Synthesis, Reactivity and Catalytic Relevance of Nickelacycles on the Aminoquinoline Scaffold

by

Pronay Roy

A dissertation submitted in partial fulfillment
of the requirements for the degree of
Doctor of Philosophy
(Chemistry)
in the University of Michigan
2022

Doctoral Committee:

Professor Melanie S. Sanford, Chair
Professor Nicolai Lehnert
Professor Stephen W. Ragsdale
Professor Nathaniel K. Szymczak

Pronay Roy

pronayry@umich.edu

ORCID iD: 0000-0002-5649-8747

Dedication

Prof. Melanie S. Sanford, Prof. Abhishek Dey and

all other friends, mentors, teachers, professors who have taught me chemistry

Acknowledgements

I could never thank Professor Melanie S. Sanford enough for all that she has taught me related to chemistry — ranging setting up experiments, analyzing data, scientific writing, teaching courses and mentoring. At some level I did realize that I joined graduate school a bit too unprepared and that too half-way across the world hence, I was a nuisance like no other. Looking back, I often wondered if I should have left graduate school but, I ultimately persevered only because of her support even though the rebuking at times was not pleasant.

I apologize to her for my blunt honesty in handling inter-personal situations in lab to having blatantly disagreeable opinions during group meetings and subgroups. I will always be grateful to her for helping me with the correction related issue and other personal incidents that followed thereafter especially considering the horrible state of mind I was in at that time which was aggravated due to the Covid-19 crisis especially back home.

Lastly, I will always be thankful to her with choosing me to be a GSI/TA with her twice where I got to learn a lot about teaching physical organic chemistry and her help with financial support from NSF grants. Instead of summarizing it all into such a *small section*, I wish I had the ability to turn my acknowledgment for her into a full thesis chapter where I could analyze the data for how our prolonged interaction over the past five years have evolved and how incredibly patient and understanding she has been amidst all the health crisis I have endured during graduate school. But all I can do is to thank her immensely for the opportunity, generosity, patience, and support, and I humbly apologize for my unpreparedness, naiveness and idiosyncrasy.

I thank Professor Nicolai Lehnert for my first experience to do chemistry research abroad, as a rotation student in Fall 2016 in his laboratory. Later on, he agreed to be a part of my doctoral thesis committee and providing letter of recommendations for fellowship applications as well. I also acknowledge professors Nathaniel K. Szymczak and Stephen W. Ragsdale for being kind enough to be part of my doctoral thesis committee and providing crucial feedback during our meetings. Professor Stephen W. Ragsdale is especially acknowledged for asking intriguing questions and providing differing insights on nickel chemistry in enzymatic systems which ultimately led me to cultivate the idea to pursue a postdoctoral research experience in biochemistry.

Additionally, Professor Vincent L. Pecoraro, Prof. Bruce A. Palfey and Professor Jennifer D. Bridwell-Rabb are acknowledged for awesome classroom instructors; especially Professor Bridwell-Rabb for boosting my confidence to pursue postdoctoral research in biochemistry. Lastly, Dr. Jeff W. Kampf for always having the time to take a look at the crystal samples, collecting data and solving the crystal structures of all the nickel complexes which has helped immensely towards the completion of my thesis.

A generous thank you to everyone in the Sanford lab as all of you have made my experience a cherish able one especially since I have always been slow in learning and understanding anything, hence can generally be annoying to deal with. First and foremost, my mentors, (*i*) Dr. James R. Bour has been an amazingly inspirational mentor and friend with his vast knowledge from every corner of science and the never-ending curiosity and thank you so much for helping me grasp the philosophy of *the usefulness of useless knowledge*. (*ii*) Dr. Devin M. Ferguson was an absolute legend especially the camaraderie we shared while being desk-buddies during the early years of my Ph.D. Thank you for explaining your entire thesis in extensive detail such that people from the lab still ask me about what experiments you ran in 2017 and I believe that shows how well you

helped me understand everything. (*iii*) Dr. Yiyang See — you are and always will be a walking encyclopedia in chemistry and although we overlapped for a short time you were kind enough to teach me so much about organic chemistry, total synthesis and the Baran lab that would last me a lifetime.

Dr. Ellen Y. Aguilera for always being an amazing friend, the better scientist and I am proud to have been in the same cohort as you. Also thank you for graduating before me as I used your thesis as a model of reference because you were always incredible at presentation and being on time with everything unlike me. Dr. Yichao Yan thank you for keeping the lab lively with all the witty and sometimes silly stuff we used to talk about. I am so certain about you will end up very high up in academia with a ginormous research lab like you always wanted to and yes, I still want to grow up to be a B-grade Yichao, someday.

Dr. Melissa Lee and Dr. Elizabeth A. Meucci for being the matured adults in 2812 while Devin, Yichao and myself were always the kids getting into trouble for our shenanigans. A special thanks to Dr. Elizabeth A. Meucci for helping me pick-up all glovebox related responsibilities and I apologize to her for my initial weird and annoying personality.

Both, Maria T. Morales, and Geraldo Duran Camacho have been so supportive and taught me a lot by being two of the hardest working chemists that I know of and for the kind conversations, daily. A special acknowledgement for Ryan Walser-Kuntz (*a nerd like no other*) for your vast knowledge and interest ranging from science to music to philosophy to cryptocurrency and even heavy-atom tunneling and especially for being such an amazing lab-mate and taking care of numerous group jobs. Dr. Anuska Shrestha for being so understanding with my *weird* personality and helping me understand how to pay US taxes. Dr. Liam S. Sharninghausen and Dr. Abebu A. Kassie for discussing so much of the copper and nickel chemistry with me and

for being such incredible people to talk with on a daily basis. Dr. Scott M. Thullen thank you for teaching me so much about photochemistry, stories from the Rovis lab, train jokes and yes, your picture will forever stay up on the ceiling in 2830. Dr. Tolani Kuam Salvador thank you so much for all the chemistry discussions ranging from Fukuzumi's back-electron transfer to research from the Warren lab. Especially for always being kind to joke around with me as well as boost my confidence to pursuing chemistry research and lastly for entertaining us at the Friday happy hours.

My deepest regards to all other current graduate students who have been amazingly kind to help me learn and understand different aspects of chemistry research from their respective theses — Conor Brigham, Naish Lalloo, Isaac Blythe, Michael Milbauer, Brianna Jett, Matthew Lasky, Frances Gu, Mami Horikawa, Jonathan Hall, and Alexander Bunnell; all the very best to all of you for your future endeavors. Especially to Michael, Isaac, and Emily on carrying forward the aminoquinoline project.

I wish I had the time and space to write separate acknowledgements for all the other senior grad students and postdocs that I have had the good fortune to overlap with during my time in the Sanford lab. All of them have been amazing mentors and lab mates who have inspired me to become a better chemist through numerous daily interactions and thank you to — Dr. Tom P. Vaid, Dr. Christian A. Malapit, Dr. Eugene Chong, Dr. Nomaan M. Rezayee, Dr. Katarina J. Makaravage, Dr. Pablo J. Cabrera, Dr. Sydonie D. Schimler, Dr. Danielle C. Samblanet, Dr. Christo S. Sevov, Dr. Koen H. Hendriks, Dr. Joshua Laffoon, Dr. Patrick R. Melvin, Dr. Courtney C. Roberts, Dr. Andrew T. Higgs, Dr. Mark A. Mantell, Dr. Bryant R. James and Monique E. Cook.

Prof. Abhishek Dey will always be a father figure to me in chemistry and life in general. I have always appreciated your blind passion for science, entertaining my absolutely ridiculous

questions ranging from chemistry to life related decisions and thank you for your endearing support for me. I would never have been able to apply for graduate school abroad if it was not for your help with the application and referral also financial help by availing my CSIR-SPM fellowship and joining your research group. I had an amazing time in the SOMADLAB and will always be a part of that and want to thank Prof. Somdatta Ghosh-Dey for being kind and supportive as well and all other SOMADLAB members for their love, support, and chemistry. Just to mention a few people who made my journey even better: Subhra da — an amazing mentor, Subal da — my elder brother and Wikipedia in chemistry, Estak da and Aman da — probably two of the hardest working and smartest chemists I know, Manjistha di — for being such a dear friend and taking frequent updates to check if I am alive or not and discussing so much of her thesis, Sarmistha di and Atanu da — for being mentors, colleagues and coauthors. Chandra da, Manas da, Biswa da, Pradip da, Kaustuv da, Sudipta da and Kushal da for being amazing lab-mates and mentors as well. Lastly Saborni di — for guiding me with my graduate school applications and keeping me on track to meet the submission deadlines over the innumerous discussions during our daily auto and metro rides back home.

I want to acknowledge the University of Michigan, Ann Arbor for supporting me with medical insurance services like Grad Care and both my doctors Dr. April L. Marquardt and Dr. Susan G. Elner − both of whom have helped me get resources and letters to the insurance companies to justify my need for proper (prohibitively expensive) medications.

Experimental research in chemistry did take away a lot of time from having a social life outside the lab but, a very special thank you to Srijoni Majhi for being an amazing person (*stalker*) who has kept me mentally sane in more ways than I can explain. I apologize for *wasting hundreds of hours of your precious time* during the regular coffee breaks and trips to the Maize & Blue

cupboard. I will forever cherish those memories of you explaining so much about everything ranging from biochemistry to economics to philosophy. Hopefully, you learn to put your massive *imposter syndrome* (*nekami*) aside and I am sure you will be an amazing scientist in the near future who will change the world for the better.

I am aware of how weirdly forgetful and quirky I am, but, *family is family*. And I humbly thank my parents (*maa* and *baba*), my brother (*bonny*) and my *in-laws*, for all of their unconditional love, and for making innumerous sacrifices so that I could pursue a PhD abroad.

Lastly but, most importantly to appreciate Debatrayee Sinha — best-friend, critic, philosopher, roommate, and wife, for literally ***everything***. I completely understand that my melancholic, eccentric, and childish nature makes it quite difficult, if not impossible at times to deal with. I thank her for entertaining all my dumb questions in biology to ludicrous interests in everything else and tolerating my unpredictable nature. I was, am and always will be incredibly grateful to her for the love, patience, friendship, and support.

Table of Contents

List of Schemes

xiv

List of Tables

List of Figures

Abstract

Metal-catalyzed C–H functionalization has revolutionized the field of synthetic chemistry with widespread implementation in the synthesis of pharmaceuticals and agrochemicals. In the past few decades, seminal work from numerous groups across the fields of organic and inorganic chemistry have demonstrated that noble metals generally serve as the most efficient catalysts. While these reactions are mechanistically well understood, the noble metal catalysts are often prohibitively expensive for large scale applications. Recently, base-metal catalysts like nickel and copper have been shown to functionalize inert C–H bonds in aminoquinoline directed systems. However, these remain mechanistically less understood than the noble metal analogs. Reactive high-valent nickel intermediates have been proposed but not isolated nor spectroscopically observed. Hence, the major focus of this thesis was to synthesize, isolate, and characterize structurally relevant nickel complexes on the aminoquinoline scaffold and to test their catalytic relevance.

Chapter 1 describes a general overview of aminoquinoline directed C–H functionalization reactions with nickel (II) catalysts. This chapter highlights the general mechanistic scenarios for these reactions in which *high-valent* (Ni^{III} and Ni^{IV}) species have been proposed as reactive intermediates.

Chapter 2 contains experimental details describing attempts to isolate the aminoquinoline σ-alkyl and σ-aryl nickelacycle complexes via C–H functionalization. Under certain conditions formation of the target nickelacycles is observed by NMR spectroscopy, but all attempts at isolation were unsuccessful owing to poor conversion. Other routes were pursued to isolate these

nickelacycle complexes, and ultimately a decarbonylation strategy proved successful to isolate a phosphine bound Ni^{II} species on both the alkyl and aryl scaffolds. Oxidation studies on the isolated phosphine complexes predominantly lead to ligand-based reactivity *i.e.,* C–P bond formation.

Chapter 3 describes exchange of the phosphine ligands for more oxidatively stable pyridine ligands, which eliminated ligand-based reactivity upon oxidation. Stoichiometric oxidation of these pyridine ligated Ni^{II} complexes with I_2 resulted in $C(sp^3)$–N and $C(sp^2)$–I bond-forming reactions. Furthermore, these complexes were shown to be catalytically relevant as noted by turnover under catalytic conditions of the aforementioned bond-forming reactions.

Chapter 4 describes the oxidation of pyridine ligated Ni^{II} complexes to form and isolate high-valent Ni^{III} complexes, which have been previously proposed in the literature as reactive intermediates in C–H functionalization catalysis. Electrochemical studies informed the appropriate choice of one-electron oxidants for isolation of these Ni^{III} complexes. The isolated complexes were shown to be catalytically inert species under catalytic reaction conditions unlike the previously isolated Ni^{II} species in Chapter 3. An aryl-aryl coupling reaction was also discovered from the isolated Ni^{III} complex on the aryl scaffold.

Chapter 5 describes general strategies employed in attempts to isolate Ni^{IV} complexes with these aminoquinoline bound nickelacycles. These involve the use of strong two-electron oxidants and polydentate ligands to access and stabilize Ni^{IV} intermediates. The synthesis, isolation, characterization of the polydentate Ni^{III} complexes is described, and general results from the oxidation reactions are summarized. Although the isolation of a Ni^{IV} complex was unsuccessful on this scaffold, based on the findings, some general guiding principles have been proposed as future directions.

Chapter 1 Introduction

1.1 C–H Functionalization Reactions

Organic compounds are composed of carbon atoms that are chemically bonded to other elements to satisfy their chemical valency, with hydrogen being the most prevalent one. Hence, the selective chemical transformation of these ubiquitous C–H bonds into more functionalized chemical bonds (i.e., C–H to C–X) is an ongoing research pursuit.[1] In the past few decades, chemists from different sub-disciplines ranging from biochemistry to inorganic to organic chemistry have developed methodologies for the selective functionalization of C–H bonds aided by catalysts (Scheme 1.1).[2] New catalytic methodologies often have a proposed mechanism that involves the intermediacy of highly reactive intermediates. Thus, there is a significant impetus to test the feasibility of the proposed reaction model via experimental mechanistic studies, often targeted at establishing the viability of the proposed reactive intermediates.

Scheme 1.1 C–H Functionalization Reactions
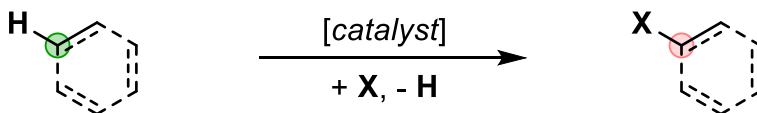
1.2 Group 10 Metal Catalyzed C–H Functionalization

Seminal work from numerous groups have shown that late transition metal catalysts, particularly noble metals like platinum and palladium, are efficient at selectively activating and then functionalizing strong C–H bonds.[3] One of the major bottlenecks for these reactions being broadly employed by chemists is the prohibitive expense of the commonly used palladium and

platinum catalysts. Nickel, a group 10 congener to Pd and Pt, is drastically cheaper owing to higher natural abundance (Figure 1.1). Although numerous palladium and platinum catalyzed C–H functionalization reactions have been reported in the literature in past few decades, analogous reports with nickel are recent and few. Hence, the development and mechanistic understanding of Ni-catalyzed C–H functionalization reactions remain in their infancy. [4,5]

Figure 1.1 Natural Abundance of Elements[6]
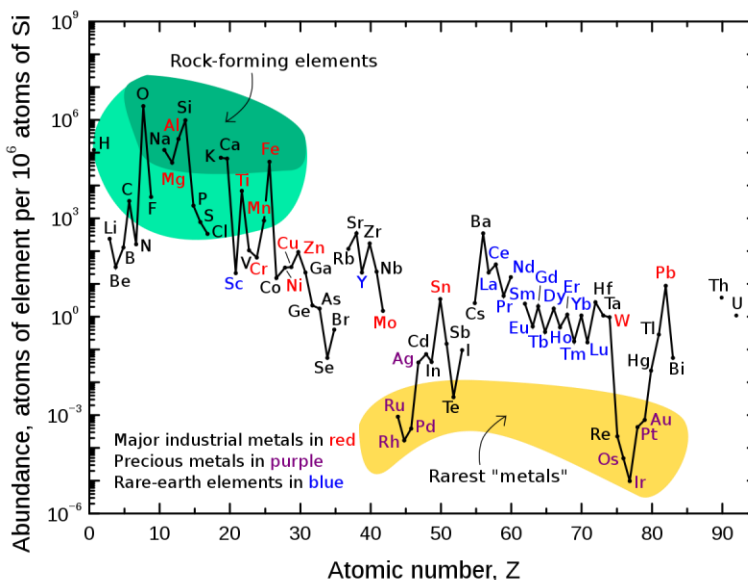
Based on the previous studies with palladium and platinum as catalysts, a seemingly simple substitution to nickel generally fails because: (*i*) it has not yet been established if the reactions proceed through similar intermediates, and (*ii*) the analogously proposed intermediates on nickel are drastically more reactive than its group congeners as inferred from studies on model systems.[7] The higher reactivity of the nickel complexes is associated with a fundamental atomic property, namely the accessibility of radical nodes, which is based on its elemental position on the periodic table. This ultimately is responsible for elemental properties like smaller ionic radii, higher electronegativity, and less covalent bonding in nickel complexes compared to palladium and

2

platinum analogues (Figure 1.2).[8] These factors lead to reduced stability of nickel complexes and decomposition through multiple deleterious pathways.

Figure 1.2 Comparing Group 10 Organometallic Complexes

Ni : *ionic, weaker − reactive*
Pd & Pt: *covalent, stronger − stable*
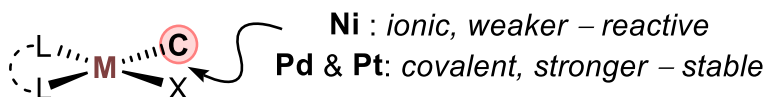
1.3 Pincer Ligands in Catalytic C–H Functionalization with Palladium and Nickel

The generalized mechanistic model for the C–H functionalization reactions involves C–H cleavage to form a metal-carbon bond (M–C) that subsequently reacts with electrophilic or oxidative reagents of general type **X** to form the desired C–X bond of interest (Scheme 1.2).[1,3]

Scheme 1.2 Organometallic Intermediate in Metal Catalyzed C–H Functionalization

organometallic intermediate
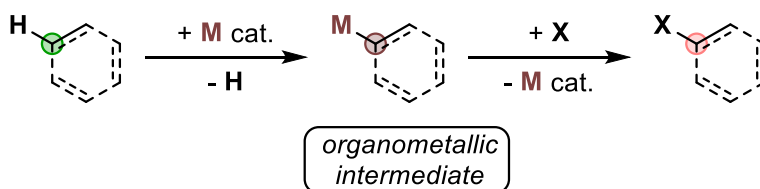
There are two major facets of metal mediated C–H activation: (*i*) the selectivity for a specific C–H bond and (*ii*) the mechanism. The C–H selectivity depends on the inherent electronics or sterics or a combination of both for the molecule. However, these factors limit (*i*) the generality of the C–H activation step, as it ends up being inherently substrate driven and (*ii*) selectivity, which is a major issue in more complex substrates as it leads to an often-intractable mixture of products. To tackle this problem, chemists have turned to the use of directing groups.[2,9] A directing group is a chemical moiety attached to the substrate that helps to scaffold the substrate onto the metal catalyst. This scaffolding controls the site of C–H activation, both aided by thermodynamic and kinetic factors. The directing group reduces the overall enthalpic and entropic cost of the reaction by pre-coordination to the metal. This also impacts the kinetics of the C–H activation step because

of the proximity effect. As previously discussed, Ni–C bonds are more reactive than Pd–C or Pt–C bonds, and one of the common modes of decomposition is through radical homolysis pathways. The tethering of the hydrocarbyl unit to the ligand of interest significantly reduces these deleterious decomposition pathways for both thermodynamic as well as kinetic reasons (Scheme 1.3).[10]

Scheme 1.3 Ligand Directed and Stabilized Organometallic Intermediates

Since the late 1990s, the C–H activation community has explored a plethora of directing groups. The one that has been most extensively employed is the aminoquinoline directing group.[11,12] This group was initially pioneered by Daugulis in the context of Pd[II]-mediated C–H functionalization reactions and was ultimately extended to other transition metal mediated reactions. The major benefits of this directing group are three-fold. It is (*i*) multidentate, (*ii*) rigid, and (*iii*) easily tunable.

The aminoquinoline directing group is a bidentate ligand, and along with hydrocarbyl unit, the metal templated C–H activated organometallic complex is a meridional tridentate ligand. Tridentate meridional ligands are commonly referred to as *pincer* ligands in the inorganic chemistry literature owing to their similarity with crustacean claws. These ligands have been employed in a plethora of applications ranging from the synthesis of transition metal complexes to the isolation and spectroscopic observation of reactive intermediates and even in the design of tunable and versatile transition metal catalysts (Figure 1.3).[13]

Figure 1.3 Pincer Ligand Scaffold
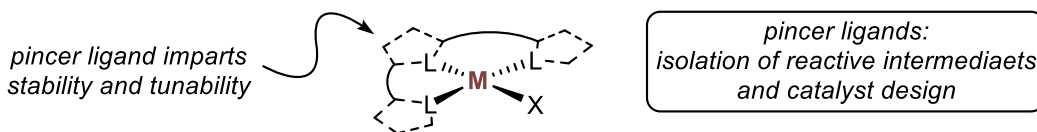
The aminoquinoline moiety is tethered onto the hydrocarbyl unit through an amide bond. This is a simple and versatile linkage that can be used to generate libraries of chemical compounds. The quinoline backbone is inherently planar and rigid thus imparting overall structural rigidity to the scaffold (Scheme 1.4). The steric and electronic properties of quinolines can easily be tuned by installation of functional groups on the heterocyclic core. Numerous methods have also been developed for easy removal of this directing group for accessing the functionalized C–X species. Overall, both of these factors contribute to the practical applicability of the aminoquinoline directing group.[14]

Scheme 1.4 Aminoquinoline Directed Metallacycle Formation
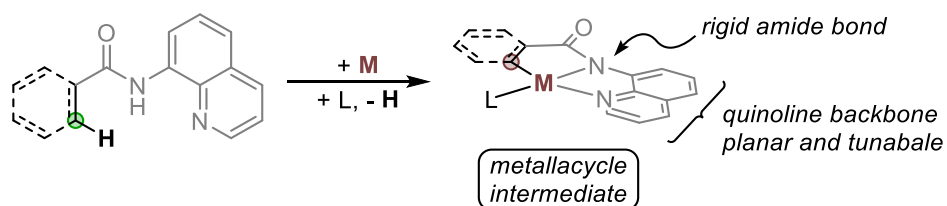
1.4 Nickel Catalyzed C–H Functionalization on the Aminoquinoline Scaffold

In 2013 Chatani first reported a broad substrate scope for nickel catalyzed C–H alkylation on the aminoquinoline-based substrates using primary alkyl halides.[15] This was further extended by reports from the groups of Ackerman and Sundararaju with more substituted alkyl and allyl halides as functionalizing reagents.[9,10] Subsequently, C–H arylation reactions on this scaffold were reported by the groups of Chatani, You, Shi, and Hoover using either aryl electrophiles or aryl nucleophiles coupled with silver oxidants.[16–19] Subsequently, this was expanded to alkynylation, alkenylation, and annulation methodologies, thereby demonstrating a wide variety of C–H to C–C bond constructions on this scaffold (Scheme 1.5).[17,20–22] Overall, these initial reports highlighted the viability of the aminoquinoline directing group in nickel catalyzed C–H functionalization.

Scheme 1.5 Aminoquinoline Directed Nickel Catalyzed C–H Carbo-Functionalization
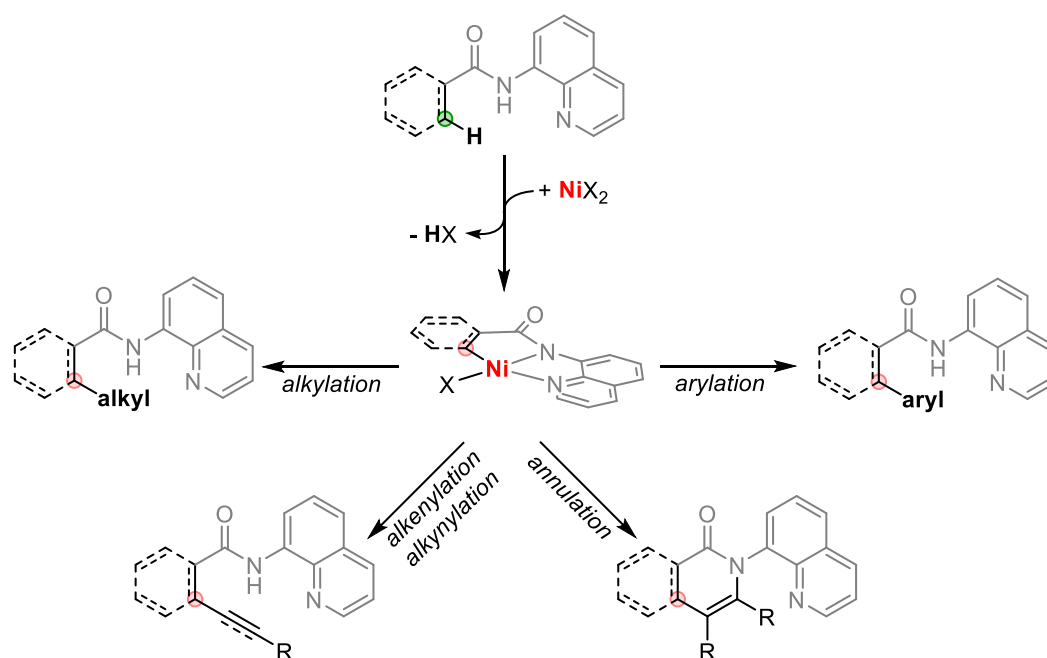
Inspired from the aforementioned generality of the C–H carbo-functionalization reports on the aminoquinoline scaffold, it was envisioned to extend this to generate C–heteroatom (heteroatom = O, N, Cl, I, P) bond-forming reactions. But, only recently in 2016 two concurrent reports were published by Chatani and Koley on C–H iodination[23,24] and by Chang in 2021 on C–H amidation.[25,26] These sparse reports in the context of C–heteroatom bond forming reactions is intriguing and prefaces the challenges involved in the C–heteroatom bond formations. A closer look at the general mechanistic model for these reaction highlights the key challenges.

The general mechanism of these nickel mediated C–H functionalization reactions involves initial formation of a nickelacycle intermediate. As discussed previously, the aminoquinoline pincer scaffold aids in accessing this crucial Ni^{II}–C intermediate. Both computational studies from Liu and Musaev as well as H/D exchange studies by Chatani indicate that the C–H bond activation step at Ni^{II} is thermodynamically uphill and reversible under most of the catalytic

6

conditions.[15,16,24,27] Hence, experimental probing of reactions steps after the formation of the nickelacycle by traditional kinetic studies has largely proven futile.

Scheme 1.6 Nickel Catalyzed Aminoquinoline Directed C–H Functionalization
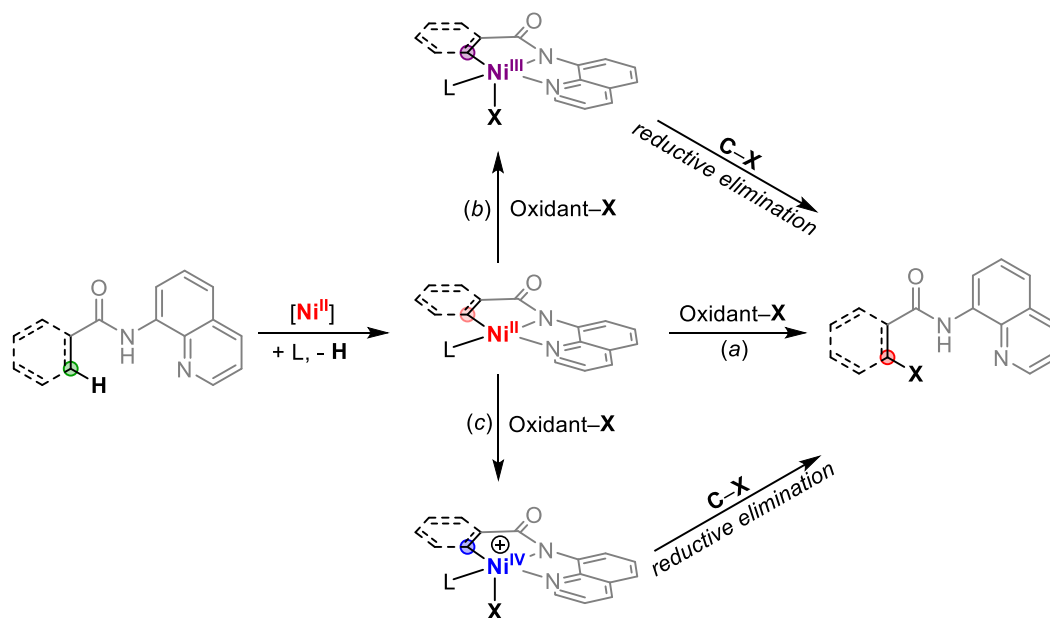
The Ni^{II} organometallic intermediate formed then encounters a branching point in the general mechanism, which is primarily based on the electrophile or oxidant employed in the reaction. The three pathways invoke the intermediacy of nickel species in three different oxidation states, Ni^{II}, Ni^{III}, or Ni^{IV} (Scheme 1.6).[28] Pathway (*a*) involves direct C–X bond formation via either an electrophilic cleavage or a σ-bond metathesis step. Pathway (*b*) involves the intermediacy of discrete Ni^{III} intermediates, and pathway (*c*) generates Ni^{IV} species. Using the redox potentials of the electrophile or oxidant under consideration, the feasibility of pathway (*b*) or pathway (*c*) can be analyzed. However, that does not provide definitive evidence, as literature reports have shown that minor changes to reaction conditions can lead to different pathways for organometallic reactions. Moreover, studies on model systems have shown that Ni^{III} species are common intermediates en route to Ni^{IV} (Figure 1.4) owing to the prevalence of facile one-electron redox events among the first-row transition metals.[29]

7

Figure 1.4 Ni$^{II/III/IV}$ Catalytic Redox Cycles
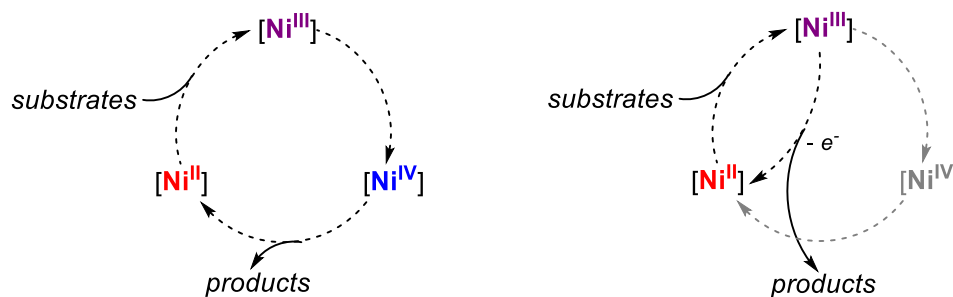
1.5 High-Valent Nickel Intermediates in Aminoquinoline Directed C–H Functionalization

The prevalence of heavier group 10 metals in C–H functionalization reactions is noteworthy. Nickel is one of the late transition metals in the chemical periodic table and is at the top of group 10. Nickel has five available oxidation states from 0 to +4.[4,5,7] Unlike Pd and Pt, the +1 and +3 oxidation states are readily accessible at Ni. The inert pair effect primarily stems from the core atomic properties *i.e.*, the radial wave function which is ultimately responsible for lack of both radial nodes and relativistic contraction in nickel, thereby leveraging one-electron redox events in nickel compared to its group congeners.[8]

As mentioned in section 1.4, three oxidation states of nickel are often invoked in aminoquinoline directed C–H functionalization reactions. Ni^{III} and Ni^{IV} are generally considered as high-valent oxidation states of the metal, with Ni^{II} being the most stable one. Considerable effort has been deployed into the isolation of these high-valent nickel complexes in model systems with the major focus of the studies being directed towards: (*i*) the isolation of Ni^{III} and Ni^{IV} species and (*ii*) C–X bond-forming reductive elimination studies. Although Ni^{III} and Ni^{IV} complexes are considered as highly reactive, Chatani, Shi, and others have regularly invoked the feasibility of these species in proposed catalytic mechanisms (Scheme 1.6).[30,31]

Hence, there is significant impetus to test the feasibility of the proposed high-valent intermediates in the context of Ni-catalyzed C–H functionalization reactions. Understanding the intermediates can allow tuning of: (*i*) selectivity of bond formations, (*ii*) choice of electrophiles and oxidants, and (iii) development of other C–X bond-forming reactions via a mechanism-guided approach. However, it is often challenging to probe the reactive high-valent species generated under catalytic conditions via traditional kinetic experiments. This thesis leverages a decarbonylative strategy to isolate and test the reactivity and catalytic relevance of some of the Ni^{II} complexes, as described in Chapters 2–3. In Chapter 4, the studies elaborate on efforts to isolate Ni^{III} complexes, and Chapter 5 focuses on attempts towards the isolation of Ni^{IV} complexes on the aminoquinoline scaffold.

Notably, recent computational and spectroscopy studies have established that the metal-ligand bonding in these high oxidation state complexes lead to higher covalency of the chemical bond. Thus, there is a significant controversy regarding the "actual" oxidation state at the metal center based on the electronic structure.[32] To reduce ambiguity in the context of this thesis the semantic references to *high-valent* nickel complexes have primarily been inferred from routine electron counting methods as used in organometallic chemistry textbooks and lectures. The exact nature of the chemical bonding in the high-valent nickel complexes was not investigated. However, that <u>does not impact the isolation, characterization, and reactivity studies</u> of these catalytically relevant high-valent nickel complexes on the aminoquinoline scaffold, as per the current common knowledge in the field.[33]

1.6 References

(1)   Labinger, J. A.; Bercaw, J. E. Understanding and Exploiting C–H Bond Activation. *Nature 2002 417:6888* **2002**, *417* (6888), 507–514. https://doi.org/10.1038/417507a.

(2)   Davies, H. M. L.; Morton, D. Recent Advances in C–H Functionalization. *The Journal of Organic Chemistry* **2016**, *81* (2), 343–350. https://doi.org/10.1021/acs.joc.5b02818.

(3)   Crabtree, R. H.; Lei, A. Introduction: CH Activation. *Chemical Reviews* **2017**, *117* (13), 8481–8482. https://doi.org/10.1021/acs.chemrev.7b00307.

(4)   P. Ananikov, V. Nickel: The "Spirited Horse" of Transition Metal Catalysis. *ACS Catalysis* **2015**, *5* (3), 1964–1971. https://doi.org/10.1021/acscatal.5b00072.

(5)   Tasker, S. Z.; Standley, E. A.; Jamison, T. F. Recent Advances in Homogeneous Nickel Catalysis. *Nature 2014 509:7500* **2014**, *509* (7500), 299–309. https://doi.org/10.1038/nature13274.

(6)   Haxel, G. B.; Hedrick, J. B.; Orris, G. J.; Stauffer, P. H.; Wendley II, J. W.; Boore, S.; Mayfield, S.; Donlin, C. Rare Earth Elements—Critical Resources for High Technology https://pubs.usgs.gov/fs/2002/fs087-02/ (accessed 2022 -01 -01).

(7)   Heberer, N.; Hu, C.-H.; Mirica, L. M. 6.09 - High-Valent Ni Coordination Compounds. In *Comprehensive Coordination Chemistry III*; Constable, E. C., Parkin, G., Que Jr, L., Eds.; Elsevier: Oxford, 2021; pp 348–374. https://doi.org/https://doi.org/10.1016/B978-0-08-102688-5.00104-5.

(8)   Kaupp, M. The Role of Radial Nodes of Atomic Orbitals for Chemical Bonding and the Periodic Table. *Journal of Computational Chemistry* **2007**, *28* (1), 320–325. https://doi.org/https://doi.org/10.1002/jcc.20522.

(9)   Khake, S. M.; Chatani, N. Chelation-Assisted Nickel-Catalyzed C-H Functionalizations. *Trends in Chemistry* **2019**, *1* (5), 524–539. https://doi.org/10.1016/j.trechm.2019.06.002.

(10)   Gandeepan, P.; Müller, T.; Zell, D.; Cera, G.; Warratz, S.; Ackermann, L. 3d Transition Metals for C–H Activation. *Chemical Reviews* **2018**, *119* (4), 2192–2452. https://doi.org/10.1021/acs.chemrev.8b00507.

(11)   Shabashov, D.; Daugulis, O. Auxiliary-Assisted Palladium-Catalyzed Arylation and Alkylation of Sp^2 and Sp^3 Carbon−Hydrogen Bonds. *Journal of the American Chemical Society* **2010**, *132* (11), 3965–3972. https://doi.org/10.1021/ja910900p.

(12)   T. Nadres, E.; Ivan Franco Santos, G.; Shabashov, D.; Daugulis, O. Scope and Limitations of Auxiliary-Assisted, Palladium-Catalyzed Arylation and Alkylation of Sp2 and Sp3 C–H Bonds. *The Journal of Organic Chemistry* **2013**, *78* (19), 9689–9714. https://doi.org/10.1021/jo4013628.

(13)   Peris, E.; Crabtree, R. H. Key Factors in Pincer Ligand Design. *Chem. Soc. Rev.* **2018**, *47* (6), 1959–1968. https://doi.org/10.1039/C7CS00693D.

(14)   Fitzgerald, L. S.; O'Duill, M. L. A Guide to Directing Group Removal: 8-Aminoquinoline. *Chemistry – A European Journal* **2021**, *27* (33), 8411–8436. https://doi.org/https://doi.org/10.1002/chem.202100093.

(15)   Y Aihara, N. C. Nickel-Catalyzed Direct Alkylation of C–H Bonds in Benzamides and Acrylamides with Functionalized Alkyl Halides via Bidentate-Chelation Assistance. *J. Am. Chem. Soc.* **2013**, *135* (14), 5308–5311. https://doi.org/10.1021/ja401344e.

(16)   Aihara, Y.; Chatani, N. Nickel-Catalyzed Direct Arylation of C(Sp3)–H Bonds in Aliphatic Amides via Bidentate-Chelation Assistance. *Journal of the American Chemical Society* **2014**, *136* (3), 898–901. https://doi.org/10.1021/ja411715v.

(17) Honeycutt, A. P.; M. Hoover, J. Nickel-Catalyzed Oxidative Decarboxylative Annulation for the Synthesis of Heterocycle-Containing Phenanthridinones. *Organic Letters* **2018**, *20* (22), 7216–7219. https://doi.org/10.1021/acs.orglett.8b03144.

(18) P. Honeycutt, A.; M. Hoover, J. Nickel-Catalyzed Oxidative Decarboxylative (Hetero)Arylation of Unactivated C–H Bonds: Ni and Ag Synergy. *ACS Catalysis* **2017**, *7* (7), 4597–4601. https://doi.org/10.1021/acscatal.7b01683.

(19) Zhao, S.; Liu, B.; Zhan, B.-B.; Zhang, W.-D.; Shi, B.-F. Nickel-Catalyzed Ortho-Arylation of Unactivated (Hetero)Aryl C–H Bonds with Arylsilanes Using a Removable Auxiliary. *Organic Letters* **2016**, *18* (18), 4586–4589. https://doi.org/10.1021/acs.orglett.6b02236.

(20) He, Z.; Huang, Y. Diverting C–H Annulation Pathways: Nickel-Catalyzed Dehydrogenative Homologation of Aromatic Amides. *ACS Catalysis* **2016**, *6* (11), 7814–7823. https://doi.org/10.1021/acscatal.6b02477.

(21) Misal Castro, L. C.; Obata, A.; Aihara, Y.; Chatani, N. Chelation-Assisted Nickel-Catalyzed Oxidative Annulation via Double C−H Activation/Alkyne Insertion Reaction. *Chemistry – A European Journal* **2016**, *22* (4), 1362–1367. https://doi.org/https://doi.org/10.1002/chem.201504596.

(22) Wan, J.-P.; Li, Y.; Liu, Y. Annulation Based on 8-Aminoquinoline Assisted C–H Activation: An Emerging Tool in N-Heterocycle Construction. *Organic Chemistry Frontiers* **2016**, *3* (6), 768–772. https://doi.org/10.1039/C6QO00077K.

(23) Khan, B.; Kant, R.; Koley, D. Nickel(II)-Mediated Regioselective C□H Monoiodination of Arenes and Heteroarenes by Using Molecular Iodine. *Advanced Synthesis and Catalysis* **2016**, *358* (14). https://doi.org/10.1002/adsc.201600177.

(24) Aihara, Y.; Chatani, N. Nickel-Catalyzed Reaction of C–H Bonds in Amides with I2: Ortho-Iodination via the Cleavage of C(Sp2)–H Bonds and Oxidative Cyclization to β-Lactams via the Cleavage of C(Sp3)–H Bonds. *ACS Catalysis* **2016**, *6* (7), 4323–4329. https://doi.org/10.1021/acscatal.6b00964.

(25) Bum Kim, Y.; Won, J.; Lee, J.; Kim, J.; Zhou, B.; Park, J.-W.; Baik, M.-H.; Chang, S. Ni-Catalyzed Intermolecular C(Sp3)–H Amidation Tuned by Bidentate Directing Groups. *ACS Catalysis* **2021**, *11* (5), 3067–3072. https://doi.org/10.1021/acscatal.1c00070.

(26) Xu, S.; Hirano, K.; Miura, M. Nickel-Catalyzed Regio- and Stereospecific C–H Coupling of Benzamides with Aziridines. *Organic Letters* **2021**, *23* (14), 5471–5475. https://doi.org/10.1021/acs.orglett.1c01821.

(27) Omer, H. M.; Liu, P. Computational Study of Ni-Catalyzed C–H Functionalization: Factors That Control the Competition of Oxidative Addition and Radical Pathways. *Journal of the American Chemical Society* **2017**, *139* (29), 9909–9920. https://doi.org/10.1021/jacs.7b03548.

(28) Roy, P.; R. Bour, J.; W. Kampf, J.; S. Sanford, M. Catalytically Relevant Intermediates in the Ni-Catalyzed C(Sp2)–H and C(Sp3)–H Functionalization of Aminoquinoline Substrates. *Journal of the American Chemical Society* **2019**, *141* (43), 17382–17387. https://doi.org/10.1021/jacs.9b09109.

(29) Bour, J. R.; M. Ferguson, D.; J. McClain, E.; W. Kampf, J.; S. Sanford, M. Connecting Organometallic Ni(III) and Ni(IV): Reactions of Carbon-Centered Radicals with High-Valent Organonickel Complexes. *Journal of the American Chemical Society* **2019**, *141* (22), 8914–8920. https://doi.org/10.1021/jacs.9b02411.

(30) Yokota, A.; Aihara, Y.; Chatani, N. Nickel(II)-Catalyzed Direct Arylation of C–H Bonds in Aromatic Amides Containing an 8-Aminoquinoline Moiety as a Directing Group. *The*

Journal of Organic Chemistry **2014**, *79* (24), 11922–11932. https://doi.org/10.1021/jo501697n.

(31) Iyanaga, M.; Aihara, Y.; Chatani, N. Direct Arylation of C(Sp3)–H Bonds in Aliphatic Amides with Diaryliodonium Salts in the Presence of a Nickel Catalyst. *The Journal of Organic Chemistry* **2014**, *79* (24), 11933–11939. https://doi.org/10.1021/jo501691f.

(32) T. Shreiber, S.; M. DiMucci, I.; N. Khrizanforov, M.; J. Titus, C.; Nordlund, D.; Dudkina, Y.; E. Cramer, R.; Budnikova, Y.; M. Lancaster, K.; A. Vicic, D. [(MeCN)Ni(CF3)3]− and [Ni(CF3)4]2–: Foundations toward the Development of Trifluoromethylations at Unsupported Nickel. *Inorganic Chemistry* **2020**, *59* (13), 9143–9151. https://doi.org/10.1021/acs.inorgchem.0c01020.

(33) Hartwig, J. F. *Organotransition Metal Chemistry: From Bonding to Catalysis*; University Science Books, 2010, 2010.

Chapter 2 Synthesis and Reactivity of Phosphine Ligated Ni^{II} Complexes

Note: Results from section **2.2.1** was published in <u>Roy, P.</u>; Bour, J. R.; Kampf, J. W.; Sanford, M. S.* Catalytically Relevant Intermediates in the Ni-Catalyzed C(sp^2)–H and C(sp^3)–H Functionalization of Aminoquinoline Substrates. *J. Am. Chem. Soc.* **2019**, *141*, 17382–17387 and *J. Am. Chem. Soc.* **2021**, *143*, 14021.

2.1 Introduction

Over the past decade there has been significant progress in the development of Ni-catalyzed reactions for the oxidative functionalization of unactivated C–H bonds. The vast majority of these transformations involve the use of aminoquinoline-based substrates and result in the formation of new carbon–carbon or carbon–heteroatom bonds (Scheme 2.1).[1,2]

Scheme 2.1 Proposed Pathways for Ni-catalyzed Oxidative Functionalization of C–H Bonds
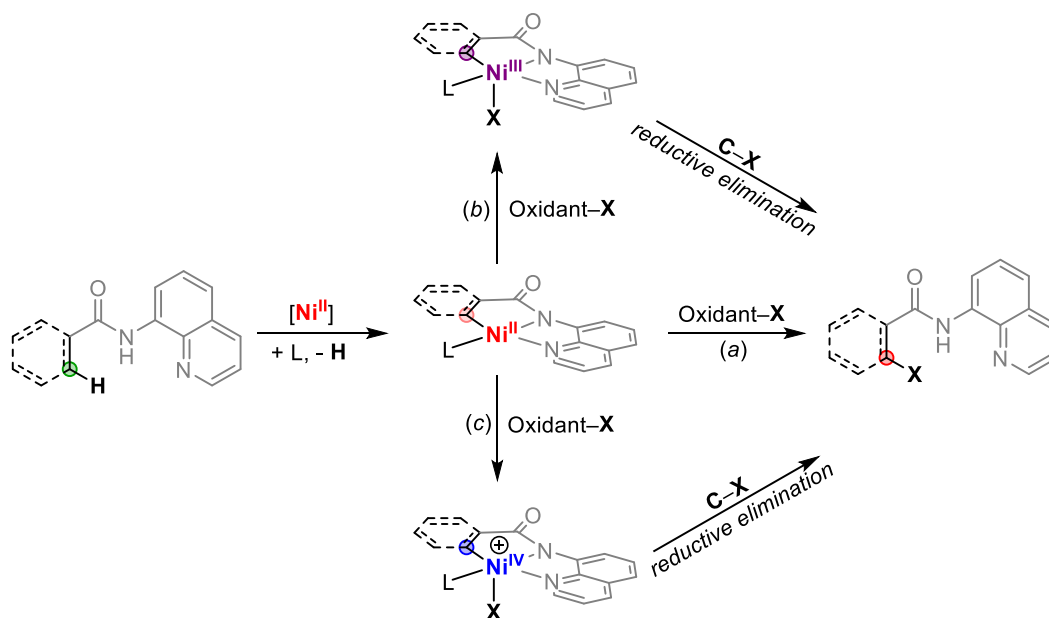
Mechanistically, these aminoquinoline-directed C–H functionalization reactions are proposed to involve initial C–H bond activation at Ni^{II} centers to form nickelacycles. However, at the time that this work was initiated (in 2017), the nickelacycle intermediates had neither been detected spectroscopically nor isolated during catalysis. However, their intermediacy was supported by computational investigations, experimental H/D exchange studies, kinetic isotope effect studies, and model systems.[3–7] In contrast, considerable debate remains to this day about the mechanism of the oxidative functionalization step. Various pathways have been proposed, including (*i*) direct electrophilic functionalization of the Ni–C bond without a change in oxidation state at Ni (Scheme 2.1, *a*), (*ii*) C–X bond-forming reductive elimination from a Ni^{III} intermediate (Scheme 2.1, *b*), or (*iii*) C–X bond-forming reductive elimination from a Ni^{IV} intermediate (Scheme 2.1, *c*).[2,8]

Several reports by Chatani concluded that the Ni^{II}-mediated C–H activation step is reversible. This was experimentally probed under catalytic conditions via H/D exchange, using a substrate in which the proximal C–H bonds were labeled with deuterium on the aminoquinoline substrate. Quenching of the reaction at shorter times both in the presence and absence of the oxidant showed exchange of deuterium for hydrogen in the substrate, as analyzed by ^{1}H NMR spectroscopy (Scheme 2.2).[4,5,9–11]

Scheme 2.2 Isotopic H/D Exchange Studies in Ni-catalyzed C–H Functionalization Reactions

functionalized product   H/D exchanged product

Erosion of D content
(shorter reaction duration)
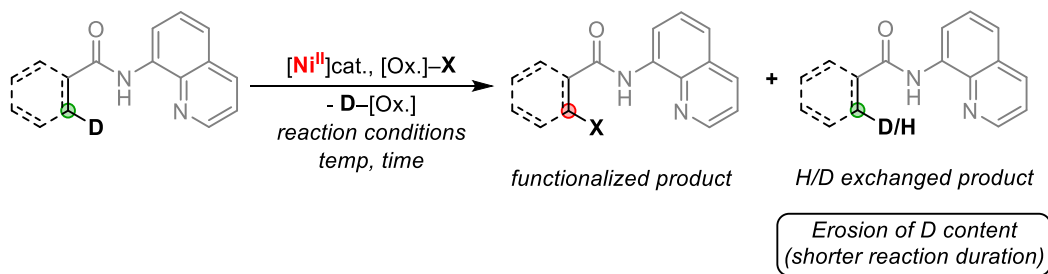
This was further corroborated with computational studies, which reported an energy barrier of ~21 kcal/mol for the $C(sp^3)$–H activation step.[6] This report also noted that the barrier for the formation of the analogous palladacycle was lower by ~2 kcal/mol. Although the barrier for the $C(sp^3)$–H activation step was comparable for both nickel and palladium, the overall reaction was endergonic (~2 kcal/mol) for the formation of the nickelacycle whereas it was exergonic (~–7 kcal/mol) for the palladacycle (Figure 2.1).[6]

Figure 2.1 C–H activation at Pd vs. Ni — Computational Studies by Liu[6]
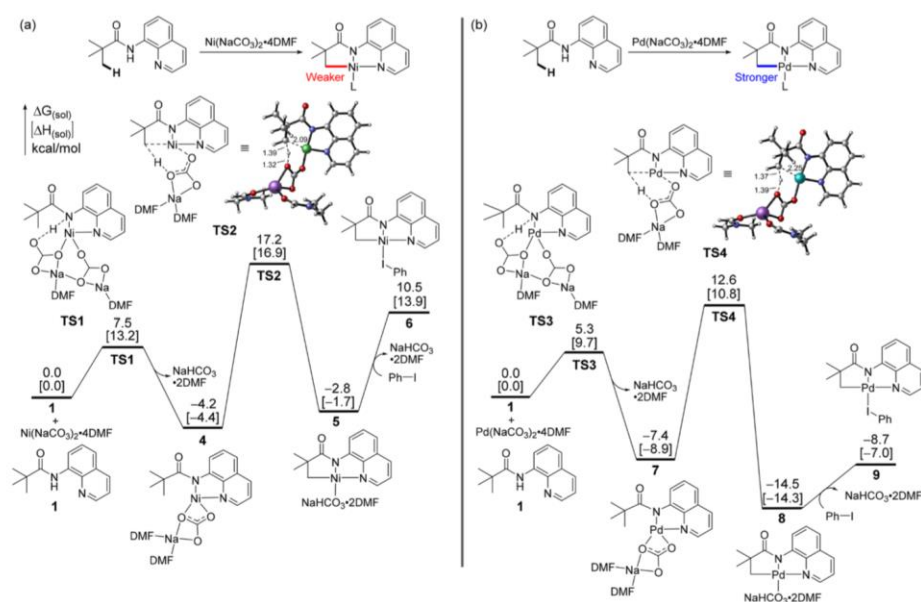
The first part of this chapter details our attempts to study the formation and isolation of the nickelacycle via C–H activation of aminoquinoline substrates. Reaction parameters including ligand, solvent, temperature, and time were screened for both the aminoquinoline $C(sp^2)$ and $C(sp^3)$ substrates. Among the conditions screened, only one reaction showed the formation of a cyclometalated aminoquinoline species. Based on the color and ^{1}H NMR spectrum of the reaction, the product was tentatively assigned as a nickelacycle species. However, all attempts to isolate this species failed owing to low conversion.

Thereafter, inspired by literature reports, a decarbonylative route was pursued for the isolation of the triethylphosphine-ligated σ-alkyl and σ-alkyl nickelacycles. These Ni[II] complexes were characterized using a variety of analytical techniques. Oxidative functionalization of these Ni[II] complexes was also explored. These studies primarily showed reactivity of the PEt$_3$ ligand, but the organic products varied as a function of oxidant (ferrocenium versus O$_2$ versus iodine versus methyl iodide).

2.2 Result and Discussion

2.2.1 C–H Activation Routes to Nickelacycles

In general, the activation of a sp^2 C–H bond via a concerted metalation deprotonation mechanism (like that proposed in Figure 2.1, above) is more facile than that of a sp^3 C–H bond because of lower pK$_a$.[12–14] Thus, our first target was isolation of the cyclometalated σ-aryl Ni[II] species **2b-MeCN** (M = Ni). Notably, analogous palladacycles have been isolated by Chen and Maiti via C(sp^2)–H activation with M = Pd (Scheme 2.3)[15,16] following similar procedures reported by Daugulis for the C(sp^3) analog.[17,18]

Scheme 2.3 Metallacycle — C(sp^2)–H Activation with M[II]
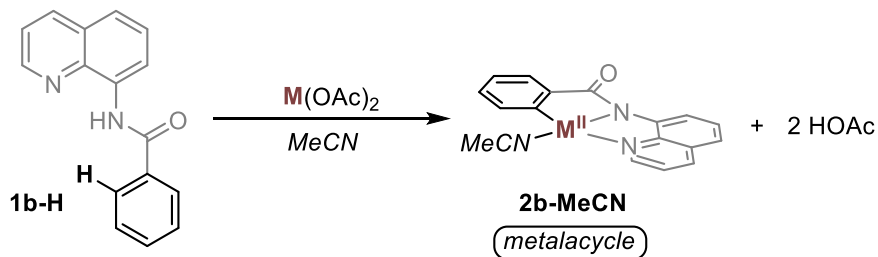
We first examined the reaction of 1 equiv of **1b-H** with 1 equiv of Ni(OAc)$_2$ in MeCN-d_3 at temperatures ranging from 25 to 90 ℃ and times from 1 to 24 h. However, these reactions only showed the presence of starting material by ^{1}H NMR spectroscopy. We next screened reaction conditions by varying the polarity of the solvent, temperatures up to 160 °C, and reaction times up

to 30 h. The above reactions mostly showed unconsumed starting material, along with some paramagnetic broadening, as analyzed by ^{1}H NMR spectroscopy. These results are in accord with previously reported conclusions by Chatani from H/D exchange studies as well as computational calculations by Musaev that predict an overall endergonic C–H activation step in this system.[19]

Scheme 2.4 C–H Activation Route to σ-aryl Ni[II] Complex

1b-H   Ni(OAc)$_2$, NMe$_4$OAc / DMSO-d_6, 12 h   **2b-L**   +   2 HOAc

yield: 12% (brsm)
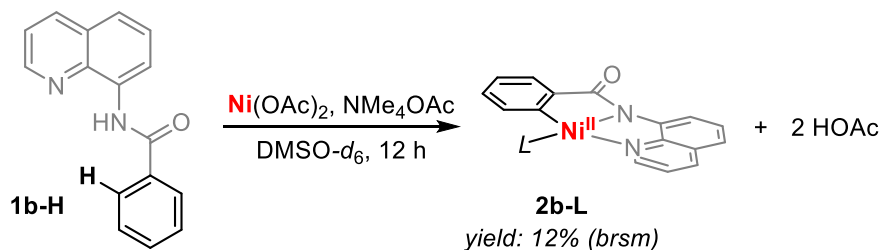
Since the stoichiometric reaction (Scheme 2.3) involves the formation of acid as a by-product alongside the desired metallacycle product **2b-MeCN**, we hypothesized that the addition of a base would drive the reaction to the right. Acetate bases are commonly used in C–H activation reactions,[20] and quaternary ammonium cations enhance their solubility in organic solvents. Thus, tetramethylammonium acetate was examined as the base. A series of reactions were conducted using 1 equiv of **1b-H**, 1 equiv of Ni(OAc)$_2$, and 1 equiv of NMe$_4$OAc in different solvents. When this transformation was conducted in DMSO-d_6 there was a color change from pale yellow to orange along with the formation of a new diamagnetic species in a maximum yield of 12% after 12 h at 160 °C as analyzed by ^{1}H NMR spectroscopy. This species was tentatively assigned as the σ-aryl nickelacycle **2b-L** (L is likely DMSO), as it showed chemical shifts akin to that of the palladacycle isolated by Chen.[15] However, attempts to isolate the complex resulted in decomposition, largely due to the challenges associated with removing DMSO from the reaction mixture. Although the identity of the nickelacycle was a tentative assignment, it was further confirmed by comparing this ^{1}H NMR spectrum to that of the picoline-bound σ-aryl nickelacycle that was synthesized in Chapter 3.

Scheme 2.5 C–H Activation Route to σ-alkyl Ni^{II} Complex
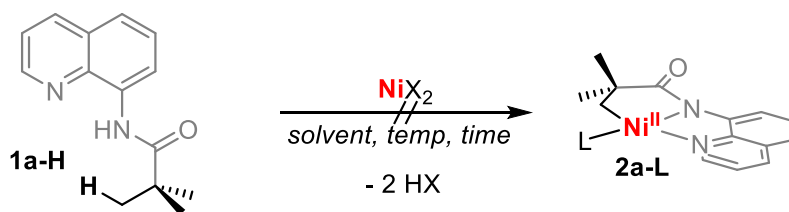
In parallel, we examined analogous conditions for the reaction **1a-H** with Ni salts to afford the corresponding σ-alkyl nickelacycle **2a-L**. We varied the nickel salt (Ni(OAc)$_2$, Ni(OTf)$_2$, or NiBr$_2$•DME), solvent (MeCN, toluene, or DMSO), and temperature (up to 160 °C) and also added exogenous NMe$_4$OAc (Scheme 2.5). However, **2a-L** was not detected by ^{1}H NMR spectroscopy under any of the conditions examined. This is likely due to the higher barrier for C(sp^3)–H activation, as predicted by Liu (Figure 2.1).[6] Recently, others have reported that tuning the substrate and nickel precursor does enable the isolation of analogous aminoquinoline σ-alkyl nickelacycles via C(sp^3)–H activation (Figure 2.2). For example, in 2018, Love reported that changing the amide backbone to a urea moiety increased rigidity, thereby lowering the barrier to C(sp^3)–H bond activation.[21] Furthermore, in 2021, Johnson reported that using a pre-formed organometallic nickel precursor in conjunction with a deprotonated amide substrate significantly facilitated access to the cyclometalated Ni^{II} σ-alkyl complexes (Figure 2.2).[22]

Figure 2.2 Literature Reports to σ-alkyl Ni^{II} Complex
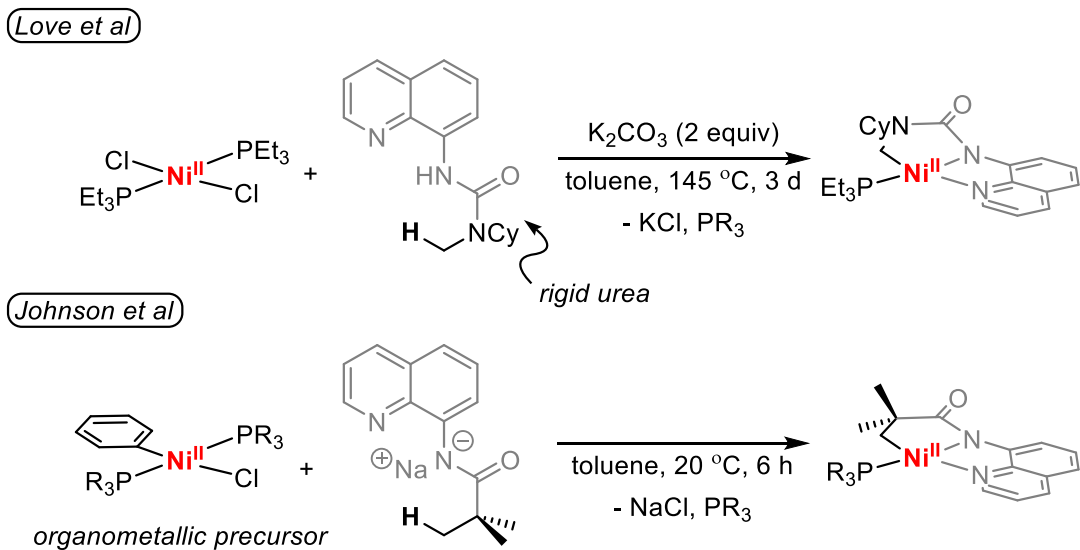
2.2.2 Decarbonylation Routes to Nickelacycles

Since the discovery of the Mond process, the fast and reversible binding of carbon monoxide (CO) with nickel has been widely explored.[23] Numerous studies have elucidated that the kinetics and thermodynamics of reversible CO binding and migratory insertion can be tuned by the ancillary ligands, especially phosphines. Ultimately, the reversible insertion and de-insertion reaction between CO and nickel–carbon bonds have been widely exploited, ranging from the synthesis of organometallic complexes to decarbonylative reactions in organic synthesis. [24–26]

In 2014, Maleckis and Sanford reported the isolation of perfluoroalkyl-ligated Ni^{II} complexes via a decarbonylation reaction. This reaction leveraged the strong electrophilic reactivity of carboxylic acid anhydrides with the nucleophilicity of Ni^{0} precursors, tuned by the phosphine ligands.[24] Subsequently, both catalytic and stoichiometric decarbonylation reactions at Ni have been developed with the appropriate use of organic nucleophiles. These reactions are primarily limited by the electrophilicity of the acyl precursor. Thus, reports with weaker electrophiles such as amides are rare.[27]

Scheme 2.6 Decarbonylation of Phthalimides by Johnson
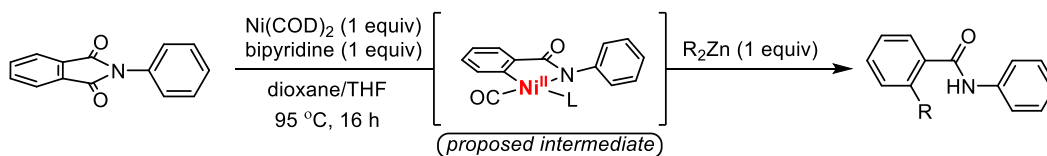
In 2011, Johnson reported a Ni^0-mediated decarbonylative reaction of *N*-arylphthalimides to form *o*-arylated *N*-aryl benzamides (Scheme 2.6).[28] This reaction was proposed to proceed through a σ-aryl nickelacycle. Owing to their structural similarity with the target aminoquinoline nickelacycle, we proposed a similar decarbonylative approach to access **2-L**. A retrosynthetic analysis of this approach implicates 8-imidoquinoline **1′** as the organic electrophile/ligand precursor in combination with an appropriate Ni^0 source (Scheme 1.7).

Scheme 2.7 Retrosynthetic Disconnection via Decarbonylation Route
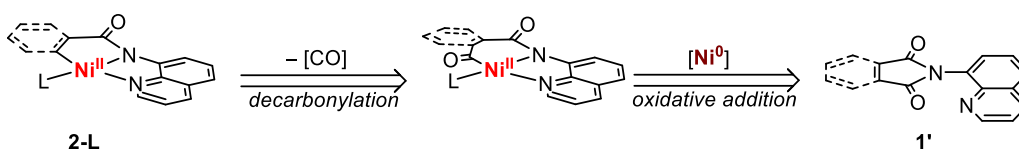
Preliminary reaction screening involved the use of $Ni(COD)_2$ as the Ni^0 precursor and 2-4 equiv of various monodentate phosphines as ligands. In some cases, the formation of new species was noted by NMR spectroscopy but attempts at isolation failed due to low conversion. We hypothesized that more nucleophilic nickel sources were needed to facilitate the oxidative addition reaction, as imides are weak electrophiles. Ultimately, a general route was developed using highly nucleophilic $Ni(PEt_3)_4$ as the Ni^0 source and conducting the reactions at 100 ºC for 16 h. This afforded the triethylphosphine (PEt_3) ligated $C(sp^2)$ (**2b-PEt₃**) and $C(sp^3)$ (**2a-PEt₃**) nickelacycles both in 87% yield (Scheme 2.8). The diamagnetic Ni^{II} products were characterized by ^1H, ^{13}C, and ^{31}P NMR spectroscopy. In addition, **2a-PEt₃** was characterized by X-ray crystallography as discussed below.

Scheme 2.8 Synthesis of PEt$_3$-ligated σ-alkyl and σ-aryl Ni^{II} Complex
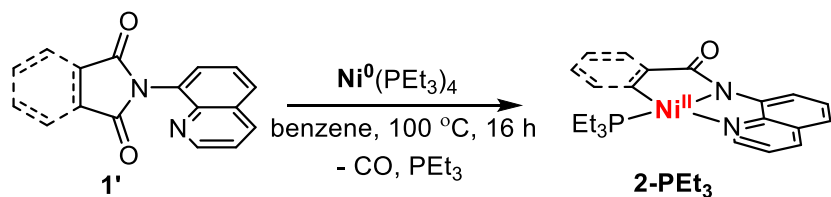
Table 2.1 compares the X-ray crystal structure of **2a-PEt$_3$** to related nickelacycles reported by Love and Johnson. Minor deviation in bond length (± 0.02 Å) is observed amongst the nitrogen atoms bound to the Ni^{II} center. The Ni^{II}–C bond of **2a-PEt$_3$** is slightly (0.03 Å) longer compared to those in the other reports. All the complexes are distorted square planar in geometry, but comparison of the τ_4 and τ'_4 structural parameters indicates that **2a-PEt$_3$** is slightly more distorted and closer to the seesaw geometry.

Figure 2.3 Comparison of Solid-state Structures of Phosphine-ligated σ-alkyl Ni^{II} complexes on the Aminoquinoline Pincer Scaffold
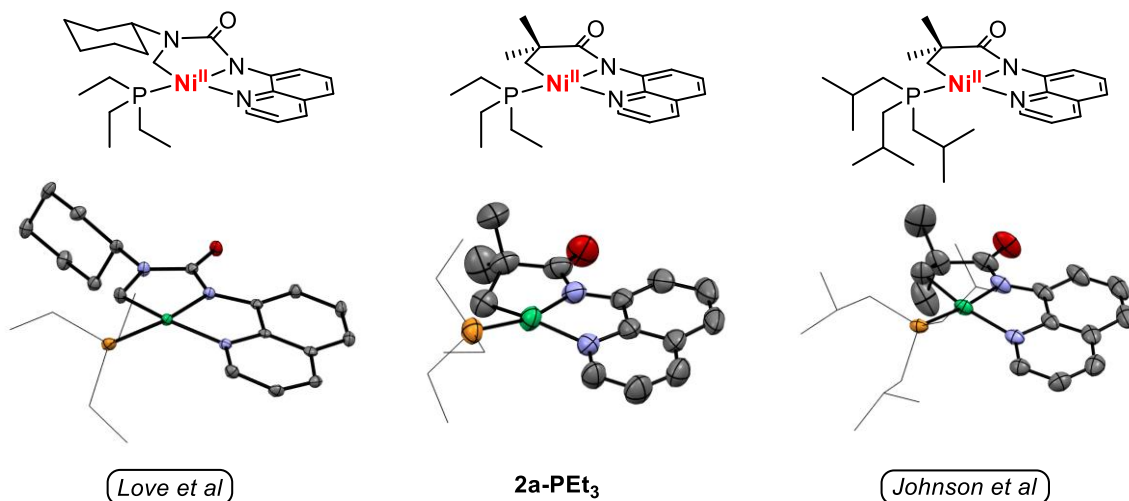
Table 2.1 Comparison of Bond Lengths and Structural Parameters of Phosphine Ligated
σ-alkyl Ni^{II} complexes on the Aminoquinoline Pincer Scaffold

entry	Love et al	2a-PEt$_3$	Johnson et al
Ni-P (Å)	**2.197(5)**	**2.170**	**2.175**
Ni-N$_q$ (Å)	**1.968(5)**	**1.976**	**1.977**
Ni-N$_a$ (Å)	**1.860**	**1.879**	**1.877**
Ni-C (Å)	**1.925(5)**	**1.957**	**1.934**
τ_4	**0.163**	**0.249**	**0.142**
τ'_4	**0.142**	**0.231**	**0.123**

2.2.3 Oxidative Reactivity Studies of σ-alkyl Nickelacycles

Our primary reason for synthesizing aminoquinoline nickelacycles was to attempt to access

high-valent Ni^{III} and Ni^{IV} analogues. To probe the feasibility of oxidation chemistry, the

electrochemical oxidation of complex **2a-PEt$_3$** was interrogated via cyclic voltammetry (CV). The

CV in MeCN/NBu$_4$PF$_6$ shows a quasi-reversible one electron redox event at approximately -0.15

V versus Ag/Ag$^+$, which was assigned as the Ni$^{II/III}$ couple. Scan rate dependent CV experiments

showed a minor shift during the oxidative scan. However, a shift of the reduction of peak current

was noted with decreasing scan rates during the reductive scan (Figure 2.3).

Figure 2.4 Scan Rate Dependent CV of **2a-PEt$_3$**
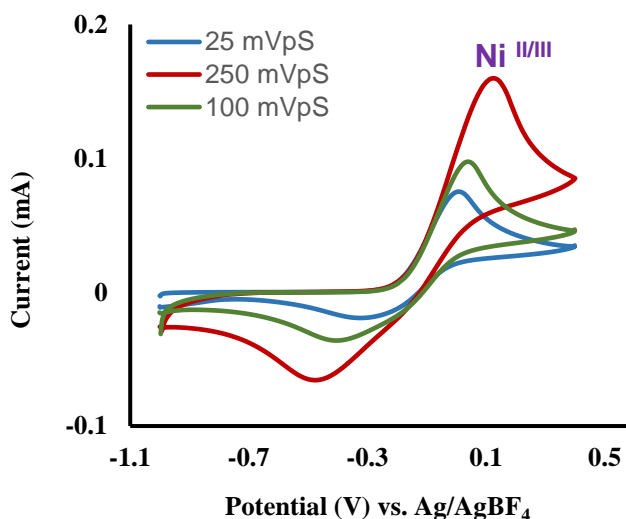
The observed redox potential suggests that Ag^I or ferrocenium salts should promote the single electron oxidation of **2a-PEt₃**. Treatment of the Ni^{II} complex **2a-PEt₃** with 1 equiv of $AgBF_4$ or 1 equiv of ferrocenium tetrafluoroborate ($FcBF_4$) in MeCN-d_3 at room temperature led to the formation of a new diamagnetic species, which confirmed to be the product of $C(sp^3)$–P coupling between the σ-alkyl group of the ligand and the PEt_3 (**5a-P**). The ferrocenium reaction was monitored by ^1H NMR spectroscopy over time, which showed the growth of the product up to a maximum yield of 70% after 6 h at 25 °C. The organic product **5a-P** was characterized based on a singlet at 38.42 ppm in the $^{31}P\{^1H\}$ NMR and a diagnostic doublet at 2.55 ppm ($J = 13.0$ Hz) in the ^1H NMR spectrum.

An EPR spectrum of this reaction was recorded after ~2 min, and it showed the presence of a Ni^{III} species, as characterized by a rhombic EPR signal that is consistent with a (S = ½) Ni^{III} species. Thus, we propose that the $C(sp^3)$–P coupling likely occurs from a transient Ni^{III} species of proposed structure **3a-PEt₃**. Although $C(sp^3)$–P coupling from Ni^{III} has not been reported in the literature, other C–heteroatom bond-forming reductive elimination reactions have been observed at Ni^{III} centers.[7,29–32]

Figure 2.5 $C(sp^3)$–P coupling with $AgBF_4$ and $FcBF_4$ via putative Ni^{III} intermediate at 25 °C
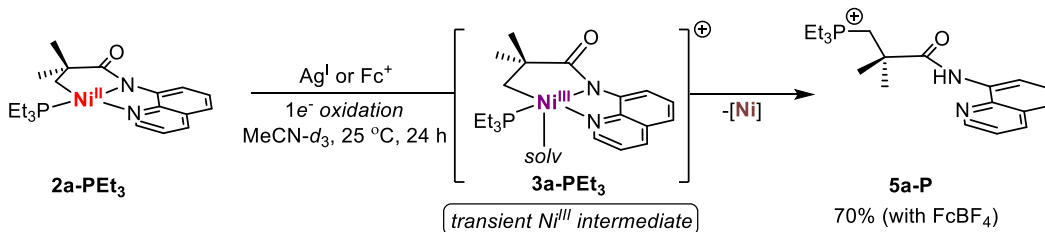
In 1994 Hillhouse reported that the oxidation of alkyl-amido Ni^{II} bipyridine complexes with ferrocenium, I_2, and O_2 leads to $C(sp^3)$–N bond formation.[30] They proposed a similar mechanism to that suggested in Figure 2.4: initial Ni-based single electron oxidation followed by C–N reductive elimination from the Ni^{III} center.

Figure 2.6 Oxidative C(sp^3)–N coupling from Ni^{II} by Hillhouse

proposed intermediate
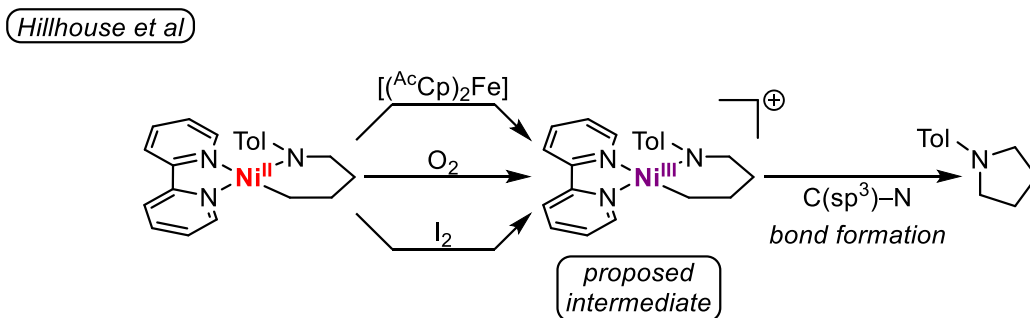
Based on this precedent, we next explored I$_2$ and O$_2$ as oxidants in order to compare their reactivity to that of FcBF$_4$. When complex **2a-PEt$_3$** was exposed to air in DMF-d_7 at 25 ℃, C(sp^3)–P coupling to form **5a-P** was observed in 16% yield after 2 h. However, the yield of **5a-P** did not increase further with time, and no other diamagnetic species were observed by ^{1}H or ^{31}P NMR spectroscopy. As such, the rest of the mass balance of this reaction is ascribed to the formation of unidentified paramagnetic Ni species.

In contrast, the reaction of **2a-PEt$_3$** with 1.1 equiv of I$_2$ under similar conditions (MeCN-d_3, 25 ℃, 24 h) resulted in exclusive formation of a C(sp^3)–I bond to generate **5a-I** in 68% yield as determined by diagnostic singlet peak at 3.62 ppm in the ^{1}H NMR spectrum. The identity of this organic product was confirmed by comparing an authentic sample of **5a-I** with the crude reaction mixture. No Ni^{III} intermediate was detected by EPR spectroscopy in an aliquot extracted from this reaction mixture after 5 min. This is in marked contrast to the reaction of **2a-PEt$_3$** with ferrocenium described above. As such, we hypothesize that this reaction may proceed by a different mechanism, possibly involving direct electrophilic cleavage of the Ni^{II}–C bond by I$_2$ without a change in oxidation state at Ni

Scheme 2.9 C(sp^3)–I coupling of **2a-PEt₃** with I₂

2a-PEt₃

I₂ (1.1 equiv)
MeCN-d_3, 25 °C, 24 h

5a-I
68%
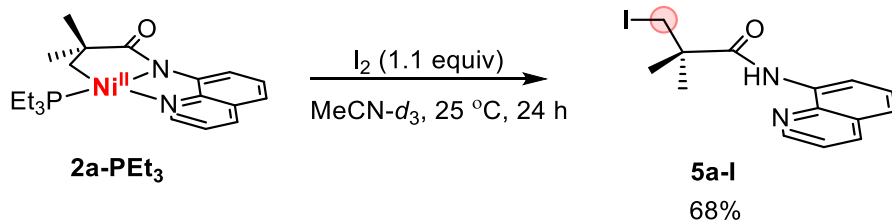
2.2.4 Methylation Studies of σ-alkyl Nickelacycles

Methyl electrophiles such as CH₃I are known to undergo oxidative addition at group 10 metal complexes in the +2 oxidation state. Thus, they have frequently been used for the isolation of high-valent Pd^{IV}, Pt^{IV}, and Ni^{IV} complexes. For example, Klein leveraged this reactivity as a route to Ni^{IV} products by reacting 5 equiv of CH₃I with a Ni^{II} phosphine precursor (Figure 2.5).[33] Notably, the synthesis involves methylation followed by loss of one trimethylphosphine (PMe₃) as tetramethylphosphonium from the Ni^{II} starting material. Subsequent oxidation addition of CH₃I furnishes the isolable Ni^{IV} species. Notably, this complex undergoes slow C–C bond-forming reductive elimination between the methyl and acyl ligands, but no PMe₃ ligand-based decomposition products were reported.[34]

Figure 2.7 Literature Reports for High-Valent Ni–CH₃ Complexes

Klein, **1997**

CH₃I (excess)
- PMe₄I

- 1/2 Ni^{II}(PMe₃)₂I₂

Tilley, **2013**
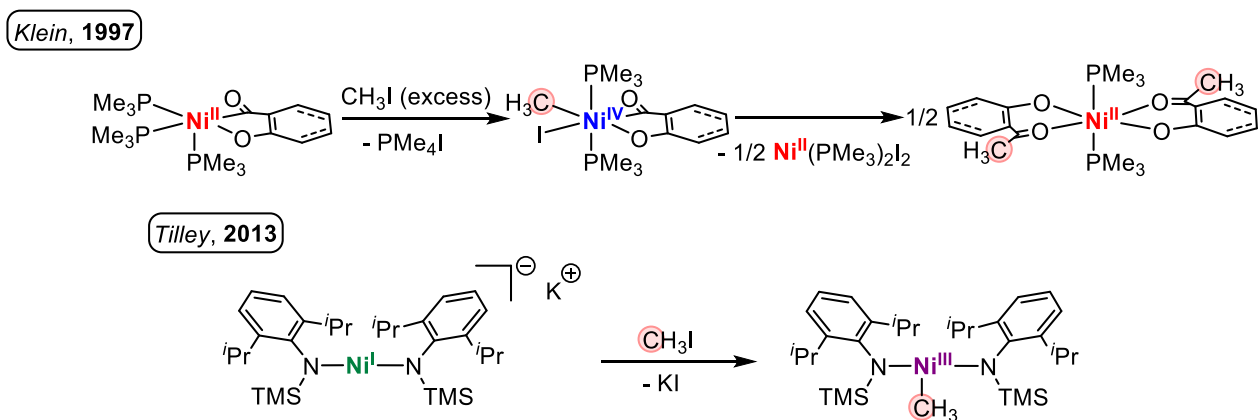
CH₃I
- KI

Recently, Tilley used a related analogous approach for the isolation of a Ni^{III}–CH_3 species, by reacting CH_3I with an anionic Ni^I precursor.[35] The Ni^{III} complex rapidly decomposed at ambient temperature over 24 h with exclusive ethane formation. Although a mechanism for ethane formation was not proposed, a bimetallic mechanism is likely, by analogy to work the work of Diao.[36] Interestingly, no ligand-based decomposition product (i.e., N–CH_3 bond formation) was observed, despite the fact that amido ligands are strong nucleophiles.

Scheme 2.10 Reaction of Equimolar Ratio of CH_3I with **2a-PEt₃** in MeCN-d_3 at 25 °C
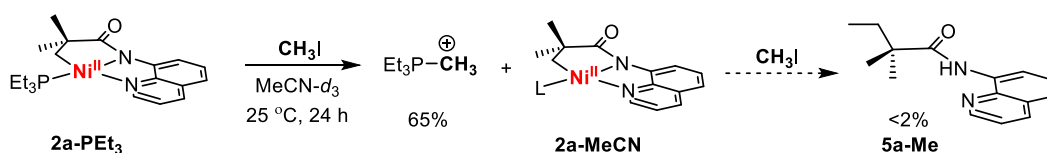
Based on these reports, we hypothesized that the reaction of the σ-alkyl Ni^{II} complex **2a-PEt₃** with CH_3I might furnish a Ni^{IV} species, by analogy to the work of Klein. However, instead the reaction of **2a-PEt₃** with 1 equiv of CH_3I in MeCN-d_3 primarily formed the methylated phosphine, Et_3P–Me^+, over 24 h at 25 ºC. The time course of this reaction is shown in Figure 2.6. This phosphonium salt was characterized by ^1H NMR spectroscopy based on a diagnostic doublet at 1.7 ppm ($J = 13.6$ Hz) and by $^{31}P\{^1H\}$ NMR spectroscopy based on a singlet at 37.67 ppm. Its identity was confirmed by comparing to an independently isolated sample of this product. The phosphonium salt was formed in 65% yield after 25 h at 25 ºC along with the acetonitrile bound Ni^{II} complex **2a-MeCN**. Traces (<2%) of the methylated σ-alkyl ligand **5a-Me** were also detected. This latter product is readily identified based on a characteristic triplet at 0.9 ppm ($J = 7.5$ Hz) in the ^1H NMR spectrum, and its identity was confirmed by comparing to an independently isolated sample of this product.

Figure 2.8 Time Evolution for the Formation of Et$_3$P–CH$_3$ with CH$_3$I and **2a-PEt$_3$** at 25 °C
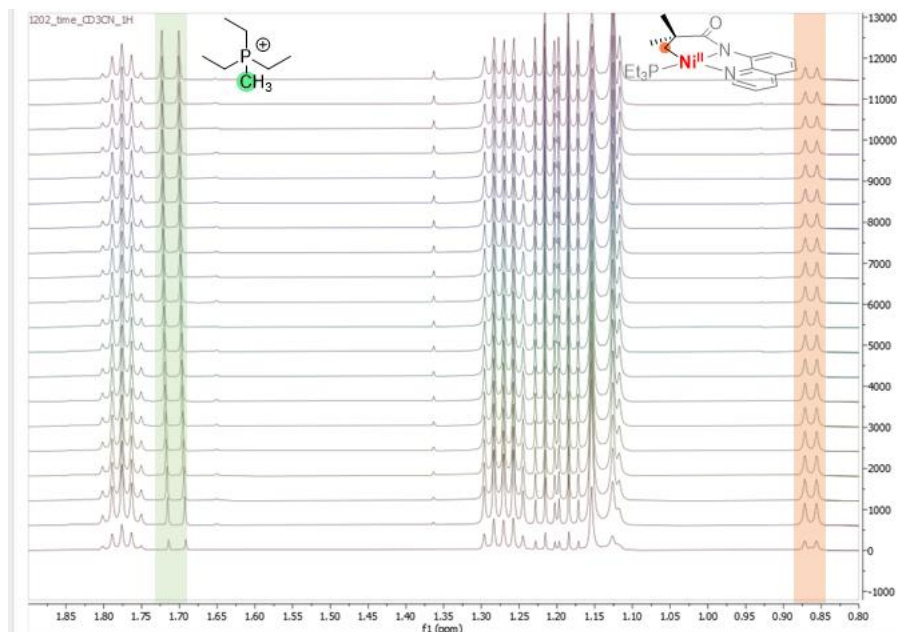
To drive the reaction to completion, it was heated to 90 °C for 24 h. This resulted in an increased yield of 95% for the phosphonium salt, Et$_3$P–CH$_3$$^+$. There was also a small increase in the yield of **5a-Me** to 6% at this higher temperature.

Scheme 2.11 Reaction of Equimolar Ratio of CH$_3$I with **2a-PEt$_3$** in MeCN-d_3 at 90 °C

We next sought to probe the reactivity of **2a-MeCN** with CH$_3$I. Thus, the reaction was repeated with an excess (3 equiv) of CH$_3$I at 90 °C for 24 h. This only led to a small increase in the yield of **5a-Me** (to 10%). This result implies that the acetonitrile bound complex **2a-MeCN** is drastically less reactive with CH$_3$I compared to **2a-PEt$_3$**, at least under these conditions. All attempts to isolate **2a-MeCN** failed, likely due to the lability of the acetonitrile ligand. However, the Et$_3$P–CH$_3$$^+$ product was isolated from this reaction mixture and confirmed by comparison with separately synthesized authentic product.
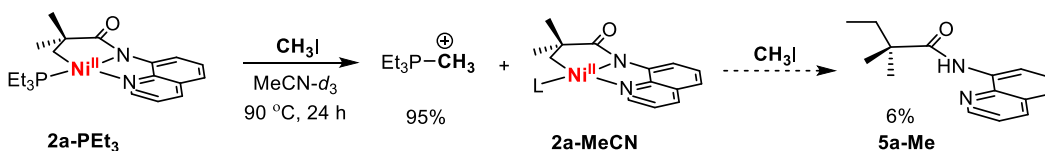
27

Scheme 2.12 Proposed Mechanism of PEt$_3$ Dissociation and Capture with CH$_3$I
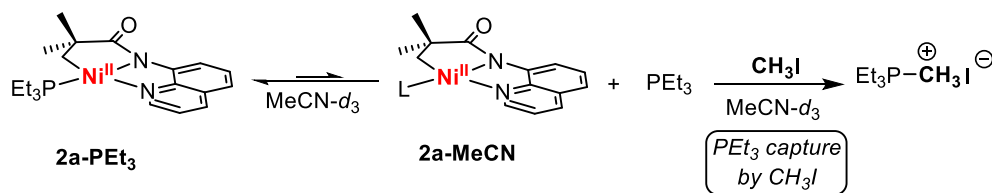
As discussed above, Klein successfully isolated a PMe$_3$-ligated Ni^{IV} species using CH$_3$I as the oxidant and did not observe the formation of Me$_3$P–CH$_3$$^+$. Based on this, we believe that formation of Et$_3$P–CH$_3$$^+$ from **2a-PEt$_3$** is not likely to occur via a high valent Ni-intermediate nor via electrophilic cleavage of Ni–PEt$_3$ bond by CH$_3$I. Instead, the most likely mechanism involves PEt$_3$ ligand dissociation followed by an S$_N$2 reaction between free PEt$_3$ and CH$_3$I. Although no free PEt$_3$ ligand was observed via ^{1}H or ^{31}P NMR spectroscopy we have seen fast ligand exchange in related systems, suggesting that free phosphine is accessible under these conditions. Future studies should focus on changing solvent polarity and nucleophilicity to test the viability of this proposed mechanism.

2.3 Conclusions

Although C–H activation routes were largely unsuccessful, a decarbonylative strategy led to the isolation of both the C(sp^3) and C(sp^2) Ni^{II} complexes on the aminoquinoline pincer. Electrochemical experiments implicated Ag^I and ferrocenium salts as viable oxidants for the formation of a Ni^{III} complex. Although a transient Ni^{III} species was detected by EPR spectroscopy with both of these oxidants, this putative intermediate underwent facile C(sp^3)–P bond-forming reductive elimination. Similar reactivity was also observed using O$_2$ as the oxidant. In contrast, with iodine, C(sp^3)–I coupling was observed, and no Ni^{III} signals were detected by EPR spectroscopy. Overall, these observations stand in contrast to Hillhouse's report showing that I$_2$, O$_2$, and FcBF$_4$ all afford the same product when used to oxidize related Ni^{II} metallacycles. Instead,

the PEt$_3$-ligated aminoquinoline pincer complexes show divergent reactivity with alkyl ligand-based electrophilic reactivity with I$_2$ versus likely metal-centered oxidation and subsequent P–C coupling with ferrocenium or O$_2$.

Reactions of **2a-PEt$_3$** with CH$_3$I as the oxidant showed exclusive formation of Et$_3$P–Me$^+$ as the product, demonstrating a third reactivity mode for this system. This reaction could proceed via (*i*) an electrophilic Ni–P bond cleavage, (*ii*) a transient (undetectable) high-valent species, or (*iii*) rapid methylation of dissociated PEt$_3$ ligand. We believe that the final mechanism is most likely, owing to observed immediate methylation of PEt$_3$ on treatment with stoichiometric amount of CH$_3$I in MeCN-d_3 at 25 °C, in quantitative yield. Further, experiments will need to be performed to test this mechanistic proposal by varying the polarity of the solvent, which is likely to impact the PEt$_3$ dissociation step.

Although rapid methylation of the PEt$_3$ ligated complex was observed at 25 °C, negligible methylation of the tentatively assigned acetonitrile bound Ni^{II} species generated under these conditions (**2a-MeCN**) was observed. All attempts to isolate **2a-MeCN** were unsuccessful, but this strikingly sluggish reactivity prompted us to consider other nitrogen-based supporting ligands for stabilizing the nickelacycle. In Chapter 3 we move from PEt$_3$ to picoline-ligated Ni^{II} complexes in order to focus on reactivity of the σ-alkyl ligand rather than the PEt$_3$.

2.4 References

(1)   Khake, S. M.; Chatani, N. Chelation-Assisted Nickel-Catalyzed C-H Functionalizations. *Trends in Chemistry* **2019**, *1* (5), 524–539. https://doi.org/10.1016/j.trechm.2019.06.002.

(2)   Gandeepan, P.; Müller, T.; Zell, D.; Cera, G.; Warratz, S.; Ackermann, L. 3d Transition Metals for C–H Activation. *Chemical Reviews* **2018**, *119* (4), 2192–2452. https://doi.org/10.1021/acs.chemrev.8b00507.

(3)   Camasso, N. M.; Sanford, M. S. Design, Synthesis, and Carbon-Heteroatom Coupling Reactions of Organometallic Nickel(IV) Complexes. *Science* **2015**, *347* (6227), 1218–1220. https://doi.org/10.1126/SCIENCE.AAA4526.

(4)   Y Aihara, N. C. Nickel-Catalyzed Direct Alkylation of C–H Bonds in Benzamides and Acrylamides with Functionalized Alkyl Halides via Bidentate-Chelation Assistance. *J. Am. Chem. Soc.* **2013**, *135* (14), 5308–5311. https://doi.org/10.1021/ja401344e.

(5)   Aihara, Y.; Chatani, N. Nickel-Catalyzed Direct Arylation of C(Sp3)–H Bonds in Aliphatic Amides via Bidentate-Chelation Assistance. *Journal of the American Chemical Society* **2014**, *136* (3), 898–901. https://doi.org/10.1021/ja411715v.

(6)   Omer, H. M.; Liu, P. Computational Study of Ni-Catalyzed C–H Functionalization: Factors That Control the Competition of Oxidative Addition and Radical Pathways. *Journal of the American Chemical Society* **2017**, *139* (29), 9909–9920. https://doi.org/10.1021/jacs.7b03548.

(7)   Heberer, N.; Hu, C.-H.; Mirica, L. M. 6.09 - High-Valent Ni Coordination Compounds. In *Comprehensive Coordination Chemistry III*; Constable, E. C., Parkin, G., Que Jr, L., Eds.; Elsevier: Oxford, 2021; pp 348–374. https://doi.org/https://doi.org/10.1016/B978-0-08-102688-5.00104-5.

(8)   Roy, P.; R. Bour, J.; W. Kampf, J.; S. Sanford, M. Catalytically Relevant Intermediates in the Ni-Catalyzed C(Sp2)–H and C(Sp3)–H Functionalization of Aminoquinoline Substrates. *Journal of the American Chemical Society* **2019**, *141* (43), 17382–17387. https://doi.org/10.1021/jacs.9b09109.

(9)   Aihara, Y.; Chatani, N. Nickel-Catalyzed Reaction of C–H Bonds in Amides with I2: Ortho-Iodination via the Cleavage of C(Sp2)–H Bonds and Oxidative Cyclization to β-Lactams via the Cleavage of C(Sp3)–H Bonds. *ACS Catalysis* **2016**, *6* (7), 4323–4329. https://doi.org/10.1021/acscatal.6b00964.

(10)   Yokota, A.; Aihara, Y.; Chatani, N. Nickel(II)-Catalyzed Direct Arylation of C–H Bonds in Aromatic Amides Containing an 8-Aminoquinoline Moiety as a Directing Group. *The Journal of Organic Chemistry* **2014**, *79* (24), 11922–11932. https://doi.org/10.1021/jo501697n.

(11)   Iyanaga, M.; Aihara, Y.; Chatani, N. Direct Arylation of C(Sp3)–H Bonds in Aliphatic Amides with Diaryliodonium Salts in the Presence of a Nickel Catalyst. *The Journal of Organic Chemistry* **2014**, *79* (24), 11933–11939. https://doi.org/10.1021/jo501691f.

(12)   Labinger, J. A.; Bercaw, J. E. Understanding and Exploiting C–H Bond Activation. *Nature 2002 417:6888* **2002**, *417* (6888), 507–514. https://doi.org/10.1038/417507a.

(13)   H. Crabtree, R. Introduction to Selective Functionalization of C−H Bonds. *Chemical Reviews* **2010**, *110* (2), 575–575. https://doi.org/10.1021/cr900388d.

(14)   Crabtree, R. H.; Lei, A. Introduction: CH Activation. *Chemical Reviews* **2017**, *117* (13), 8481–8482. https://doi.org/10.1021/acs.chemrev.7b00307.

(15) Zhang, S.-Y.; Li, Q.; He, G.; Nack, W. A.; Chen, G. Pd-Catalyzed Monoselective *Ortho* - C–H Alkylation of *N* -Quinolyl Benzamides: Evidence for Stereoretentive Coupling of Secondary Alkyl Iodides. *Journal of the American Chemical Society* **2015**, *137* (1), 531– 539. https://doi.org/10.1021/ja511557h.

(16) Deb, A.; Hazra, A.; Peng, Q.; Paton, R. S.; Maiti, D. Detailed Mechanistic Studies on Palladium-Catalyzed Selective C–H Olefination with Aliphatic Alkenes: A Significant Influence of Proton Shuttling. *Journal of the American Chemical Society* **2017**, *139* (2), 763–775. https://doi.org/10.1021/jacs.6b10309.

(17) Shabashov, D.; Daugulis, O. Auxiliary-Assisted Palladium-Catalyzed Arylation and Alkylation of sp^2 and sp^3 Carbon−Hydrogen Bonds. *Journal of the American Chemical Society* **2010**, *132* (11), 3965–3972. https://doi.org/10.1021/ja910900p.

(18) T. Nadres, E.; Ivan Franco Santos, G.; Shabashov, D.; Daugulis, O. Scope and Limitations of Auxiliary-Assisted, Palladium-Catalyzed Arylation and Alkylation of Sp2 and Sp3 C– H Bonds. *The Journal of Organic Chemistry* **2013**, *78* (19), 9689–9714. https://doi.org/10.1021/jo4013628.

(19) Haines, B. E.; Yu, J. Q.; Musaev, D. G. The Mechanism of Directed Ni(II)-Catalyzed C– H Iodination with Molecular Iodine. *Chemical Science* **2018**, *9* (5), 1144–1154. https://doi.org/10.1039/C7SC04604A.

(20) Ackermann, L. Carboxylate-Assisted Transition-Metal-Catalyzed C-H Bond Functionalizations: Mechanism and Scope. *Chemical Reviews* **2011**, *111* (3), 1315–1345. https://doi.org/10.1021/CR100412J.

(21) Dawson Beattie, D.; C. Grunwald, A.; Perse, T.; L. Schafer, L.; A. Love, J. Understanding Ni(II)-Mediated C(Sp3)–H Activation: Tertiary Ureas as Model Substrates. *Journal of the American Chemical Society* **2018**, *140* (39), 12602–12610. https://doi.org/10.1021/jacs.8b07708.

(22) Liu, J.; A. Johnson, S. Mechanism of 8-Aminoquinoline-Directed Ni-Catalyzed C(Sp3)–H Functionalization: Paramagnetic Ni(II) Species and the Deleterious Effect of Carbonate as a Base. *Organometallics* **2021**, *40* (17), 2970–2982. https://doi.org/10.1021/acs.organomet.1c00265.

(23) Mond, L.; Langer, C.; Quincke, F. L.—Action of Carbon Monoxide on Nickel. *Journal of the Chemical Society, Transactions* **1890**, *57* (0), 749–753. https://doi.org/10.1039/CT8905700749.

(24) Maleckis, A.; S. Sanford, M. Synthesis of Fluoroalkyl Palladium and Nickel Complexes via Decarbonylation of Acylmetal Species. *Organometallics* **2014**, *33* (14), 3831–3839. https://doi.org/10.1021/om500535x.

(25) Malapit, C. A.; Bour, J. R.; Brigham, C. E.; Sanford, M. S. Base-Free Nickel-Catalysed Decarbonylative Suzuki–Miyaura Coupling of Acid Fluorides. *Nature* **2018**, *563* (7729), 100–104. https://doi.org/10.1038/s41586-018-0628-7.

(26) Malapit, C. A.; R. Bour, J.; R. Laursen, S.; S. Sanford, M. Mechanism and Scope of Nickel-Catalyzed Decarbonylative Borylation of Carboxylic Acid Fluorides. *Journal of the American Chemical Society* **2019**, *141* (43), 17322–17330. https://doi.org/10.1021/jacs.9b08961.

(27) Shiba, T.; Kurahashi, T.; Matsubara, S. Nickel-Catalyzed Decarbonylative Alkylidenation of Phthalimides with Trimethylsilyl-Substituted Alkynes. *Journal of the American Chemical Society* **2013**, *135* (37), 13636–13639. https://doi.org/10.1021/ja4068172.

(28)   Havlik, S. E.; Simmons, J. M.; Winton, V. J.; Johnson, J. B. Nickel-Mediated Decarbonylative Cross-Coupling of Phthalimides with in Situ Generated Diorganozinc Reagents. *The Journal of Organic Chemistry* **2011**, *76* (9), 3588–3593. https://doi.org/10.1021/jo200347j.

(29)   Zheng, B.; Tang, F.; Luo, J.; W. Schultz, J.; P. Rath, N.; M. Mirica, L. Organometallic Nickel(III) Complexes Relevant to Cross-Coupling and Carbon–Heteroatom Bond Formation Reactions. *Journal of the American Chemical Society* **2014**, *136* (17), 6499–6504. https://doi.org/10.1021/ja5024749.

(30)   Koo, K.; Hillhouse, G. L. Carbon-Nitrogen Bond Formation by Reductive Elimination from Nickel(II) Amido Alkyl Complexes. *Organometallics* **1995**, *14* (9), 4421–4423. https://doi.org/10.1021/om00009a054.

(31)   Iluc, V. M.; Hillhouse, G. L. Three-Coordinate Nickel Carbene Complexes and Their One-Electron Oxidation Products. *Journal of the American Chemical Society* **2014**, *136* (17), 6479–6488. https://doi.org/10.1021/ja501900j.

(32)   M. Iluc, V.; J. M. Miller, A.; S. Anderson, J.; J. Monreal, M.; P. Mehn, M.; L. Hillhouse, G. Synthesis and Characterization of Three-Coordinate Ni(III)-Imide Complexes. *Journal of the American Chemical Society* **2011**, *133* (33), 13055–13063. https://doi.org/10.1021/ja2024993.

(33)   Klein, H.-F.; Bickelhaupt, A.; Jung, T.; Cordier, G. Syntheses and Properties of the First Octahedral Diorganonickel(IV) Compounds. *Organometallics* **1994**, *13* (7), 2557–2559. https://doi.org/10.1021/om00019a007.

(34)   Klein, H.-F.; Bickelhaupt, A.; Lemke, M.; Sun, H.; Brand, A.; Jung, T.; Röhr, C.; Flörke, U.; Haupt, H.-J. Trimethylphosphine Complexes of Diorganonickel(IV) Moieties. *Organometallics* **1997**, *16* (4), 668–676. https://doi.org/10.1021/om960436g.

(35)   I. Lipschutz, M.; Yang, X.; Chatterjee, R.; Don Tilley, T. A Structurally Rigid Bis(Amido) Ligand Framework in Low-Coordinate Ni(I), Ni(II), and Ni(III) Analogues Provides Access to a Ni(III) Methyl Complex via Oxidative Addition. *Journal of the American Chemical Society* **2013**, *135* (41), 15298–15301. https://doi.org/10.1021/ja408151h.

(36)   Diccianni, J.; Lin, Q.; Diao, T. Mechanisms of Nickel-Catalyzed Coupling Reactions and Applications in Alkene Functionalization. *Accounts of Chemical Research* **2020**, *53* (4), 906–919. https://doi.org/10.1021/acs.accounts.0c00032.

2.5 Experimental Procedures

2.5.1 General Procedures, Materials and Methods

General Procedures

NMR spectra were recorded on a Varian VNMRS 600 (600 MHz for ^{1}H and 151 MHz for ^{13}C). ^{1}H and ^{13}C NMR chemical shifts are reported in parts per million (ppm) and are referenced to the solvent lock. ^{1}H NMR quantification was conducted using internal standards as mentioned in the experimental procedures. Abbreviations used to report NMR peaks: singlet (s); doublet (d); triplet (t); quartet (q); doublet of doublets (dd); triplet of doublets (td); doublet of triplets (dt); multiplet (m). GC-FID data were collected on a Shimadzu 17A GC using a Restek Rtx®-5 (crossbond 5% diphenyl–95% dimethyl polysiloxane; 15 m, 0.25 mm ID, 0.25 µm df) column. High-resolution mass spectra were recorded on a Micromass AutoSpec Ultima Magnetic Sector mass spectrometer. Cyclic voltammetry was performed using a CHI600C potentiostat from CH Instruments. EPR spectra were collected at temperatures mentioned in the experimental procedures using a Bruker EMX ESR Spectrometer with a nitrogen-cooled cryostat. Elemental analyses were performed by Midwest Microlab located in Indianapolis. X-ray crystallographic data were obtained on a Rigaku AFC10K Saturn 944+ CCD-based X-ray diffractometer. Chromatographic separations were carried out on a Biotage Isolera One system using Sfär Silica HC D (High-capacity Duo 20 µm) columns (10 g, 25 g, or 50 g cartridges depending on the scale of isolations), as mentioned in the synthetic procedures.

Acronyms: Dichloromethane (DCM), Tetrahydrofuran (THF), Water in NMR solvent (HDO), Tetramethylsilane (TMS), Nitromethane (CH_3NO_2), residual moisture in solvent (HDO).

Note: All ^{1}H NMR spectra of nickel complexes and their reactivity studies with iodine (I_2) were recorded on a 600 MHz Varian Vnmrs instrument with a 100% lock efficiency and a relaxation

delay of 25 s at 25 °C. These specifications are crucial for proper quantification and analysis uncommonly high T1 relaxation times have been noted for these nickel complexes.

Materials and Methods

All commercial reagents were used as received without further purification unless otherwise noted. [Ni(PEt$_3$)$_4$] was prepared via literature procedures.1 Bis(1,5-cyclooctadiene)nickel(0) ([Ni(COD)$_2$]) was purchased from Strem Chemical, 2,2-dimethylsuccinic anhydride and 8-aminoquinoline from Ark Pharm. Tetramethylammonium acetate (NMe$_4$OAc) from TCI America. Nickel(II) acetate (Ni(OAc)$_2$), nickel(II) trifluoromethanesulfonate 96% (Ni(OTf)$_2$), silver(I) carbonate (Ag$_2$CO$_3$), triethylphosphine (PEt$_3$), triethylamine (Et$_3$N) and acetonitrile (electronic grade) were purchased from Millipore-Sigma or Aldrich. All deuterated solvents were obtained from Cambridge Isotope Laboratories and deaerated via a nitrogen sparge prior to storage over activated 4 Å molecular sieves (EMD Millipore). Anhydrous N,N-dimethylformamide and acetone were purchased from Acros Organics in AcroSeal® bottles. Anhydrous benzene was purchased from Alfa Aesar and ethanol from VMR international. Pentane (Fisher), diethyl ether (Millipore-Sigma), tetrahydrofuran (Fisher), and toluene (Fisher) were deaerated via a nitrogen sparge and further purified using a solvent purification system for usage inside the glovebox. Sodium carbonate, potassium carbonate, sodium sulfate, hexanes, diethyl ether, ethyl acetate, dichloromethane, sulfuric acid (Certified ACS Plus) and glacial acetic acid were purchased from Fisher. Celite was purchased from Aqua Solutions and was dried under vacuum at 150 °C for 24 h for usage inside the glovebox. All glassware used in the glovebox was dried in an oven at 150 °C for at least 6 h and cooled under an inert atmosphere. All experiments and synthetic procedures were setup inside a nitrogen-filled glovebox unless otherwise mentioned.

34

2.5.2 Synthesis and Characterization of Organic Molecules

All synthesis in this subsection was performed outside the glovebox unless otherwise mentioned. All modified reaction procedures and confirmation of characterization data were referenced against previous literature reports as cited.
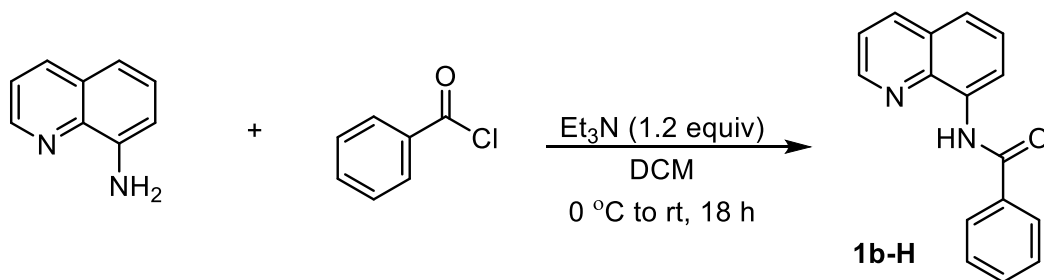
1b-H: Benzoyl chloride (0.65 mL, 6 mmol, 1.2 equiv) and then triethylamine (0.9 mL, 6 mmol, 1.2 equiv) were added dropwise to a solution of 8-aminoquinoline (0.72 g, 5 mmol, 1.0 equiv) dissolved in DCM (10 mL) cooled in an ice bath. The reaction was slowly warmed up to room temperature and then stirred overnight for 18 h. The reaction was quenched with water (30 mL) and extracted with DCM (3 x 20 mL). The organic extracts were combined, dried over anhydrous sodium sulfate, and concentrated under vacuum. The crude product was purified by chromatography using a Sfär Silica HC D (High-capacity Duo 20 µm) 50 g cartridge on a Biotage Isolera One system (hexanes : DCM, gradient from 80:20 to 10:90). This afforded compound **1b-H** as a white solid (1.10 g, 89% yield) or 1a-Cl as a white solid (1.32 g, 94% yield). The ^{1}H NMR spectra of the products matched those reported in the literature.[4,6]
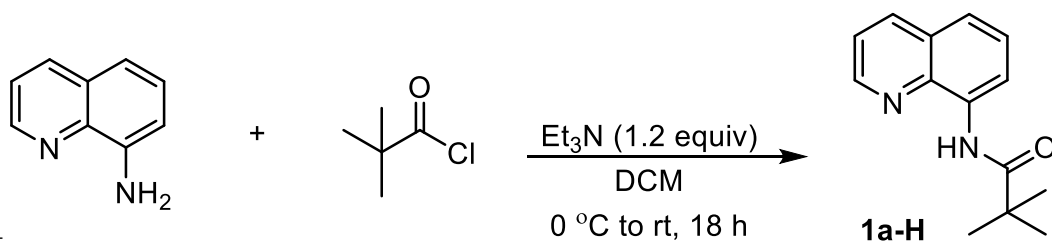
1a-H: Trimethylacetyl chloride (0.75 mL, 6 mmol, 1.2 equiv) and then triethylamine (0.9 mL, 6 mmol, 1.2 equiv) were added dropwise to a solution of 8-aminoquinoline (0.72 g, 5 mmol, 1.0 equiv) in DCM (10 mL) cooled in an ice bath. The reaction was stirred overnight for 18 h at room temperature. The reaction was quenched with water (30 mL) and extracted with DCM (3 x 20 mL). The organic extracts were combined, dried over anhydrous sodium sulfate, and concentrated under vacuum. The crude product was purified by chromatography using a Sfär Silica HC D (High-capacity Duo 20 µm) 50 g cartridge on a Biotage Isolera One system (hexanes : DCM, gradient from 80:20 to 10:90). This afforded compound **1a-H** as a pale-yellow oil (0.95 g, 83% yield) or 1a-Cl as a white solid (0.95 g, 73% yield). The ^{1}H NMR spectra of the products matched those reported in the literature.6,7
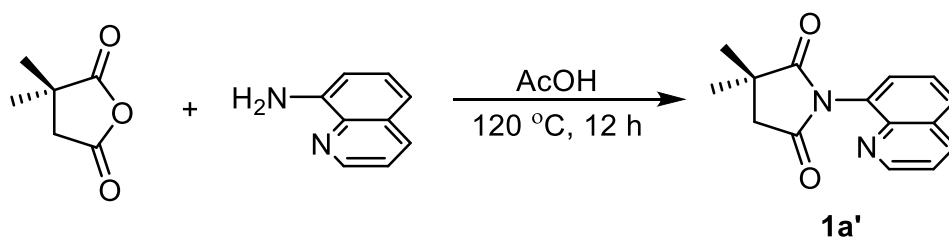
1a′:8-Aminoquinoline (1.44 g, 10 mmol, 1 equiv) and 2,2-dimethylsuccinic anhydride (1.54 g, 12 mmol, 1.2 equiv) were weighed into a 20 mL vial equipped with an oven-dried magnetic stir-bar. Glacial acetic acid (10 mL) was added to the vial, which was then sealed with a Teflon-lined screw cap. The reaction mixture was stirred and heated at 120 °C for 12 h. The reaction mixture slowly change color from yellow to brown. The reaction was then allowed to cool down to room temperature, diluted with DCM (30 mL), and neutralized with a saturated aqueous solution of sodium carbonate. The organic layer was collected, and the aqueous layer was washed with DCM (2 x 15 mL). The organic extracts were combined, dried over anhydrous sodium sulfate, and concentrated under vacuum to afford a yellow solid. The crude mixture was purified by chromatography using a Sfär Silica HC D (High-capacity Duo 20 µm) 50 g cartridge on a Biotage

Isolera One system (hexanes : ethyl acetate, gradient from 95:5 to 80:20). This afforded compound **1a′** as a grey solid (2.31 g, 91% yield). The ^{1}H NMR spectrum of the product matched that reported in the literature.[3]

1b'
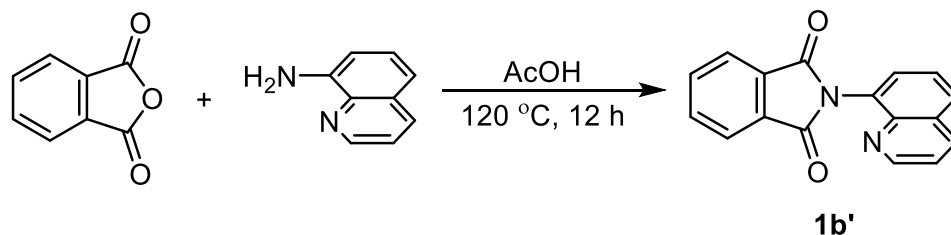
1b′: 8-Aminoquinoline (1.44 g, 10 mmol, 1 equiv) and phthalic anhydride (1.63 g, 11 mmol, 1.1 equiv) were weighed into a 20 mL vial equipped with an oven-dried magnetic stir-bar. Glacial acetic acid (10 mL) was added to the vial, which was then sealed with a Teflon-lined screw cap. The reaction mixture was heated at 120 °C for 12 h. The reaction mixture slowly changed color from pale yellow to dark yellow. The reaction was then allowed to cool to room temperature, diluted with DCM (30 mL), and neutralized with a saturated aqueous solution of sodium carbonate. The organic layer was collected, and the aqueous layer was washed with DCM (2 x 15 mL). The organic extracts were combined, dried over anhydrous sodium sulfate, and concentrated under vacuum to afford a yellow solid. The crude mixture was purified by chromatography using a Sfär Silica HC D (High-capacity Duo 20 µm) 50 g cartridge on a Biotage Isolera One system (hexanes : ethyl acetate, gradient from 95:5 to 80:20). This afforded compound **1b′** as a white solid (2.33 g, 85% yield). The ^{1}H NMR spectrum of the product matched that reported in the literature.[2]
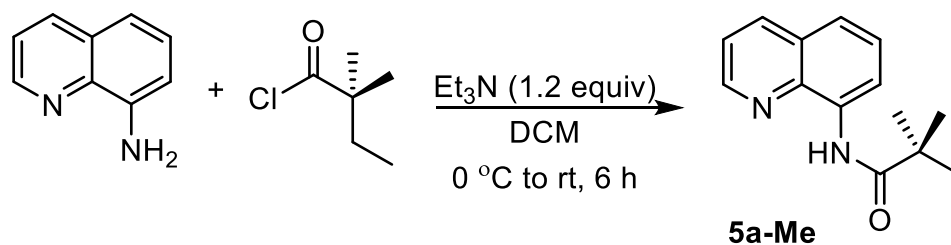

5a-Me

5a-Me: 2,2-dimethylbutanoyl chloride (0.83 mL, 6 mmol, 1.2 equiv) and then triethylamine (0.9 mL, 6 mmol, 1.2 equiv) were added dropwise to a solution of 8-aminoquinoline (0.72 g, 5 mmol, 1.0 equiv) in DCM (10 mL) cooled in an ice bath. The reaction was stirred overnight for 18 h at room temperature. The reaction was quenched with water (30 mL) and extracted with DCM (3 x 20 mL). The organic extracts were combined, dried over anhydrous sodium sulfate, and concentrated under vacuum. The crude product was purified by chromatography using a Sfär Silica HC D (High-capacity Duo 20 µm) 50 g cartridge on a Biotage Isolera One system (hexanes : DCM, gradient from 80:20 to 10:90). This afforded compound **5a-Me** as a pale-yellow oil (1.03 g, 85% yield). The ^{1}H NMR spectra of the products matched those reported in the literature.[6,7]
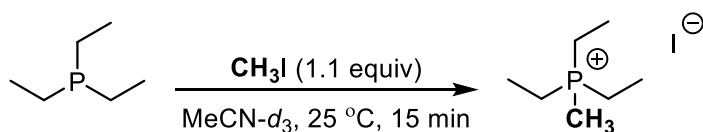
This synthesis was performed inside the glovebox as triethylphosphine is a volatile pyrophoric substance.

Triethylphosphine (5.9 mg, 5.0 mmol 1.0 equiv) was weighed out in a 4 mL vial and to it MeCN-d_3 (2.5 mL) was added. To the above mixture a 0.5 mL aliquot from a stock solution of MeCN-d_3 (1 mL) containing methyl iodide (17 mg, 12.0 mmol) was added. An aliquot (0.6 mL) from the above reaction mixture was transferred to an NMR tube and was characterized by ^{1}H and ^{31}P NMR spectroscopy. Some of the ^{1}H NMR peaks were noted to shift significantly with respect to concentration hence, proper caution was taken for characterization of product.

2.5.3 Attempted C–H Activation Routes to Isolate Nickelacycle
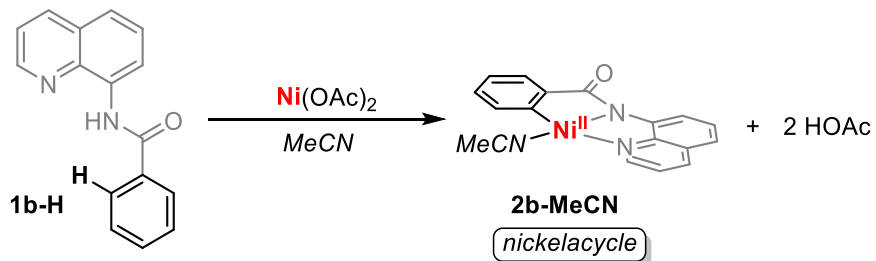
1b-H (9.9 mg, 0.04 mmol, 1 equiv), nickel(II) acetate (7.1 mg, 0.04 mmol, 1 equiv) were weighed into a 4 mL vial. MeCN-d_3 (0.6 mL) was added, and the resulting mixture was transferred to a J. Young NMR tube. (Note: the reaction mixture was not homogeneous). The reaction in the J. Young NMR tube was heated in an oil bath and monitored over time by 1H NMR up to 30 h at 110 ºC during which no significant color change was noted. Analysis by ^{1}H NMR spectroscopy only showed signals consistent starting material as shown below.

1b-H (9.9 mg, 0.04 mmol, 1 equiv), nickel(II) acetate (7.1 mg, 0.04 mmol, 1 equiv) or nickel(II) acetyl acetonate (10.3 mg, 0.04 mmol, 1 equiv) were weighed into a 4 mL vial. Solvent (0.6 mL) was added, and the resulting mixture was transferred to a Teflon-lined screw cap NMR tube. (Note: In general, the reaction mixtures were not homogeneous) The reaction in the NMR tubes were heated in an oil bath and monitored over time by ^{1}H NMR up to 30 h at 110 ºC during which no significant color change was noted for most. Analysis by ^{1}H NMR spectroscopy only showed signals consistent with starting material with occasional paramagnetic broadening in some case as shown below.

2b-L
yield: 12% (brsm)

1b-H (9.9 mg, 0.04 mmol, 1 equiv), nickel(II) acetate (7.1 mg, 0.04 mmol, 1 equiv), and tetramethylammonium acetate (5.33 mg, 0.04 mmol, 1 equiv) were weighed into a 4 mL vial. DMSO-d_6 (0.6 mL) was added, and the resulting mixture was transferred to a J. Young NMR tube. (Note: the reaction mixture was not homogeneous). The reaction in the J. Young NMR tube was heated in an oil bath and monitored over time. The reaction was heated for 12 h at 160 °C during which it changed color from light yellow to orange. Analysis by ^{1}H NMR spectroscopy showed signals consistent with the formation of 2a in 12% yield with 88% starting material remaining (yields calculated based on integration of the remaining starting material **1b-H**). However, numerous attempts to isolate clean Ni^{II} product(s) from this mixture proved unsuccessful.

(**a**) ^{1}H NMR spectrum following the attempted synthesis of **2b-L** via C–H activation (eq. 3 in manuscript). (**b**) Expanded aromatic region of the ^{1}H NMR spectrum from (**a**). Integrated resonances correspond to resonances assigned to **2b-L** . (**c**) Stacked ^{1}H NMR spectra from reaction in eq. 3 (top) and ^{1}H NMR spectrum of isolated **2b-L** in DMSO-d_6 (bottom)

C-H activation route from 1a-H_Eq 2

8.65
8.63
8.55
8.53

5.72

Ni(OAc)$_2$, NMe$_4$OAc
DMSO-d_6, 160 °C, 12 h

(1a-H)

(2a)
12% yield
(^{1}H NMR relative to remaining 1a-H)

^{1}H NMR (DMSO-d_6, 600 MHz)

(2a)
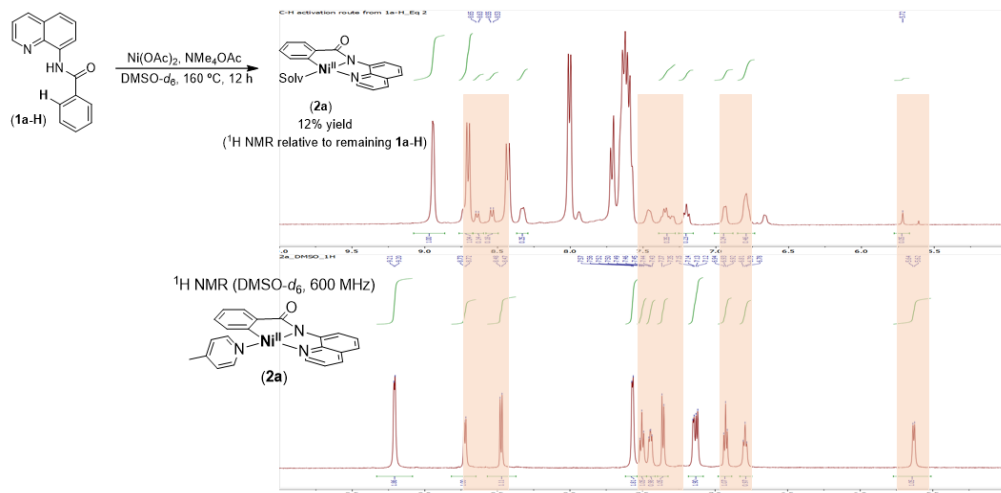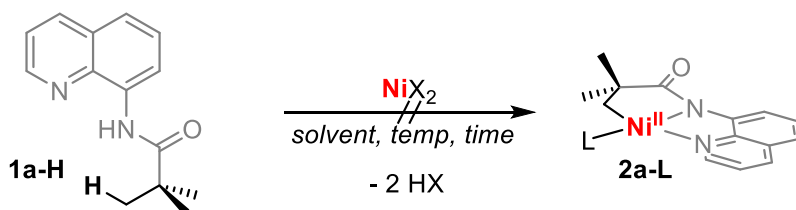
1a-H (9.9 mg, 0.04 mmol, 1 equiv), nickel(II) acetate (7.1 mg, 0.04 mmol, 1 equiv) or nickel(II) acetyl acetonate (10.3 mg, 0.04 mmol, 1 equiv) or Ni(II) trifluoromethanesulfonate (10.3 mg, 0.04 mmol, 1 equiv) were weighed into a 4 mL vial. Solvent (0.6 mL) was added, and the resulting mixture was transferred to a Teflon-lined screw cap NMR tube. (Note: In general, the reaction mixtures were not homogeneous) The reaction in the NMR tubes were heated in an oil bath and monitored over time by ^{1}H NMR up to 30 h at 110 ºC during which no significant color change was noted for most. Analysis by ^{1}H NMR spectroscopy only showed signals consistent with starting material with occasional paramagnetic broadening in some case as shown below.

2.5.4 Synthesis and Characterization of Nickel Complexes

$$\text{Ni(COD)}_2 \quad + \quad 4 \ \text{PEt}_3 \quad \xrightarrow[\substack{-35 \ ^\circ\text{C, 18 h} \\ -\text{COD}}]{\text{Et}_2\text{O}} \quad$$
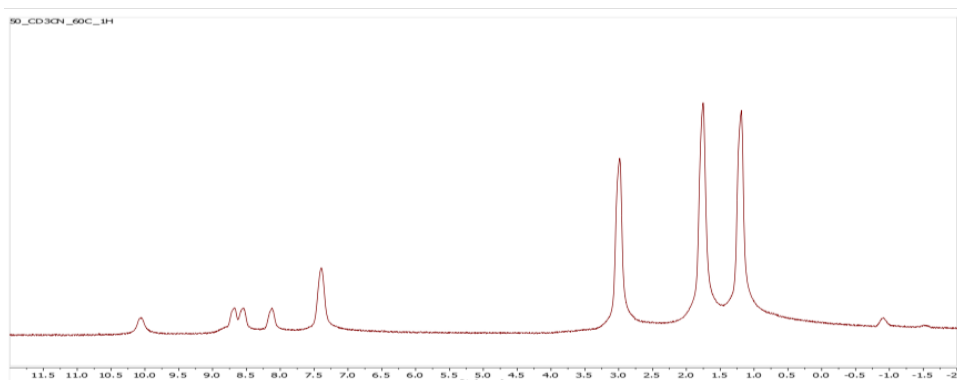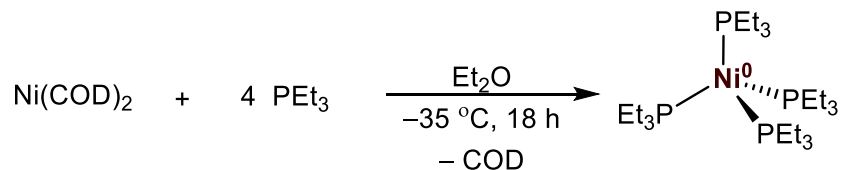
Triethylphosphine (5.00 g, 42 mmol, 4 equiv) in diethyl ether (10 mL) was added dropwise to a stirring suspension of bis(1,5-cyclooctadiene)nickel(0) (2.90 g, 10.5 mmol, 1 equiv) in diethyl ether (10 mL) in a 20 mL vial, at room temperature. The solution changed color from a yellow suspension to an intermediate dark orange and then to a final homogeneous dark purple solution with the complete addition of the triethylphosphine in 2–3 mins. The vial was sealed with a Teflon-lined cap and left inside the glove box freezer at –35 °C for 18 h. Then the vial was brought out of the freezer and the pale-yellow liquid was decanted out with the help of a glass pipette. The resulting residue was twice washed with pre-cooled (–35 °C) pentane (5 mL) and filtrate was decanted off again. The crystalline white solid was dried on a vacuum line from inside the glovebox to remove trace solvent. This afforded $\text{Ni}^0(\text{PEt}_3)_4$ as a crystalline white solid (3.80 g, 68% yield). The ^{1}H and ^{31}P NMR spectra of the product matched that reported in the literature.[2]

Notes:

1. A further ~5% increase in yield of the reaction could be ascertained with prolonged (36 h) duration of slow crystallization of white solid from the filtrate after the first decantation step at –35 °C.

2. Triethylphosphine is a pyrophoric reagent and was handled with proper care only inside the glovebox.

3. All solid waste containers were carefully handled while transferring to outside the glovebox. Depending on the scale of the reaction, trace liquids inside the vacuum trap or on the vials, glass pipettes and used kimwipes often started smoking in contact with air.

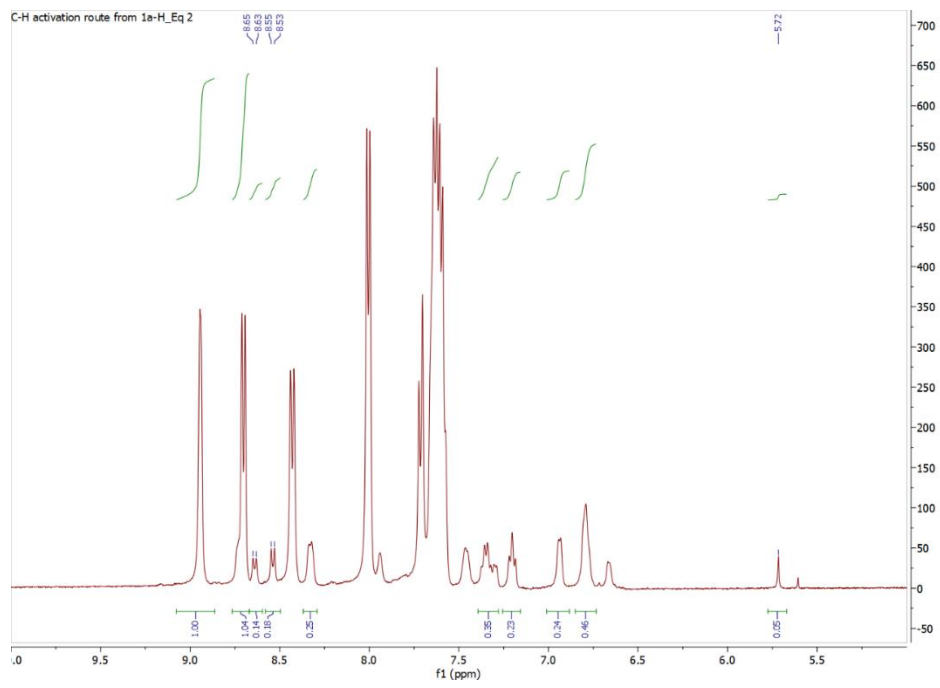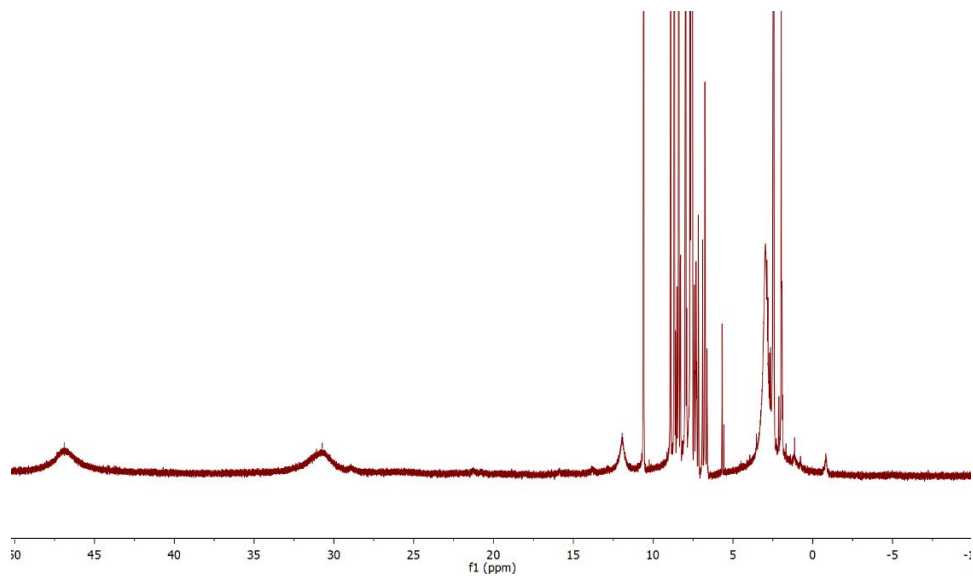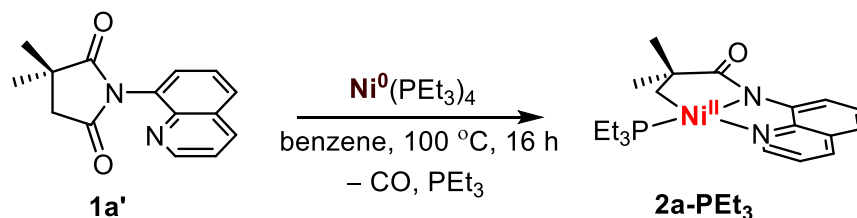**2a-PEt₃**: 3,3-Dimethyl-1-(quinolin-8-yl)pyrrolidine-2,5-dione (**1a′**) (508 mg, 2 mmol, 1 equiv) and [Ni(PEt₃)₄] (2.125 g, 4 mmol, 2 equiv) were weighed into a 20 mL vial. Anhydrous benzene (15 mL) was added, and the resulting mixture was stirred vigorously. Over the course of 30 min, **1a′** dissolved, and the solution changed color from purple to dark red-brown. The reaction mixture was transferred to a 50 mL Schlenk tube, and the reaction vial was washed with an additional 10 mL of anhydrous benzene. The Schlenk tube was sealed and then heated in an oil bath at 100 °C for 16 h. The reaction turned dark brown-black. The Schlenk tube was brought into a glovebox, the reaction mixture was transferred to a 100 mL round bottom flask, and the Schlenk tube was washed with THF (10 mL). The solvent was then removed under vacuum to afford a brown-black residue. The residue was washed with pentane (2 x 15 mL) and diethyl ether (2 x 5 mL), and the liquid extracts (which contained a fine black solid) were discarded. The residue was next dissolved in THF (15 mL), and a 5:2 mixture of pentane: diethyl ether (35 mL) was added to precipitate a dark red-orange powder. Next this residue was dissolved in THF (15 mL), and the product was precipitated with pentane (30 mL) (two times). The product **2a-PEt₃** was obtained as an ochre-yellow powder (702 mg, 87% yield).

1H NMR (600 MHz, Acetone-d_6) δ 9.07-8.88 (m, 1H), 8.59 (d, J = 4.8 Hz, 1H), 8.38 (d, J = 8.2 Hz, 1H), 7.59-7.39 (m, 2H), 7.29 (d, J = 7.9 Hz, 1H), 1.82 (p, J = 7.6 Hz, 3H), 1.29 (dt, J = 15.4, 7.7 Hz, 5H), 1.14 (s, 2H), 0.85 (d, J = 9.2 Hz, 1H).

^{31}P NMR (243 MHz, Acetone-d_6) δ 20.19.

^{13}C NMR (151 MHz, Acetone-d_6) δ 191.03, 150.57 (d, J = 1.5 Hz), 149.14, 146.44 (d, J = 3.8 Hz), 138.76, 130.28, 129.83, 122.42, 119.05, 117.67, 49.28 (d, J = 3.0 Hz), 30.95, 25.91 (d, J = 24.2 Hz), 16.03 (d, J = 24.8 Hz), 9.05.

Elemental analysis: calculated for $C_{22}H_{17}N_3NiO$, C: 59.59, H: 7.25, N: 6.95; Found: C: 60.21, H: 7.39, N: 7.58

HRMS-electrospray (m/z): [M$^+$] calcd. for $C_{20}H_{29}N_2NiOP$, 402.1371; found, 403.1528 [M+H]
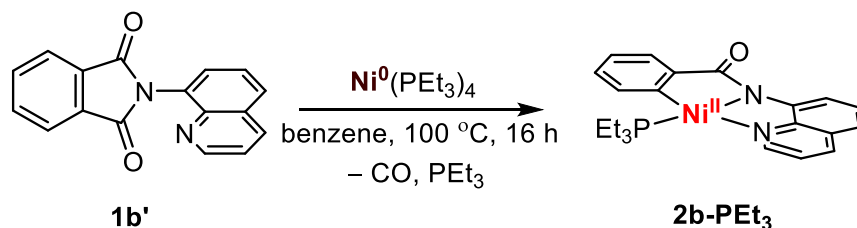
2b-PEt₃: 2-(Quinolin-8-yl)isoindoline-1,3-dione (**1b′**) (548 mg, 2 mmol, 1 equiv) and Ni(PEt₃)₄ (2.125 g, 4 mmol, 2 equiv) were weighed into a 20 mL vial. Anhydrous benzene (15 mL) was added, and the resulting mixture was stirred vigorously. Over the course of 30 min, **1b′** dissolved, and the solution changed color from purple to dark red-brown. The reaction mixture was transferred to a 50 mL Schlenk tube, and the reaction vial was washed with an additional 10 mL of anhydrous benzene. The Schlenk tube was sealed and then heated in an oil bath at 100 °C for 16 h. The reaction turned dark brown-black. The Schlenk tube was brought into a glovebox, the reaction mixture was transferred to a 100 mL round bottom flask, and the Schlenk tube was washed with THF (10 mL). The solvent was then removed under vacuum to afford a brown-black residue. The residue was washed with pentane (2 x 15 mL) and diethyl ether (2 x 5 mL), and the liquid extracts (which contained a fine black solid) were discarded. The residue was next dissolved in THF (15 mL), and a 5:2 mixture of pentane: diethyl ether (35 mL) was added to precipitate a dark red-orange powder. This procedure was repeated three times, first dissolving in acetone (10 mL) and precipitating with a 5:2 mixture of pentane: diethyl ether (15 mL) and next dissolving in THF (15 mL) and precipitating with pentane (30 mL) (two times). The product **2b-PEt₃** was obtained as an ochre-yellow powder (736 mg, 87% yield).

[^1]H NMR (700 MHz, Benzene-d_6) δ 9.95 (d, J = 7.8 Hz, 1H), 8.32 (d, J = 7.7 Hz, 1H), 7.76 (d, J = 5.0 Hz, 1H), 7.55 (t, J = 8.1 Hz, 1H), 7.50 (d, J = 8.3 Hz, 1H), 7.16 (t, J = 7.3 Hz, 1H), 7.03 (t, J

= 7.6 Hz, 1H), 6.92 (d, J = 8.1 Hz, 1H), 6.74 (d, J = 7.7 Hz, 1H), 6.59 (t, J = 6.7 Hz, 1H), 1.54 (q, J = 8.2 Hz, 6H), 1.14 (dt, J = 13.6, 7.6 Hz, 9H).

^{31}P NMR (283 MHz, Benzene-d_6) δ 15.31.

^{13}C NMR (176 MHz, Benzene-d_6) δ 204.78 (d, J = 5.9 Hz), 175.19, 149.82, 149.04, 148.94, 147.99, 146.97, 137.19, 135.44, 131.18, 130.09, 128.82, 123.35, 120.42, 119.31, 114.86, 23.57 – 21.96 (m), 8.43.

HRMS-electrospray (m/z): [M$^+$] calcd. for $C_{22}H_{25}N_2NiOP$, 422.1058; found, 422.1066 [M+H]

2.5.5 Reactivity of Nickel Complexes
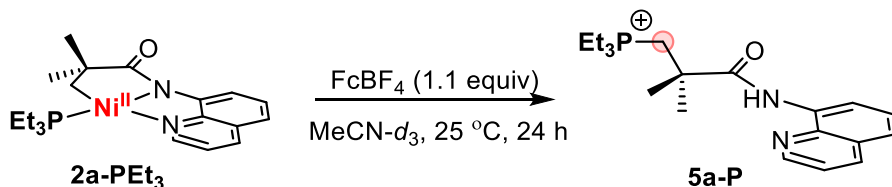
2a-PEt₃   →   FcBF₄ (1.1 equiv), MeCN-d_3, 25 °C, 24 h   →   **5a-P**

Complex **2a-PEt₃** (4.0 mg, 10 µmol, 1 equiv) was weighed into a 4 mL glass vial and dissolved in MeCN-d_3 (0.5 mL) containing tetramethylsilane (0.9 mg, 10 µmol) as an internal standard. The sample was transferred an NMR tube that was sealed with a Teflon septa-lined screw cap. Traces of undissolved **2a-PEt₃** was noted in the vial; to correct for any changes in concentration as a result, an NMR spectrum was recorded at this stage, and the ratio of **2a-PEt₃** : tetramethylsilane standard was quantified. The NMR tube was transferred back into the glovebox, and ferrocenium tetrafluoborate (3.0 mg, 11.0 µmol, 1.1 equiv) was added. This addition resulted in an immediate color change from orangish-yellow to dark green. An EPR spectrum of the above reaction mixture was recorded at 100K in a PrCN glass by transferring an aliquot and diluting in PrCN. The color faded over the course of the reaction. The yield of **5a-P** was quantified by ^{1}H NMR spectroscopy to be 70% after 24 min as determined by relative integration values as based on the internal standard (TMS). Reaction was monitored by ^{1}H and ^{31}P NMR spectroscopy, and these data as shown .
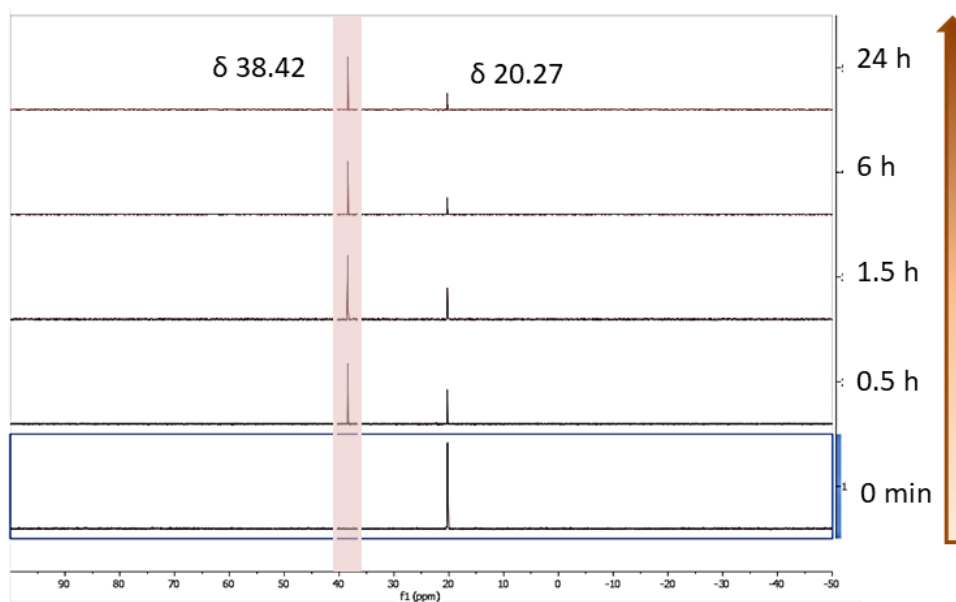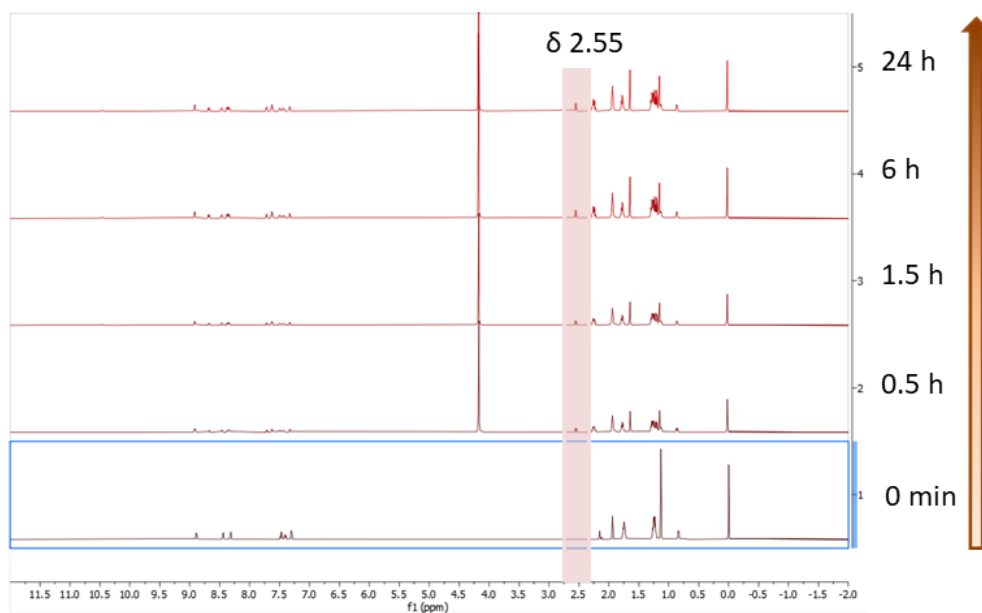
Time evolution of ^{1}H (doublet at δ 2.55 ppm) and ^{31}P (singlet at δ 38.42 ppm) NMR spectra

show formation of product **5a-P** on treatment of **2a-PEt₃** with FcBF₄
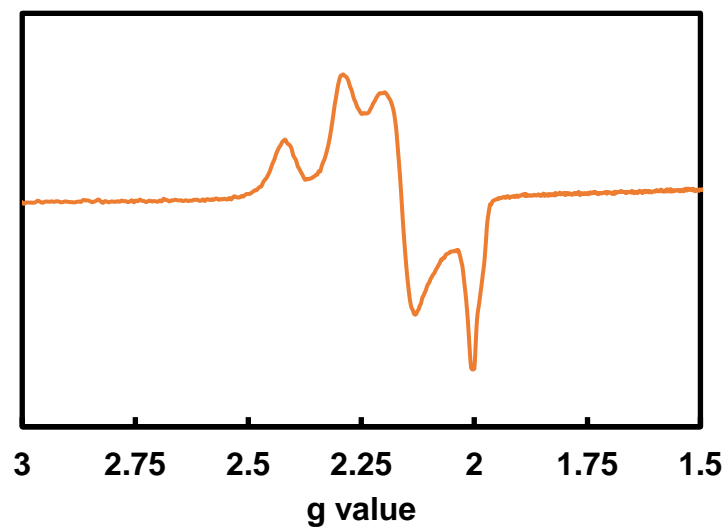
EPR spectrum of putative Ni^{III} (S = ½) species formed during formation of product **5a-P** on treatment of **2a-PEt$_3$** with FcBF$_4$

2a-PEt₃ → aerobic oxidation, MeCN-*d₃*, 25 °C, 2 h → **5a-P** 16%

Complex **2a-PEt₃** (4.0 mg, 10 µmol, 1 equiv) was weighed into a 4 mL glass vial and dissolved in MeCN-*d₃* (0.5 mL) containing tetramethylsilane (0.9 mg, 10 µmol) as an internal standard. The sample was transferred an NMR tube that was sealed with a Teflon septa-lined screw cap. Traces of undissolved **2a-PEt₃** was noted in the vial; to correct for any changes in concentration as a result, an NMR spectrum was recorded at this stage, and the ratio of **2a-PEt₃** : tetramethylsilane standard was quantified. The NMR screwcap was opened, and the NMR tube was left exposed to air under ambient conditions inside a laboratory hood. The reaction slowly changed color from the initial orange to a more brownish orange and finally to a yellowish-brown. The reaction was monitored ¹H and ³¹P NMR spectroscopy as shown in. After 2 h, the complete disappearance of NMR signals from the starting material was noted along with the formation of diamagnetic signals attributed to **5a-P** and some paramagnetic nickel species as characterized by broad ¹H NMR signals. The yield of **5a-P** was quantified by ¹H NMR spectroscopy to be 16% after 2 h as determined by relative integration values as based on the internal standard (TMS).
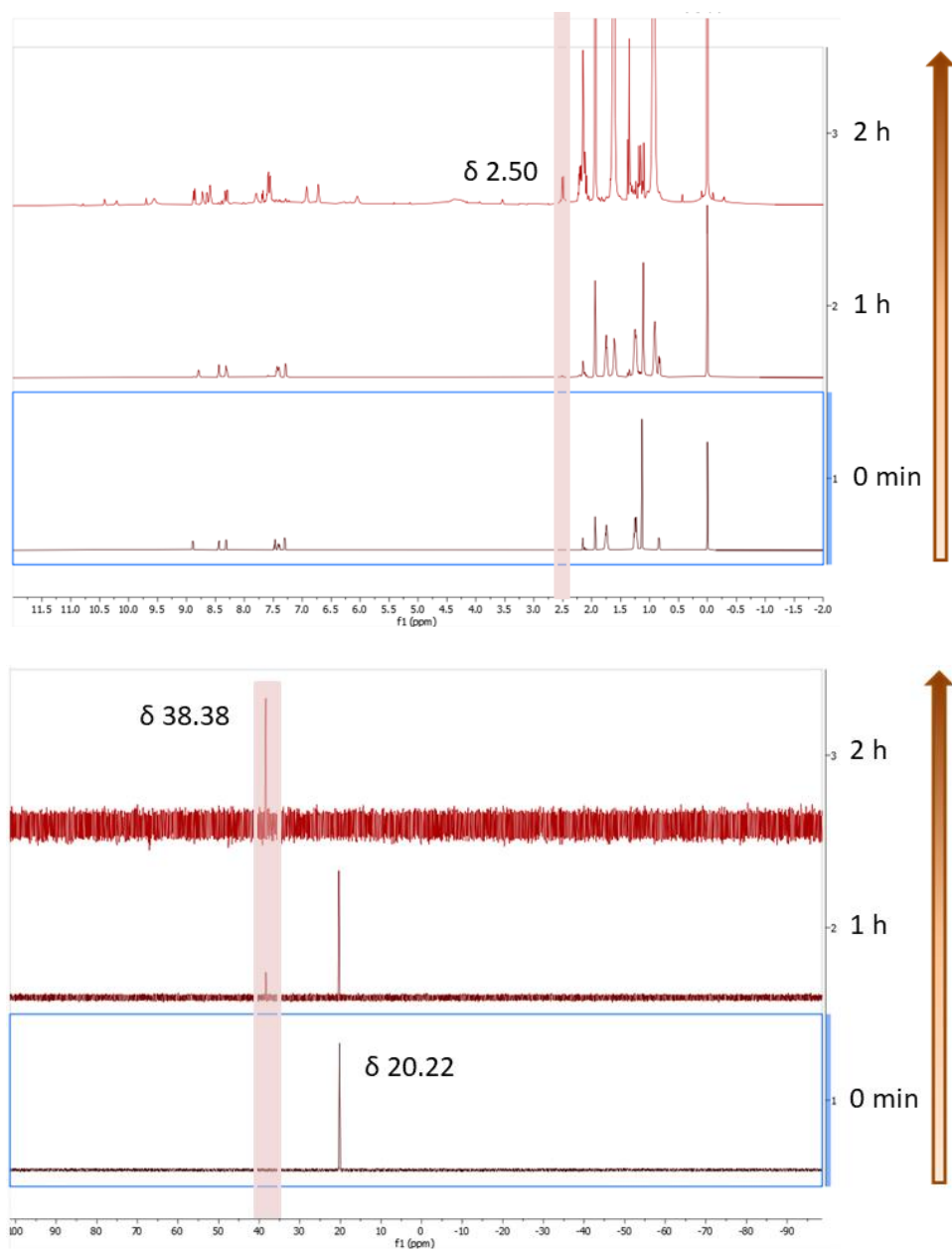
Time evolution of ^{1}H (doublet at δ 2.50 ppm) and ^{31}P (singlet at δ 38.38 ppm) NMR spectra

show formation of product **5a-P** on aerobic oxidation of **2a-PEt₃**

2a-PEt₃   I₂ (1.1 equiv)   **5a-I**

MeCN-d_3, 25 °C, 24 h

68%

Complex **2a-PEt₃** (4.0 mg, 10 µmol, 1 equiv) was weighed into a 4 mL glass vial and dissolved in MeCN-d_3 (0.5 mL) containing tetramethylsilane (0.9 mg, 10 µmol) as an internal standard. The sample was transferred an NMR tube that was sealed with a Teflon septa-lined screw cap. Traces of undissolved **2a-PEt₃** was noted in the vial; to correct for any changes in concentration as a result, an NMR spectrum was recorded at this stage, and the ratio of **2a-PEt₃** : tetramethylsilane standard was quantified. The NMR tube was transferred back into the glovebox, and I₂ (0.1 mL of a 0.118 M stock solution in MeCN-d_3, 11.8 µmol, 1.18 equiv) was added. This addition resulted in an immediate color change from orangish-yellow to purplish-red. The NMR tube was vigorously shaken to ensure immediate and thorough mixing and was then removed from the glovebox and analyzed by ¹H NMR spectroscopy.

The yield of **5a-I** was quantified by ¹H NMR spectroscopy to be 70% (singlet at 3.62 ppm) after 24 min as determined by relative integration values as based on the internal standard (TMS). NMR data are shown below.
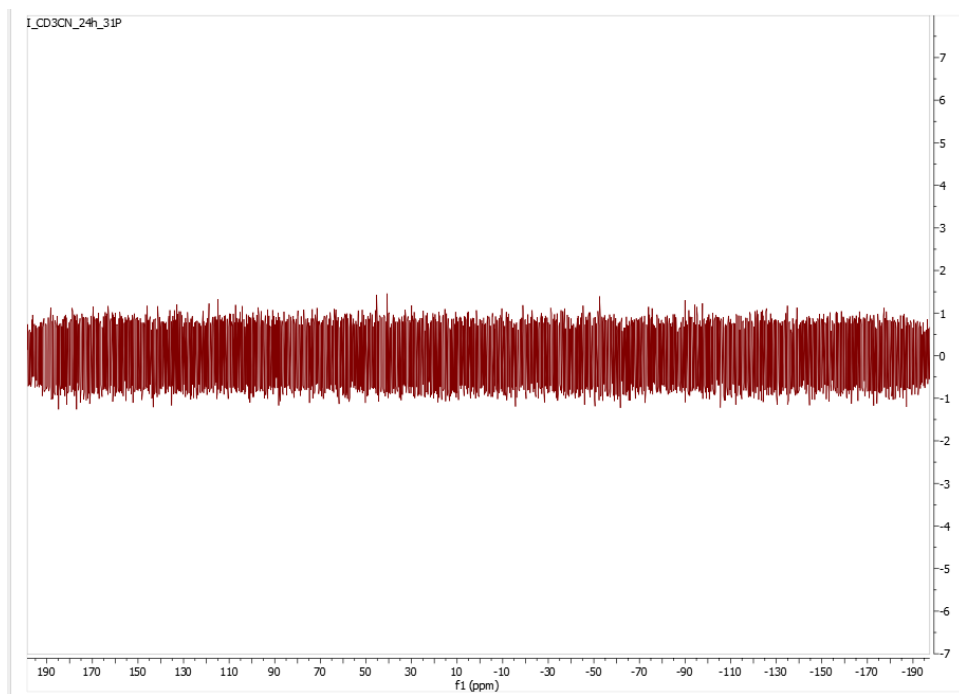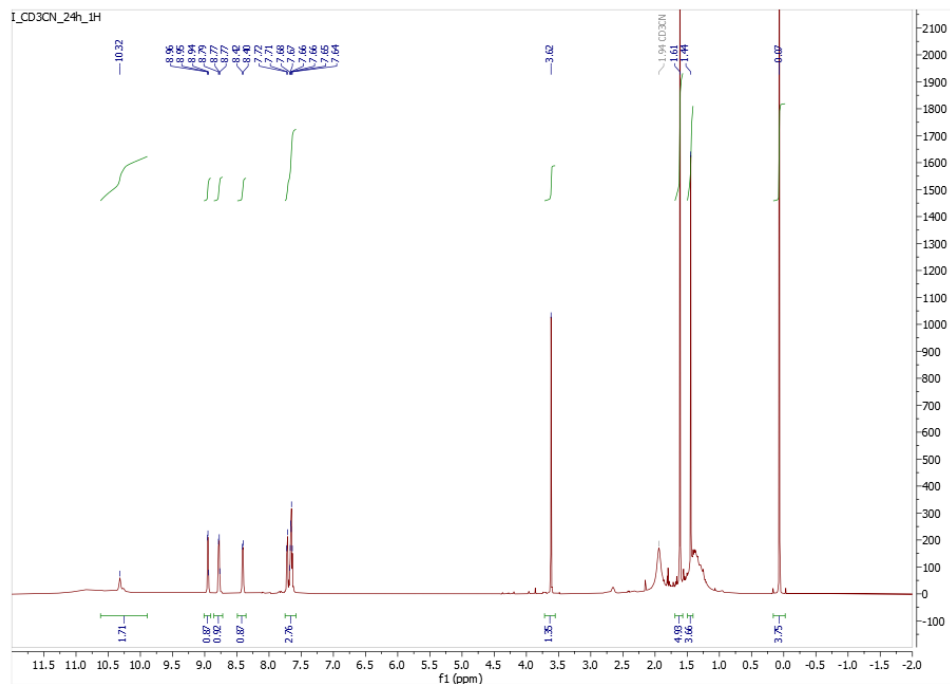
^{1}H NMR (singlet at δ 3.62 ppm) show formation of **5a-I** on treatment of **2a-PEt₃** with I₂ and no

signals were observed in the ^{31}P NMR
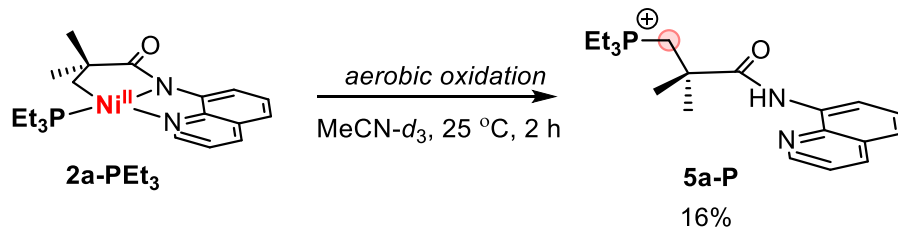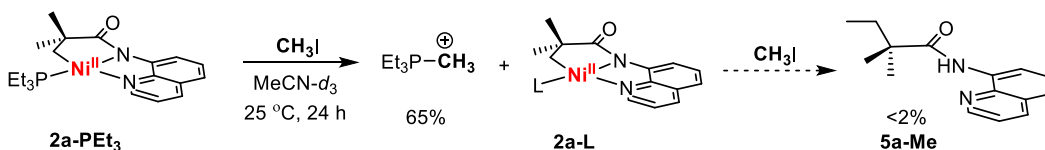
Complex **2a-PEt₃** (4.0 mg, 10 µmol, 1 equiv) was weighed into a 4 mL glass vial and dissolved in MeCN-d_3 (0.5 mL) containing tetramethylsilane (0.9 mg, 10 µmol) as an internal standard. The sample was transferred an NMR tube that was sealed with a Teflon septa-lined screw cap. Traces of undissolved **2a-PEt₃** was noted in the vial; to correct for any changes in concentration as a result, an NMR spectrum was recorded at this stage, and the ratio of **2a-PEt₃** : tetramethylsilane standard was quantified. The NMR tube was transferred back into the glovebox, and CH₃I (0.1 mL of a 0.118 M stock solution in MeCN-d_3, 11.8 µmol, 1.18 equiv) was added. This addition resulted in an immediate color change from orangish-yellow to pale-yellow. The NMR tube was then removed from the glovebox formation of **5a-Me** was tracked and analyzed by ¹H NMR spectroscopy.
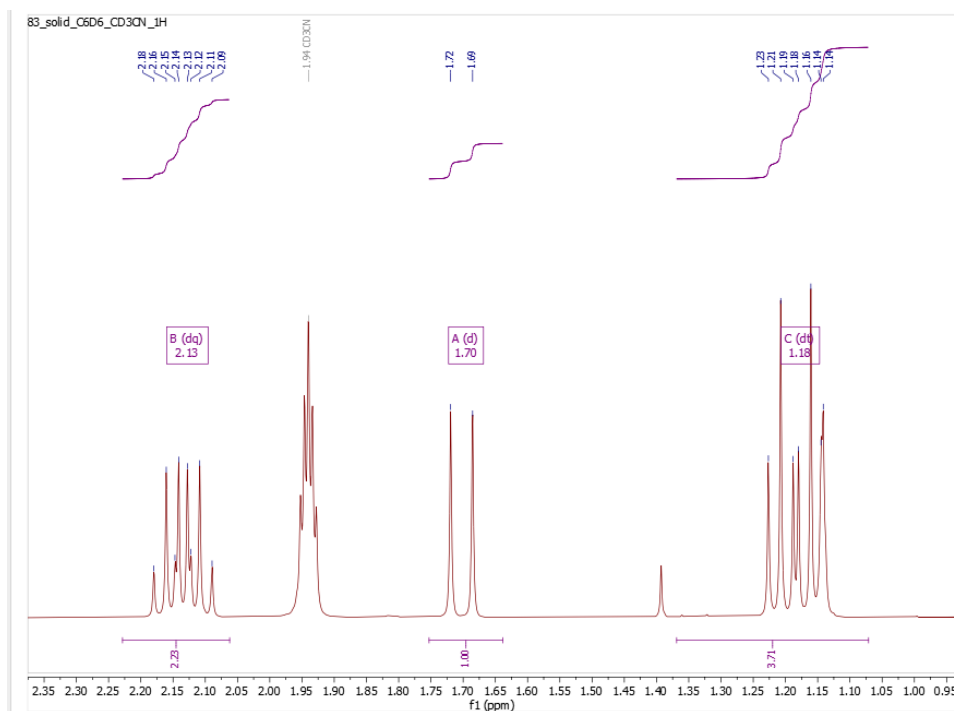
¹H NMR spectrum of isolated Et₃−CH₃⁺ from above reaction

2.5.6 X-Ray Crystallography Data

X-Ray Crystallographic Data of 2a-PEt₃

Orange prisms of **2a-PEt₃** were grown from a tetrahydrofuran/pentane solution of the compound at 22 deg. C. A crystal of dimensions 0.16 x 0.09 x 0.05 mm was mounted on a Rigaku AFC10K Saturn 944+ CCD-based X-ray diffractometer equipped with a low temperature device and Micromax-007HF Cu-target micro-focus rotating anode (l = 1.54187 A) operated at 1.2 kW power (40 kV, 30 mA). The X-ray intensities were measured at 225(1) K with the detector placed at a distance 42.00 mm from the crystal. A total of 2028 images were collected with an oscillation width of 1.0° in w. The exposure times were 1 sec. for the low angle images, 3 sec. for high angle. Rigaku d*trek images were exported to CrysAlisPro for processing and corrected for absorption. The integration of the data yielded a total of 30563 reflections to a maximum 2q value of 138.81° of which 3806 were independent and 3761 were greater than 2s(I). The final cell constants (Table 1) were based on the xyz centroids 22853 reflections above 10s(I). Analysis of the data showed negligible decay during data collection. The structure was solved and refined with the Bruker SHELXTL (version 2016/6) software package, using the space group Pna2(1) with Z = 4 for the formula C20H29N2OPNi. All non-hydrogen atoms were refined anisotropically with the hydrogen atoms placed in idealized positions. Full matrix least-squares refinement based on F2 converged at R1 = 0.0401 and wR2 = 0.1148 [based on I > 2sigma(I)], R1 = 0.0410 and wR2 = 0.1154 for all data. Additional details are presented in Table 1 and are given as Supporting

Table 2.2 Crystal Data and Structure Refinement for **2a-PEt₃**

Empirical formula	$C_{20} H_{29} N_2 O P Ni$
Formula weight	403.13
Temperature	85(2) K
Wavelength	1.54184 A
Crystal system, space group	Orthorhombic, Pna2(1)
Unit cell dimensions	a = 17.56881(9) A alpha = 90° b = 9.67658(4) A beta = 90° c = 12.06282(6) A gamma = 90°
Volume	2050.752(18) A^3
Z, Calculated density	4, 1.306 Mg/m^3
Absorption coefficient	2.166 mm^-1
F(000)	856
Crystal size	0.160 x 0.090 x 0.050 mm

Theta range for data collection	5.035° to 69.406°
Limiting indices	-18<=h<=20, -11<=k<=11, -14<=l<=14
Reflections collected / unique	30563 / 3806 [R(int) = 0.0239
Completeness to theta = 67.684	99.8%
Absorption correction	Semi-empirical from equivalents
Max. and min. transmission	1.00000 and 0. 86719
Refinement method	Full-matrix least-squares on F^2
Data / restraints / parameters	3806 / 1 / 232
Goodness-of-fit on F^2	1.037
Final R indices [I>2sigma(I)]	R1 = 0.0401, wR2 = 0.1148
R indices (all data)	R1 = 0.0410, wR2 = 0.1154
Absolute structure parameter	-0.013(9)
Extinction coefficient	0.0035(4)
Largest diff. peak and hole	0.620 and -0.452 e.A^-3

Chapter 3 Synthesis, Reactivity and Catalytic Relevance of Picoline Ligated Ni^{II} Complexes

Note: This chapter is partly based on work published in Roy, P.; Bour, J. R.; Kampf, J. W.; Sanford, M. S.* Catalytically Relevant Intermediates in the Ni-Catalyzed C(sp^2)–H and C(sp^3)–H Functionalization of Aminoquinoline Substrates. *J. Am. Chem. Soc.* **2019**, *141*, 17382–17387 and *J. Am. Chem. Soc.* **2021**, *143*, 14021.

3.1 Introduction

In 2004 Daugulis introduced the aminoquinoline pincer ligand as a directing group for the palladium-catalyzed oxidative functionalization of unactivated C–H bonds.[1,2] Subsequently, this directing group has been used in a variety of C–H functionalization reactions catalyzed by other transition metals to form both carbon–carbon and carbon–heteroatom bonds.[3] As one example, nickel, a group congener of palladium, has recently been employed as a catalyst in aminoquinoline-directed C–H functionalization reactions.[4] Mechanistically, these reactions are proposed to proceed through the intermediacy of a cyclometalated Ni^{II} intermediate, **2-L**. Subsequently, this Ni^{II} intermediate undergoes oxidatively-induced C–C or C–heteroatom bond formation. Depending on the oxidant, reactive intermediates in varying oxidation states at the nickel center have been proposed (Figure 3.1).

Figure 3.1 Ni-Catalyzed Oxidative Functionalization of C–H Bonds

61
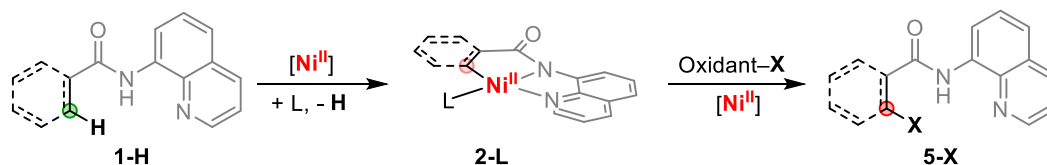
When we initiated our studies, this cornerstone Ni^{II} species had not been isolated nor spectroscopically observed under catalytic conditions, and its feasibility had only been supported by kinetic isotope experiments and computational investigations. [5-7] In 2018, Love isolated a model complex with connectivity analogous to that of the cyclometalated Ni^{II}–alkyl species, by swapping the amide unit with a urea core. Although no mechanistic model for oxidative functionalization was proposed in this system, the feasibility of $C(sp^3)$–C bond formation from **3a** was established using alkyl halides, aryl halides, and aryliodonium salts (Figure 3.2).[8]

Figure 3.2 $C(sp^3)$–C Bond Formation with Carbon Electrophiles by Love[8]
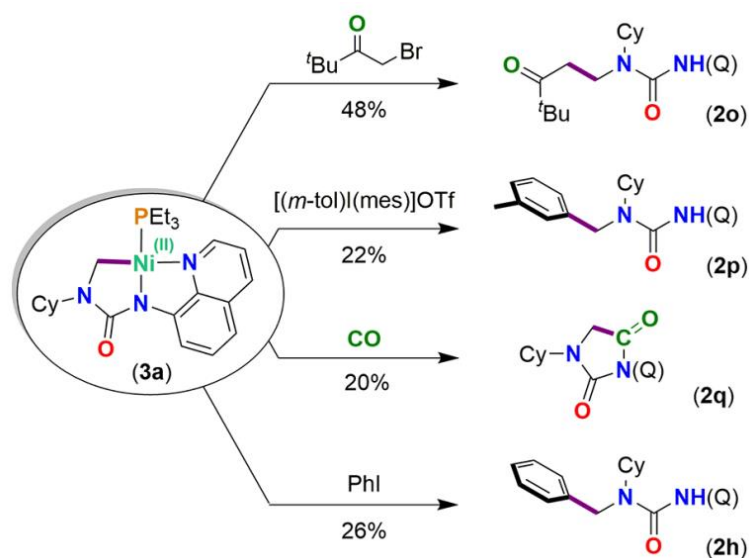
The previous chapter detailed the isolation of a triethylphosphine-ligated cyclometalated Ni^{II} complex (**2a-PEt₃**) via a decarbonylation reaction. In pursuit of high-valent nickel analogues, oxidative functionalization studies were conducted at **2a-PEt₃**. However, these predominantly showed PEt_3-based reactivity (Figure 3.3). Although mechanistically novel, the observed P–C coupling reactions precluded (*i*) probing the catalytic relevance of this complex as well as (*ii*) the isolation of high valent nickel complexes.

Figure 3.3 C(sp^3)–P Coupling with One-electron Oxidants via Putative Ni^{III} Intermediate
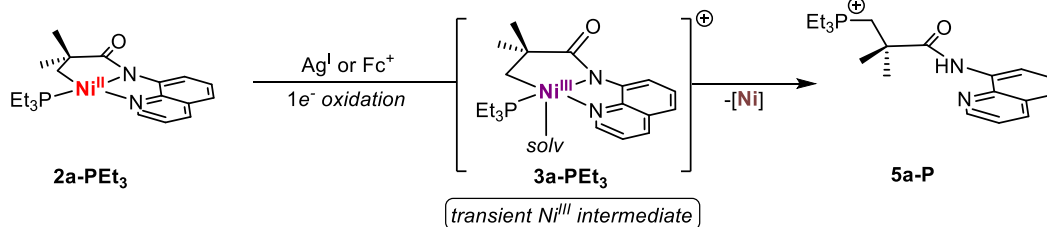
Previously isolated high-valent nickel complexes have contained nitrogen-based ligands like pyridines, which are generally inert towards C–N coupling reactions.[9,10] Thus, we hypothesized that swapping PEt$_3$ for a pyridine ligand would potentially enable to detection and/or isolation of high valent Ni intermediates upon the oxidation of **2**. Ligand exchange studies showed that the PEt$_3$ ligand could be swapped with 4-picoline in acetone, and subsequent oxidative studies were performed with the 4-picoline complex (Figure 3.4).

Figure 3.4 Proposal for C–X Coupling from Nitrogen Ligated Ni^{II} Complex
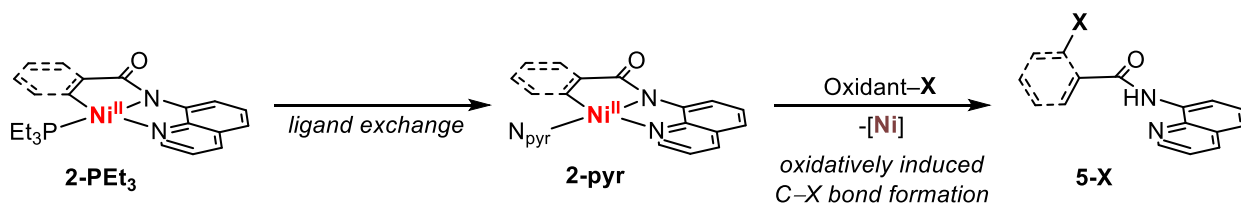
As detailed below, the oxidation studies showed a striking difference in reactivity between the picoline and phosphine complexes for both the σ-alkyl and σ-aryl nickelacycles. Oxidation studies of the σ-alkyl analogue **2a-pic** with I$_2$ revealed exclusive C(sp^3)–N bond formation to form a β-lactam product, in accord with Chatani's catalytic report for this bond forming reaction.[11] Interestingly, in the same report Chatani also reported a C(sp^2)–I bond-forming reaction, which was similarly observed with our σ-aryl nickelacycle **2b-pic**. The catalytic relevance of these complexes was established in the respective C(sp^3)–N and C(sp^2)–I coupling reactions. Finally, the reaction of **2a-pic** with CH$_3$I showed the formation of the organic product **5a-Me** at 90 °C in

24 h, consistent with reactivity of the Ni^{II}–C bond. Overall, these results indicate that ligand exchange of triethylphosphine with picoline suppresses is effective for promoting oxidatively induced C–X coupling from these Ni^{II} complexes.

3.2 Results and Discussion

3.2.1 Synthesis of Ni^{II}–picoline Complexes

Our initial attempts to study ligand exchange of PEt_3 for pyridine used 1 equiv of complex **2a-PEt$_3$** and 1 equiv of pyridine in MeCN-d_3 at 25 °C. We noted the rapid formation of a new species (after 15 min at 25 ºC) via ^{1}H NMR spectroscopy; however, detailed analysis of the spectrum was difficult owing to overlapping signals. Similar issues were encountered with substituted pyridines such as 4-picoline. In order to obtain higher resolution NMR spectra, pyridine-d_5 was next selected as the ligand. The addition of 1 equiv of pyridine-d_5 to a solution of complex **2a-PEt$_3$** in MeCN-d_3 showed the formation of a new diamagnetic species by ^{1}H NMR spectroscopy after 15 min at 25 ºC. Notably, a new singlet at 0.95 ppm was observed in the alkyl region of the ^{1}H NMR spectrum, with a concomitant decrease in intensity of the diagnostic doublet at 0.85 ppm. This new signal was tentatively assigned as the hydrogens associated with the Ni-σ-alkyl group (Figure 3.5).

Figure 3.5 Reaction of **2-PEt₃** with 1 equiv of Pyridine-*d₅* in MeCN-*d₃* (¹H NMR spectra)
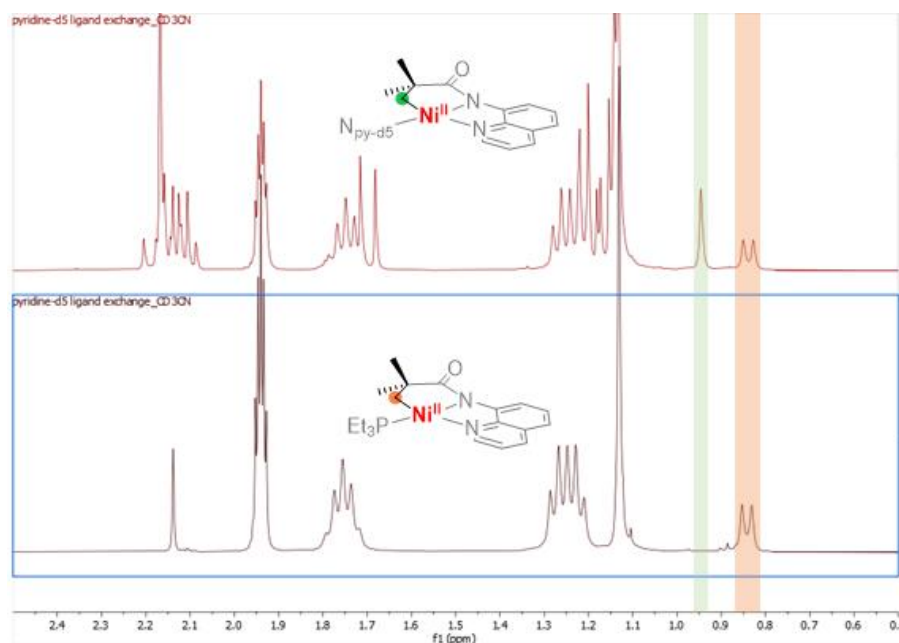
Although this result was promising, an equilibrium mixture of the two complexes was always observed, even upon the addition of an excess of pyridine-*d₅*. As such, isolation of the pyridine-*d₅* complex proved to be low yielding, owing to the requirement for repeated recrystallizations. Recently, Zargarian reported that ligand substitution on Ni^{II} pincer complexes in MeCN tends to be complicated by the nucleophilicity of the solvent.[12] This report also noted that several other solvents (e.g., THF and DCM) are also problematic for such ligand exchange reactions because of low dielectric constants. To address these issues, acetone was chosen as the solvent, because it is less nucleophilic and more volatile than MeCN but has a comparable dielectric constant.

Ligand exchange studies in acetone showed that the use of 4-picoline instead of pyridine-*d₅* led to higher conversion. However, the yield remained moderate owing to incomplete conversion. Ultimately, this was addressed by conducting the ligand exchange with 4-picoline under active vacuum to promote removal of the volatile phosphine ligand and thus drive the reaction to completion (Scheme 3.1). This was feasible because the boiling point of PEt₃ is 20 °C

lower than that of 4-picoline. Throughout the reaction, additional acetone was added (3 x 10 mL), and the mixture was placed under dynamic vacuum until full conversion was achieved.

Scheme 3.1 Synthesis of Picoline-ligated Ni^{II}–$C(sp^3)$ Complex
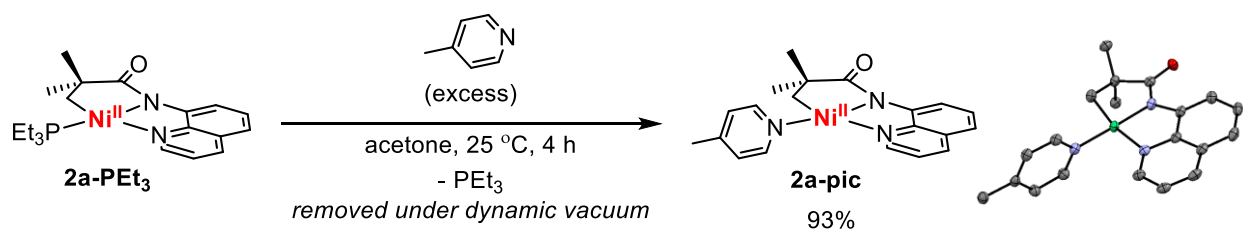
The picoline-ligated complex **2a-pic** was isolated in 93% yield as a diamagnetic Ni^{II} species that was characterized by elemental analysis, NMR spectroscopy, and X-ray crystallography. The X-ray crystal structure of **2a-pic** shows a slightly distorted square planar nickel center, consistent with other pincer Ni^{II} complexes. The structure of this complex is similar to that of its palladium analogue except that the M–C and M–N bonds are ~0.1 Å shorter than those in the corresponding palladacycle.[1]

Scheme 3.2 Synthesis of Picoline-ligated Ni^{II}–$C(sp^2)$ Complex
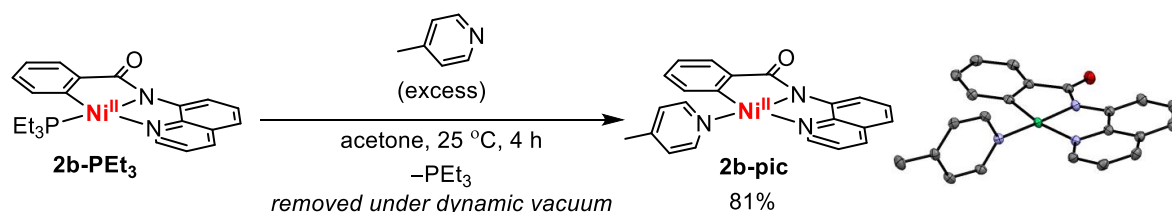
An analogous ligand exchange procedure was also effective for the σ-aryl nickelacycle **2b-PEt₃** (Scheme 3.2). The Ni^{II}-picoline product **2b-pic** was isolated and characterized by NMR spectroscopy and X-ray crystallography. It is noteworthy that the isolation protocol for **2b-pic** required at least four sequential recrystallizations to obtain pure material. The X-ray crystal structure of **2b-pic** shows a slightly distorted square planar nickel center, consistent with other pincer Ni^{II} complexes, with analogous traits with **2a-pic** and the Pd-analogs isolated by Chen and

66

Maiti.[13,14] Later, both the decarbonylation and ligand exchange steps were telescoped for isolation of both the complexes (Scheme 3.3).

Scheme 3.3 Generalized Route to Picoline-ligated Ni[II] Aminoquinoline Pincer Complexes
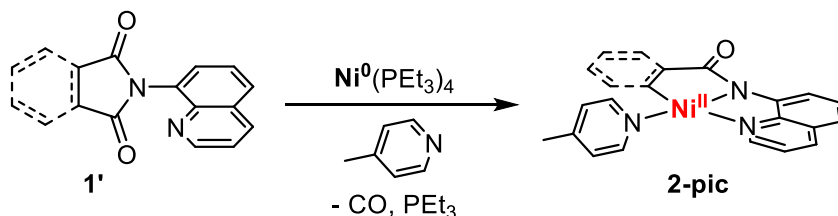
3.2.2 Iodination Reactivity and Catalytic Relevance of σ-alkyl Ni[II] complex

The oxidation potentials of **2a-pic** and **2b-pic** were interrogated using cyclic voltammetry. A small (~100 mV) positive shift in the Ni[II/III] potentials was observed upon changing the PEt$_3$ ligand to 4-picoline. In general, higher reversibility of scans was noted based on the ratio of anodic to cathodic peak current (Figure 3.6, 3.7). For instance, the i_a/i_c was 1.2 for **2a-pic** compared to 2.0 for **2a-PEt$_3$** at scan rates of 100 mVps. The observed potentials suggest that one-electron oxidants like Ag[I] and ferrocenium salts should be capable of oxidizing **2a-pic** and **2b-pic** to form Ni[III] intermediates.

Figure 3.6 CV Data for **2a-pic**

67
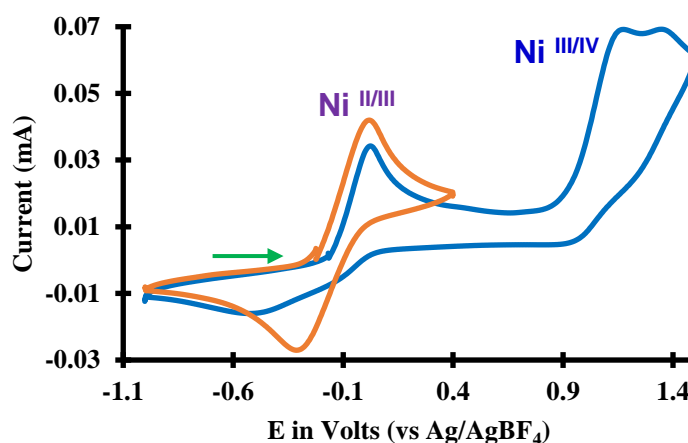
Figure 3.7 CV Data for **2a-PEt₃**
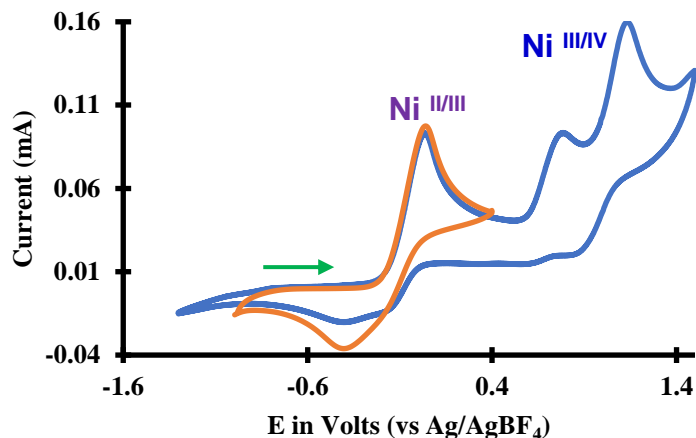
Indeed, both **2a-pic** and **2b-pic** underwent facile one-electron oxidation to form the Ni^{III} products **3a-s** and **3b-s**, respectively. In contrast to the PEt₃ analogue, no coupling with the picoline ligand (**5-pic**) was observed (Scheme 3.4). Instead, the Ni^{III} pincer complexes of general structure **3-s** were not isolated but characterized by EPR spectroscopy, as exemplified in Figure 3.8.

Figure 3.8 EPR Spectrum attributed to (S = ½) Ni^{III} species on Oxidation of **2a-pic** with AgBF₄ at 25 °C in MeCN-d_3
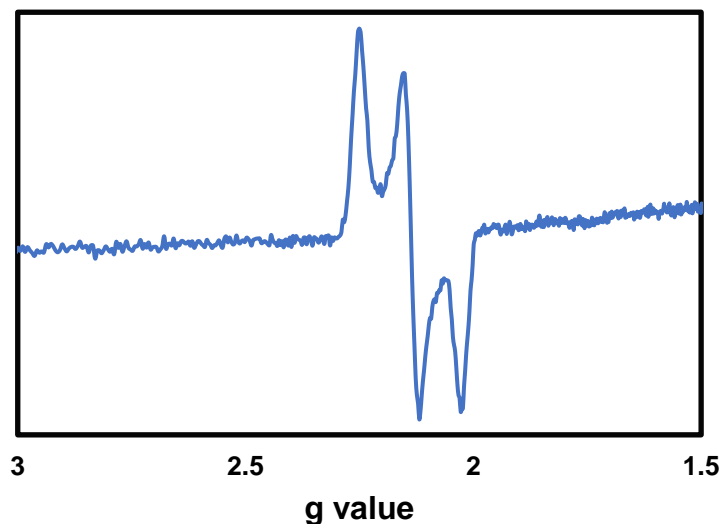
Attempts to isolate **3-s** were unsuccessful, which was attributed to the lability of a solvent molecule as the ligand. Hence, Ag^I-mediated oxidation was carried out in the presence of various

added nitrogen-based supporting ligands. The isolation, characterization, reactivity studies and catalytic relevance of these isolated Ni[III] complexes have been summarized in Chapter 4.

Scheme 3.4 One-electron Oxidation Exclusively Led to Ni[III] Complexes
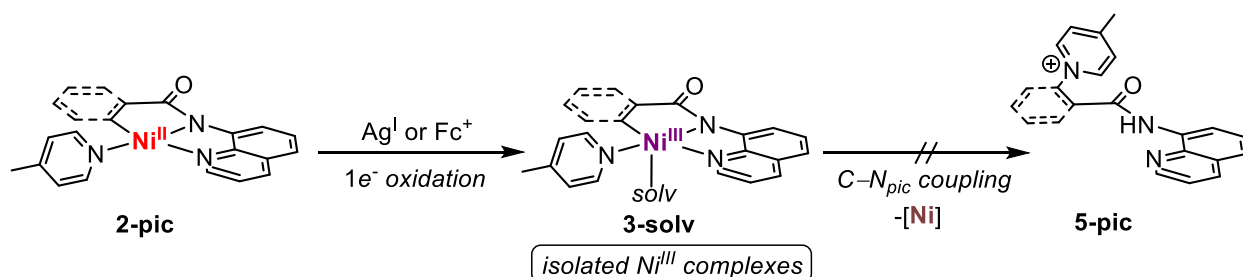
The PEt$_3$ complex **2a-PEt$_3$** showed very different results when oxidized with Ag[I] salts (which led to C(sp^3)–P coupling) as compared to with I$_2$ (which led to C(sp^3)–I coupling). As such, we aimed to conduct the same comparison with the picoline-ligated complex **2a-pic**. The stoichiometric reaction of the σ-alkyl Ni[II] complex **2a-pic** with I$_2$ in DMF-d_7 solution at 25 °C resulted in an immediate color change from orange to purple to yellow. Analysis of the crude reaction mixture by ^{1}H NMR spectroscopy revealed that the Ni[II] starting material was completely consumed within 90 min, with concomitant formation of the C(sp^3)–N coupled β-lactam product **3a** in 65% yield (Scheme 3.5). No intermediates were observed via ^{1}H NMR spectroscopy during the transformation.

Scheme 3.5 C(sp^3)–N Coupling from σ-alkyl Ni[II] complex with I$_2$ at 25 °C in DMF-d_7
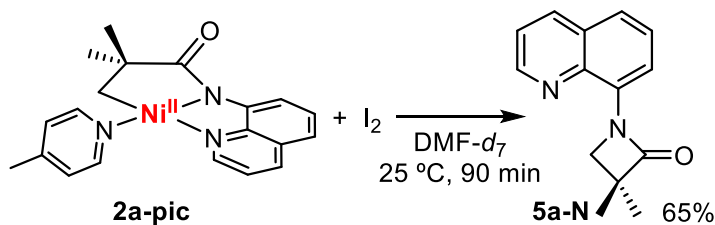
Chatani previously reported that an analogous β-lactam product, **5a-N**, is formed in the Ni(OTf)$_2$-catalyzed reaction of ^{Cl}**1a-H** with I$_2$ (Scheme 3.6). This report proposed two possible mechanisms for the generation of **5a-N**.[11] The first involves C(sp^3)–N bond-forming reductive

elimination from a high valent Ni center. The second involves the generation of a $C(sp^3)$–I bond

and subsequent intramolecular S_N2 cyclization to generate the β-lactam.

Scheme 3.6 Ni-catalyzed $C(sp^3)$–H amidation by Chatani
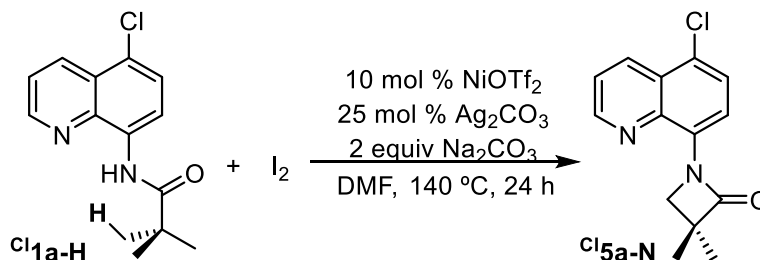
Overall, these results demonstrate that $C(sp^3)$–N bond formation is fast at room temperature

and suggest that the functionalization step is unlikely to be turnover limiting during catalysis.

Furthermore, this **2a-pic** closely resembles the putative nickel(II) intermediate proposed in Ni-

catalyzed $C(sp^3)$–H amidation reaction. Based on the reaction conditions reported by Chatani, the

fourth ligand during catalysis is likely triflate, carbonate, or solvent rather than picoline. To assess

whether **2a-pic** can enter the catalytic cycle, we examined this complex as a catalyst for the $C(sp^3)$–

H amidation reaction in Scheme 3.7 and Table 3.1.

Scheme 3.7 Catalytic Competence of σ-alkyl Ni^{II} Complex
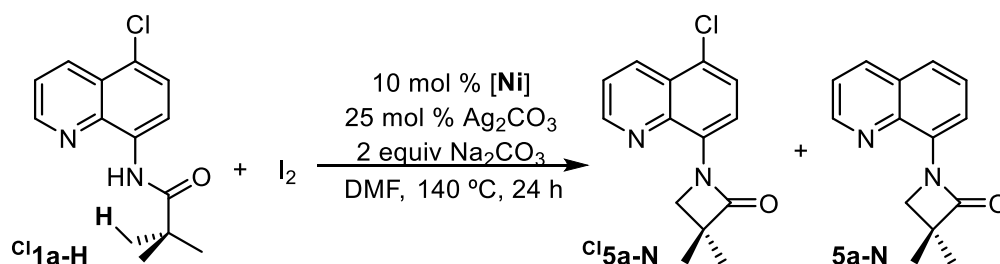
Indeed, use of 10 mol % of **2a-pic** as catalyst for the reaction of ^{Cl}**1a-H** with I_2 resulted in

47% yield of ^{Cl}**5a-N** along with 7% of **5a-N** (derived from the nickelacycle; Scheme 3.7). For

comparison, in our hands the analogous reaction with $Ni(OTf)_2$ as catalyst afforded ^{Cl}**5a-N** in 58%

yield. These results demonstrate that the σ-alkyl Ni^{II} complex **2a-pic** is catalytically competent for this transformation.

Table 3.1 Catalytic Competence of σ-alkyl Ni^{II} Complex for Intramolecular C(sp^3)–H Amidation

entry	[Ni]	Yield ^{Cl}5a-N	Yield 5a-N
1	Ni(OTf)$_2$	58%	–
2	2a-pic	47%	7%

3.2.3 Iodination Reactivity and Catalytic Relevance of σ-aryl Ni^{II} complex

The stoichiometric reaction of the σ-aryl Ni^{II} complex **2b-pic** with I$_2$ in acetone-d_6 at 25 °C resulted in an immediate color change from orange to purple to yellow. Analysis of the crude reaction mixture by ^{1}H NMR spectroscopy revealed that the complex was completely consumed within 1 h, with concomitant formation of the C(sp^2)–I coupling product **5b-I** in 20% yield. The reaction was quenched with D$_2$O to cleave the product from the nickel center, which led to a final yield of 70% (Scheme 3.8). No intermediates were observed via ^{1}H NMR spectroscopy nor EPR spectroscopy during this transformation.

Scheme 3.8 C(sp^2)–I coupling from σ-aryl Ni^{II} complex with I$_2$ at 25 °C in acetone-d_6
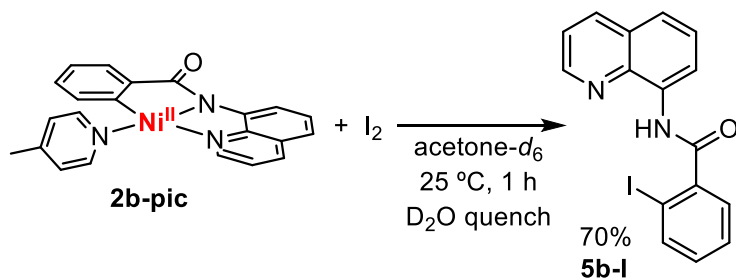
Overall, these results demonstrate that C(sp^2)–I bond formation is extremely fast at room temperature and suggest that the functionalization step is unlikely to be turnover limiting during catalysis. Furthermore, this complex closely resembles the putative nickelacycle intermediate

proposed in Chatani's Ni-catalyzed C(sp^2)–H iodination reaction. Based on the reaction conditions, the fourth ligand during catalysis is likely triflate, carbonate, or solvent. To assess whether this complex can enter the catalytic cycle, we examined **2b-pic** as a catalyst for the C(sp^2)–H iodination reaction in Scheme 3.9.

Scheme 3.9 Catalytic Competence of σ-aryl Ni^{II} Complex
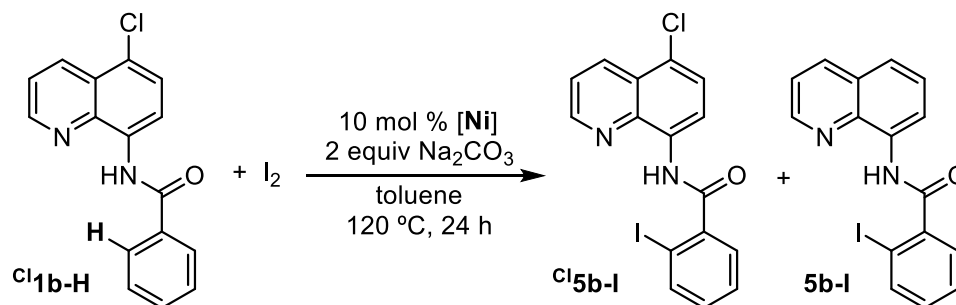
The use of 10 mol % of **2b-pic** afforded 48% yield of ^{Cl}**5b-I** along with 0.6% of **5b-I** (derived from **2b-pic**; Scheme 3.9). For comparison, in our hands the analogous reaction with Ni(OTf)$_2$ afforded ^{Cl}**5b-I** in 47% yield. These results demonstrate that the σ-aryl Ni^{II} complex is catalytically competent for this transformation.

Table 3.2 Catalytic Competence of σ-aryl Ni^{II} Complex for Intramolecular C(sp^2)–H Iodination

entry	[Ni]	Yield ^{Cl}5b-I	Yield 5b-I
1	**Ni(OTf)₂**	**48%**	–
2	**2b-pic**	**47%**	**0.6%**

3.2.4 *Methylation of σ-alkyl Ni^{II} complex*

Scheme 3.10 Reaction of **2a-pic** with 5 equiv of CH$_3$I in MeCN-d_3 at 90 °C
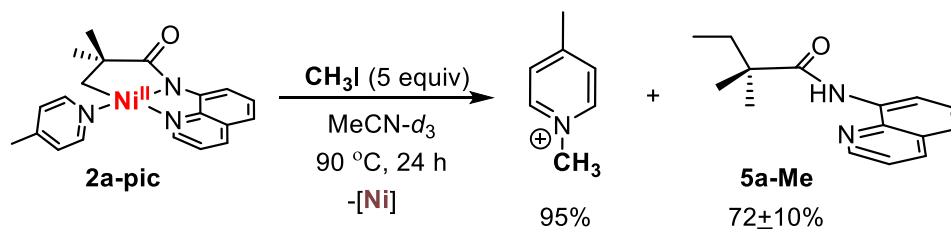
In attempts to isolate Ni^{IV} complexes, similar methylation studies with CH$_3$I were performed with **2a-pic** as compared to **2a-PEt$_3$** in Chapter 2. The reaction of **2a-pic** with 5 equiv of CH$_3$I in MeCN-d_3 showed the formation of methylated 4-picoline, $^{4\text{-Me}}$Py–Me$^+$, over 24 h at 90 °C. The methylated 4-picoline salt was characterized by ^{1}H NMR spectroscopy based on a diagnostic singlet at 4.44 ppm. Its identity was confirmed by comparing to an independently isolated sample of this product. The pyridinium salt was formed in 95% yield after 24 h at 90 °C along with the ligand-methylation product **5a-Me** in 72±10% yield[1]. Notably, the high yield of this methylated product is in striking contrast to that observed with **2a-PEt$_3$** in Chapter 2, where **5a-Me** was observed in trace yield even with excess (5 equiv) of CH$_3$I, under similar conditions. This latter product is readily identified based on a characteristic triplet at 0.81 ppm ($J = 7.5$ Hz) in the ^{1}H NMR spectrum, and its identity was confirmed by comparing to an independently isolated sample of this product. Overall, this striking difference in reactivity between **2a-PEt$_3$** and **2a-pic** is likely due to the nature of the supporting ligand. The mechanistic details of this reaction can be a target of future mechanistic investigations.

Figure 3.9 ^{1}H NMR spectrum of reaction of **2a-pic** with 5 equiv of CH$_3$I in MeCN-d_3 at 90 °C after 24 h

---
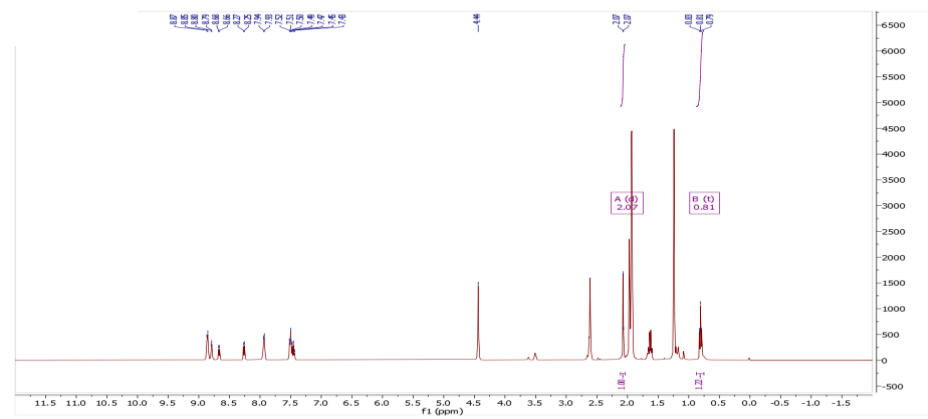
[1] The yield of this reaction was quantified using the internal standard of the NMR instrument. Later, studies had revealed high error bars in estimation of yield via this method as represented by the ±10%, as had been noted for similar reactions of **2a-pic** and **2b-pic** with I$_2$.

3.3 Conclusions

Overall, this chapter describes the synthesis of picoline-ligated Ni^{II} complexes via ligand exchange reactions. These Ni^{II} complexes react with I_2 at room temperature to afford $C(sp^3)$–N and $C(sp^2)$–I coupled products. Furthermore, these complexes were also shown to be relevant to catalytic $C(sp^2)$–H and $C(sp^3)$–H functionalization reactions with I_2 as the oxidant. These studies suggest that direct electrophilic cleavage of the Ni^{II}–C bond is plausible with I_2 or the intermediacy of other high-valent intermediates. Since, these studies did not definitively rule out the reactivity from higher valent Ni intermediates, the next chapter deals with the isolation and reactivity from isolated Ni^{III} complexes. More broadly, this study opens the door for further detailed interrogations of organometallic intermediates in Ni-catalyzed C–H functionalization reactions on a catalytically relevant scaffold.

3.4 References

(1)   Shabashov, D.; Daugulis, O. Auxiliary-Assisted Palladium-Catalyzed Arylation and Alkylation of sp ^{2} and sp ^{3} Carbon−Hydrogen Bonds. *Journal of the American Chemical Society* **2010**, *132* (11), 3965–3972. https://doi.org/10.1021/ja910900p.

(2)   T. Nadres, E.; Ivan Franco Santos, G.; Shabashov, D.; Daugulis, O. Scope and Limitations of Auxiliary-Assisted, Palladium-Catalyzed Arylation and Alkylation of Sp2 and Sp3 C–H Bonds. *The Journal of Organic Chemistry* **2013**, *78* (19), 9689–9714. https://doi.org/10.1021/jo4013628.

(3)   Gandeepan, P.; Müller, T.; Zell, D.; Cera, G.; Warratz, S.; Ackermann, L. 3d Transition Metals for C–H Activation. *Chemical Reviews* **2018**, *119* (4), 2192–2452. https://doi.org/10.1021/acs.chemrev.8b00507.

(4)   Khake, S. M.; Chatani, N. Chelation-Assisted Nickel-Catalyzed C-H Functionalizations. *Trends in Chemistry* **2019**, *1* (5), 524–539. https://doi.org/10.1016/j.trechm.2019.06.002.

(5)   Y Aihara, N. C. Nickel-Catalyzed Direct Alkylation of C–H Bonds in Benzamides and Acrylamides with Functionalized Alkyl Halides via Bidentate-Chelation Assistance. *J. Am. Chem. Soc.* **2013**, *135* (14), 5308–5311. https://doi.org/10.1021/ja401344e.

(6)   Aihara, Y.; Chatani, N. Nickel-Catalyzed Direct Arylation of C(Sp3)–H Bonds in Aliphatic Amides via Bidentate-Chelation Assistance. *Journal of the American Chemical Society* **2014**, *136* (3), 898–901. https://doi.org/10.1021/ja411715v.

(7)   Omer, H. M.; Liu, P. Computational Study of Ni-Catalyzed C–H Functionalization: Factors That Control the Competition of Oxidative Addition and Radical Pathways. *Journal of the American Chemical Society* **2017**, *139* (29), 9909–9920. https://doi.org/10.1021/jacs.7b03548.

(8)   Dawson Beattie, D.; C. Grunwald, A.; Perse, T.; L. Schafer, L.; A. Love, J. Understanding Ni(II)-Mediated C(Sp3)–H Activation: Tertiary Ureas as Model Substrates. *Journal of the American Chemical Society* **2018**, *140* (39), 12602–12610. https://doi.org/10.1021/jacs.8b07708.

(9)   Heberer, N.; Hu, C.-H.; Mirica, L. M. 6.09 - High-Valent Ni Coordination Compounds. In *Comprehensive Coordination Chemistry III*; Constable, E. C., Parkin, G., Que Jr, L., Eds.; Elsevier: Oxford, 2021; pp 348–374. https://doi.org/https://doi.org/10.1016/B978-0-08-102688-5.00104-5.

(10)   Nebra, N. High-Valent NiIII and NiIV Species Relevant to C–C and C–Heteroatom Cross-Coupling Reactions: State of the Art. *Molecules* **2020**, *25* (5). https://doi.org/10.3390/molecules25051141.

(11)   Aihara, Y.; Chatani, N. Nickel-Catalyzed Reaction of C–H Bonds in Amides with I2: Ortho-Iodination via the Cleavage of C(Sp2)–H Bonds and Oxidative Cyclization to β-Lactams via the Cleavage of C(Sp3)–H Bonds. *ACS Catalysis* **2016**, *6* (7), 4323–4329. https://doi.org/10.1021/acscatal.6b00964.

(12)   Lapointe, S.; Vabre, B.; Zargarian, D. POCOP-Type Pincer Complexes of Nickel: Synthesis, Characterization, and Ligand Exchange Reactivities of New Cationic Acetonitrile Adducts. *Organometallics* **2015**, *34* (14), 3520–3531. https://doi.org/10.1021/acs.organomet.5b00272.

(13)   Zhang, S.-Y.; Li, Q.; He, G.; Nack, W. A.; Chen, G. Pd-Catalyzed Monoselective *Ortho* -C–H Alkylation of *N* -Quinolyl Benzamides: Evidence for Stereoretentive Coupling of

Secondary Alkyl Iodides. *Journal of the American Chemical Society* **2015**, *137* (1), 531–539. https://doi.org/10.1021/ja511557h.

(14) Deb, A.; Hazra, A.; Peng, Q.; Paton, R. S.; Maiti, D. Detailed Mechanistic Studies on Palladium-Catalyzed Selective C–H Olefination with Aliphatic Alkenes: A Significant Influence of Proton Shuttling. *Journal of the American Chemical Society* **2017**, *139* (2), 763–775. https://doi.org/10.1021/jacs.6b10309.

3.5 Experimental Procedures

3.5.1 General Procedures, Materials and Methods

General Procedures

NMR spectra were recorded on a Varian VNMRS 600 (600 MHz for ^{1}H and 151 MHz for ^{13}C). ^{1}H and ^{13}C NMR chemical shifts are reported in parts per million (ppm) and are referenced to the solvent lock. ^{1}H NMR quantification was conducted using internal standards as mentioned in the experimental procedures. Abbreviations used to report NMR peaks: singlet (s); doublet (d); triplet (t); quartet (q); doublet of doublets (dd); triplet of doublets (td); doublet of triplets (dt); multiplet (m). GC-FID data were collected on a Shimadzu 17A GC using a Restek Rtx®-5 (crossbond 5% diphenyl–95% dimethyl polysiloxane; 15 m, 0.25 mm ID, 0.25 µm df) column. High-resolution mass spectra were recorded on a Micromass AutoSpec Ultima Magnetic Sector mass spectrometer. Cyclic voltammetry was performed using a CHI600C potentiostat from CH Instruments. EPR spectra were collected at temperatures mentioned in the experimental procedures using a Bruker EMX ESR Spectrometer with a nitrogen-cooled cryostat. Elemental analyses were performed by Midwest Microlab located in Indianapolis. X-ray crystallographic data were obtained on a Rigaku AFC10K Saturn 944+ CCD-based X-ray diffractometer. Chromatographic separations were carried out on a Biotage Isolera One system using Sfär Silica HC D (High-capacity Duo 20 µm) columns (10 g, 25 g, or 50 g cartridges depending on the scale of isolations), as mentioned in the synthetic procedures.

Acronyms: Dichloromethane (DCM), Tetrahydrofuran (THF), Water in NMR solvent (HDO), Tetramethylsilane (TMS), Nitromethane (CH_3NO_2), residual moisture in solvent (HDO)

Note: All ^{1}H NMR spectra of nickel complexes and their reactivity studies with iodine (I_2) were recorded on a 600 MHz Varian Vnmrs instrument with a 100% lock efficiency and a relaxation

delay of 25 s at 25 °C. These specifications are crucial for proper quantification and analysis as we have noted high T1 relaxation times for the nickel complexes.

Materials and Methods

All commercial reagents were used as received without further purification unless otherwise noted. [Ni(PEt$_3$)$_4$] was prepared via literature procedures.[1] Bis(1,5-cyclooctadiene)nickel(0) ([Ni(COD)$_2$]) was purchased from Strem Chemical, 2,2-dimethylsuccinic anhydride and 8-aminoquinoline from Ark Pharm. Tetramethylammonium acetate (TMAOAc) from TCI America. Nickel(II) acetate (Ni(OAc)$_2$), nickel(II) trifluoromethanesulfonate 96% (Ni(OTf)$_2$), silver(I) carbonate (Ag$_2$CO$_3$), triethylphosphine (PEt$_3$), triethylamine (Et$_3$N) and acetonitrile (electronic grade) were purchased from Millipore-Sigma or Aldrich. All deuterated solvents were obtained from Cambridge Isotope Laboratories and deaerated via a nitrogen sparge prior to storage over activated 4 Å molecular sieves (EMD Millipore). Anhydrous N,N-dimethylformamide and acetone were purchased from Acros Organics in AcroSeal® bottles. Anhydrous benzene was purchased from Alfa Aesar and ethanol from VMR international. Pentane (Fisher), diethyl ether (Millipore-Sigma), tetrahydrofuran (Fisher), and toluene (Fisher) were deaerated via a nitrogen sparge and further purified using a solvent purification system for usage inside the glovebox. Sodium carbonate, potassium carbonate, sodium sulfate, hexanes, diethyl ether, ethyl acetate, dichloromethane, sulfuric acid (Certified ACS Plus) and glacial acetic acid were purchased from Fisher. Celite was purchased from Aqua Solutions and was dried under vacuum at 150 °C for 24 h for usage inside the glovebox. All glassware used in the glovebox was dried in an oven at 150 °C for at least 6 h and cooled under an inert atmosphere. All experiments and synthetic procedures were setup inside a nitrogen-filled glovebox unless otherwise mentioned.

3.5.2 Synthesis and Characterization of Organic Molecules

All synthesis in this subsection was performed outside the glovebox. All modified reaction procedures and confirmation of characterization data were referenced against previous literature reports as cited.

X = H: **5a-N**
X = Cl: **Cl5a-N**
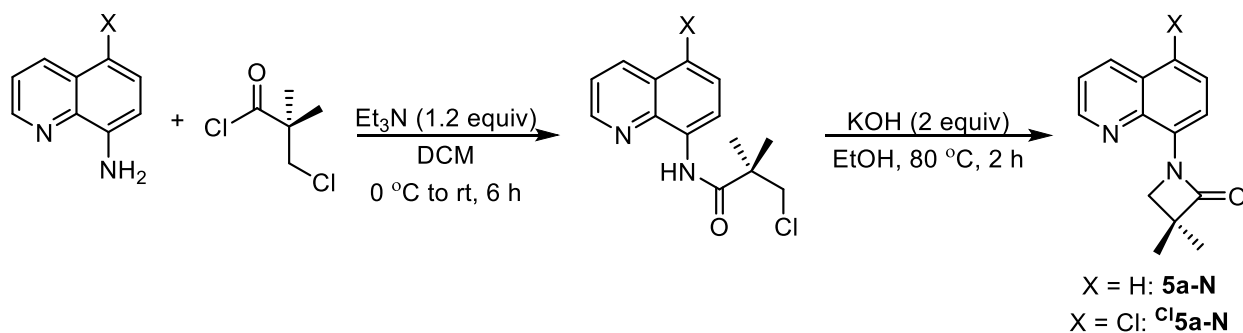
5a-N and **Cl5a-N**: A 1 M solution of 3-chloro-2,2-dimethylpropionyl chloride in DCM (2.2 mL, 2.2 mmol, 1.1 equiv) was slowly added to a solution of 5-chloro-8-aminoquinoline (0.36 g, 2 mmol, 1.0 equiv) or 8-aminoquinoline (0.29 g, 2 mmol, 1.0 equiv) in DCM (10 mL) cooled in an ice bath. The resulting solution was stirred for 6 h at room temperature. The reaction was quenched with water (30 mL) and extracted with DCM (3 x 20 mL). The organic extracts were combined, dried over anhydrous sodium sulfate, concentrated under vacuum. The resulting crude material was carried forward to the next step without further purification.

The crude product was dissolved in ethanol (3 mL), and potassium hydroxide (0.22 g, 4 mmol, 2.0 equiv) was added in a 4 mL glass vial equipped with a magnetic stir-bar. The vial was sealed with a Teflon-lined screw cap and heated in a hot plate at 80 °C for 2 h. The reaction was cooled to room temperature, quenched with water (10 mL), and extracted with diethyl ether (3 x 20 mL). The organic extracts were combined, dried over anhydrous sodium sulfate, and concentrated under vacuum. The crude product was purified by chromatography using a Sfär Silica HC D (High-capacity Duo 20 µm) 50 g cartridge on a Biotage Isolera One system (hexanes : DCM, gradient

79

from 80:20 to 10:90). This afforded compound **5a-N** as a white solid (0.28 g, 63% yield) or [Cl]**5a-N** as a white solid (0.36 g, 70% yield). The ^{1}H NMR spectra of the products matched those reported in the literature.[7,8]

X = H: **5b-I**
X = Cl: [Cl]**5b-I**
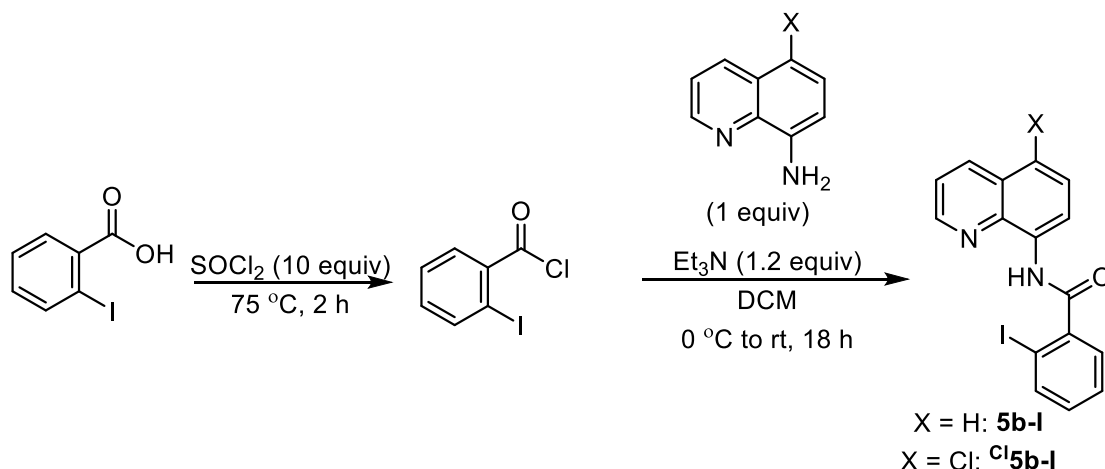
5b-I and [Cl]**5b-I**: 2-Iodobenzoic acid (0.27 g, 2.2 mmol, 1.1 equiv) was weighed out in a 4 mL glass vial and then dissolved in thionyl chloride (1.60 mL, 22 mmol, 11 equiv). The vial was sealed with a Teflon-lined screw cap and heated on a hot plate at 75 °C for 2 h. The excess thionyl chloride was removed under vacuum to afford a tan oil. This crude material was then diluted with DCM (2 mL), and the resulting solution added dropwise to a solution of 5-chloro-8-aminoquinoline (0.36 g, 2 mmol, 1.0 equiv) in DCM (10 mL) cooled in an ice bath. To this mixture, triethylamine (0.45 mL, 3 mmol, 1.5 equiv) was added, and the resulting mixture was stirred overnight for 18 h at room temperature. The reaction was quenched with water (20 mL) and extracted with DCM (3 x 20 mL). The organic extracts were combined, dried over anhydrous sodium sulfate, and concentrated under vacuum. The crude product was purified by chromatography using a Sfär Silica HC D (High-capacity Duo 20 µm) 25 g cartridge on a Biotage Isolera One system (hexanes : DCM, gradient from 80:20 to 10:90). This afforded compound [Cl]**5b-I** as a white solid (0.51 g, 62% yield). The ^{1}H NMR spectra of the products matched those reported in the literature.[6]

3.5.3 Synthesis and Characterization of Nickel Complexes
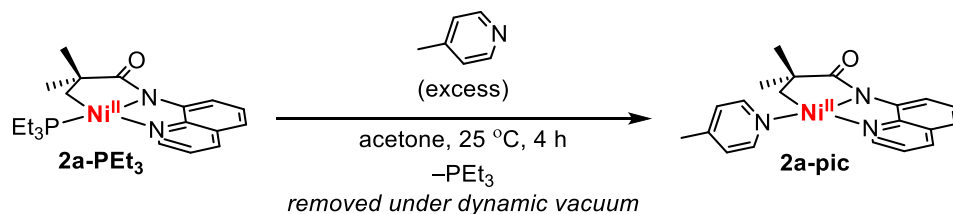
2a-PEt₃ (403 mg) was weighed into a 20 mL vial and dissolved in acetone (10 mL). 4-Picoline

(0.3 mL, 287 mg, 3.1 mmol, 3.1 equiv) was added, the reaction was stirred for 5 min, and the

solvent was slowly removed under vacuum while stirring . This procedure was repeated three times

to afford a dark-red gummy residue. This residue was washed with diethyl ether (3 x 15 mL). The

resulting orange solid was dissolved in acetone (5 mL) and precipitated with a 3:2 mixture of

pentane: diethyl ether (10 mL). This precipitation was repeated twice to afford **2a-pic** as a dark

yellow powder (352 mg, 93% yield from **2a-PEt₃**; 81% overall yield). Complex **2a-pic** was

characterized via ^{1}H and ^{13}C NMR spectroscopy. A single crystal was obtained by vapor diffusion

of pentane into an acetone solution of **2a-pic**.

^{1}H NMR (600 MHz, acetone-d_6) δ 9.01 (s, 2H), 8.85 (d, J = 7.8 Hz, 1H), 8.35 (dd, J = 7.8, 2.1 Hz,

1H), 7.44-7.33 (m, 5H), 7.26 (d, J = 8.1 Hz, 1H), 2.45 (s, 3H), 1.12 (s, 6H), 0.94 (s, 2H).

^{13}C NMR (151 MHz, acetone-d_6) δ 191.40, 152.31, 150.19, 148.89, 146.03, 145.66, 138.17,

130.11, 129.80, 127.12, 122.49, 119.60, 117.23, 48.22, 30.77, 27.71, 21.13.

^{1}H NMR (600 MHz, Benzene-d_6) δ 9.86 (d, J = 7.8 Hz, 1H), 8.22 (d, J = 5.7 Hz, 2H), 7.47 (d, J =

8.2 Hz, 1H), 7.35 (t, J = 8.0 Hz, 1H), 6.86 (d, J = 8.0 Hz, 1H), 6.80 (d, J = 4.7 Hz, 1H), 6.39 (dd,

J = 8.2, 4.8 Hz, 1H), 6.16 (d, J = 5.7 Hz, 2H), 1.81 (s, 6H), 1.55 (s, 3H), 1.34 (s, 2H).

^{13}C NMR (151 MHz, Benzene-d_6) δ 190.20, 151.14, 149.04, 147.48, 145.51, 143.33, 136.83,

130.39, 129.30, 125.25, 120.68, 120.23, 115.94, 48.32, 30.93, 28.59, 20.39.

Elemental analysis: calculated for $C_{20}H_{21}N_3NiO$, C: 63.53, H: 5.60, N:11.11; Found: C: 63.87, H: 5.72, N: 11.15

HRMS-electrospray (m/z): [M$^+$] calcd. for $C_{20}H_{21}N_3NiO$, 377.1038; found, 378.1114 [M+H]
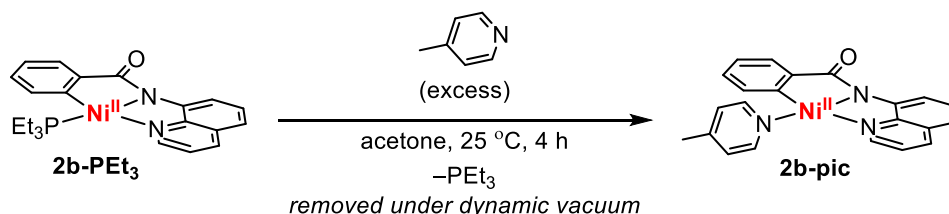
2b-PEt₃ (423 mg, 1 mmol, 1 equiv) was weighed into a 20 mL vial and dissolved in acetone (10 mL). 4-Picoline (0.3 mL, 287 mg, 3.1 mmol, 3.1 equiv) was added, the reaction was stirred for 5 min, and then the solvent was slowly removed under vacuum while stirring. This procedure was repeated five times to afford a dark-red gummy residue. This residue was washed with a 1:1 mixture of pentane/diethyl ether (3 x 15 mL). The resulting yellow-orange solid was dissolved in acetone (5 mL) and precipitated with a 3:2 mixture of pentane: diethyl ether (10 mL). This precipitation was repeated twice to afford **2b-pic** as a dark yellow powder (322 mg, 81% yield from **2b-PEt₃**; 71% yield overall). Complex **2b-pic** was characterized via ^{1}H and ^{13}C NMR spectroscopy. A single crystal was obtained by slow vapor diffusion of pentane into a THF solution of **2b-pic**.

^{1}H NMR (600 MHz, acetone-d_6) δ 9.31-9.16 (m, 2H), 8.88 (d, J = 7.8 Hz, 1H), 8.37 (dd, J = 8.2, 1.5 Hz, 1H), 7.58 (d, J = 5.8 Hz, 2H), 7.47 (t, J = 7.9 Hz, 1H), 7.35 (dd, J = 8.2, 4.9 Hz, 1H), 7.31 -7.24 (m, 2H), 7.20 (dd, J = 5.0, 1.6 Hz, 1H), 6.92 (t, J = 7.3 Hz, 1H), 6.77 (td, J = 7.3, 1.6 Hz, 1H), 5.71 (d, J = 7.3 Hz, 1H), 2.56 (s, 3H).

^{13}C NMR (151 MHz, acetone-d_6) δ 177.67, 152.75, 151.59, 150.33, 149.46, 148.42, 146.78, 146.28, 139.02, 134.27, 130.46, 130.23, 129.74, 127.80, 125.54, 124.88, 122.70, 118.65, 116.95, 21.33.

Elemental analysis: calculated for $C_{22}H_{17}N_3NiO$, C: 66.38, H: 4.30, N: 10.56; Found: C: 66.67, H: 4.32, N: 10.58

HRMS-electrospray (m/z): [M$^+$] calcd. for $C_{22}H_{17}N_3NiO$, 397.0725; found, 398.0806 [M+H]

3.5.4 Reactivity of Nickel Complexes
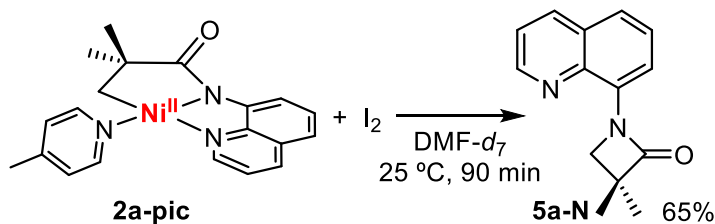
Complex **2a-pic** (3.8 mg, 10 µmol, 1 equiv) was weighed into a 4 mL glass vial and dissolved in DMF-d_7 (0.5 mL) containing tetramethylsilane (0.9 mg, 10 µmol) as an internal standard. The sample was transferred an NMR tube that was sealed with a Teflon septa-lined screw cap. Traces of undissolved **2a-pic** was noted in the vial; to correct for any changes in concentration as a result, an NMR spectrum was recorded at this stage, and the ratio of **2a-pic** : tetramethylsilane standard was quantified. The NMR tube was transferred back into the glovebox, and I$_2$ (0.1 mL of a 0.118 M stock solution in DMF-d_7, 11.8 µmol, 1.18 equiv) was added. This addition resulted in an immediate color change from orangish-yellow to purplish-red. The NMR tube was vigorously shaken to ensure immediate and thorough mixing and was then removed from the glovebox and analyzed by ^{1}H NMR spectroscopy at 30 min intervals. The yield of **5a-N** was quantified by ^{1}H NMR spectroscopy to be 65% after 90 min as determined by relative integration values as based on the internal standard (TMS). NMR data are shown below.

2b+I2@90min_TMS_DMF_1H_stacked-with-authentic-3b-H

2b+I2@90min_TMS_DMF_1H_stacked-with-authentic-3b-H
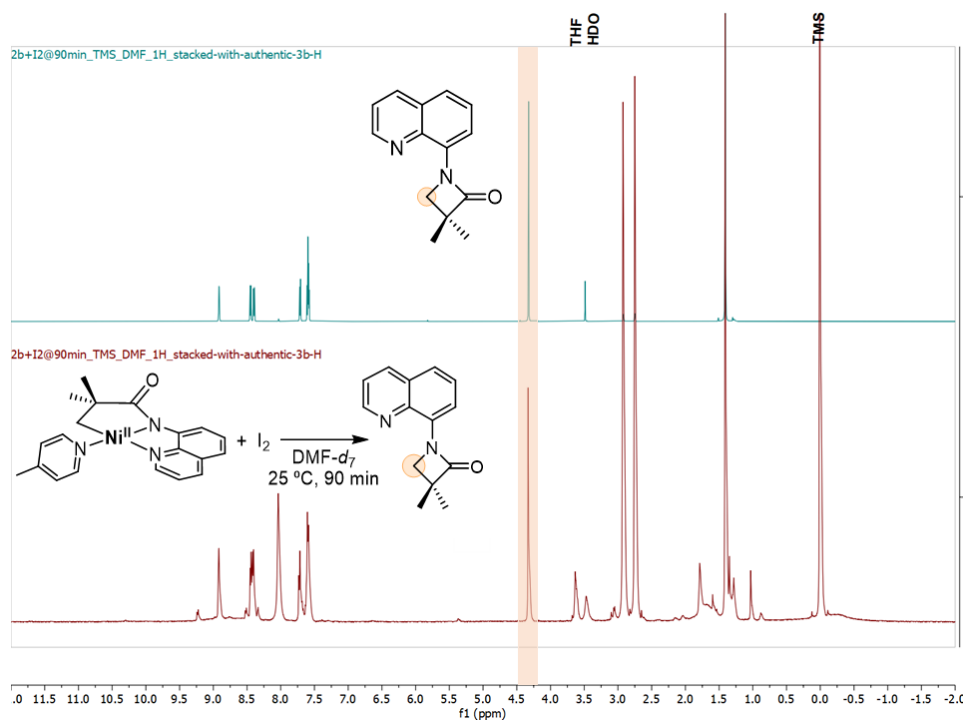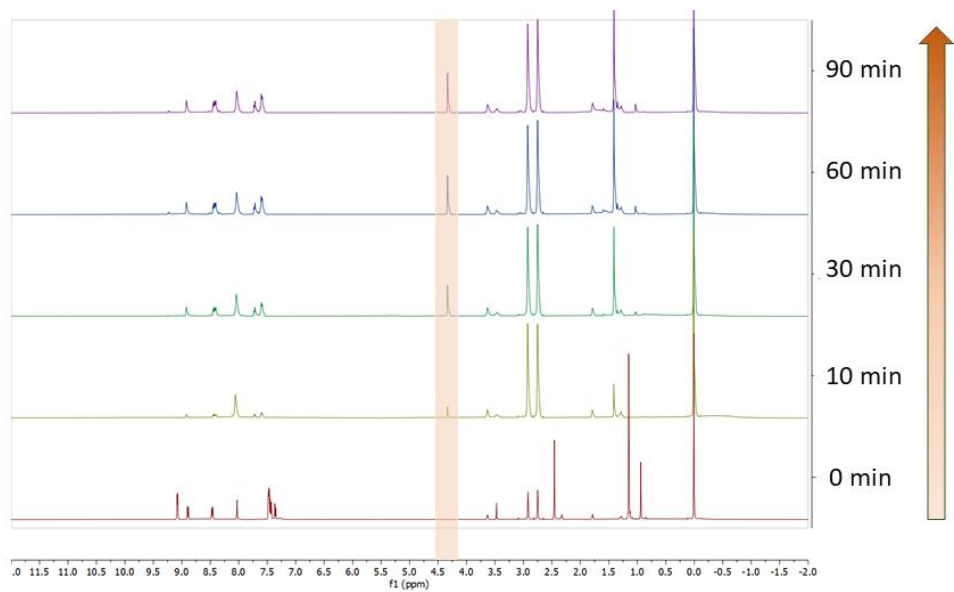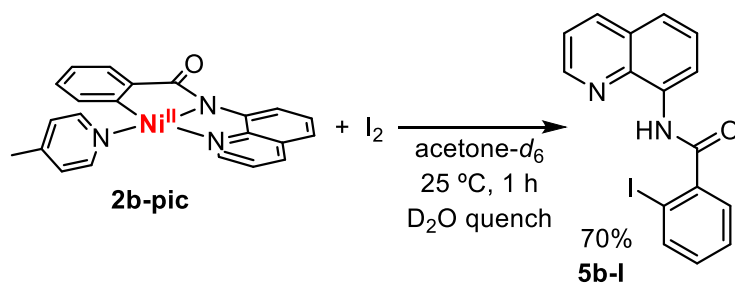
Complex **2b-pic** (4.0 mg, 10 µmol, 1 equiv) was weighed into a 4 mL glass vial and dissolved in acetone-d_6 (0.5 mL) containing CH_3NO_2 (1.2 mg, 20 µmol) as an internal standard. The sample was transferred into an NMR tube that was sealed with a Teflon septum-lined screw cap. Traces of undissolved **2b-pic** were noted to remain in the vial; to correct for any changes in concentration as a result, an NMR spectrum was recorded at this stage, and the ratio of **2b-pic** : CH_3NO_2 standard was quantified. The NMR tube was transferred back into the glovebox, and I_2 (0.1 mL of a 0.118 M stock solution in acetone-d_6, 11.8 µmol, 1.18 equiv) was added. This addition resulted in an immediate color change from orangish-yellow to purplish-red. The tube was vigorously shaken to ensure immediate and thorough mixing. The reaction was allowed to stand at room temperature for 1 h and was then removed from the glovebox and analyzed by ^{1}H NMR spectroscopy.

D_2O (0.05 mL, 55.5 mg, 2.77 mmol) was added to the NMR tube by puncturing the septum of the cap. The NMR tube was shaken vigorously to facilitate proper and immediate mixing and a slight fade in color was noted. A ^{1}H NMR spectra was recorded, which showed the formation of product **5b-I** in 70% yield as determined by relative integration values based on the internal standard. NMR data are shown in figure below.

Before D$_2$O quench

After D$_2$O quench
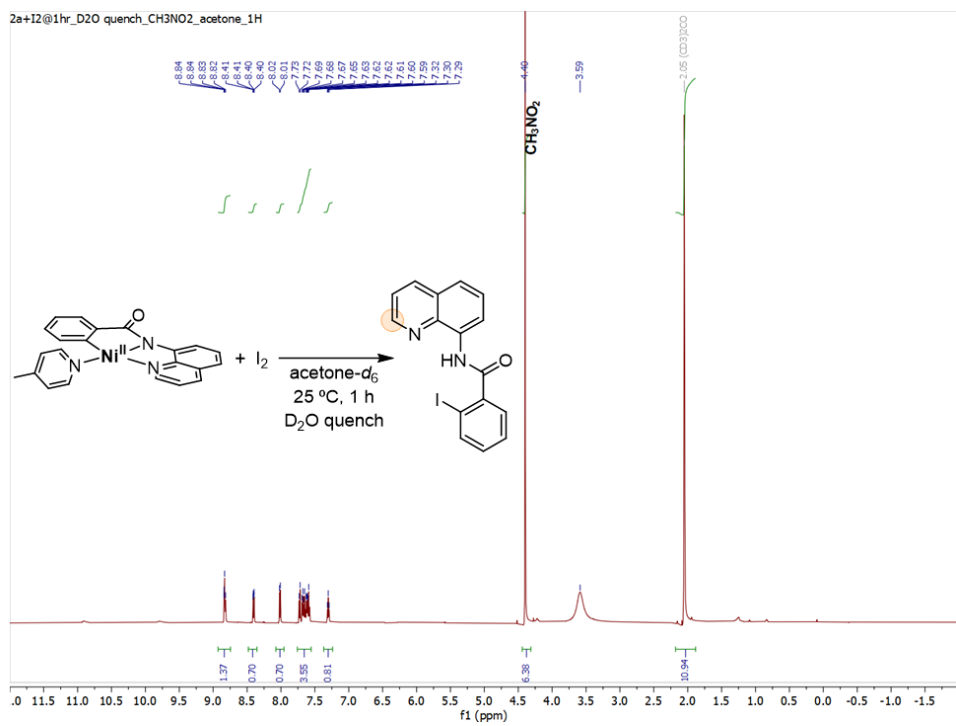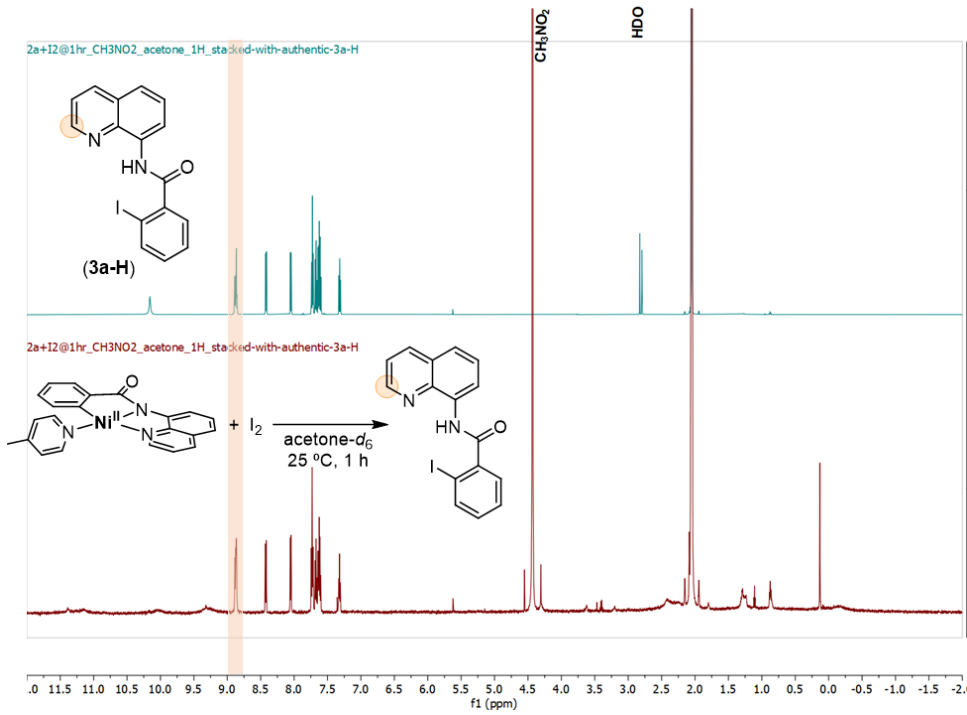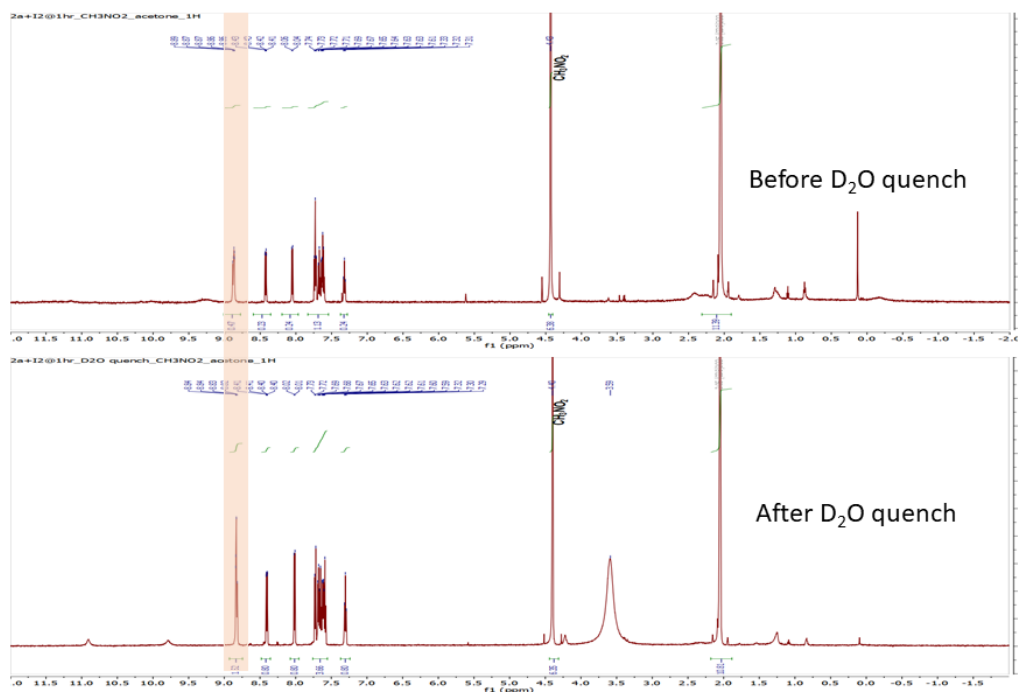
3.5.5 Catalytic Relevance of Nickel Complexes

Catalytic Relevance of 2a-pic: GC data
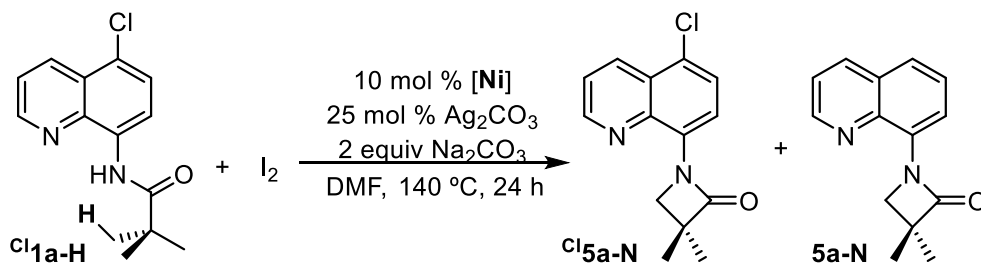
Entry 1: In a glove box, N-(5-chloroquinolin-8-yl)-pivalamide ^{Cl}**1a-H** (39 mg, 0.15 mmol, 1 equiv), iodine (76 mg, 0.3 mmol, 2 equiv), Ni(OTf)$_2$ (5.3 mg, 0.015 mmol, 0.1 equiv), Ag$_2$CO$_3$ (10 mg, 0.0375 mmol, 0.25 equiv), Na$_2$CO$_3$ (32 mg, 0.3 mmol, 2 equiv), and DMF (0.5 mL) were combined in an oven-dried 4 mL vial equipped with a magnetic stirbar. The vial was equipped with a reflux condenser, the mixture was placed under an N$_2$ atmosphere, and the reaction was stirred for 24 h at 140 °C. The reaction mixture was cooled to room temperature, quenched with DI water (1 mL), and diluted with 3 mL of a 50 mM (0.15 mmol) stock solution of 1,3,5-trimethoxybenzene (standard) in DCM. The resulting mixture was filtered through a Celite pad, and the Celite was washed with of DCM (2-3 mL). The yields of **5a-N** and ^{Cl}**5a-N** were quantified via gas chromatography.

Entry 2: The same procedure as entry 1, but using **2a-pic** (6 mg, 0.015 mmol) as the [Ni] source.

(a)

(b)

Ratio = 1.38 (PD:SM); yield = 58.0%

Peak#	Ret. Time	Area	Height	Mark	Conc.	Unit	ID#	Name	Area%
	0.479	38768033	22837584		91.325				91.325
	0.606	3187906	2308534	V	7.510				7.510
	3.795	334572	142926		0.788				0.788
	11.073	67189	30184		0.158				0.158
	11.693	92734	39614		0.218				0.218
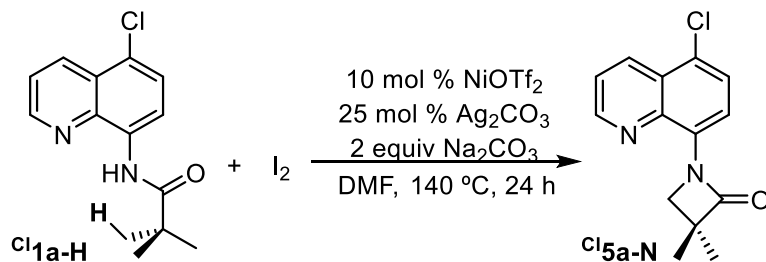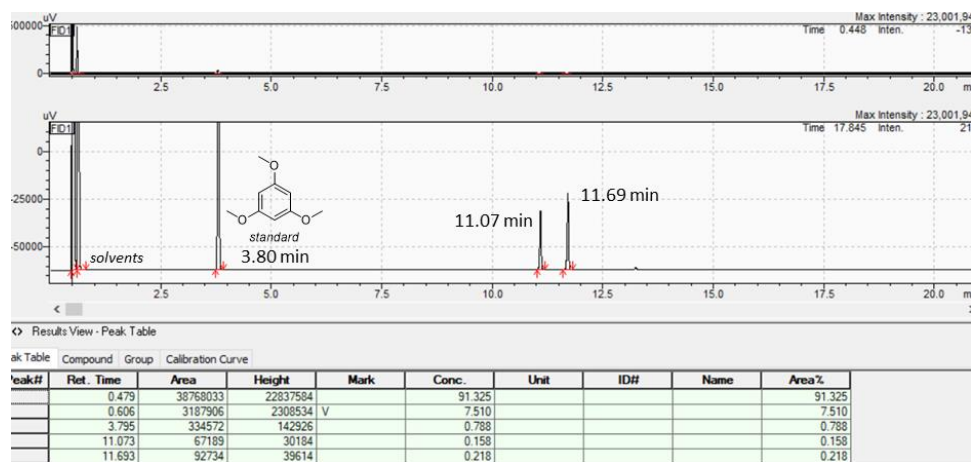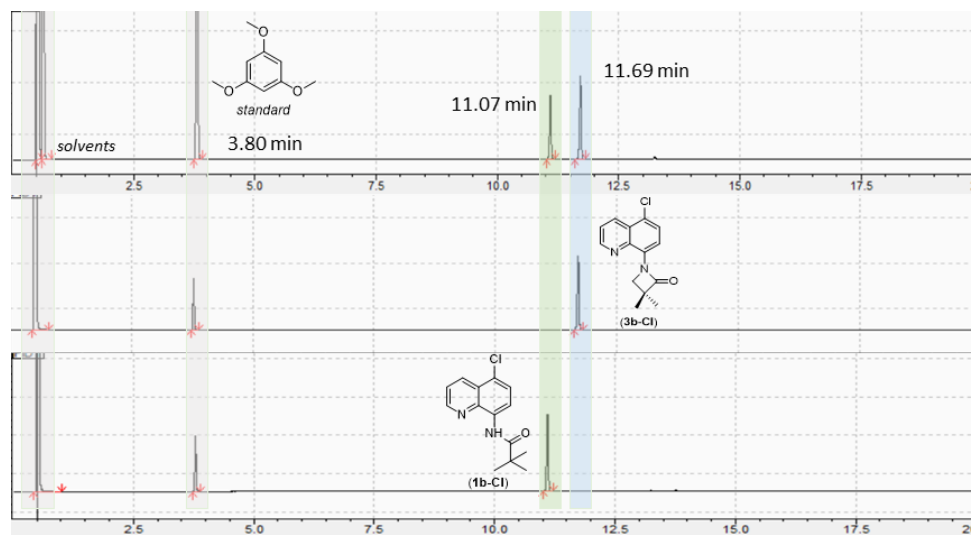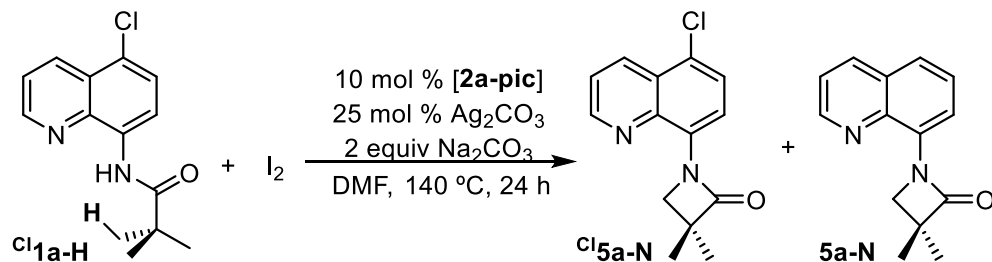
(a)
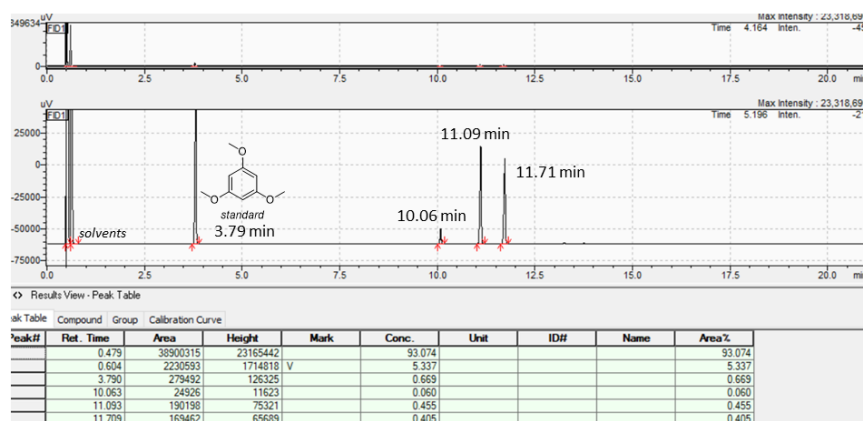
Ratio = 0.891 (PD:SM); yield = 47.1%
Ratio = 0.147 (3b-H:3b-Cl); yield = 6.93%

(b)

91
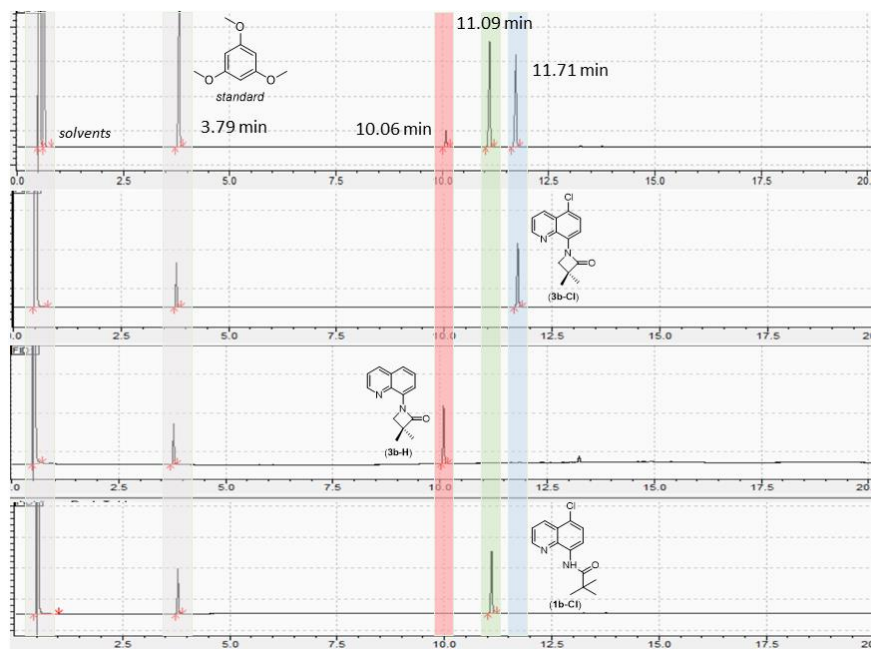
Catalytic Relevance of 2b-pic: GC data
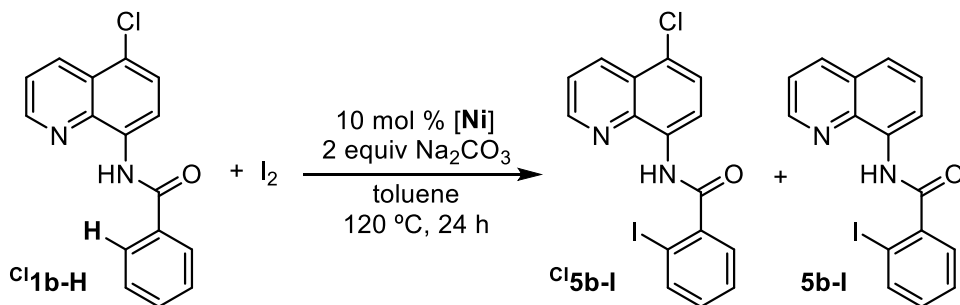
Entry 1: In a glove box, N-(5-chloroquinolin-8-yl)-benzamide ^{Cl}**1b-H** (45 mg, 0.15 mmol, 1 equiv), iodine (76 mg, 0.3 mmol, 2 equiv), Ni(OTf)$_2$ (5.3 mg, 0.015 mmol, 0.1 equiv), Na$_2$CO$_3$ (32 mg, 0.3 mmol, 2 equiv), and toluene (0.7 mL) were combined in an oven-dried 4 mL vial equipped with a magnetic stirbar. The vial was equipped with a reflux condenser, the mixture was placed under an N$_2$ atmosphere, and the reaction was stirred for 24 h at 120 °C. The reaction mixture was cooled to room temperature, quenched with DI water (1 mL), and diluted with 3 mL of a 50 mM (0.15 mmol) stock solution of 1,3,5-trimethoxybenzene (standard) in DCM. The resulting mixture was filtered through a Celite pad, and the Celite was washed with of DCM (2-3 mL). The yields of ^{Cl}**5b-I** and **5b-I** were quantified via gas chromatography.

Entry 2: The same procedure as entry 1, but using **2b-pic** (6 mg, 0.015 mmol) as the [Ni] source.

(a)

(b)
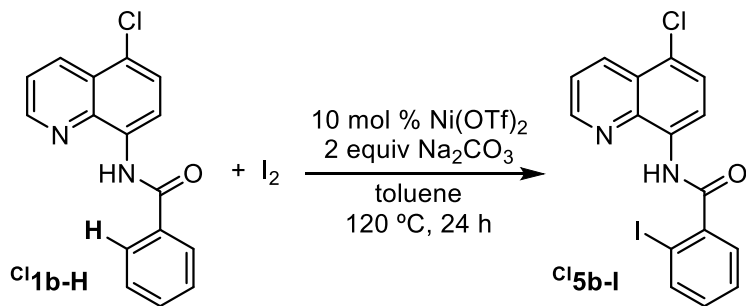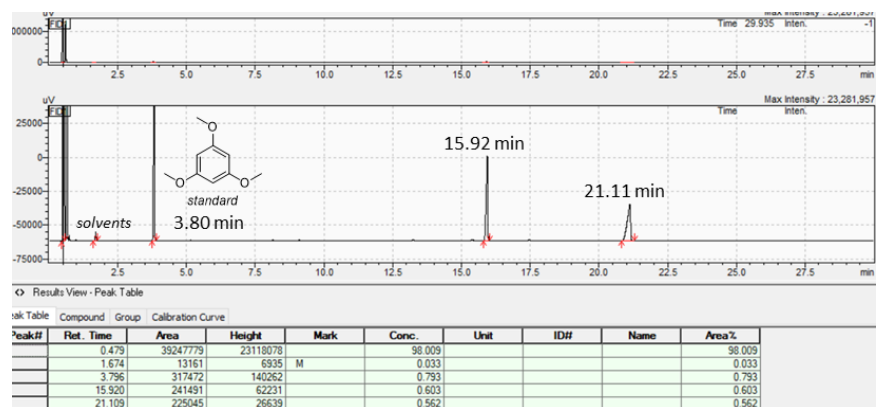
Ratio = 0.932 (PD:SM); yield = 48.2%

93

(a)

(b)

Peak Table | Compound | Group | Calibration Curve

Peak#	Ret. Time	Area	Height	Mark	Conc.	Unit	ID#	Name	Area%
	0.479	39552532	23627282	M	54.096				54.096
	0.596	32432850	24430473	V M	44.359				44.359
	3.815	645180	231983		0.882				0.882
	15.923	240594	63608	M	0.329				0.329
	17.926	2781	741		0.004				0.004
	19.217	18433	1787		0.025				0.025
	21.104	213684	25915	M	0.292				0.292
	25.081	9062	992		0.012				0.012
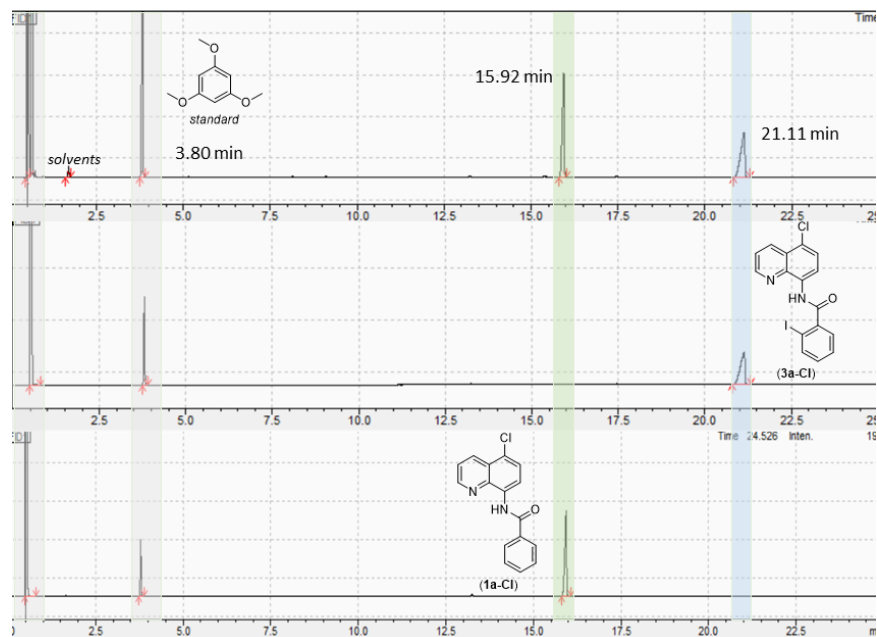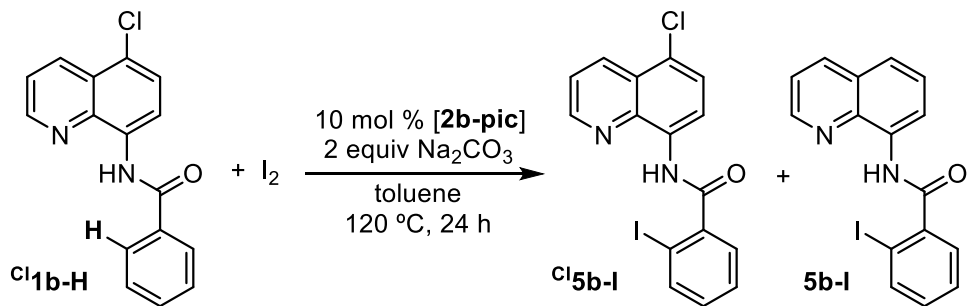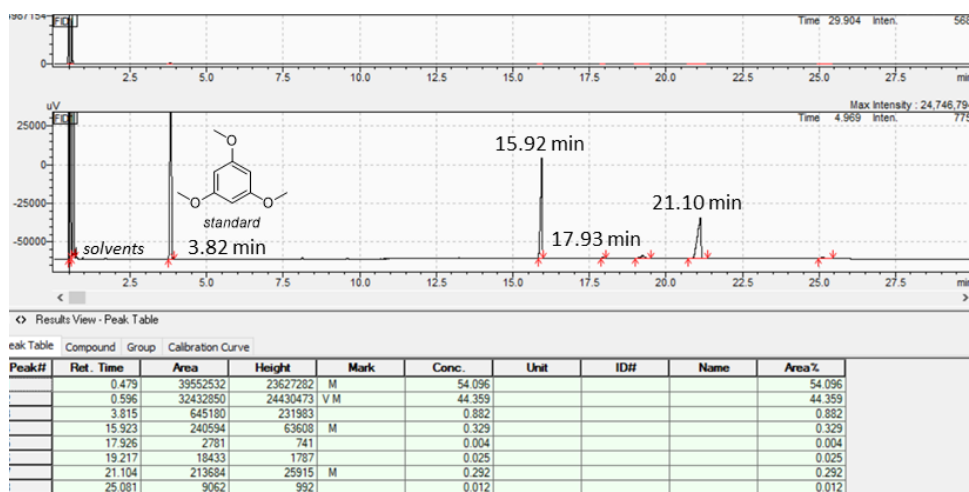
Ratio = 0.888 (PD:SM); yield = 47.0%
Ratio = 0.0130 (3b-H:3b-Cl); yield = 0.612%

Peak Table | Compound | Group | Calibration Curve

Peak#	Ret. Time	Area	Height	Mark	Conc.	Unit	ID#	Name	Area%
	0.479	39552532	23627282	M	54.095				54.095
	0.596	32432850	24430473	V M	44.357				44.357
	3.815	645180	231983		0.882				0.882
	15.923	242850	63840	M	0.332				0.332
	17.926	2781	741		0.004				0.004
	19.217	18433	1787		0.025				0.025
	21.104	213684	25915	M	0.292				0.292
	25.081	9062	992		0.012				0.012

94
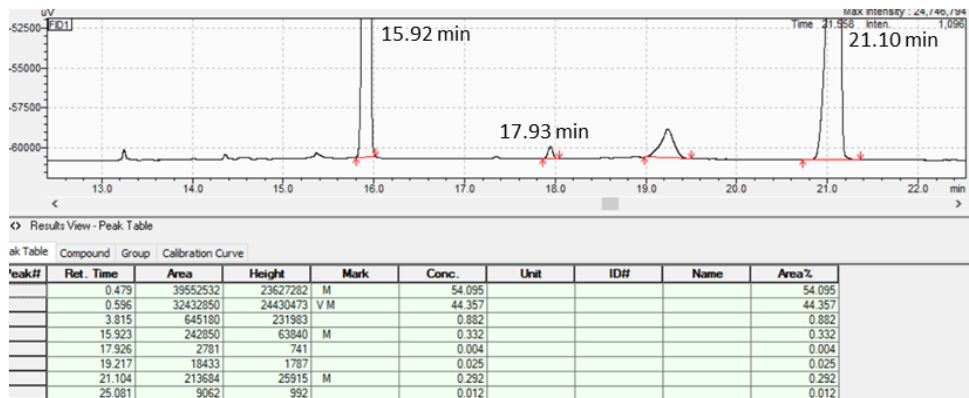
(c)
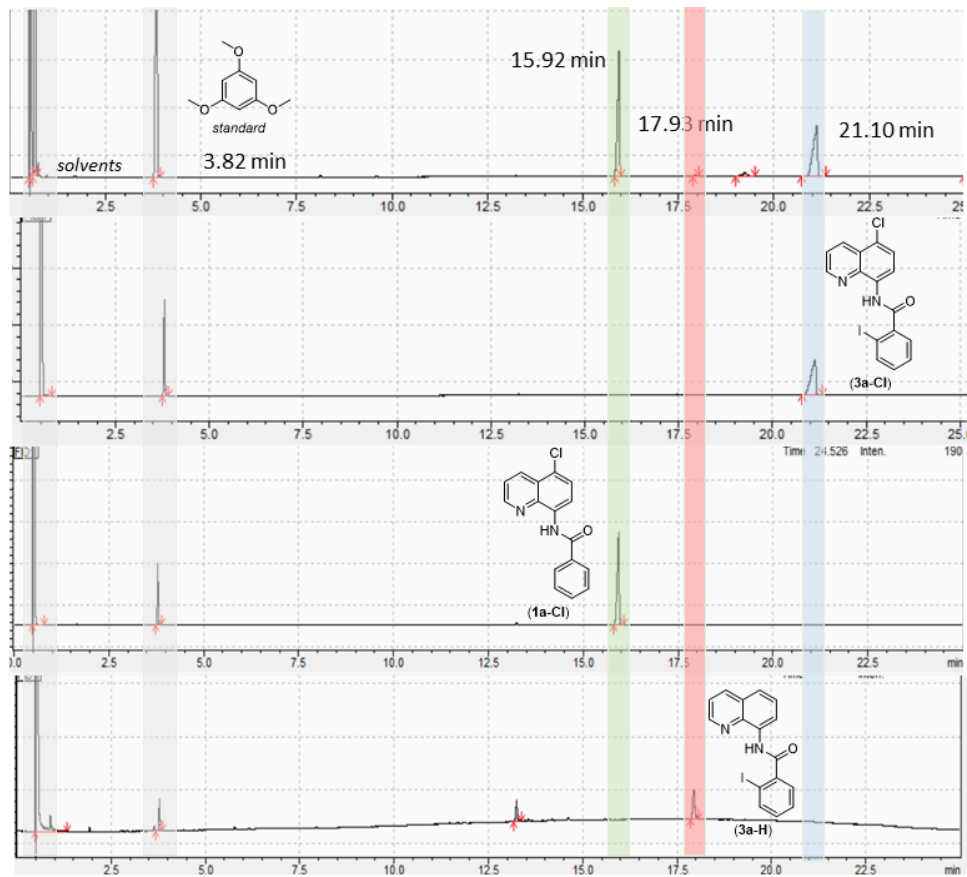
3.5.6 X-Ray Crystallography Data

X-Ray Crystallographic Data of 2a-pic
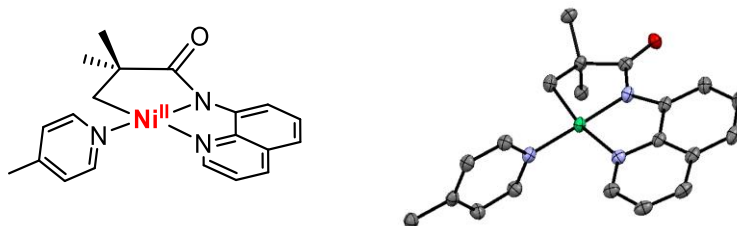
Orange plates of **2a-pic** were grown from a THF/pentane solution of the compound at 23 °C. A crystal of dimensions 0.12 x 0.09 x 0.03 mm was mounted on a Rigaku AFC10K Saturn 944+ CCD-based X-ray diffractometer equipped with a low temperature device and Micromax-007HF Cu-target micro-focus rotating anode (λ = 1.54187 A) operated at 1.2 kW power (40 kV, 30 mA). The X-ray intensities were measured at 85(1) K with the detector placed at a distance 42.00 mm from the crystal. A total of 2028 images were collected with an oscillation width of 1.0° in ω. The exposure times were 1 sec. for the low angle images, 4 sec. for high angle. Rigaku d*trek images were exported to CrysAlisPro for processing and corrected for absorption. The integration of the data yielded a total of 26553 reflections to a maximum 2θ value of 138.62° of which 6429 were independent and 6144 were greater than 2σ(I). The final cell constants (Table 1) were based on the xyz centroids of 17510 reflections above 10σ(I). Analysis of the data showed negligible decay during data collection. The structure was solved and refined with the Bruker SHELXTL (version 2016/6) software package, using the space group P1bar with Z = 4 for the formula $C_{20}H_{21}N_3ONi$. All non-hydrogen atoms were refined anisotropically with the hydrogen atoms placed in idealized positions. Full matrix least-squares refinement based on F^2 converged at R1 = 0.0373 and wR2 = 0.1018 [based on I > 2sigma(I)], R1 = 0.0385 and wR2 = 0.1041 for all data. Additional details

are presented in Table 1 and are given as Supporting Information in a CIF file. Acknowledgement is made for funding from NSF grant CHE-0840456 for X-ray instrumentation.

G.M. Sheldrick (2015) "Crystal structure refinement with SHELXL", Acta Cryst., C71, 3-8 (Open Access).

CrystalClear Expert 2.0 r16, Rigaku Americas and Rigaku Corporation (2014), Rigaku Americas, 9009, TX, USA 77381-5209, Rigaku Tokyo, 196-8666, Japan.

CrysAlisPro 1.171.38.41 (Rigaku Oxford Diffraction, 2015).

Table 3.3 Crystal Data and Structure Refinement for **2a-pic**

Empirical formula	C20 H21 N3 Ni O
Formula weight	378.11
Temperature	85(2) K
Wavelength	1.54184 A
Crystal system, space group	Triclinic, P-1
Unit cell dimensions	a = 9.9239(3) A alpha = 95.269(2)° b = 10.4834(3) A beta = 90.932(2)° c = 17.2050(4) A gamma = 93.893(2)°
Volume	1777.81(9) A^3
Z, Calculated density	4, 1.413 Mg/m^3
Absorption coefficient	1.664 mm^-1
F(000)	792
Crystal size	0.120 x 0.090 x 0.030 mm

Theta range for data collection	2.580 to 69.309°
Limiting indices	-12<=h<=11, -12<=k<=12, -19<=l<=20
Reflections collected / unique	26553 / 6429 [R(int) = 0.0539]
Completeness to theta = 67.684	97.70%
Absorption correction	Semi-empirical from equivalents
Max. and min. transmission	1.00000 and 0.92041
Refinement method	Full-matrix least-squares on F^2
Data / restraints / parameters	6429 / 0 / 458
Goodness-of-fit on F^2	1.014
Final R indices [I>2sigma(I)]	R1 = 0.0373, wR2 = 0.1018
R indices (all data)	R1 = 0.0385, wR2 = 0.1041
Extinction coefficient	0.00068(18)
Largest diff. peak and hole	0.297 and -0.453 e.A^-3

X-Ray Crystallographic Data of 2b-pic
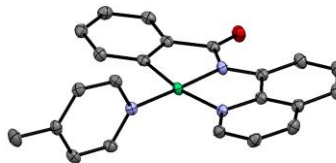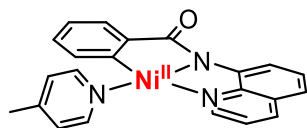
Dark yellow plates of **2b-pic** were grown from a pentane solution of the compound at 23 °C. A crystal of dimensions 0.10 x 0.08 x 0.06 mm was mounted on a Rigaku AFC10K Saturn 944+ CCD-based X-ray diffractometer equipped with a low temperature device and Micromax-007HF Cu-target micro-focus rotating anode (λ = 1.54187 A) operated at 1.2 kW power (40 kV, 30 mA). The X-ray intensities were measured at 85(1) K with the detector placed at a distance 42.00 mm from the crystal. A total of 2028 images were collected with an oscillation width of 1.0° in ω. The exposure times were 1 sec. for the low angle images, 3 sec. for high angle. Rigaku d*trek images were exported to CrysAlisPro for processing and corrected for absorption. The integration of the data yielded a total of 26466 reflections to a maximum 2θ value of 138.95° of which 3364 were independent and 3309 were greater than $2\sigma(I)$. The final cell constants (Table 1) were based on the xyz centroids of 18039 reflections above $10\sigma(I)$. Analysis of the data showed negligible decay during data collection. The structure was solved and refined with the Bruker SHELXTL (version 2018/3) software package, using the space group P2(1)/c with Z = 4 for the formula C22H17N3ONi. All non-hydrogen atoms were refined anisotropically with the hydrogen atoms placed in idealized positions. Full matrix least-squares refinement based on F^2 converged at R1 = 0.0309 and wR2 = 0.0874 [based on I > 2sigma(I)], R1 = 0.0313 and wR2 = 0.0879 for all data.

Additional details are presented in Table 1 and are given as Supporting Information in a CIF file.

G.M. Sheldrick (2015) "Crystal structure refinement with SHELXL", Acta Cryst., C71, 3-8 (Open Access).

CrystalClear Expert 2.0 r16, Rigaku Americas and Rigaku Corporation (2014), Rigaku Americas, 9009, TX, USA 77381-5209, Rigaku Tokyo, 196-8666, Japan.

CrysAlisPro 1.171.38.41 (Rigaku Oxford Diffraction, 2015).

Table 3.4 Crystal Data and Structure Refinement for **2b-pic**

Empirical formula	C22 H17 N3 Ni O
Formula weight	398.09
Temperature	85(2) K
Wavelength	1.54178 A
Crystal system, space group	Monoclinic, P2(1)/c
Unit cell dimensions	a = 10.36830(10) A alpha = 90° b = 9.11630(10) A beta = 90.7060(10)° c = 19.1021(2) A gamma = 90°
Volume	1805.40(3) A^3
Z, Calculated density	4, 1.465 Mg/m^3
Absorption coefficient	1.678 mm^-1
F(000)	824
Crystal size	0.100 x 0.080 x 0.060 mm
Theta range for data collection	4.264 to 69.476°
Limiting indices	-12<=h<=12, -10<=k<=11, -22<=l<=23
Reflections collected / unique	26446 / 3364 [R(int) = 0.0332]

Completeness to theta = 67.679	99.9%
Absorption correction	Semi-empirical from equivalents
Max. and min. transmission	1.00000 and 0.83499
Refinement method	Full-matrix least-squares on F^2
Data / restraints / parameters	3364 / 0 / 246
Goodness-of-fit on F^2	1.008
Final R indices [I>2sigma(I)]	R1 = 0.0309, wR2 = 0.0874
R indices (all data)	R1 = 0.0313, wR2 = 0.0879
Extinction coefficient	0.0019(2)
Largest diff. peak and hole	0.340 and -0.298 e.A^-3
Empirical formula	C22 H17 N3 Ni O

Chapter 4 Synthesis, Reactivity and Catalytic Relevance of Ni[III] Complexes

Note: This chapter is partly based on work published in <u>Roy, P.</u>; Bour, J. R.; Kampf, J. W.; Sanford, M. S.* Catalytically Relevant Intermediates in the Ni-Catalyzed C(sp^2)–H and C(sp^3)–H Functionalization of Aminoquinoline Substrates. *J. Am. Chem. Soc.* **2019**, *141*, 17382–17387 and *J. Am. Chem. Soc.* **2021**, *143*, 14021.

4.1 Introduction

Transition metal catalyzed cross-coupling and C–H functionalization have been developed for carbon-carbon and carbon-heteroatom bond formation.[1–3] Noble metals such as platinum and palladium have been widely used as catalysts. Seminal reports from Sanford and others have demonstrated that challenging bond-forming reductive elimination reactions (e.g. C–F, C–CF$_3$, C–N) are facile from higher oxidation states such as Pd[IV] or Pt[IV] compared to the Pd[II] or Pt[II] analogues.[4–6] Although fleeting Pd[III] intermediates have been connected to the formation of Pd[IV], challenging bond formations occur almost exclusively from Pd[IV].[7] In this context, the ease of reductive elimination has been attributed to the higher electrophilicity at the metal center with increase in oxidation state.[5,6]

Figure 4.1 Transient Pd^{III} Species Compared to Persisting Ni^{III} Intermediates

Rare Pd^{III} intermediate
Pd^{III} disproportionates

Common Ni^{III} intermediate
Ni^{III} formed via comproportionation
Connecting Ni^{III} to Ni^{IV}
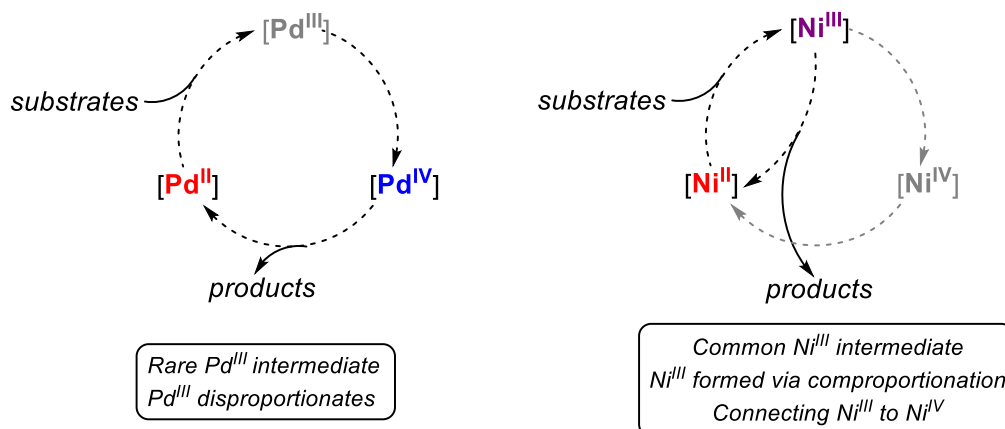
Analogous to Pd^{IV}, challenging bond-forming reactions (e.g., C–N, C–O and C–CF$_3$) have recently been demonstrated from Ni^{IV} model complexes.[8,9] In general, Pd^{III} species often undergo disproportionation reactions to form Pd^{II} and Pd^{IV} species whereas, Ni^{III} complexes can be formed via comproportionation of Ni^{II} and Ni^{IV} species (Figure 4.1).[10] Furthermore, Ni^{III} species have also been shown to promote challenging bond-forming reactions such as C–Br and C–C coupling.[11–14]

Figure 4.2 Dichotomy of Proposed Ni^{III} or Ni^{IV} Intermediates
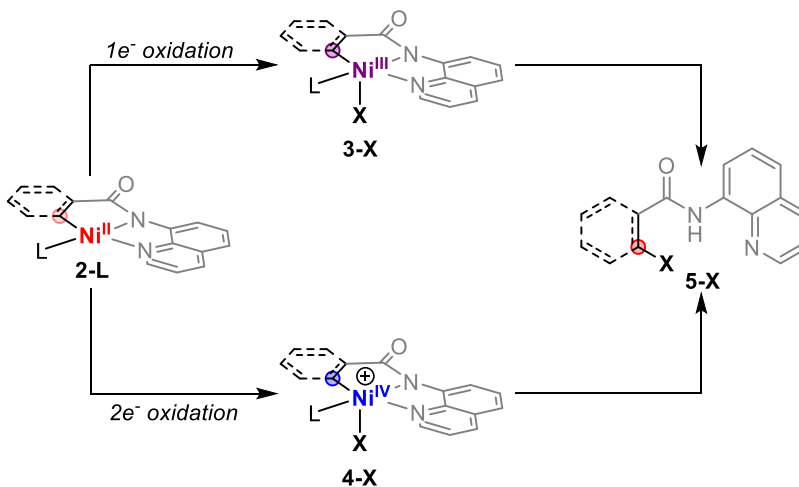
This dichotomy of proposed Ni^{III} and Ni^{IV} intermediates prevails in the Ni-catalyzed C–H functionalization reactions as well. Literature reports have proposed that the cyclometalated Ni^{II} species **2-L** undergoes either one or two electron oxidation to a Ni^{III} or Ni^{IV} (**3-X** or **4-X**)

intermediate (Figure 4.2). Each of these species could then participate in C–X reductive elimination to generate a functionalized organic product.[15–17] To date, no high-valent intermediates have been spectroscopically observed nor isolated from these catalytic reactions. This chapter focuses on the isolation and reactivity studies of σ-alkyl and σ-aryl Ni^{III} complexes bearing the aminoquinoline scaffold.

Figure 4.3 Literature Report of Isolated Ni^{III} Complexes

| van Koten, **1983** | Zargarian, **2007** | Sanford, **2016** | Mirica, **2016** |
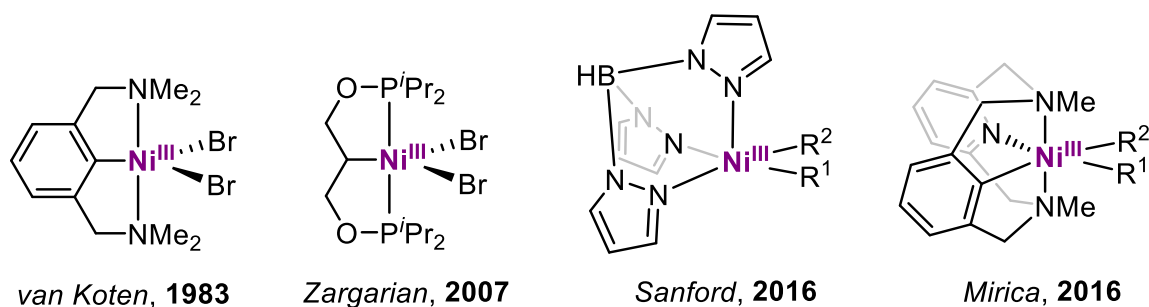
Ni^{III} complexes have been successfully isolated with polydentate supporting ligands, with tridentate ligands being the most common. Both meridional (mer) and facial (fac) geometrical arrangements of ligands on a tridentate scaffold are possible, and both mer and fac ligands have been employed for the isolation of Ni^{III} species, examples of which are shown in Figure 4.3. These paramegnetic d^7 complexes are typically characterized via X-ray crystallography and EPR spectroscopy. The most common methodology employed for the isolation of such species involves the treatment of Ni^{II} starting materials with single-electron oxidants. Pioneering studies by van Koten and Zargarian employed $CuBr_2$ as a single-electron inner sphere oxidant that transferred Br•　to a Ni^{II} center to generate Ni^{III} (Figure 4.4). Outer sphere 1-electron oxidants such as Ag^I and ferrocenium(I) salts have also been demonstrated by Sanford and Mirica for the isolation of Ni^{III} species (Figure 4.4). In this Chapter, analogous approaches are employed to access aminoquinoline-ligated σ-alkyl and σ-aryl Ni^{III} complexes and to study their reactivity in bond-forming reactions.

Figure 4.4 General Routes for Isolation of Ni^{III} Complexes

van Koten, **1983** and Zargarian, **2007**
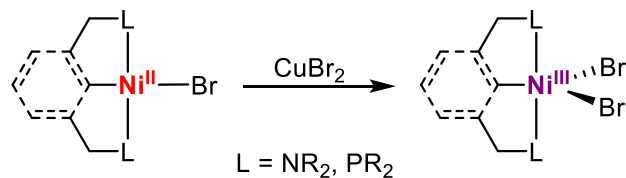
Sanford, **2016** and Mirica, **2016**

L = NR$_2$, PR$_2$

L = NR$_2$, N$_{Ar}$
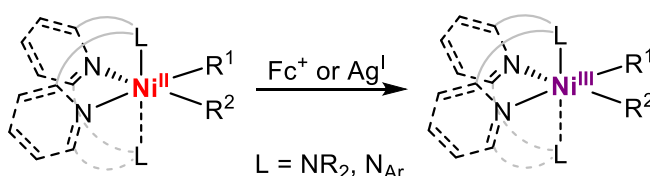
4.2 Result and Discussion

4.2.1 Synthesis and Probing for C(sp^3)–N Reductive Elimination from σ-alkyl Ni^{III}

In Chapter 3, electrochemical experiments with the Ni(II) complex **2a-pic** showed that one-electron oxidants such as ferrocenium and Ag^I salts have appropriate potentials for the single electron oxidation of this species. Consistent with the CV data, the addition of 1 equiv of AgOTf to **2a-pic** in acetone resulted in an immediate color change of the solution from orange-red to dark brown along with the precipitation of colloidal silver. After 30 min, the ^{1}H NMR spectrum of the reaction mixture showed complete disappearance of diamagnetic signals attributed to **2a-pic**. The silver(0) precipitate was removed by filtering this reaction mixture through a plug of Celite. The Ni^{III} product (**3a-OTf**) was then isolated by removal of solvent under reduced pressure and recrystallization twice from a ternary mixture of acetone, diethyl ether, and pentane (Scheme 4.1).

Scheme 4.1 Synthesis of **3a-OTf** via Oxidation of **2a-pic** with AgOTf
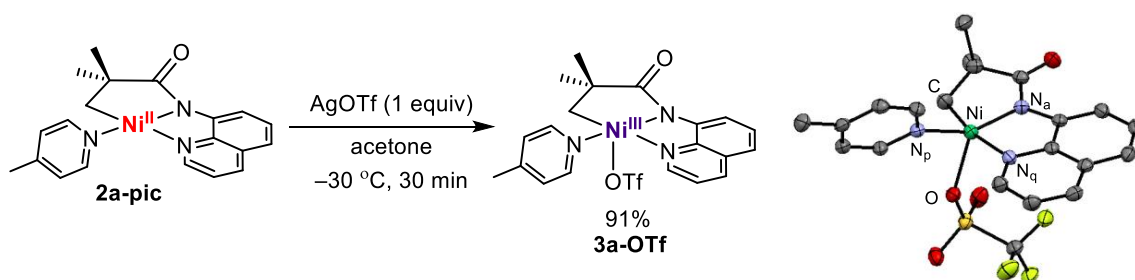
Complex **3a-OTf** was characterized by X-ray crystallography and EPR spectroscopy. X-ray quality crystals were obtained by vapor diffusion of pentane into a THF of **3a-OTf**. The solid state structure of **3a-OTf** is shown in Scheme 4.1 and relevant bond distances and bond angles are summarized in Table 4.1. A τ value of 0.25 was noted, which is similar to that of reported Ni^{III} pincer complexes. A characteristic $S = \frac{1}{2}$ rhombic signal was observed in the EPR spectrum of **3a-OTf**, consistent with a low spin d^7 complex.

Table 4.1 Bond Lengths, Angles and Geometrical Structural Parameters of **3a-OTf**

entry	3a-OTf
Ni-C (Å)	**1.988**
Ni-N_q (Å)	**2.009**
Ni-N_a (Å)	**1.861**
Ni-N_p (Å)	**1.960**
Ni-O (Å)	**2.087**
N_a-Ni-N_p	**152.27°**
τ	**0.25**

Scheme 4.2 Ni-Catalyzed Intramolecular C(sp^3)–H Amination by Chatani
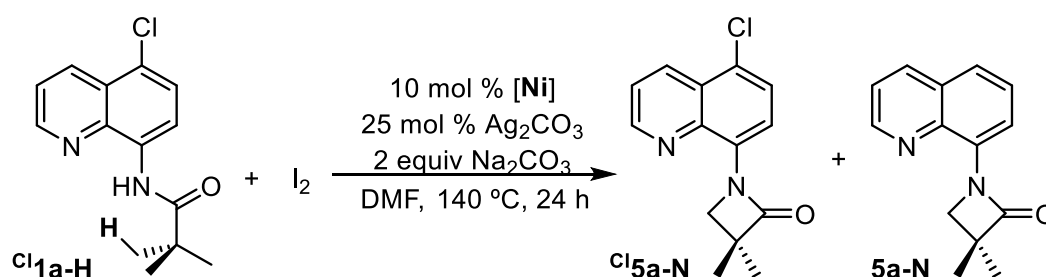
Chatani proposed two possible routes to *β*-lactam product **5a-N** in the Ni-catalyzed C–H amination of **1a-Cl** (Scheme 4.2).[15] The first involves direct C(sp^3)–N bond-forming reductive elimination from a high valent Ni-center similar to **3a-OTf**. The second involves the generation of a C(sp^3)–I bond and subsequent intramolecular S$_N$2 cyclization to form the lactam. To test the reactivity of **3a-OTf** towards C(sp^3)–N bond-forming reductive elimination, we heated this complex in various solvents (MeCN-d_3, DMSO-d_6, and DMF-d_7) to temperatures up to 140 ℃ and for times up to 16 h. Under all of these conditions, the *β*-lactam **5a-N** was not detected by ^{1}H NMR spectroscopy or GCMS analysis (Scheme 4.3).

Scheme 4.3 *β*-lactam product (**5a-N**) was not observed from **3a-OTf** at 140 °C after 16 h in DMF-*d₇*

3a-OTf

DMF-*d₇*, 140 ºC, 16 h

5a-N
not detected
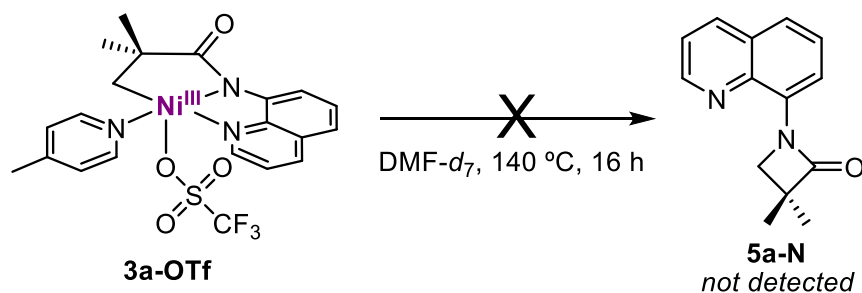
We also probed the viability of C(sp³)–I coupling at **3a-OTf** by examining the thermolysis of this complex in the presence of 1–2 equiv of NBu₄I (Scheme 4.4). In DMF-*d₇* at 140 ºC, none of the iodinated product **5a-I** nor **5a-N** was detected by ¹H NMR spectroscopy.

Scheme 4.4 C(sp³)–N nor C(sp³)–I Coupling was Observed from **3a-OTf** with NBu₄I in DMF-*d₇*

3a-OTf

1-2 equiv NBu₄I

DMF-*d₇*, 140 ºC, 16 h

5a-N
not detected

+

5a-I
not detected
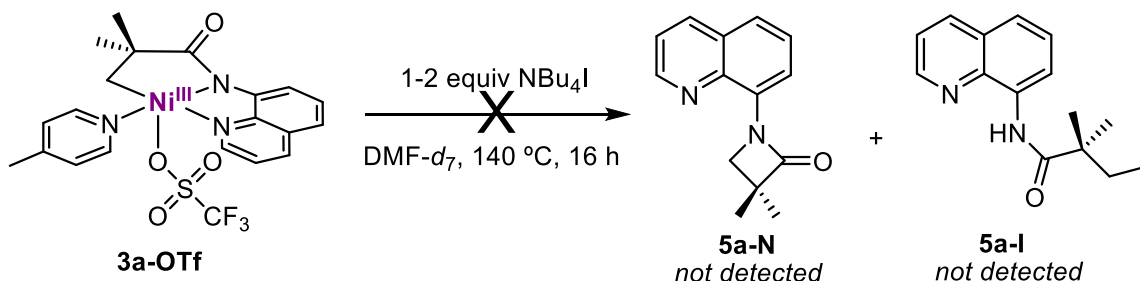
These results suggest that complex **3a-OTf** is not a productive intermediate in Chatani's catalytic reaction in Scheme 4.2. To test this directly, we examined the competency of **3a-OTf** as a catalyst for the conversion of **1a-Cl** to the *β*-lactam ᶜˡ**5a-N**. As shown in Table 4.2, the use of 10 mol % of **3a-OTf** as the Ni source resulted in <1% yield of the *β*-lactam product. In contrast, Ni(OTf)₂ (the original catalyst employed by Chatani) afforded **4a-Cl** in 58% yield under analogous conditions.

Table 4.2 Catalytic Competence of σ-alkyl Ni^{III} Complex for Intramolecular $C(sp^3)$–H Amidation

entry	[Ni]	Yield ^{Cl}5a-N	Yield 5a-N
1	Ni(OTf)$_2$	58%	–
2	3a-OTf	<1%	0%

4.2.2 Synthesis and Probing for C(sp^2)–I Reductive Elimination from σ-aryl Ni^{III}

We next carried out analogous one-electron oxidation reactions of the σ-aryl Ni(II) complex **3b-pic**. The reaction of **3b-pic** with 1 equiv of AgOTf or AgOTFA in acetone resulted in an immediate color change of the solution from orange-red to dark brown along with the precipitation of colloidal silver. After 30 min, the ^{1}H NMR spectrum of the reaction mixture showed complete disappearance of the diamagnetic signals attributed to **3b-pic**. The silver(0) precipitate was removed by filtration through a Celite column. The Ni^{III} products **3b-OTf** and **3b-OTFA** were then isolated in 65% and 80% yield, respectively (Scheme 4.5).

Scheme 4.5 Synthesis of **3b-OTf** and **3b-OTFA** via Oxidation of **2b-pic** with Ag^I Salts
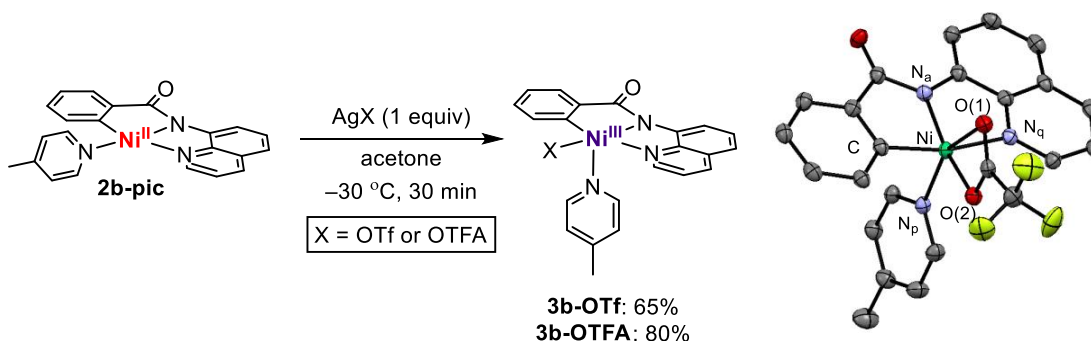
Table 4.3 Bond Lengths, Angles and Geometrical Structural Parameters of **3a-OTf**

entry	3b-OTFA
Ni-C (Å)	1.930
Ni-N$_q$ (Å)	1.991
Ni-N$_a$ (Å)	1.888
Ni-N$_p$ (Å)	2.041
Ni-O^1 (Å)	2.628
Ni-O^2 (Å)	1.954
τ	0.03

Both **3b-OTf** and **3b-OTFA** are paramagnetic Ni^{III} complexes that were characterized by elemental analysis as well as EPR spectroscopy. Both EPR spectra are consistent with S = ½ Ni^{III} rhombic signals. Complex **3b-OTFA** was further characterized by X-ray crystallography, and the solid state structure shows a slightly distorted square pyramidal geometry with a τ value of 0.03 (Table 4.3). Similar geometries have been reported for related organometallic Ni^{III} PCP and NCN pincer complexes.[18,19] Notably, the carbonyl oxygen of the carboxylate ligand is also in the proximity of the Ni^{III} center and could potentially act as a sixth ligand. However, the bond distance (Ni–O^1 = 2.628 Å) suggests that this interaction is relatively weak, particularly compared to that of Ni–O^2 (1.954 Å).

Scheme 4.6 Ni-Catalyzed Intramolecular C(sp^2)–H Iodination by Chatani
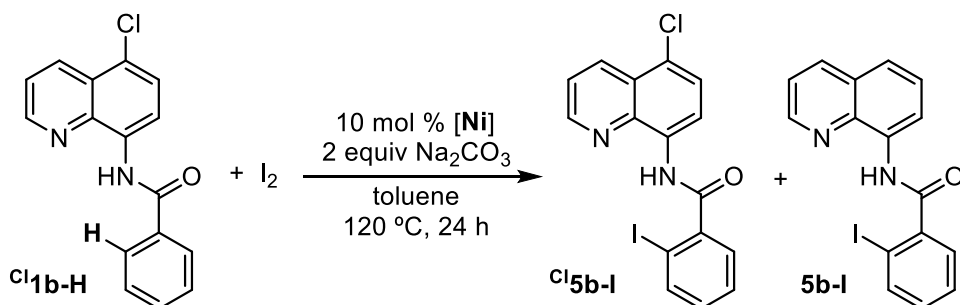
We next explored the reactivity of the isolated Ni^{III} complexes toward C(sp^2)–heteroatom coupling. Importantly, a number of reports have shown the feasibility of C(sp^2)–halogen coupling

at isolated Ni^{III} centers.[9,20] Furthermore, Chatani has proposed C(sp^2)–I bond formation from reactive Ni^{III} intermediates in his C(sp^2)–H iodination of substrate ^{Cl}1b-H (Scheme 4.6).[15] Heating 3b-OTf and 3b-OTFA for up to 16 h at 140 °C in DMF-d_7 solvent did not lead to traces of the C–O coupling products 5b-OTFA or 5b-OTf as analyzed by ^{1}H NMR spectroscopy (Scheme 4.7). Instead, a different coupling reaction occurred, which is discussed in Section 4.2.3 below. In addition, the addition of 1-2 equiv of NBu$_4$I or I$_2$ to analogous thermolysis reactions did not afford traces of the C(sp^2)–I coupled product 5b-I (Scheme 4.8).

Scheme 4.7 5b-OTf or **5b-OTFA** was not observed from **3b-X** at 140 °C after 16 h in DMF-d_7

(3b-OTf *or* 3b-OTFA)

various conditions up to 140 ºC for 16 h

5b-OTf (X = OTf)
5b-OTFA (X = OTFA)

not detected
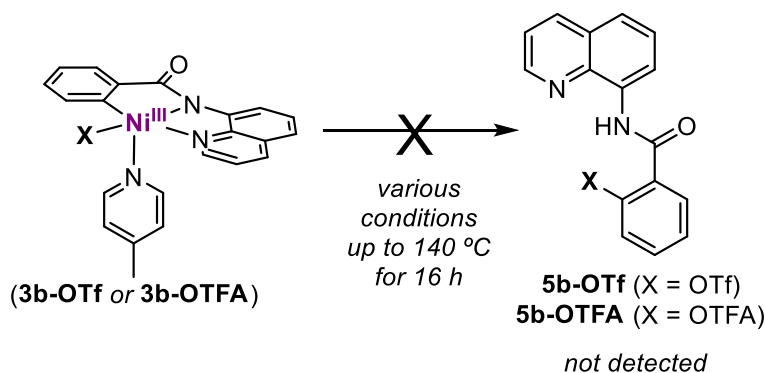
Scheme 4.8 5b-I was not observed from **3b-OTf** or **3b-OTFA** at 140 °C after 16 h in DMF-d_7

(3b-OTf *or* 3b-OTFA)

I$_2$, NBu$_4$I

various conditions up to 140 ºC for 16 h

5b-I
not detected
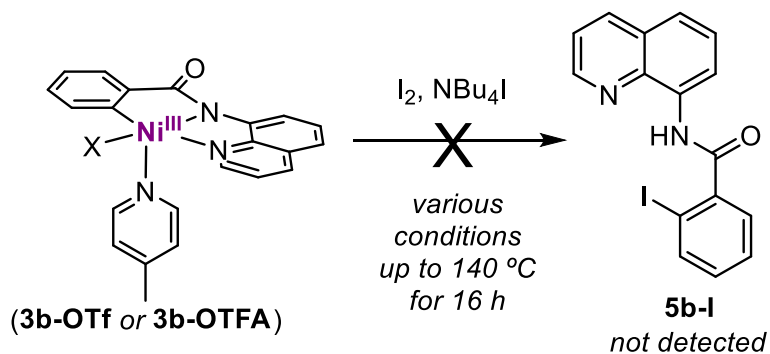
The results in Schemes 4.7 and 4.8 suggest that Ni^{III} complexes like **3b-OTf** or **3b-OTFA** are not catalytically competent intermediates in Chatani's C(sp^2)–H iodonation of substrate ^{Cl}1b-H. To test this directly, we examined **3b-OTf** and **3b-OTFA** as catalysts for the conversion of

^{Cl}**1b-H** to the iodinated product ^{Cl}**5b-I**. As shown in Table 4.4, the use of 10 mol % of either **3b-OTf** or **3b-OTFA** as the Ni source resulted in <1% yield of the iodinated product. In contrast, Ni(OTf)$_2$ (the original catalyst employed by Chatani, Scheme 4.6) afforded ^{Cl}**5b-I** in 48% yield under analogous conditions (Table 4.4).

Table 4.4 Catalytic Competence of σ-aryl Ni^{III} Complex for Intramolecular C(sp^2)–H Iodination

entry	[Ni]	Yield ^{Cl}5b-I	Yield 5b-I
1	Ni(OTf)$_2$	48%	–
2	3b-OTf	<1%	<1%
3	3b-OTFA	<1%	<1%

4.2.3 Probing for C(sp^2)–X Reductive Elimination from σ-aryl Ni^{III}

Scheme 4.9 Probing for C(sp^2)–X Coupling from **3b-OTf**
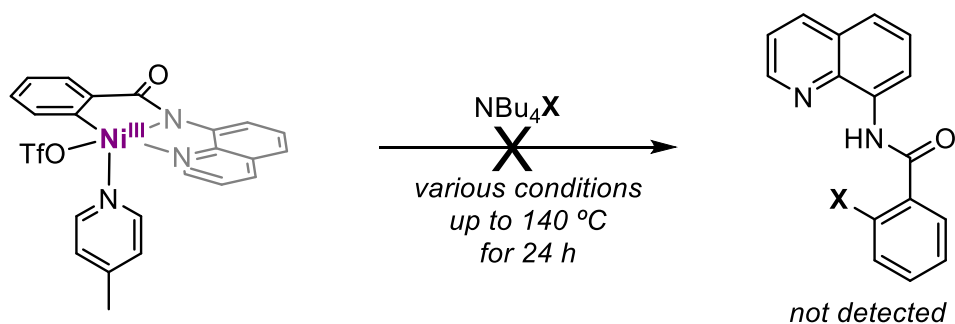
We continued to probe for reductive elimination reactions from the σ-aryl Ni^{III} species by adding various tetrabutylammonium salts to **3b-OTf**, reasoning that more coordinating X-type ligands would displace the weakly bound triflate. These studies were performed by treating **3b-OTf** with stoichiometric quantity of NBu$_4$X salts (X = OAc, Cl, Br) in MeCN-d_3 or DMF-d_7 at temperatures up to 140 °C for up to 24 h. In some cases, a change in color from brownish-green to pale brown was observed. However, no C(sp^2)–X coupling products were detected via ^{1}H NMR spectroscopy (Scheme 4.9).

We were puzzled by these observations, since C(sp^2)–heteroatom coupling from Ni^{III} centers is well-established in the literature.[9,20] Thus, we next attempted to isolate the products formed in these thermolysis reactions. Intriguingly these studies revealed that heating **3b-OTf** in DMF-d_7 for 4 h at 140 ºC followed by direct crystallization of this sample (by adding THF and pentane) affords the Ni^{II} complex ^{Ni}**5b-dimer**, in which the two σ-aryl ligands have undergone C(sp^2)–C(sp^2) coupling. The yield of this product is 30%[2] (assuming that 2 moles of **3b-OTf** should afford 1 mole of product ^{Ni}**5b-dimer**). Ni^{II}(pic)$_4$(OTf)$_2$ byproducts (**Ni$_1$** and **Ni$_2$**) were also isolated from this reaction mixture and characterized by X-ray crystallography.

Scheme 4.10 Isolation of ^{Ni}**5b-dimer** from heating **3b-OTf** in DMF-d_7 at 140 °C for 4 h
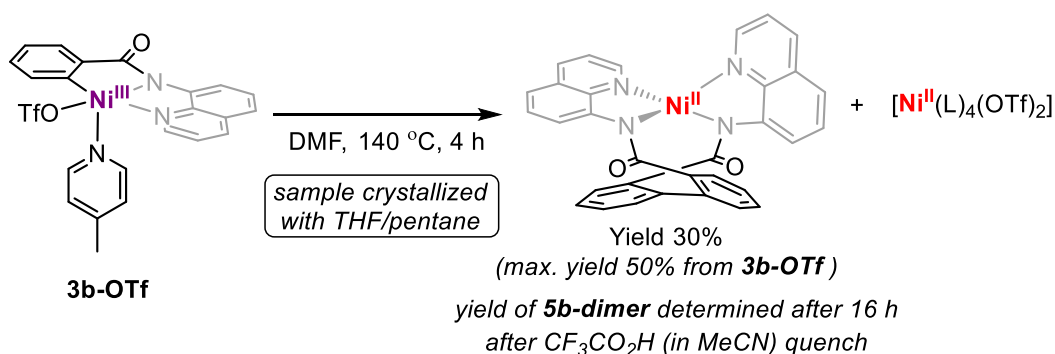
This Ni^{II} product ^{Ni}**5b-dimer** was characterized by X-ray crystallography (Scheme 4.10). The X-ray structure shows a distorted tetrahedral structure resembling a seesaw-like geometry. Based on the solid-state structure of ^{Ni}**5b-dimer** it was expected to be paramagnetic. Indeed, the ^{1}H NMR spectrum of **3b-OTf** in DMF-d_7 showed 12 broad signals from 5.75-9.35, owing to paramagnetic broadening.[3] Upon heating this sample for 16 h at 140 °C in DMF-d_7 in a J-Young

---

[2] The yield of this reaction was quantified using the internal standard of the NMR instrument. Later, studies had revealed high error bars in estimation of yield via this method as represented by the $\pm$10%, as had been noted for similar reactions of **2a-pic** and **2b-pic** with I$_2$.

[3] The NMR spectrum was recorded with 1 s relaxation delay for 256 scans which showed extensive paramagnetic broadening (Figure 4.6, bottom).

NMR tube, the color changed from greenish-brown to pale-brown, and the number of broad NMR

signals decreased.

Figure 4.5 Solid-state structure of isolated [Ni]**5b-dimer**
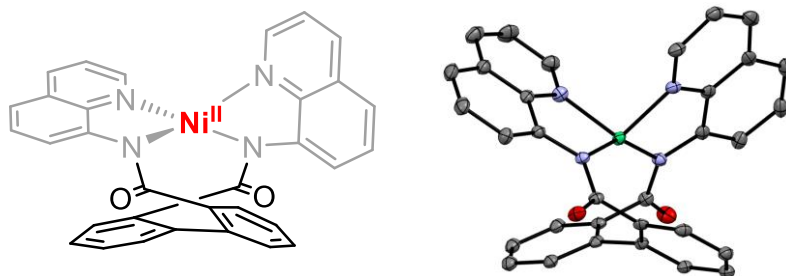
Figure 4.6 ^{1}H NMR Spectra of **3b-OTf** (bottom), NMR Sample after heating of **3b-OTf** for 16 h at 140 °C (middle) and synthesized authentic sample of **5b-dimer** (top), in DMF-d_7
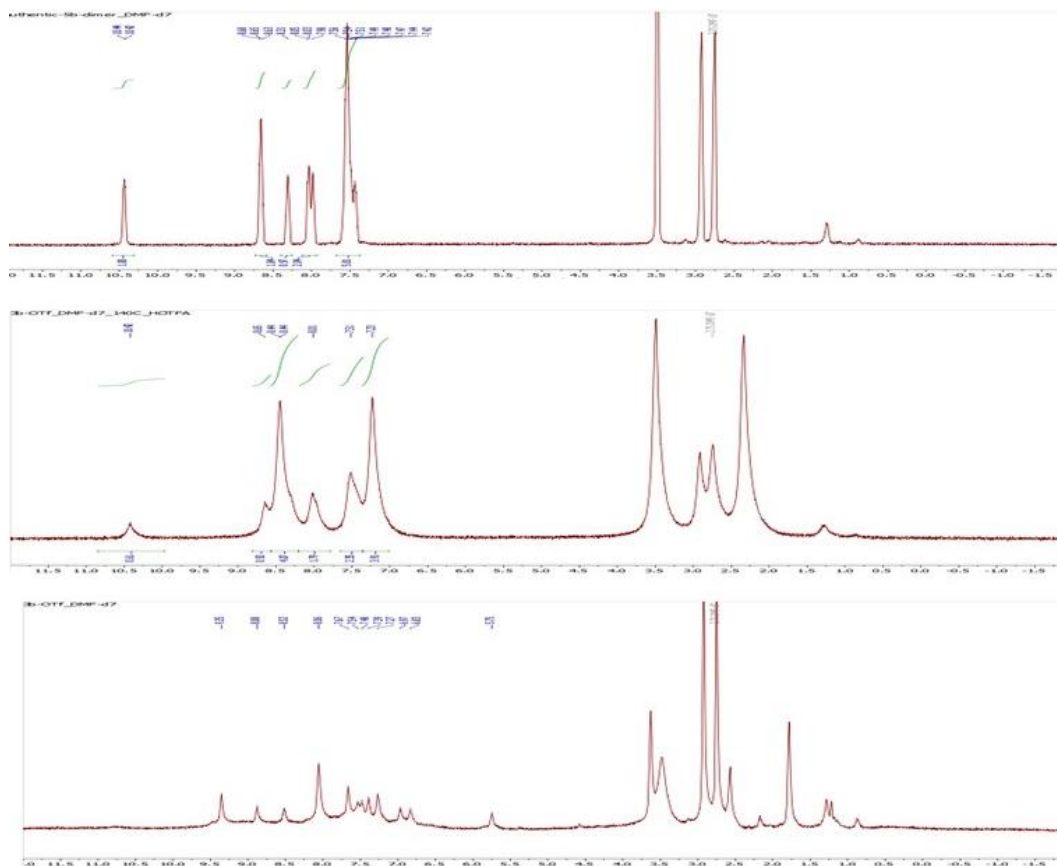
The addition of 10 equiv of trifluoroacetic acid to the NMR sample was performed to de-ligate the dimerized organic product, **5b-dimer** (Figure 4.6, middle)[4]. The ^{1}H NMR spectrum of this reaction mixture showed a cluster of aromatic signals between 7.2-8.7 ppm and a broad signal at 10.4 ppm, which is tentatively assigned as the amide proton of **5b-dimer**. Although the ^{1}H NMR spectrum still shows the presence of paramagnetic species (as indicated by the broadening of signals), the observed resonances are in line with those of an authentic sample of **5b-dimer** (Figure 4.6, top).

Scheme 4.11 Effect of X-type Ligand on Formation of **5b-dimer** in DMF-d_7 at 140 °C for 16 h
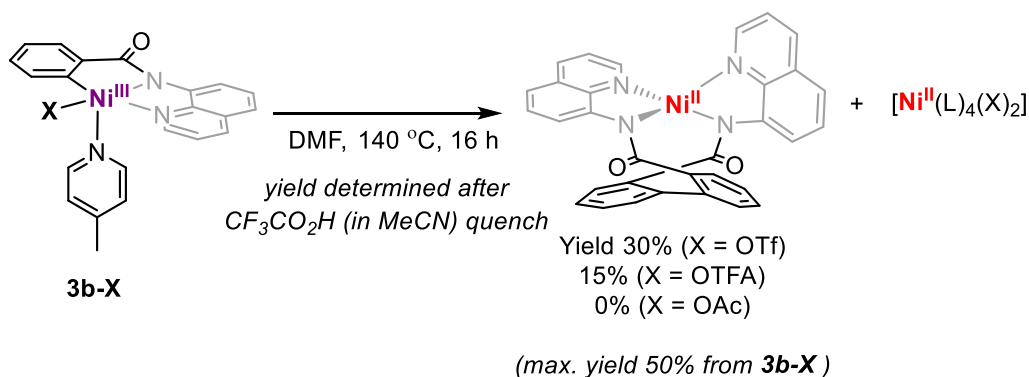
We next sought to assess the impact of the X-type ligand on Ni on this C–C coupling reaction (Scheme 4.11). The formation of the dimerized ligand product **5b-dimer** was observed upon heating **3b-OTFA** in DMF-d_7 at 140 °C for 16 h albeit in a lower yield of 15%. In contrast, under similar reaction conditions the formation of **5b-dimer** was not observed from the analogous actetate Ni^{III} complex **3b-OAc**. These results suggest that the C(sp^2)–C(sp^2) bond-forming step may involve a bimetallic mechanism and occur via a dissociative pathway. The dissociative mechanism is proposed based on the higher yield of **5b-dimer** (post acid quench) from **3b-OTf**

---

[4] The yield of this reaction was quantified using the internal standard of the NMR instrument using the overlapping broad signals at 7.23 and 7.51 accountable for 6 H-atoms (Figure 4.6, middle). This was analysis was based on the ^{1}H NMR signal of the separately synthesized authentic sample of **5b-dimer** based on a literature report as an overlapping signal from 7.4–7.6 was noted for 6 H-atoms (Figure 4.6, top).

and **3b-OTFA** over **3b-OAc**, since OAc is a stronger ligand than OTFA than OTf. Further investigations will be required to definitively confirm the mechanism of this bimetallic pathway of biaryl formation.

Scheme 4.12 Literature Reports for the Formation of **5b-dimer** from **1b-H** by Co and Cu Catalysis
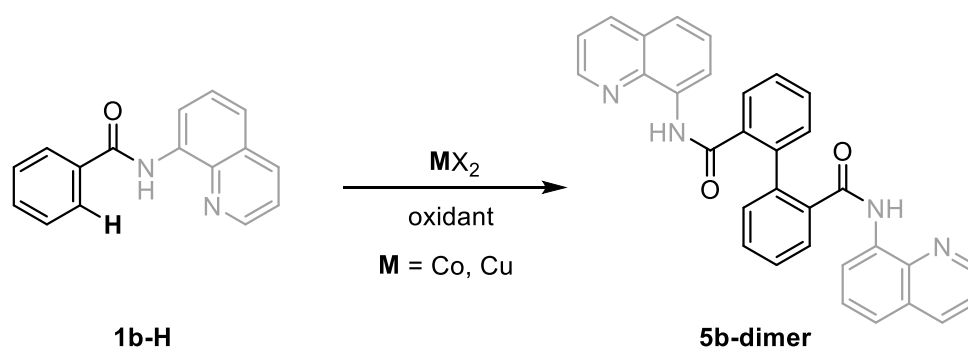
A key question that this result raises is the relevance of this C–C coupling to Ni catalysis. A search of the literature revealed that Ni has not been reported to catalyze the oxidative coupling of **1b-H** to form **5b-dimer** (Scheme 4.12). In contrast, this transformation has been reported using Co and Cu-based catalysts.[21,22]

4.3 Conclusions

This Chapter focuses on the synthesis of isolable Ni[III] complexes bearing both σ-alkyl and σ-aryl ligands along with the aminoquinoline directing group. Silver(I)-based oxidants are effective for oxidizing the pincer Ni[II] picoline staring materials. The Ni[III] σ-alkyl species (**3a-OTf**) did not undergo intramolecular $C(sp^3)$–N bond-forming reductive elimination at 140 ℃ to form a β-lactam. Furthermore, this complex is not a competent catalyst for the Ni-catalyzed $C(sp^3)$–H functionalization reaction that generates this product. Similarly, although $C(sp^2)$–halogen coupling has been demonstrated from a variety of other Ni[III] model complexes, the σ-aryl analogue proved

inert to $C(sp^2)$–I bond formation under both stoichiometric and catalytic conditions. Instead, this complex undergoes a C–C coupling reaction.

Overall, these experiments do not definitively rule out a role for all possible Ni^{III} intermediates in aminoquinoline-directed Ni-catalyzed C–H functionalization reactions. However, they strongly suggest that other pathways, such as direct electrophilic cleavage of the Ni^{II}–C bond and/or the formation of more reactive higher valent Ni intermediates such as Ni^{IV}, should be closely considered/examined as alternatives. More broadly, this study opens the door for further detailed interrogations of organometallic intermediates in Ni-catalyzed C–H functionalization reactions. Thus, the next chapter deals with exploring the feasibility of a Ni^{IV} species bearing the the aminoquinoline ligand scaffold.

4.4 References

(1) Davies, H. M. L.; Morton, D. Recent Advances in C–H Functionalization. *The Journal of Organic Chemistry* **2016**, *81* (2), 343–350. https://doi.org/10.1021/acs.joc.5b02818.

(2) H. Crabtree, R. Introduction to Selective Functionalization of C−H Bonds. *Chemical Reviews* **2010**, *110* (2), 575–575. https://doi.org/10.1021/cr900388d.

(3) Crabtree, R. H.; Lei, A. Introduction: CH Activation. *Chemical Reviews* **2017**, *117* (13), 8481–8482. https://doi.org/10.1021/acs.chemrev.7b00307.

(4) D. Ball, N.; S. Sanford, M. Synthesis and Reactivity of a Mono-σ-Aryl Palladium(IV) Fluoride Complex. *Journal of the American Chemical Society* **2009**, *131* (11), 3796–3797. https://doi.org/10.1021/ja8054595.

(5) Hickman, A. J.; Sanford, M. S. High-Valent Organometallic Copper and Palladium in Catalysis. *Nature 2012 484:7393* **2012**, *484* (7393), 177–185. https://doi.org/10.1038/nature11008.

(6) W. Lyons, T.; S. Sanford, M. Palladium-Catalyzed Ligand-Directed C−H Functionalization Reactions. *Chemical Reviews* **2010**, *110* (2), 1147–1169. https://doi.org/10.1021/cr900184e.

(7) C. Powers, D.; Lee, E.; Ariafard, A.; S. Sanford, M.; F. Yates, B.; J. Canty, A.; Ritter, T. Connecting Binuclear Pd(III) and Mononuclear Pd(IV) Chemistry by Pd–Pd Bond Cleavage. *Journal of the American Chemical Society* **2012**, *134* (29), 12002–12009. https://doi.org/10.1021/ja304401u.

(8) Camasso, N. M.; Sanford, M. S. Design, Synthesis, and Carbon-Heteroatom Coupling Reactions of Organometallic Nickel(IV) Complexes. *Science* **2015**, *347* (6227), 1218–1220. https://doi.org/10.1126/SCIENCE.AAA4526.

(9) Heberer, N.; Hu, C.-H.; Mirica, L. M. 6.09 - High-Valent Ni Coordination Compounds. In *Comprehensive Coordination Chemistry III*; Constable, E. C., Parkin, G., Que Jr, L., Eds.; Elsevier: Oxford, 2021; pp 348–374. https://doi.org/https://doi.org/10.1016/B978-0-08-102688-5.00104-5.

(10) Bour, J. R.; M. Ferguson, D.; J. McClain, E.; W. Kampf, J.; S. Sanford, M. Connecting Organometallic Ni(III) and Ni(IV): Reactions of Carbon-Centered Radicals with High-Valent Organonickel Complexes. *Journal of the American Chemical Society* **2019**, *141* (22), 8914–8920. https://doi.org/10.1021/jacs.9b02411.

(11) B. Watson, M.; P. Rath, N.; M. Mirica, L. Oxidative C–C Bond Formation Reactivity of Organometallic Ni(II), Ni(III), and Ni(IV) Complexes. *Journal of the American Chemical Society* **2016**, *139* (1), 35–38. https://doi.org/10.1021/jacs.6b10303.

(12) B. Watson, M.; P. Rath, N.; M. Mirica, L. Oxidative C–C Bond Formation Reactivity of Organometallic Ni(II), Ni(III), and Ni(IV) Complexes. *Journal of the American Chemical Society* **2016**, *139* (1), 35–38. https://doi.org/10.1021/jacs.6b10303.

(13) W. Schultz, J.; Fuchigami, K.; Zheng, B.; P. Rath, N.; M. Mirica, L. Isolated Organometallic Nickel(III) and Nickel(IV) Complexes Relevant to Carbon–Carbon Bond Formation Reactions. *Journal of the American Chemical Society* **2016**, *138* (39), 12928–12934. https://doi.org/10.1021/jacs.6b06862.

(14) Zheng, B.; Tang, F.; Luo, J.; W. Schultz, J.; P. Rath, N.; M. Mirica, L. Organometallic Nickel(III) Complexes Relevant to Cross-Coupling and Carbon–Heteroatom Bond Formation Reactions. *Journal of the American Chemical Society* **2014**, *136* (17), 6499–6504. https://doi.org/10.1021/ja5024749.

(15)   Aihara, Y.; Chatani, N. Nickel-Catalyzed Reaction of C–H Bonds in Amides with I2: Ortho-Iodination via the Cleavage of C(Sp2)–H Bonds and Oxidative Cyclization to β-Lactams via the Cleavage of C(Sp3)–H Bonds. *ACS Catalysis* **2016**, *6* (7), 4323–4329. https://doi.org/10.1021/acscatal.6b00964.

(16)   Khake, S. M.; Chatani, N. Chelation-Assisted Nickel-Catalyzed C-H Functionalizations. *Trends in Chemistry* **2019**, *1* (5), 524–539. https://doi.org/10.1016/j.trechm.2019.06.002.

(17)   Wu, X.; Zhao, Y.; Ge, H. Nickel-Catalyzed Site-Selective Alkylation of Unactivated C(Sp3)–H Bonds. *Journal of the American Chemical Society* **2014**, *136* (5), 1789–1792. https://doi.org/10.1021/ja413131m.

(18)   Pandarus, V.; Zargarian, D. New Pincer-Type Diphosphinito (POCOP) Complexes of Nickel. *Organometallics* **2007**, *26* (17), 4321–4334. https://doi.org/10.1021/om700400x.

(19)   Lapointe, S.; Vabre, B.; Zargarian, D. POCOP-Type Pincer Complexes of Nickel: Synthesis, Characterization, and Ligand Exchange Reactivities of New Cationic Acetonitrile Adducts. *Organometallics* **2015**, *34* (14), 3520–3531. https://doi.org/10.1021/acs.organomet.5b00272.

(20)   Zheng, B.; Tang, F.; Luo, J.; W. Schultz, J.; P. Rath, N.; M. Mirica, L. Organometallic Nickel(III) Complexes Relevant to Cross-Coupling and Carbon–Heteroatom Bond Formation Reactions. *Journal of the American Chemical Society* **2014**, *136* (17), 6499–6504. https://doi.org/10.1021/ja5024749.

(21)   Grigorjeva, L.; Daugulis, O. Cobalt-Promoted Dimerization of Aminoquinoline Benzamides. *Organic Letters* **2015**, *17* (5), 1204–1207. https://doi.org/10.1021/acs.orglett.5b00155.

(22)   Wang, M.; Hu, Y.; Jiang, Z.; Shen, H. C.; Sun, X. Divergent Copper-Mediated Dimerization and Hydroxylation of Benzamides Involving C–H Bond Functionalization. *Organic & Biomolecular Chemistry* **2016**, *14* (18), 4239–4246. https://doi.org/10.1039/C6OB00392C.

4.5 Experimental Procedures

4.5.1 General Procedures, Materials and Methods

General Procedures

NMR spectra were recorded on a Varian VNMRS 600 (600 MHz for ^{1}H and 151 MHz for ^{13}C). ^{1}H and ^{13}C NMR chemical shifts are reported in parts per million (ppm) and are referenced to the solvent lock. ^{1}H NMR quantification was conducted using internal standards as mentioned in the experimental procedures. Abbreviations used to report NMR peaks: singlet (s); doublet (d); triplet (t); quartet (q); doublet of doublets (dd); triplet of doublets (td); doublet of triplets (dt); multiplet (m). GC-FID data were collected on a Shimadzu 17A GC using a Restek Rtx®-5 (crossbond 5% diphenyl–95% dimethyl polysiloxane; 15 m, 0.25 mm ID, 0.25 µm df) column. High-resolution mass spectra were recorded on a Micromass AutoSpec Ultima Magnetic Sector mass spectrometer. Cyclic voltammetry was performed using a CHI600C potentiostat from CH Instruments. EPR spectra were collected at temperatures mentioned in the experimental procedures using a Bruker EMX ESR Spectrometer with a nitrogen-cooled cryostat. Elemental analyses were performed by Midwest Microlab located in Indianapolis. X-ray crystallographic data were obtained on a Rigaku AFC10K Saturn 944+ CCD-based X-ray diffractometer. Chromatographic separations were carried out on a Biotage Isolera One system using Sfär Silica HC D (High-capacity Duo 20 µm) columns (10 g, 25 g, or 50 g cartridges depending on the scale of isolations), as mentioned in the synthetic procedures.

Acronyms: Dichloromethane (DCM), Tetrahydrofuran (THF), Water in NMR solvent (HDO), Tetramethylsilane (TMS), Nitromethane (CH_3NO_2), residual moisture in solvent (HDO)

Note: All ^{1}H NMR spectra of nickel complexes and their reactivity studies with iodine (I_2) were recorded on a 600 MHz Varian Vnmrs instrument with a 100% lock efficiency and a relaxation delay of 25 s at 25 °C. These specifications are crucial for proper quantification and analysis as we have noted high T1 relaxation times for the nickel complexes.

Materials and Methods

All commercial reagents were used as received without further purification unless otherwise noted. [Ni(PEt$_3$)$_4$] was prepared via literature procedures.1 Bis(1,5-cyclooctadiene)nickel(0) ([Ni(COD)$_2$]) was purchased from Strem Chemical, 2,2-dimethylsuccinic anhydride and 8-aminoquinoline from Ark Pharm. Tetramethylammonium acetate (TMAOAc) from TCI America. Nickel(II) acetate (Ni(OAc)$_2$), nickel(II) trifluoromethanesulfonate 96% (Ni(OTf)$_2$), silver(I) carbonate (Ag$_2$CO$_3$), triethylphosphine (PEt$_3$), triethylamine (Et$_3$N) and acetonitrile (electronic grade) were purchased from Millipore-Sigma or Aldrich. All deuterated solvents were obtained from Cambridge Isotope Laboratories and deaerated via a nitrogen sparge prior to storage over activated 4 Å molecular sieves (EMD Millipore). Anhydrous N,N-dimethylformamide and acetone were purchased from Acros Organics in AcroSeal® bottles. Anhydrous benzene was purchased from Alfa Aesar and ethanol from VMR international. Pentane (Fisher), diethyl ether (Millipore-Sigma), tetrahydrofuran (Fisher), and toluene (Fisher) were deaerated via a nitrogen sparge and further purified using a solvent purification system for usage inside the glovebox. Sodium carbonate, potassium carbonate, sodium sulfate, hexanes, diethyl ether, ethyl acetate, dichloromethane, sulfuric acid (Certified ACS Plus) and glacial acetic acid were purchased from Fisher. Celite was purchased from Aqua Solutions and was dried under vacuum at 150 °C for 24 h for usage inside the glovebox. All glassware used in the glovebox was dried in an oven at 150

°C for at least 6 h and cooled under an inert atmosphere. All experiments and synthetic procedures were setup inside a nitrogen-filled glovebox unless otherwise mentioned.

EPR Spectra of Nickel Complexes

50 µL from a 10 mM (10 µmol in 1mL) stock solution of each Ni^{III} complex was diluted with 200 µL of toluene or PrCN or toluene. This 250 µL sample was placed in a septum capped EPR tube and cooled in liquid nitrogen until it glassed. EPR spectra were recorded for complexes at 100 K.

4.5.2 Synthesis and Characterization of Organic Molecules

All synthesis in this subsection was performed outside the glovebox; modified procedures and confirmation of characterization were referenced against previous literature report as cited.

1b-H
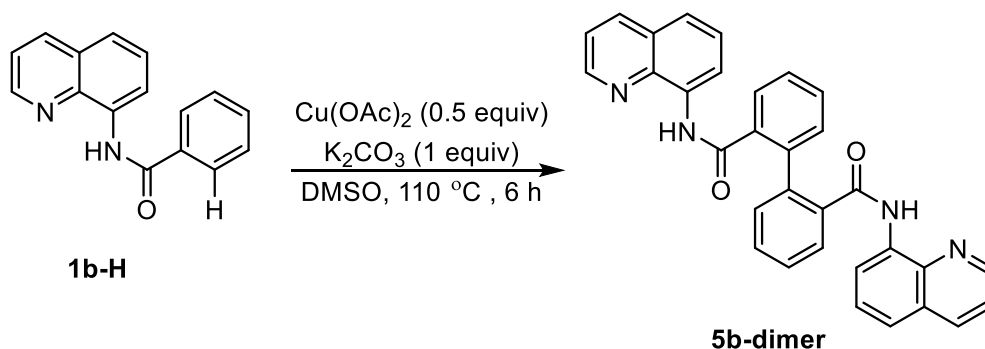
5b-dimer

5b-dimer: N-(quinolyl-8-yl)benzamide (1.242 g, 5.0 mmol, 1.0 equiv), potassium carbonate (0.690 g, 5.0 mmol, 1.0 equiv), and copper (II) acetate (0.0455 g, 2.5 mmol, 0.5 equiv) were weighed out in a 50 mL round bottom flask equipped with a magnetic stir-bar and then dissolved in DMSO (25 mL). The flask was fitted with a Liebig condenser and heated in a silicon-oil bath at 110 °C for 6 h. Then the reaction was cooled to room temperature and quenched with sodium sulfide (2.5 g), DCM (100 mL) and water (100 mL) and reaction was stirred at room temperature for 30 mins. The reaction was divided into two portions and each portion was separately filtered through a pad of Celite in a glass crucible using additional 50 mL of DCM for washing the Celite pad and then both filtrate fractions were combined. The organic phase was extracted from the aqueous phase using DCM (2 x 50 mL). All organic fractions were combined, dried over anhydrous sodium sulfate, and concentrated under vacuum. The crude product was further purified by chromatography using a Sfär Silica HC D (High-capacity Duo 20 µm) 50 g cartridge on a Biotage Isolera One system (MeOH : DCM, gradient from 0:100 to 10:90). This afforded compound **5b-dimer** as an off-white solid (0.51 g, 62% yield). The ^{1}H NMR spectrum of the product matched that reported in the literature.[6]

4.5.3 Synthesis and Characterization of Nickel Complexes
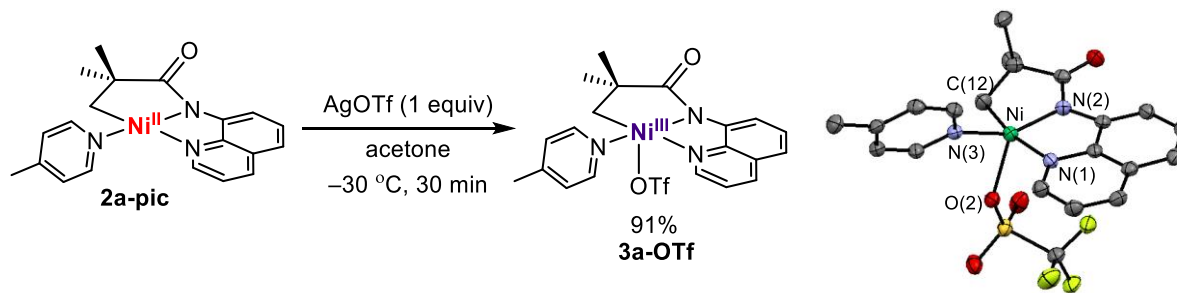
3a-OTf: Complex **2a-pic** (189 mg, 0.5 mmol, 1 equiv) was weighed into a 20 mL vial and dissolved in anhydrous acetone (5 mL), and the resulting solution was cooled to –30 °C. This solution was added dropwise to a pre-cooled (–30 °C) solution of AgOTf (131 mg, 0.51 mmol, 1.02 equiv) in acetone (5 mL). The reaction was stirred for 30 min while it slowly warmed up to ambient temperature. A color change from orange to dark green was observed, along with the formation of a gray precipitate. The solvent was removed under vacuum, and the resulting residue was re-dissolved in THF (5 mL). The reaction mixture was filtered through a Celite pad, and this pad was washed with THF (5 mL). The solvent was reduced under vacuum to ~2 mL and then a 1:1 mixture of pentane: diethyl ether (8 mL) was added to precipitate a brownish-green solid. This solid was recrystallized via slow diffusion of pentane into a THF solution. Complex **3a-OTf** was obtained as a dark orange-green solid (240 mg, 91% yield). Complex **3a-OTf** was characterized EPR spectroscopy at 93 K in a toluene glass (S = $^1/_2$; g_1 = 2.07, g_2 = 2.18, g_3 = 2.32). A single crystal of **3a-OTf** was obtained via slow vapor diffusion of pentane into a THF solution of **3a-OTf** at –30 °C.

Elemental analysis: calculated for $C_{21}H_{21}N_3F_3NiO_4S$, C: 47.85, H: 4.02, N: 7.97; Found: C: 48.07, H: 4.07, N: 7.98

HRMS-electrospray (m/z): $[M^+\text{-}OTf]$ calcd. for $C_{20}H_{21}N_3NiO$, 377.1033; found, 377.1038 [M-OTf]

EPR spectrum of **3a-OTf** (top/blue) and simulated (bottom/orange). The simulated spectrum was fit using the following parameters $g_1 = 2.07$, $g_2 = 2.18$, $g_3 = 2.32$; g-strain, $g_1 = 0.018$, $g_2 = 0.014$, $g_3 = 0.018$. The spectrum was recorded at 93 K in toluene-glass.
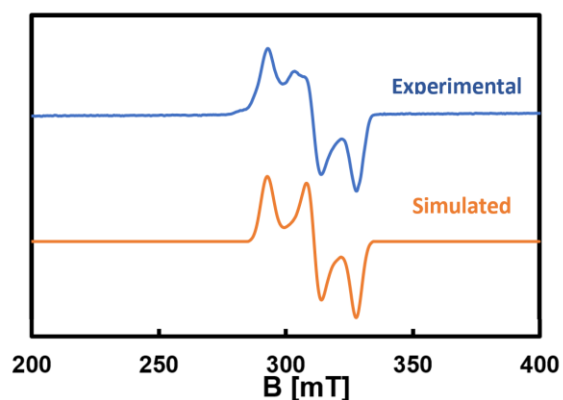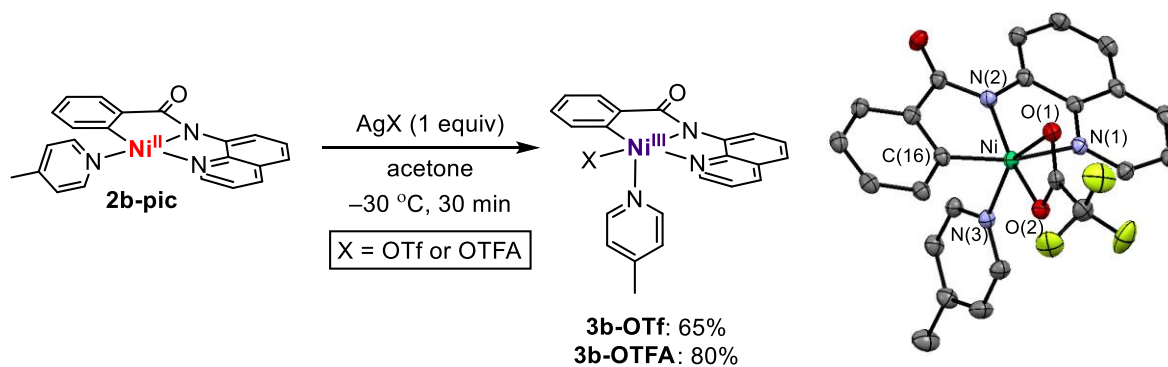
3b-OTf: Complex **2b-pic** (200 mg, 0.5 mmol, 1 equiv) was weighed into a 20 mL vial and dissolved in anhydrous acetone (5 mL), and the resulting solution was cooled to –30 °C. This solution was added dropwise to a pre-cooled (–30 °C) solution of AgOTf (131 mg, 0.51 mmol, 1.02 equiv) in acetone (5 mL). The reaction was stirred for 30 min while it slowly warmed up to ambient temperature. A color change from orange to dark brown was observed, along with the formation of a gray precipitate. The solvent was removed under vacuum, and the resulting residue was re-dissolved in THF (5 mL). The reaction mixture was filtered through a Celite pad, and this pad was washed with THF (5 mL). The solvent was reduced under vacuum to ~2 mL and then a 1:1 mixture of pentane: diethyl ether (8 mL) was added to precipitate a brownish-orange solid. This solid was re-dissolved in minimum amount of THF (~5 mL), and the resulting solution was transferred to a centrifuge tube and centrifuged at 5000 rpm for 15 min. The solution was separated from the pellet of silver particulate impurities at the bottom of the tube. This procedure was repeated twice, and then the solution was collected and the solvent was removed under vacuum to afford **3b-OTf** as a brownish orange solid (178 mg, 65% yield). Complex **3b-OTf** was characterized EPR spectroscopy at 100 K in a toluene glass (S = $^1/_2$; g_1 = 2.07, g_2 = 2.18, g_3 = 2.30).

Elemental analysis: calculated for $C_{23}H_{17}N_3F_3NiO_4S$, C: 50.49, H: 3.13, N: 7.68; Found: C: 51.27, H: 3.36, N: 7.71

HRMS-electrospray (m/z): [M$^+$-OTf] calcd. for C$_{22}$H$_{17}$N$_3$NiO, 397.0720; found, 397.0727 [M$^+$-OTf]

EPR spectrum of **3b-OTf** (bottom/blue) and simulated (top/orange). The simulated spectrum was fit using the following parameters g$_1$ = 2.07, g$_2$ = 2.18, g$_3$ = 2.30; g-strain$_{1,2,3}$ = 0.012. The spectrum was recorded at 100 K in toluene-glass.
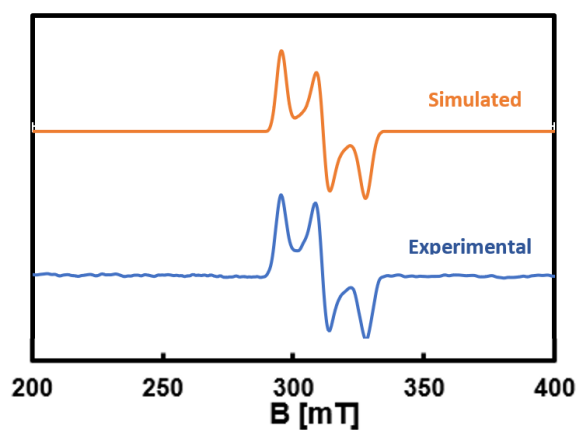
3b-OTFA: Complex **2b-pic** (200 mg, 0.5 mmol, 1 equiv) was weighed into a 20 mL vial and dissolved in anhydrous acetone (5 mL), and the resulting solution was cooled to –30 °C. This solution was added dropwise to a pre-cooled (–30 °C) solution of AgOTf (113 mg, 0.51 mmol, 1.02 equiv) in acetone (5 mL). The reaction was stirred for 45 min while it slowly warmed up to ambient temperature. A color change from orange to dark brown was observed, along with the formation of a gray precipitate. The solvent was removed under vacuum, and the resulting residue was re-dissolved in THF (5 mL). The reaction mixture was filtered through a Celite pad, and this pad was washed with THF (5 mL). The solvent was reduced under vacuum to ~2 mL and then a 1:1 mixture of pentane: diethyl ether (8 mL) was added to precipitate a brownish-orange solid. This solid was re-dissolved in minimum amount of THF (~5 mL), and the resulting solution was transferred to a centrifuge tube and centrifuged at 5000 rpm for 15 min. The solution was separated from the pellet of silver particulate impurities at the bottom of the tube. This procedure was repeated twice, and then the solution was collected and the solvent was removed under vacuum to afford **3b-OTFA** as a brownish orange solid (204 mg, 80% yield). Complex **3b-OTFA** was characterized EPR spectroscopy at 100 K in a PrCN glass ($S = {}^1/_2$; $g_1 = 2.08$, $g_2 = 2.1$, $g_3 = 2.28$; $A^N_{1,2} = 75$ G). A single crystal of **3b-OTFA** was obtained via slow vapor diffusion of pentane into a THF solution of **3b-OTFA** at –30 °C.

Notes:

1. The reagent quality of AgOTf is crucial for the isolation of complex 4a-OTf. Most vendors have traces of impurities that result in faster decomposition of complex 4a-OTf.

2. Before the Celite filter, the solvent swap from acetone to THF is important to limit decomposition during the filtration step.

3. The centrifugation step is important to remove silver and nickel impurities that impact reactivity studies.

Elemental analysis: calculated for $C_{24}H_{17}N_3F_3NiO_3$, C: 56.40, H: 3.35, N: 8.22; Found: C: 57.06, H: 3.41, N: 8.21

HRMS-electrospray (m/z): [M^+-OTFA] calcd. for $C_{22}H_{17}N_3NiO$, 397.0720; found, 397.0728 [M-OTFA]

EPR spectrum of **3b-OTFA** (blue) and simulated (orange). The simulated spectrum was fit using the following parameters $g_1 = 2.08$, $g_2 = 2.1$, $g_3 = 2.28$; $A^N_{1,2} = 75$ G. The spectrum was recorded at 100 K in PrCN-glass.

4.5.4 Reactivity of Nickel Complexes

3a-OTf → (DMF-d_7, 140 °C, 16 h) ✗ → **5a-N** *not detected*
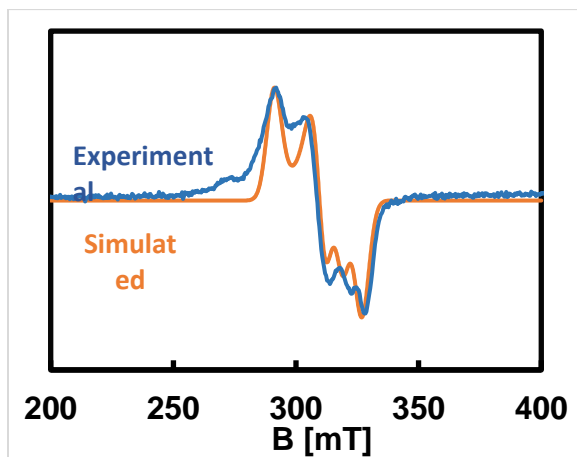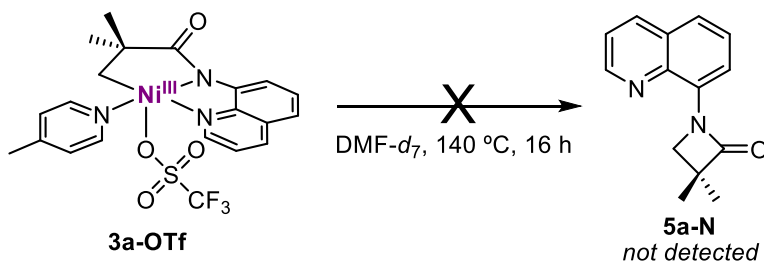
A 0.02 M stock solution of **3a-OTf** in DMF-d_7 (10.5 mg, 20 µmol in 1 mL of DMF-d_7) was prepared. A 0.5 mL aliquot of the **3a-OTf** stock solution was placed in J. Young NMR tube. The resulting mixture was heated at 140 °C for 16 h. ^{1}H NMR analysis showed no detectable formation of 3b-H, which was further confirmed via ^{1}H NMR spectroscopy by spiking in an (independently synthesized) authentic sample of **5a-N** into the reaction mixture. NMR data are shown in Figure S11, below.

authentic (**3b-H**) spiked into above reaction mixture
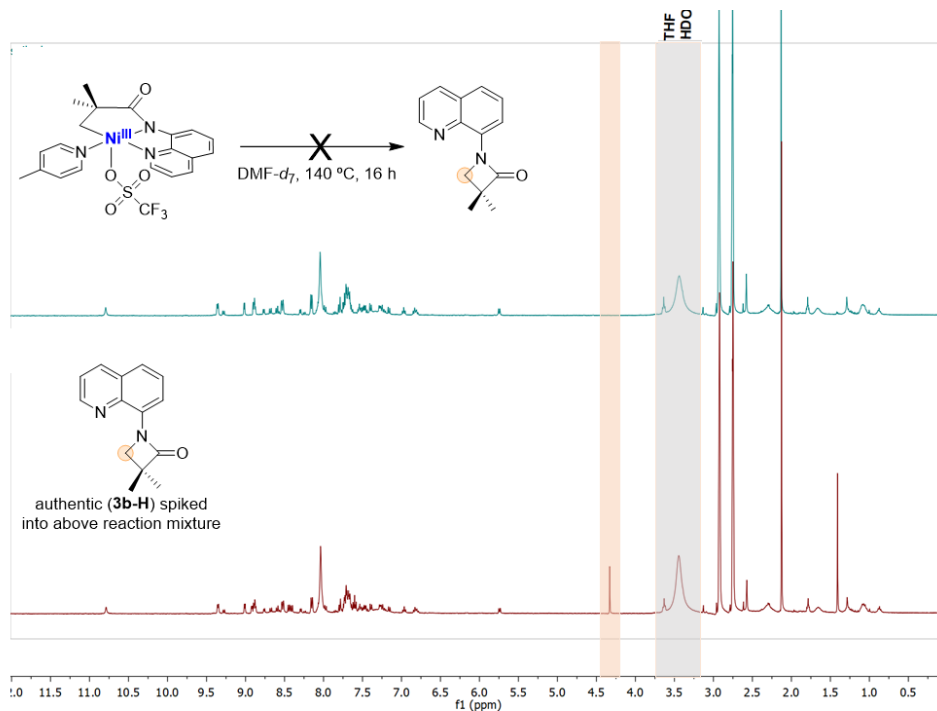
Thermolysis of 3b-OTf with NBu₄I in toluene-*d₈* and acetone- *d₆*
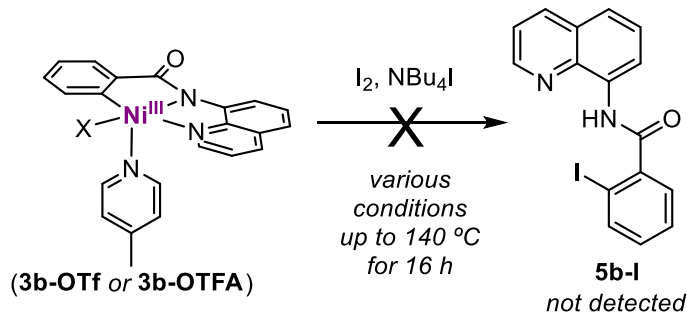
A 0.02 M stock solution of **3b-OTf** in toluene-d_8 (7.6 mg, 20 µmol in 1 mL of toluene-d_8) was prepared. A 0.5 mL aliquot of **3b-OTf** (3.8 mg, 10 µmol, 1 equiv) stock solution was placed in J. Young NMR tube, and either NBu₄I (7.4 mg, 20 µmol, 2 equiv) or I₂ (2.5 mg, 20 µmol, 2 equiv) was added. The resulting mixture was heated at 120 ºC for 16 h. ^{1}H NMR analysis showed no detectable formation of **5b-I**. Similar results were obtained for a reaction in acetone-d_6 after 16 h at 60 ºC and DMF-d_7 at 140 ºC for 16 h. Representative NMRs of the above reactions are presented below.

Analogous reactions were conducted with **3b-OTFA**, and they similarly afforded no detectable **5b-I**.

Note: **3b-OTf**, **3b-OTFA** and NBu₄I have poor to moderate solubility in toluene-d_8 but are completely soluble in acetone-d_6 and DMF-d_7.

Thermolysis of 3b-OTf with NBu₄I in toluene-*d*₈
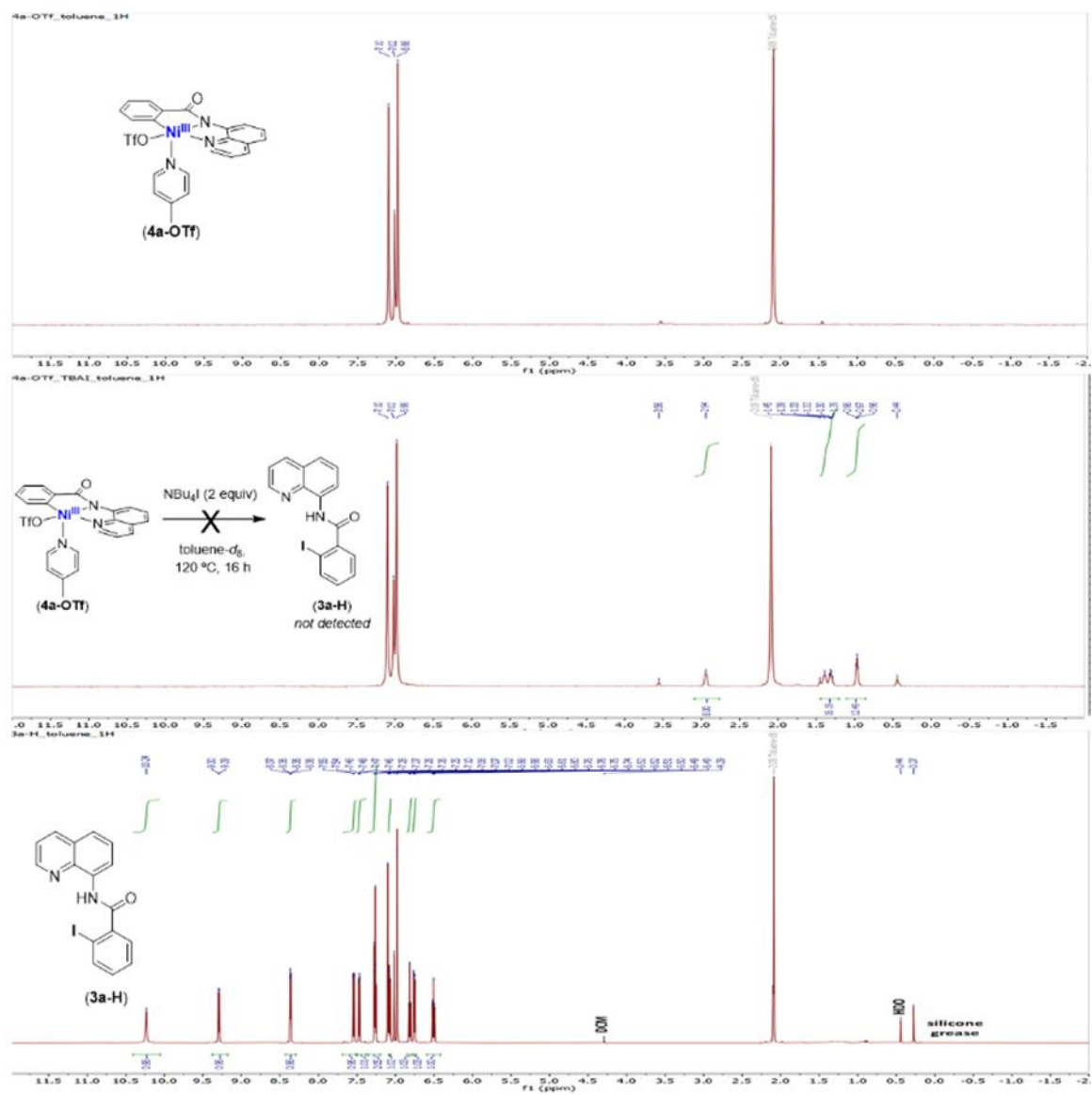
Thermolysis of 3b-OTf with NBu₄I in acetone-*d*₆
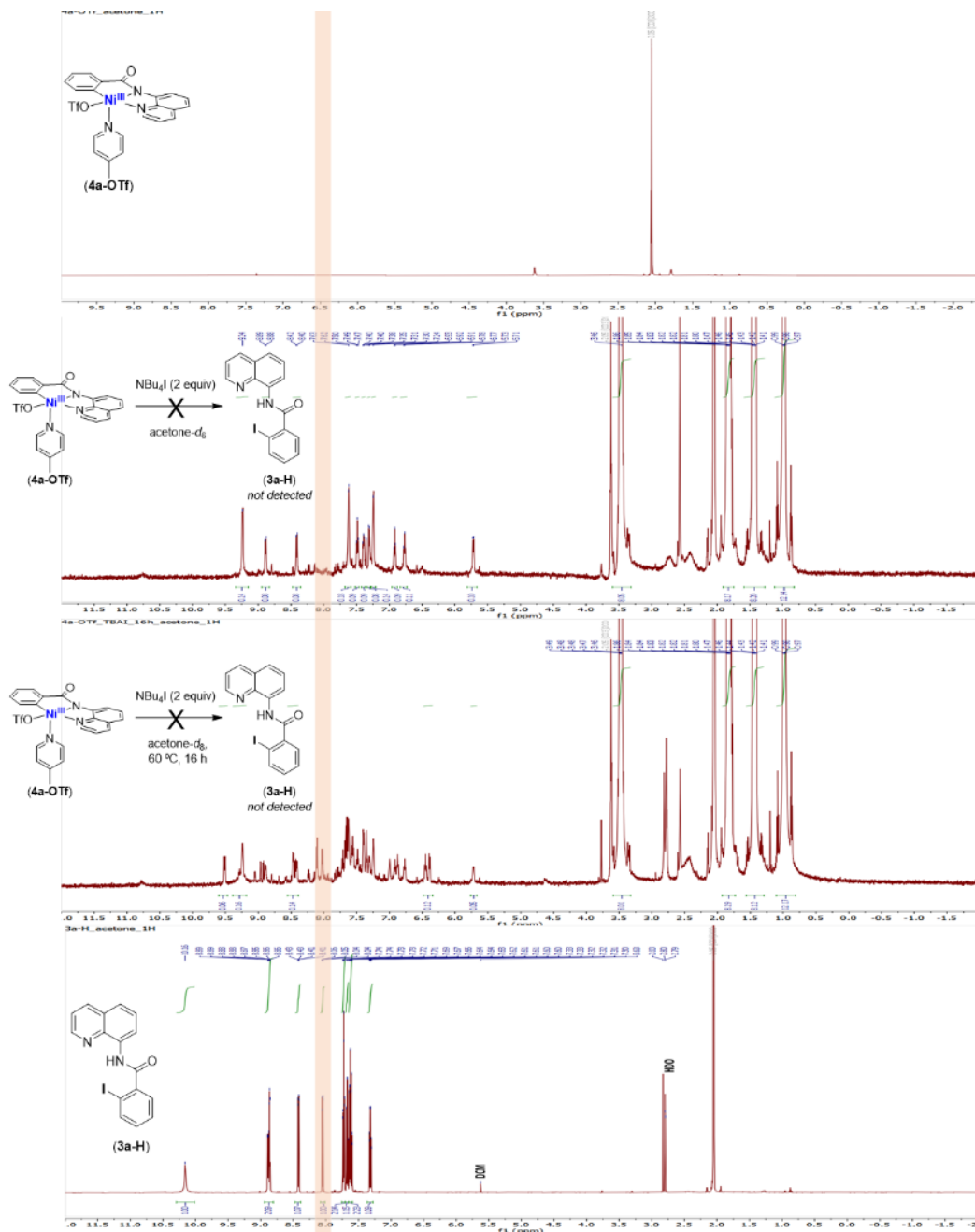
4.5.5 Catalytic Relevance of Nickel Complexes
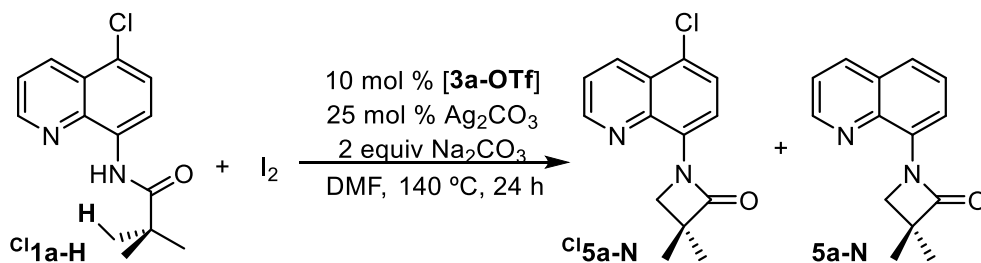
GC trace of Table 2, entry 3 with labeled retention times and experimentally observed yields; (b) Stacked GC traces (top) Table 2, entry 3, (top) and rest [Cl]1a-H, 1a-H, 5a-N, and [Cl]5a-N as labeled.

Peak#	Ret.Tim	Area	Height	Conc.	Mark	Compound ID#	Compound Name	Units
	0.751	20363742.9	1116868.5	0.00000	E			
	3.992	407974.5	97936.2	0.00000	S			
	9.612	23185.8	10775.5	0.00000				
	11.372	371004.5	73877.3	0.00000				
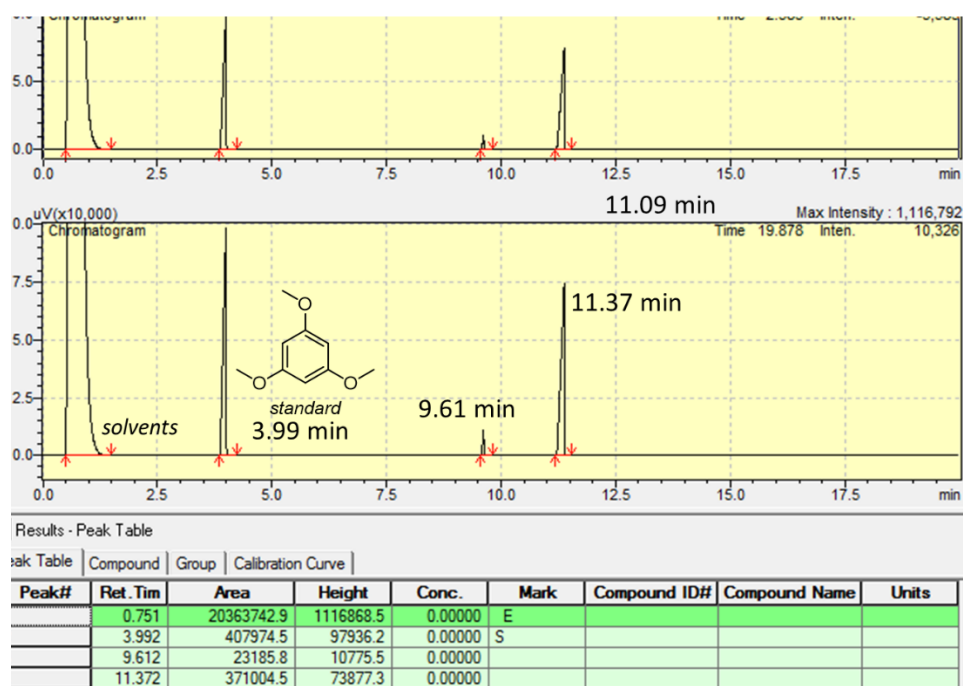
Ratio = 0.909 (SM:IS); urSM = ~91%
Ratio = 0.057 (1b-H:IS); yield = ~6%
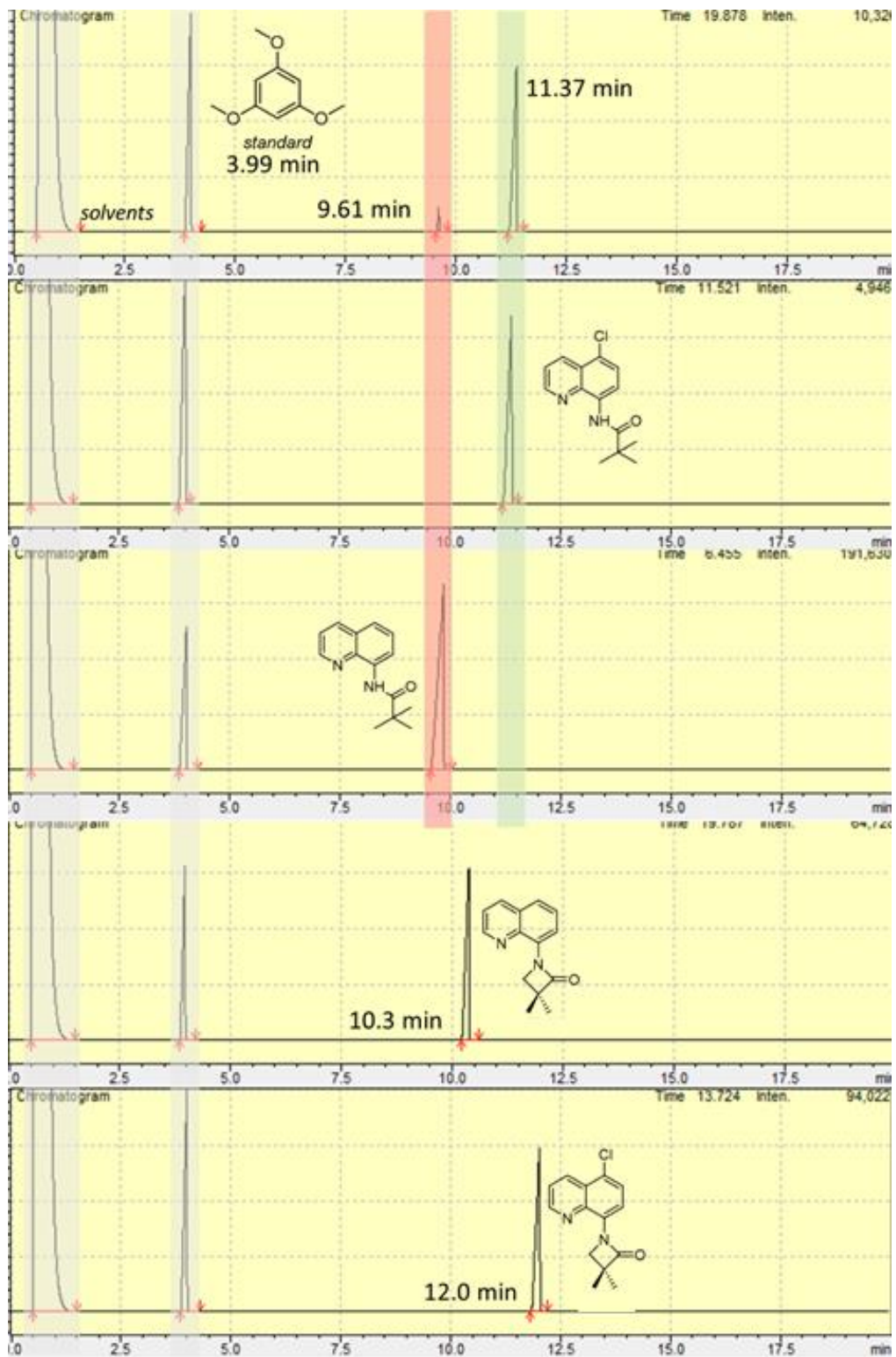
X-Ray Crystallographic Data of 3a-OTf
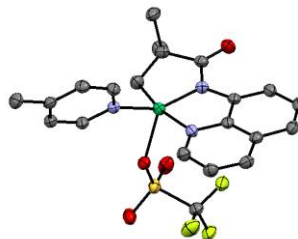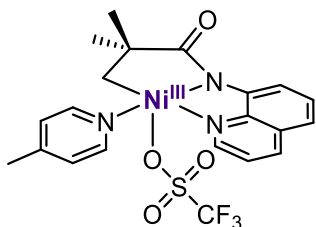
Brown plates of **3a-OTf** were grown from a THF/pentane solution of the compound at -30 °C. A crystal of dimensions 0.10 x 0.07 x 0.05 mm was mounted on a Rigaku AFC10K Saturn 944+ CCD-based X-ray diffractometer equipped with a low temperature device and Micromax-007HF Cu-target micro-focus rotating anode ($\lambda = 1.54187$ A) operated at 1.2 kW power (40 kV, 30 mA). The X-ray intensities were measured at 85(1) K with the detector placed at a distance 42.00 mm from the crystal. A total of 2028 images were collected with an oscillation width of 1.0° in ω. The exposure times were 1 sec. for the low angle images, 5 sec. for high angle. Rigaku d*trek images were exported to CrysAlisPro for processing and corrected for absorption. The integration of the data yielded a total of 32929 reflections to a maximum 2θ value of 138.67° of which 4112 were independent and 3827 were greater than 2σ(I). The final cell constants (Table 1) were based on the xyz centroids of 14911 reflections above 10σ(I). Analysis of the data showed negligible decay during data collection. The structure was solved and refined with the Bruker SHELXTL (version 2016/6) software package, using the space group P2(1)/n with Z = 4 for the formula C21H21N3O4F3SNi. All non-hydrogen atoms were refined anisotropically with the hydrogen atoms placed in idealized positions. Full matrix least-squares refinement based on F^2 converged at R1 = 0.0407 and wR2 = 0.1111 [based on I > 2sigma(I)], R1 = 0.0435 and wR2 = 0.1159 for all data. Additional details are presented in Table 1 and are given as Supporting Information in a CIF

file.   Acknowledgement is made for funding from NSF grant CHE-0840456 for X-ray instrumentation.

G.M. Sheldrick (2015) "Crystal structure refinement with SHELXL", Acta Cryst., C71, 3-8 (Open Access).

CrystalClear Expert 2.0 r16, Rigaku Americas and Rigaku Corporation (2014), Rigaku Americas, 9009, TX, USA 77381-5209, Rigaku Tokyo, 196-8666, Japan.

CrysAlisPro 1.171.38.41 (Rigaku Oxford Diffraction, 2015).

Table 4.5 Crystal data and structure refinement for **3a-OTf**

Empirical formula	C21 H21 F3 N3 Ni O4 S
Formula weight	527.17
Temperature	85(2) K
Wavelength	1.54184 A
Crystal system, space group	Monoclinic, P2(1)/n
Unit cell dimensions	a = 9.5689(2) A alpha = 90° b = 17.9404(3) A beta = 101.756(2)° c = 13.1615(3) A gamma = 90°
Volume	2212.05(8) A^3
Z, Calculated density	4, 1.583 Mg/m^3
Absorption coefficient	2.687 mm^-1
F(000)	1084
Crystal size	0.100 x 0.070 x 0.050 mm

Theta range for data collection	4.224 to 69.337°
Limiting indices	-11<=h<=11, -21<=k<=21, -15<=l<=15
Reflections collected / unique	32929 / 4112 [R(int) = 0.0662]
Completeness to theta = 67.684	99.90%
Absorption correction	Semi-empirical from equivalents
Max. and min. transmission	1.00000 and 0.61304
Refinement method	Full-matrix least-squares on F^2
Data / restraints / parameters	4112 / 0 / 301
Goodness-of-fit on F^2	1.096
Final R indices [I>2sigma(I)]	R1 = 0.0407, wR2 = 0.1111
R indices (all data)	R1 = 0.0435, wR2 = 0.1159
Extinction coefficient	n/a
Largest diff. peak and hole	0.426 and -0.516 e.A^-3

X-Ray Crystallographic Data of 3b-OTFA
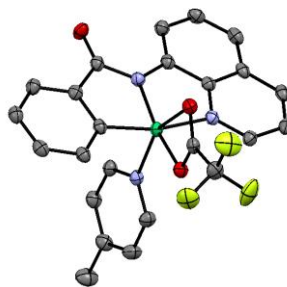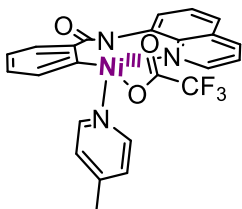
Brown needles of **3b-OTFA** were grown from a THF/pentane solution of the compound at -30 °C.

A crystal of dimensions 0.11 x 0.05 x 0.05 mm was mounted on a Rigaku AFC10K Saturn 944+

CCD-based X-ray diffractometer equipped with a low temperature device and Micromax-007HF

Cu-target micro-focus rotating anode (λ = 1.54187 A) operated at 1.2 kW power (40 kV, 30 mA).

The X-ray intensities were measured at 85(1) K with the detector placed at a distance 42.00 mm

from the crystal. A total of 2028 images were collected with an oscillation width of 1.0° in ω. The

exposure times were 1 sec. for the low angle images, 5 sec. for high angle. Rigaku d*trek images

were exported to CrysAlisPro for processing and corrected for absorption. The integration of the

data yielded a total of 16396 reflections to a maximum 2θ value of 138.32° of which 3902 were

independent and 3687 were greater than 2σ(I). The final cell constants (Table 1) were based on

the xyz centroids of 8272 reflections above 10σ(I). Analysis of the data showed negligible decay

during data collection. The structure was solved and refined with the Bruker SHELXTL (version

2018/3) software package, using the space group P1bar with Z = 2 for the formula

C24H17N3O3F3Ni. All non-hydrogen atoms were refined anisotropically with the hydrogen

atoms placed in idealized positions. Full matrix least-squares refinement based on F^2 converged

at R1 = 0.0385 and wR2 = 0.1058 [based on I > 2sigma(I)], R1 = 0.0404 and wR2 = 0.1081 for all

data. Additional details are presented in Table 1 and are given as Supporting Information in a CIF

G.M. Sheldrick (2015) "Crystal structure refinement with SHELXL", Acta Cryst., C71, 3-8 (Open Access).

CrystalClear Expert 2.0 r16, Rigaku Americas and Rigaku Corporation (2014), Rigaku Americas, 9009, TX, USA 77381-5209, Rigaku Tokyo, 196-8666, Japan.

CrysAlisPro 1.171.38.41 (Rigaku Oxford Diffraction, 2015).

Table 4.6 Crystal data and structure refinement for **3b-OTFA**

Empirical formula	C24 H17 F3 N3 Ni O3
Formula weight	511.11
Temperature	85(2) K
Wavelength	1.54184 A
Crystal system, space group	Triclinic, P-1
Unit cell dimensions	a = 8.4096(3) A alpha = 95.466(3)° b = 11.3752(4) A beta = 107.282(3)° c = 11.9729(4) A gamma = 92.626(3)°
Volume	1085.34(6) A^3
Z, Calculated density	2, 1.564 Mg/m^3
Absorption coefficient	1.816 mm^-1
F(000)	522
Crystal size	0.110 x 0.050 x 0.050 mm

Theta range for data collection	3.892 to 69.159°
Limiting indices	-9<=h<=10, -12<=k<=11, -14<=l<=14
Reflections collected / unique	16396 / 3902 [R(int) = 0.0384]
Completeness to theta = 67.684	97.6%
Absorption correction	Semi-empirical from equivalents
Max. and min. transmission	1.00000 and 0.81150
Refinement method	Full-matrix least-squares on F^2
Data / restraints / parameters	3902 / 0 / 308
Goodness-of-fit on F^2	1.044
Final R indices [I>2sigma(I)]	R1 = 0.0385, wR2 = 0.1058
R indices (all data)	R1 = 0.0404, wR2 = 0.1081
Extinction coefficient	n/a
Largest diff. peak and hole	0.443 and -0.417 e.A^-3

X-Ray Crystallographic Data of ^{Ni}5b-dimer
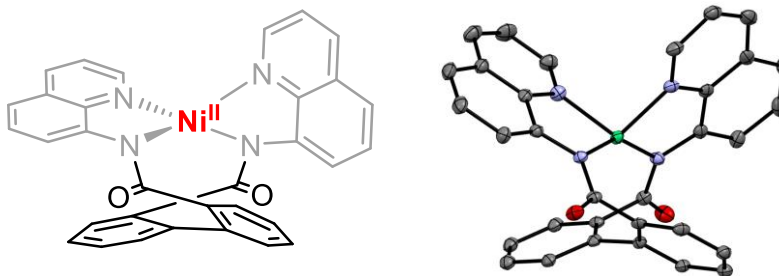
Brown prisms of ^{Ni}**5b-dimer** were grown from a tetrahydrofuran/pentane solution of the compound at 22 deg. C. A crystal of dimensions 0.09 x 0.04 x 0.04 mm was mounted on a Rigaku AFC10K Saturn 944+ CCD-based X-ray diffractometer equipped with a low temperature device and Micromax-007HF Cu-target micro-focus rotating anode (l = 1.54187 A) operated at 1.2 kW power (40 kV, 30 mA). The X-ray intensities were measured at 85(1) K with the detector placed at a distance 42.00 mm from the crystal. A total of 2028 images were collected with an oscillation width of 1.0° in w. The exposure times were 1 sec. for the low angle images, 3 sec. for high angle. Rigaku d*trek images were exported to CrysAlisPro for processing and corrected for absorption. The integration of the data yielded a total of 37571 reflections to a maximum 2q value of 138.66° of which 4645 were independent and 4464 were greater than 2s(I). The final cell constants (Table 1) were based on the xyz centroids of 23905 reflections above 10s(I). Analysis of the data showed negligible decay during data collection. The structure was solved and refined with the Bruker SHELXTL (version 2018/3) software package, using the space group P2(1)/c with Z = 4 for the formula C32H20N4O2Ni. All non-hydrogen atoms were refined anisotropically with the hydrogen atoms placed in idealized positions. Full matrix least-squares refinement based on F2 converged at R1 = 0.0329 and wR2 = 0.0824 [based on I > 2sigma(I)], R1 = 0.0341 and wR2 = 0.0835 for all data. Additional details are presented in Table 1 and are given as Supporting

Table 4.7 Crystal data and structure refinement for [Ni]**5b-dimer**

Empirical formula	C32 H20 N4 Ni O2
Formula weight	551.23
Temperature	85(2) K
Wavelength	1.54184 A
Crystal system, space group	Monoclinic, P2(1)/c
Unit cell dimensions	a = 10.01885(6) A alpha = 90° b = 14.28386(10) A beta = 92.6637(5)° c = 17.50086(11) A gamma = 90°
Volume	2501.81(3) A^3
Z, Calculated density	4, 1.463 Mg/m^3
Absorption coefficient	1.431 mm^-1
F(000)	1136
Crystal size	0.090 x 0.040 x 0.040 mm

Theta range for data collection	3.997 to 69.332°
Limiting indices	-12<=h<=12, -16<=k<=17, -21<=l<=21
Reflections collected / unique	37571 / 4645 [R(int) = 0.0404]
Completeness to theta = 67.684	99.9%
Absorption correction	Semi-empirical from equivalents
Max. and min. transmission	1.00000 and 0. 87578
Refinement method	Full-matrix least-squares on F^2
Data / restraints / parameters	4645 / 0 / 353
Goodness-of-fit on F^2	1.036
Final R indices [I>2sigma(I)]	R1 = 0.0329, wR2 = 0.0824
R indices (all data)	R1 = 0.0341, wR2 = 0.0834
Extinction coefficient	0.00098(11)
Largest diff. peak and hole	0.310 and -0.478 e.A^-3

X-Ray Crystallographic Data of Ni₁

Blue blocks of **Ni₁** were grown from a tetrahydrofuran solution of the compound at 24 deg. C. A crystal of dimensions 0.10 x 0.10 x 0.02 mm was mounted on a Rigaku AFC10K Saturn 944+ CCD-based X-ray diffractometer equipped with a low temperature device and Micromax-007HF Cu-target micro-focus rotating anode (l = 1.54187 A) operated at 1.2 kW power (40 kV, 30 mA). The X-ray intensities were measured at 85(1) K with the detector placed at a distance 42.00 mm from the crystal. A total of 2028 images were collected with an oscillation width of 1.0° in w. The exposure times were 1 sec. Rigaku d*trek images were exported to CrysAlisPro for processing and corrected for absorption. The integration of the data yielded a total of 41598 reflections to a maximum 2q value of 140.72° of which 2901 were independent and 1725 were greater than 2s(I). The final cell constants (Table 1) were based on the xyz centroids of 4392 reflections above 10s(I). Analysis of the data showed negligible decay during data collection. The structure was solved and refined with the Bruker SHELXTL (version 2018/3) software package, using the space group Pbcn with Z = 4 for the formula C26H28N4O6F6S2Ni. All non-hydrogen atoms were refined anisotropically with the hydrogen atoms placed in idealized positions. The complex lies on a two-fold rotation axis in the crystal lattice. Full matrix least-squares refinement based on F2 converged at R1 = 0.01344 and wR2 = 0.4122 [based on I > 2sigma(I)], R1 = 0.1742 and wR2 = 0.4679 for all data. Additional details are presented in Table 1 and are given as Supporting Information in a

CIF file.   Acknowledgement is made for funding from NSF grant CHE-0840456 for X-ray instrumentation.

G.M. Sheldrick (2015) "Crystal structure refinement with SHELXL", Acta Cryst., C71, 3-8 (Open Access).

CrystalClear Expert 2.0 r16, Rigaku Americas and Rigaku Corporation (2014), Rigaku Americas, 9009, TX, USA 77381-5209, Rigaku Tokyo, 196-8666, Japan.
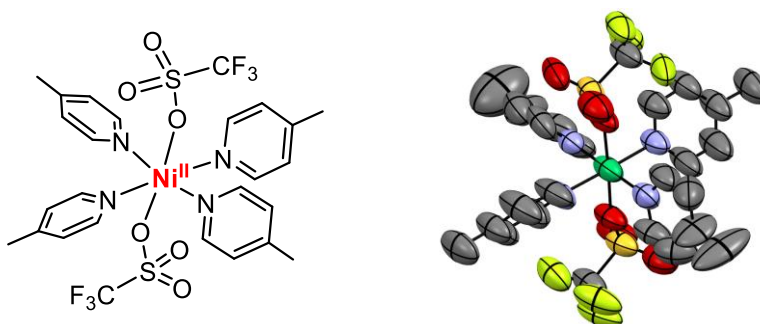
CrysAlisPro 1.171.40.53 (Rigaku Oxford Diffraction, 2019).

Table 4.8 Crystal data and structure refinement for **Ni₁**

Empirical formula	C32 H20 N4 Ni O2
Formula weight	551.23
Temperature	85(2) K
Wavelength	1.54184 A
Crystal system, space group	Monoclinic, P2(1)/c
Unit cell dimensions	a = 10.01885(6) A alpha = 90° b = 14.28386(10) A beta = 92.6637(5)° c = 17.50086(11) A gamma = 90°
Volume	2501.81(3) A^3
Z, Calculated density	4, 1.463 Mg/m^3
Absorption coefficient	1.431 mm^-1
F(000)	1136
Crystal size	0.090 x 0.040 x 0.040 mm

Theta range for data collection	3.997 to 69.332°
Limiting indices	-12<=h<=12, -16<=k<=17, -21<=l<=21
Reflections collected / unique	37571 / 4645 [R(int) = 0.0404]
Completeness to theta = 67.684	99.9%
Absorption correction	Semi-empirical from equivalents
Max. and min. transmission	1.00000 and 0. 87578
Refinement method	Full-matrix least-squares on F^2
Data / restraints / parameters	4645 / 0 / 353
Goodness-of-fit on F^2	1.036
Final R indices [I>2sigma(I)]	R1 = 0.0329, wR2 = 0.0824
R indices (all data)	R1 = 0.0341, wR2 = 0.0834
Extinction coefficient	0.00098(11)
Largest diff. peak and hole	0.310 and -0.478 e.A^-3

X-Ray Crystallographic Data of Ni₂

Pale green needles of **Ni₂** were grown from a tetrahydrofuran solution of the compound at 22 deg. C. A crystal of dimensions 0.08 x 0.05 x 0.05 mm was mounted on a Rigaku AFC10K Saturn 944+ CCD-based X-ray diffractometer equipped with a low temperature device and Micromax-007HF Cu-target micro-focus rotating anode (l = 1.54187 A) operated at 1.2 kW power (40 kV, 30 mA). The X-ray intensities were measured at 85(1) K with the detector placed at a distance 42.00 mm from the crystal. A total of 2028 images were collected with an oscillation width of 1.0° in w. The exposure times were 1 sec. for the low angle images, 2 sec. for high angle. Rigaku d*trek images were exported to CrysAlisPro for processing and corrected for absorption. The integration of the data yielded a total of 42551 reflections to a maximum 2q value of 138.48° of which 2736 were independent and 2612 were greater than 2s(I). The final cell constants (Table 1) were based on the xyz centroids of 17073 reflections above 10s(I). Analysis of the data showed negligible decay during data collection. The structure was solved and refined with the Bruker SHELXTL (version 2018/3) software package, using the space group Pbcn with Z = 4 for the formula C24H29N3O7F6S2Ni. The complex lies on a two-fold rotation axis of the crystal lattice. All non-hydrogen atoms were refined anisotropically with the hydrogen atoms placed in idealized positions. Full matrix least-squares refinement based on F2 converged at R1 = 0.0560 and wR2 = 0.1495 [based on I > 2sigma(I)], R1 = 0.0577 and wR2 = 0.1515 for all data. Additional details

are presented in Table 1 and are given as Supporting Information in a CIF file. Acknowledgement is made for funding from NSF grant CHE-0840456 for X-ray instrumentation.

G.M. Sheldrick (2015) "Crystal structure refinement with SHELXL", Acta Cryst., C71, 3-8 (Open Access).

CrystalClear Expert 2.0 r16, Rigaku Americas and Rigaku Corporation (2014), Rigaku Americas, 9009, TX, USA 77381-5209, Rigaku Tokyo, 196-8666, Japan.
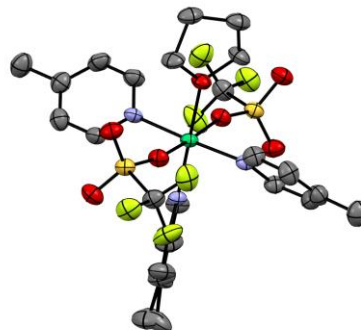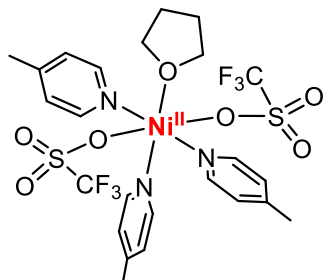
CrysAlisPro 1.171.38.41 (Rigaku Oxford Diffraction, 2015).

Table 4.9 Crystal data and structure refinement for **Ni₂**

Empirical formula	C32 H20 N4 Ni O2
Formula weight	551.23
Temperature	85(2) K
Wavelength	1.54184 A
Crystal system, space group	Monoclinic, P2(1)/c
Unit cell dimensions	a = 10.01885(6) A alpha = 90° b = 14.28386(10) A beta = 92.6637(5)° c = 17.50086(11) A gamma = 90°
Volume	2501.81(3) A^3
Z, Calculated density	4, 1.463 Mg/m^3
Absorption coefficient	1.431 mm^-1
F(000)	1136
Crystal size	0.090 x 0.040 x 0.040 mm

Theta range for data collection	3.997 to 69.332°
Limiting indices	-12<=h<=12, -16<=k<=17, -21<=l<=21
Reflections collected / unique	37571 / 4645 [R(int) = 0.0404]
Completeness to theta = 67.684	99.9%
Absorption correction	Semi-empirical from equivalents
Max. and min. transmission	1.00000 and 0. 87578
Refinement method	Full-matrix least-squares on F^2
Data / restraints / parameters	4645 / 0 / 353
Goodness-of-fit on F^2	1.036
Final R indices [I>2sigma(I)]	R1 = 0.0329, wR2 = 0.0824
R indices (all data)	R1 = 0.0341, wR2 = 0.0834
Extinction coefficient	0.00098(11)
Largest diff. peak and hole	0.310 and -0.478 e.A^-3

Chapter 5 Attempts and Outlook towards the Isolation of Ni^{IV}

5.1 Introduction

In the 1990s, the first organometallic Ni^{IV} complexes were isolated.[1] The guiding principles for isolation focused on appropriate choice of ligands. Ni^{IV} complexes are generally unstable and decompose through: (*i*) ligand homolysis, (*ii*) reductive elimination, and (*iii*) other reduction reactions. To tackle these problems, multidentate ligands binding though highly electronegative atoms (N, O, F, CF$_3$) were selected. The seminal report by Klein leveraged these guiding principles by using multidentate ligands with electronegative atoms (O, P, I) to isolate the first organometallic Ni^{IV} complex (Figure 5.1).

Figure 5.1 First Isolated Organometallic Ni^{IV} complex

multidentate ligand
electronegative O & C(O) centers

Klein, **1994**
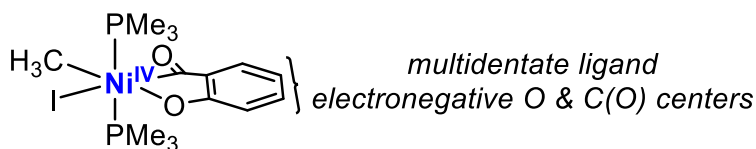
In 2015, Sanford incorporated these design principles for the isolation of a Ni^{IV} complex and then studied the reactivity of this species in C–X (X = N, O, S) bond-forming processes.[2] Here, a tridentate N-centered facial trispyrazolylborate ligand and a strong electronegative CF$_3$ ligand were employed to stabilize the high oxidation state. In 2016, Mirica independently reported the isolation of a Ni^{IV} species with a tetradentate N-centered macrocyclic ligand (Figure 5.2).[3,4] Notably, both these reports used the bidentate neophyl moiety to impart structural stability and to enable probing of C–X coupling. Subsequently, Ni^{IV} complexes with other ancillary polydentate

ligands have been isolated, highlighting the importance of polydentate ligands for the stabilization of Ni[IV] species.[5,6]

Figure 5.2 Representative Ni[IV] Complexes to Study C–X (C, N, O, S) Reductive Elimination

Sanford, **2015**   *Mirica*, **2016**
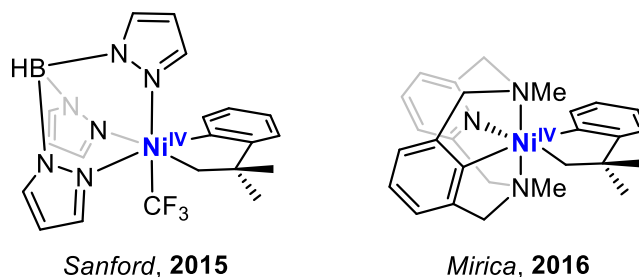
C–X bond formation from Ni[IV] species has been proposed for the catalytically relevant meridional, aminoquinoline scaffold as well. However, since the C–H activation step is believed to be thermodynamically uphill under most catalytic conditions, the veracity of the proposed Ni[IV] intermediate has yet to be tested.[7–9] This chapter summarizes our efforts to isolate and/or spectroscopically observe a Ni[IV] species with the cyclometalated aminoquinoline ligand (Figure 5.3).

Figure 5.3 Proposed Ni[IV] Intermediates on the Aminoquinoline Scaffold
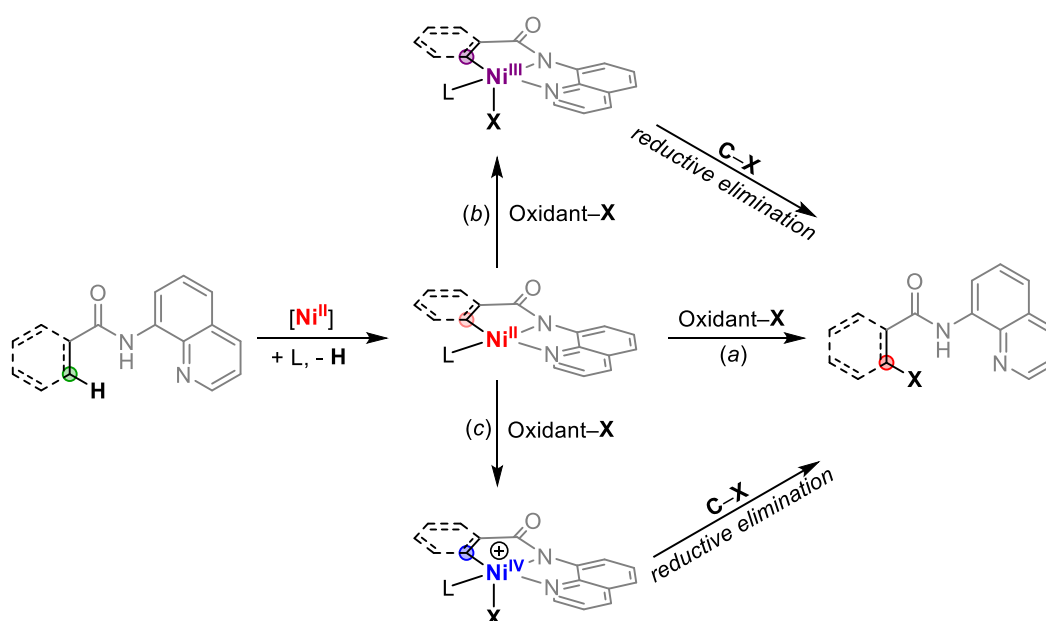
The first part of the chapter summarizes oxidative reactivity studies from the previously isolated Ni^{II} and Ni^{III} complexes with one and two electron oxidants, respectively. Although, trace C–X coupling was observed in some cases, no new Ni^{IV} species were spectroscopically observed. We hypothesized that the electron rich aromatic aminoquinoline was being functionalized at the 5-position under these oxidation reactions. Similar observations had led Chatani to install an electron-withdrawing Cl-group at this position to promote Ni- rather than ligand-centered oxidative functionalization (Figure 5.4).[10]

Figure 5.4 Derivatized 5-position for Ni-centered Oxidations by Chatani
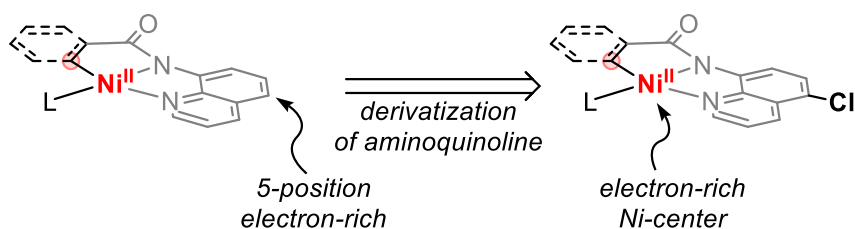
The previously established route to the Ni^{II} complexes leveraged a decarbonylation reaction of imides (weak electrophiles) with a strongly nucleophilic Ni^0 source. However, we noted that Ni^0-mediated activation of $C(sp^2)$–Cl bonds is also well-known.[11–13] Hence, the presence of Cl group on the starting aminoquinoline imide was anticipated to lead to multiple reaction products and subsequent problems with isolation.

Figure 5.5 Polydentate Ligands to Promote Ni-based Oxidation
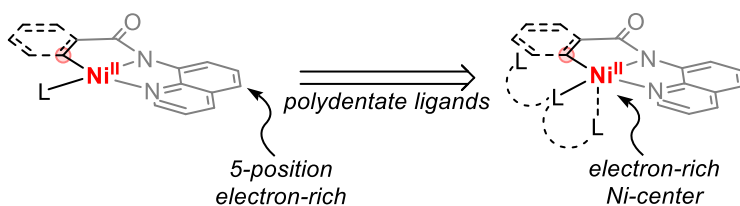
Thus, an alternative strategy to promote Ni-centered oxidation was proposed by installing a multidentate ancillary ligand (Figure 5.5). Ligand exchange at the Ni^{II} center was slow and attempts towards product isolations were unsuccessful. Thus, a one-pot procedure for ligand

153

exchange coupled with Ag^I-mediated oxidation was used to generate Ni^{III} complexes bearing polydentate ligands. However, subsequent one-electron oxidation reactions of these complexes did not lead an observable Ni^{IV} complex.

Although all attempts to observe and/or isolate a Ni^{IV} complex were unsuccessful, a concluding outlook section has been compiled. This last section is based on conclusions from the reactivity studies of all previous chapters as well as inspirations drawn from previous literature reports. This should serve as a guide for future attempts towards the isolation of a Ni^{IV} complex on this ligand scaffold.

5.2 Result and Discussion

5.2.1 Two-electron Oxidation Studies of σ-alkyl Nickelacycles

The isolation of the σ-alkyl Ni^{II} complex **2a-pic** was significantly easier that its σ-aryl analogue **2b-pic**. Thus, all oxidation studies in pursuit of Ni^{IV} were performed with **2a-pic** for scalability purposes. Cyclic voltammetry studies of **2a-pic** show that a second oxidation event at ~1.1 V versus Ag/Ag⁺. This was tentatively assigned as the $Ni^{III/IV}$ couple (Figure 5.6). This suggests that strong two-electron oxidants will be required to access Ni^{IV}. Notably, these generally contain highly electronegative groups such as fluorine (F) or trifluoromethyl (CF_3), which have frequently been employed as ligands for isolated Ni^{IV} species.[2,5,14,15]

Figure 5.6 CV of **2a-pic**
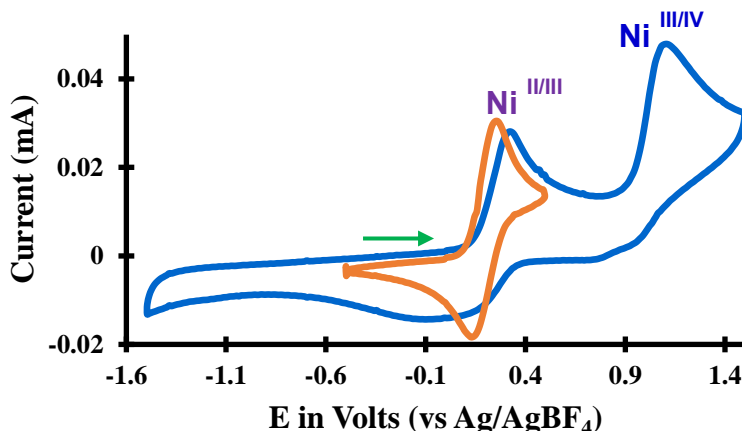
The treatment of **2a-pic** with equimolar quantities of a two-electron oxidant such as N-fluoropyridinium triflate (F$^+$-oxidant) or 2,8-difluoro-S-(trifluoromethyl)dibenzothiophenium triflate (CF$_3{}^+$-oxidant) predominantly led to formation of Ni^{III} species. This was inferred by paramagnetic broadening of ^{1}H NMR spectra and a lack of diagnostic Ni^{IV}–F or Ni^{IV}–CF$_3$ peaks in ^{19}F NMR spectra.[2] Similar results were obtained with other common oxidants, such as PhI(OAc)$_2$ (AcO$^+$-oxidant) and N-fluorobenzenesulfonimide (F$^+$-oxidant). In general, upon treatment with the oxidant at 25 °C in MeCN-d_3 an instantaneous color change was observed to either pale yellow or pale green (Scheme 5.1).

Scheme 5.1 Formation of Ni^{III} from **2a-pic** with F$^+$ and CF$_3{}^+$ oxidants
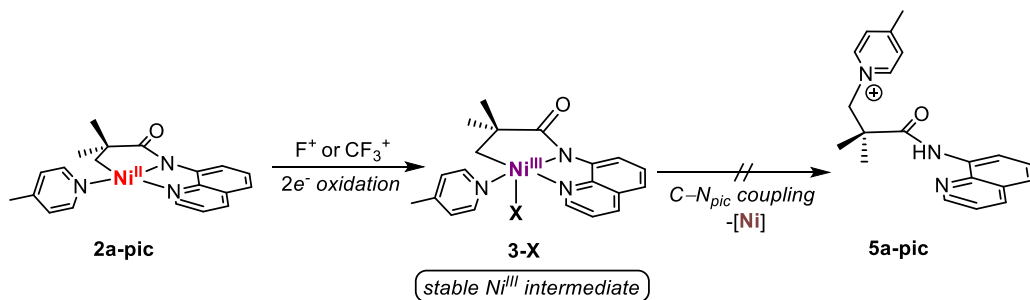
Notably, no C(sp^3)–N coupling products such as **5a-N** or **5a-pic** were observed with two-electron oxidants, similar to what was observed with one-electron oxidants in Chapter 2. These

results suggest that these oxidants promote single electron processes and fail to yield Ni^{IV}. Thus, we hypothesized that an ever stronger oxidant might be required to access the two electron oxidation of **2a-pic**.

Scheme 5.2 C(sp^3)–N Coupling from **2a-pic** with XeF$_2$ in MeCN-d_3 at 25 °C
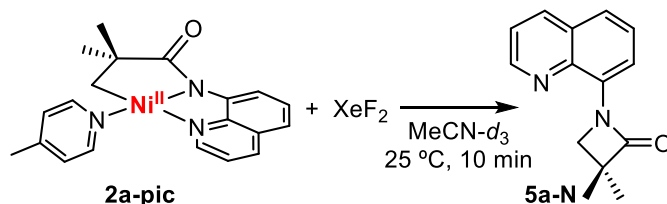
Xenon difluoride (XeF$_2$) is one of the strongest oxidants known and is commonly used as a difluorine (F$_2$) surrogate. It has been previously been used for oxidation of Pd^{II} to Pd^{IV} species.[16,17] Upon treatment of **2a-pic** with an equimolar quantity of XeF$_2$, an immediate color change from orange to pale green was observed along with the extrusion of white fumes (Scheme 5.2). No diamagnetic Ni^{IV} species were detected, but the formation of **5a-N** was observed at a maximum yield of 18% by ^{1}H NMR spectroscopy. Since, this bond formation has not been observed from previous Ni^{III} (**3a**) species, this result suggests the possibility of a transient Ni^{IV} species under these conditions. We also observed the formation of some aryl fluoride signals via ^{19}F NMR spectroscopy (at -116.3 and 129.4 ppm), which are tentatively assigned as fluorination on the 5-position of the aminoquinoline scaffold.

Scheme 5.5.3 Proposed Route to Polydentate Ligand Supported Ni^{IV} Complexes
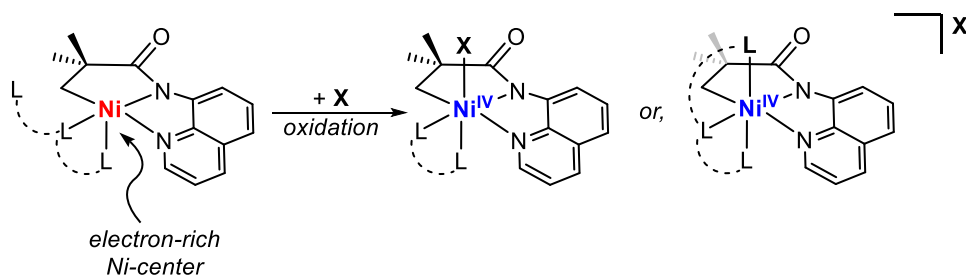
We next hypothesized that the use of polydentate ligand-supported nickel complexes would help mitigate both the challenges faced previously. Specifically, the polydentate ligand bound to the nickel center should increase electron density as well as facilitate formation of octahedral Ni^{IV} intermediates, thereby promoting selective Ni-centered oxidation over undesired aminoquinoline backbone functionalization.

5.2.2 Synthesis and Preliminary Oxidation Studies of Polydentate Ni^{III} Complexes

Literature reports and studies from Chapter 2 indicated that pyridine ligands were superior in supporting high-valent nickel complexes. Thus, in attempts to isolate polydentate ligand supported Ni-complexes, we examined the reactions of **2a-PEt₃** and **2a-pic** with multi-dentate pyridine-based ligands. However, as shown in Scheme 5.4, with both bi- and tridentate pyridines, ligand exchange was sluggish and resulted in the formation of a mixture of species. This ligand exchange could not be driven to completion even by removal of volatile PEt_3 under active vacuum with **2a-PEt₃** as the precursor.

Scheme 5.5.4 Failed Attempts at Ligand Exchange from **2a**
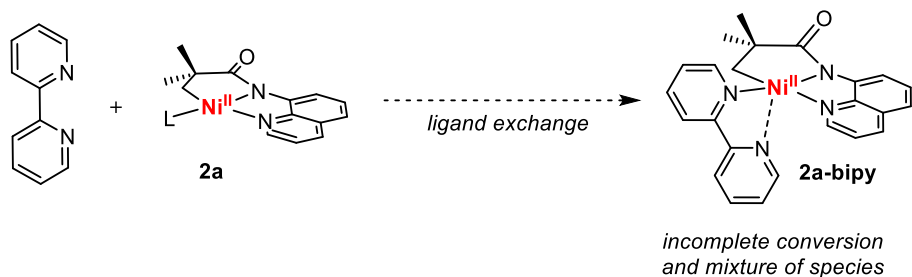
As discussed in Chapters 3 and 4, various oxidation studies with **2a-pic** resulted in the formation of stable Ni^{III} species, where the fifth ligand is either a solvent molecule or the counter-anion of the oxidant. Thus, we next conducted an analogous one-pot oxidation followed by ligand exchange to access Ni^{III} complexes bearing multidentate supporting ligands (Figure 5.7). After 30 mins, the ^1H NMR spectrum of the reaction mixture showed complete disappearance of the

diamagnetic signals attributed to **2a-pic**. The Ag^0 precipitate was removed by filtering this reaction

mixture through a plug of Celite. The Ni^{III} products (**3a-L**) were isolated by removal of solvent

under reduced pressure and recrystallization from a ternary mixture of acetone, diethyl ether, and

pentane.

Figure 5.7 General Procedure for Synthesis of **3a-L** Complexes
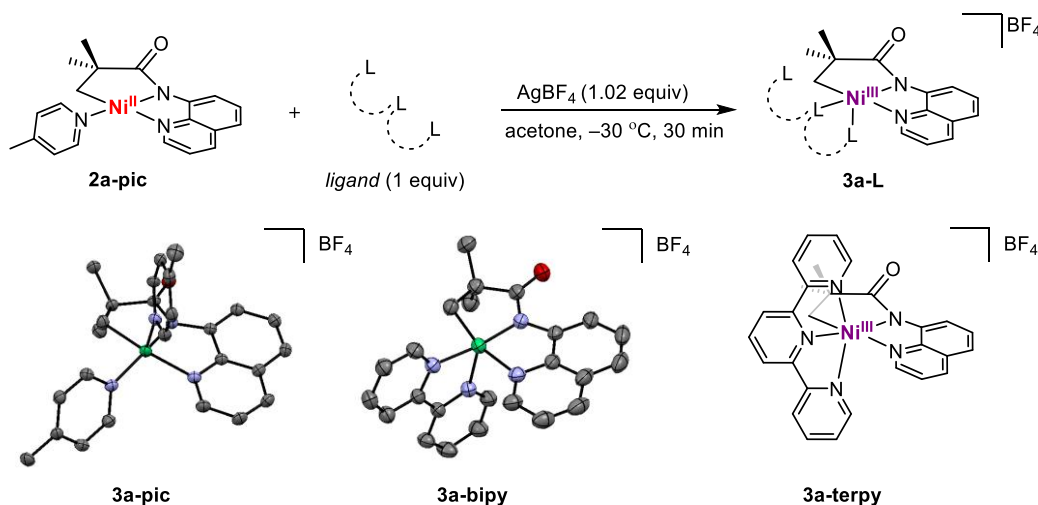
This strategy was successful for the isolation of three new Ni^{III} (**3a-L**) complexes by

treatment of **2a-pic** with stoichiometric amounts of AgBF$_4$ and ligand (ligand = picoline,

bipyridine, or terpyridine). Complexes **3a-L** depicted broad paramagnetic resonances in the ^{1}H

NMR spectrum and rhombic (S = ½) EPR signals were noted. A hyperfine splitting was observed

for **3a-terpy** but not for **3a-pic** and **3a-bipy**. Both the bis-picoline (**3a-pic**) and bipyridine (**3a-bipy**) complexes were characterized by X-ray crystal structures. In contrast, to date, attempts to

obtain a single crystal structure of the terpyridine complex (**3a-terpy**) have been unsuccessful.

Notably, Vicic has reported on the fluxional nature of the terpyridine ligand at Ni complexes,

which can result in the formation of bridged bimetallic species and thus complicate

characterization.[18–20]

Figure 5.8 CV of **3a-pic** at different scan rates,
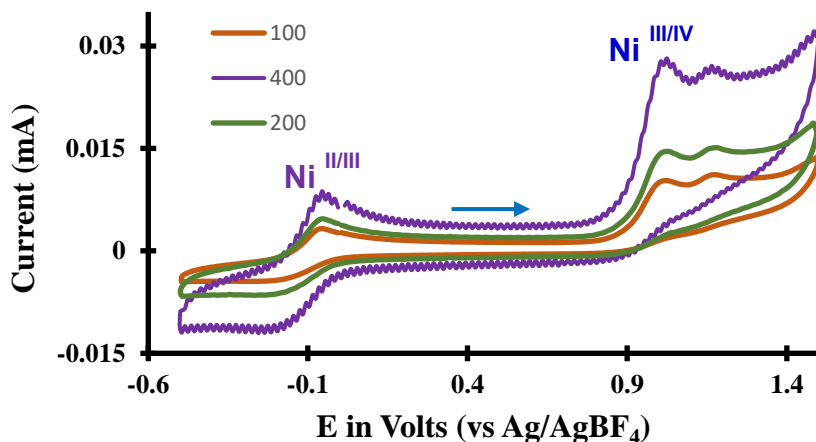
Cyclic voltammetry of isolated Ni^{III} complexes (**3a-L**) indicated a small negative shift (~50 mV) for the Ni$^{II/III}$ peak compared to that of **2a-pic**. The data for **3a-pic** are representative and are shown in Figure 5.8. Two peaks are observed at 0.95 V and 1.15 V in the tentatively assigned Ni$^{III/IV}$ region compared to the single peak at 1.1 V for **2a-pic**. Although the rationale for these split peaks was not investigated, we hypothesize that one of these species may be the 6-coordinate solvent (MeCN) bound complex. This is supported by the qualitative change in ratio of both these peaks under different scan rates (Figure 5.8).

Scheme 5.5 Preliminary Oxidative Studies from **3a-L**
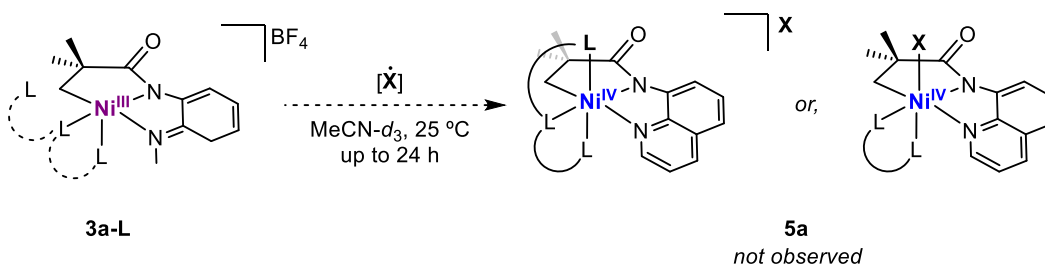
Preliminary one-electron oxidation studies of **3a-L** complexes with equimolar quantities of a strong oxidant such as NOBF$_4$ (~0.9 V vs. Fc$^+$/Fc) led to no change in color of the reaction and no noticeable change in the ^{1}H NMR spectra. This is consistent with the electrochemical results

that $NOBF_4$ is not a strong enough oxidant for this transformation. Although this did not lead to the formation of any observable Ni^{IV} species, future experiments could interrogate the use of stronger oxidants such as XeF_2 or Umemoto's reagent.

5.3 Conclusions

The reactions of **2a-pic** with two electron oxidants predominantly led to either (*i*) functionalization at the 5-position on the aminoquinoline backbone or (*ii*) formation of Ni^{III}. Thus, polydentate Ni^{III} complexes (**3a-L**) were isolated to promote Ni-centered oxidation. However, when treated with strong oxidants, the complexes **3a-L** did not lead to any observable Ni^{IV} species as probed by NMR spectroscopy. This does not rule out the feasibility of a transient Ni^{IV} species on this scaffold, as a low yield of **5a-N** ($C(sp^3)$–N coupling) was observed from oxidation of **2a-pic** with XeF_2, but not from any Ni^{III} complexes (**3a-L**).

5.4 Summary and Outlook

Studies from Chapters 2 and 3 showed that the cyclometalated aminoquinoline Ni^{II} complexes (**2-L**) can be isolated via a decarbonylation reaction. Ni^{III} complexes (**3a**) were isolable from **2a-pic** but not from **2a-PEt₃.** This highlights the stabilizing effect of nitrogen donor ligands on high valent Ni intermediates. Chapters 4 and 5 describe attempts to isolate Ni^{III} and Ni^{IV} species. Ag^{I}-mediated oxidations of **2-pic** complexes afforded isolable Ni^{III} species. In attempts to isolate a Ni^{IV} species, polydentate ligand supported Ni^{III} complexes (**3a-L**) were isolated to bias the systems towards Ni-centered oxidations. Electrophilic reactivity on the aminoquinoline backbone was minimized in these systems, and no $C(sp^3)$–N bond formation was observed. However, no Ni^{IV} species were detected, even with strong oxidants.

160

Figure 5.9 Proposal for Isolable Ni^{IV} species on the Aminoquinoline Scaffold
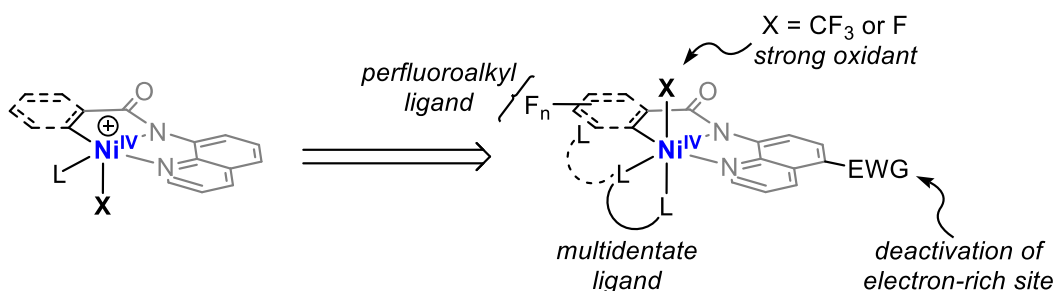
In 2015, Vicic demonstrated that perfluoroalkyl ligands stabilize high valent Ni-complexes.[18,20–22] Thus, future studies should focus on the design of Ni complexes supported by perfluoroalkyl ligands. Such Ni^{II} complexes can be synthesized via similar decarbonylation routes to that of **2-PEt₃**. This would likely significantly mitigate decomposition via C(sp^3)–N bond coupling owing to polarity mismatch required for reductive elimination.

Moreover, Vicic has observed that perfluoroalkyl bound metal complexes are more electrophilic compared to the alkyl analogs, owing to the higher electronegativity of the fluoroalkyl ligand. This enhanced electrophilicity can promote facile ligand exchange for the isolation of nickel complexes supported by tunable polydentate ligands. Subsequent oxidation may lead to isolable Ni^{IV} complexes bearing the aminoquinoline scaffold.

5.5 References

(1)   Klein, H.-F.; Bickelhaupt, A.; Jung, T.; Cordier, G. Syntheses and Properties of the First Octahedral Diorganonickel(IV) Compounds. *Organometallics* **1994**, *13* (7), 2557–2559. https://doi.org/10.1021/om00019a007.

(2)   Camasso, N. M.; Sanford, M. S. Design, Synthesis, and Carbon-Heteroatom Coupling Reactions of Organometallic Nickel(IV) Complexes. *Science* **2015**, *347* (6227), 1218–1220. https://doi.org/10.1126/SCIENCE.AAA4526.

(3)   W. Schultz, J.; Fuchigami, K.; Zheng, B.; P. Rath, N.; M. Mirica, L. Isolated Organometallic Nickel(III) and Nickel(IV) Complexes Relevant to Carbon–Carbon Bond Formation Reactions. *Journal of the American Chemical Society* **2016**, *138* (39), 12928–12934. https://doi.org/10.1021/jacs.6b06862.

(4)   B. Watson, M.; P. Rath, N.; M. Mirica, L. Oxidative C–C Bond Formation Reactivity of Organometallic Ni(II), Ni(III), and Ni(IV) Complexes. *Journal of the American Chemical Society* **2016**, *139* (1), 35–38. https://doi.org/10.1021/jacs.6b10303.

(5)   Heberer, N.; Hu, C.-H.; Mirica, L. M. 6.09 - High-Valent Ni Coordination Compounds. In *Comprehensive Coordination Chemistry III*; Constable, E. C., Parkin, G., Que Jr, L., Eds.; Elsevier: Oxford, 2021; pp 348–374. https://doi.org/https://doi.org/10.1016/B978-0-08-102688-5.00104-5.

(6)   Nebra, N. High-Valent NiIII and NiIV Species Relevant to C–C and C–Heteroatom Cross-Coupling Reactions: State of the Art. *Molecules* **2020**, *25* (5). https://doi.org/10.3390/molecules25051141.

(7)   Khake, S. M.; Chatani, N. Chelation-Assisted Nickel-Catalyzed C-H Functionalizations. *Trends in Chemistry* **2019**, *1* (5), 524–539. https://doi.org/10.1016/j.trechm.2019.06.002.

(8)   Yokota, A.; Aihara, Y.; Chatani, N. Nickel(II)-Catalyzed Direct Arylation of C–H Bonds in Aromatic Amides Containing an 8-Aminoquinoline Moiety as a Directing Group. *The Journal of Organic Chemistry* **2014**, *79* (24), 11922–11932. https://doi.org/10.1021/jo501697n.

(9)   Iyanaga, M.; Aihara, Y.; Chatani, N. Direct Arylation of C(Sp3)–H Bonds in Aliphatic Amides with Diaryliodonium Salts in the Presence of a Nickel Catalyst. *The Journal of Organic Chemistry* **2014**, *79* (24), 11933–11939. https://doi.org/10.1021/jo501691f.

(10)   Aihara, Y.; Chatani, N. Nickel-Catalyzed Reaction of C–H Bonds in Amides with I2: Ortho-Iodination via the Cleavage of C(Sp2)–H Bonds and Oxidative Cyclization to β-Lactams via the Cleavage of C(Sp3)–H Bonds. *ACS Catalysis* **2016**, *6* (7), 4323–4329. https://doi.org/10.1021/acscatal.6b00964.

(11)   Funes-Ardoiz, I.; Nelson, D. J.; Maseras, F. Halide Abstraction Competes with Oxidative Addition in the Reactions of Aryl Halides with [Ni(PMenPh(3−n))4]. *Chemistry – A European Journal* **2017**, *23* (66), 16728–16733. https://doi.org/https://doi.org/10.1002/chem.201702331.

(12)   T. Tsou, T.; K. Kochi, J. Mechanism of Oxidative Addition. Reaction of Nickel(0) Complexes with Aromatic Halides. *Journal of the American Chemical Society* **2002**, *101* (21), 6319–6332. https://doi.org/10.1021/ja00515a028.

(13)   Burling, S.; Elliott, P. I. P.; Jasim, N. A.; Lindup, R. J.; McKenna, J.; Perutz, R. N.; Archibald, S. J.; Whitwood, A. C. C–F Bond Activation at Ni(0) and Simple Reactions of

Square Planar Ni(II) Fluoride Complexes. *Dalton Transactions* **2005**, No. 22, 3686–3695. https://doi.org/10.1039/B510052F.

(14)   R. Bour, J.; M. Camasso, N.; S. Sanford, M. Oxidation of Ni(II) to Ni(IV) with Aryl Electrophiles Enables Ni-Mediated Aryl–CF3 Coupling. *Journal of the American Chemical Society* **2015**, *137* (25), 8034–8037. https://doi.org/10.1021/jacs.5b04892.

(15)   Bour, J. R.; M. Ferguson, D.; J. McClain, E.; W. Kampf, J.; S. Sanford, M. Connecting Organometallic Ni(III) and Ni(IV): Reactions of Carbon-Centered Radicals with High-Valent Organonickel Complexes. *Journal of the American Chemical Society* **2019**, *141* (22), 8914–8920. https://doi.org/10.1021/jacs.9b02411.

(16)   D. Ball, N.; S. Sanford, M. Synthesis and Reactivity of a Mono-σ-Aryl Palladium(IV) Fluoride Complex. *Journal of the American Chemical Society* **2009**, *131* (11), 3796–3797. https://doi.org/10.1021/ja8054595.

(17)   W. Kaspi, A.; Yahav-Levi, A.; Goldberg, I.; Vigalok, A. Xenon Difluoride Induced Aryl Iodide Reductive Elimination: A Simple Access to Difluoropalladium(II) Complexes. *Inorganic Chemistry* **2007**, *47* (1), 5–7. https://doi.org/10.1021/ic701722f.

(18)   Yu, S.; Dudkina, Y.; Wang, H.; Kholin, K. v.; Kadirov, M. K.; Budnikova, Y. H.; Vicic, D. A. Accessing Perfluoroalkyl Nickel(II), (III), and (IV) Complexes Bearing a Readily Attached [C4F8] Ligand. *Dalton Transactions* **2015**, *44* (45), 19443–19446. https://doi.org/10.1039/C5DT01771H.

(19)   T. Ciszewski, J.; Y. Mikhaylov, D.; v. Holin, K.; K. Kadirov, M.; H. Budnikova, Y.; Sinyashin, O.; A. Vicic, D. Redox Trends in Terpyridine Nickel Complexes. *Inorganic Chemistry* **2011**, *50* (17), 8630–8635. https://doi.org/10.1021/ic201184x.

(20)   Zhang, C.-P.; Wang, H.; Klein, A.; Biewer, C.; Stirnat, K.; Yamaguchi, Y.; Xu, L.; Gomez-Benitez, V.; A. Vicic, D. A Five-Coordinate Nickel(II) Fluoroalkyl Complex as a Precursor to a Spectroscopically Detectable Ni(III) Species. *Journal of the American Chemical Society* **2013**, *135* (22), 8141–8144. https://doi.org/10.1021/ja4030462.

(21)   Kosobokov, M. D.; Xue, T.; Vicic, D. A. Synthesis of an Anionic Derivative of the Terpyridine Ligand. *Polyhedron* **2018**, *155*, 366–369. https://doi.org/10.1016/J.POLY.2018.08.062.

(22)   T. Shreiber, S.; M. DiMucci, I.; N. Khrizanforov, M.; J. Titus, C.; Nordlund, D.; Dudkina, Y.; E. Cramer, R.; Budnikova, Y.; M. Lancaster, K.; A. Vicic, D. [(MeCN)Ni(CF3)3]− and [Ni(CF3)4]2–: Foundations toward the Development of Trifluoromethylations at Unsupported Nickel. *Inorganic Chemistry* **2020**, *59* (13), 9143–9151. https://doi.org/10.1021/acs.inorgchem.0c01020.

5.6 Experimental Procedures

5.6.1 General Procedures, Materials and Methods

General Procedures

NMR spectra were recorded on a Varian VNMRS 600 (600 MHz for ^{1}H and 151 MHz for ^{13}C). ^{1}H and ^{13}C NMR chemical shifts are reported in parts per million (ppm) and are referenced to the solvent lock. ^{1}H NMR quantification was conducted using internal standards as mentioned in the experimental procedures. Abbreviations used to report NMR peaks: singlet (s); doublet (d); triplet (t); quartet (q); doublet of doublets (dd); triplet of doublets (td); doublet of triplets (dt); multiplet (m). GC-FID data were collected on a Shimadzu 17A GC using a Restek Rtx®-5 (crossbond 5% diphenyl–95% dimethyl polysiloxane; 15 m, 0.25 mm ID, 0.25 µm df) column. High-resolution mass spectra were recorded on a Micromass AutoSpec Ultima Magnetic Sector mass spectrometer. Cyclic voltammetry was performed using a CHI600C potentiostat from CH Instruments. EPR spectra were collected at temperatures mentioned in the experimental procedures using a Bruker EMX ESR Spectrometer with a nitrogen-cooled cryostat. Elemental analyses were performed by Midwest Microlab located in Indianapolis. X-ray crystallographic data were obtained on a Rigaku AFC10K Saturn 944+ CCD-based X-ray diffractometer. Chromatographic separations were carried out on a Biotage Isolera One system using Sfär Silica HC D (High-capacity Duo 20 µm) columns (10 g, 25 g, or 50 g cartridges depending on the scale of isolations), as mentioned in the synthetic procedures.

Acronyms: Dichloromethane (DCM), Tetrahydrofuran (THF), Water in NMR solvent (HDO), Tetramethylsilane (TMS), Nitromethane (CH_3NO_2), residual moisture in solvent (HDO)

Materials and Methods

All commercial reagents were used as received without further purification unless otherwise noted. Silver(I) tetrafluoroborate ($AgBF_4$), propionitrile and acetonitrile (electronic grade) were purchased from Millipore-Sigma or Aldrich. Acetone was purchased from Acros Organics in AcroSeal® bottles. All deuterated solvents were obtained from Cambridge Isotope Laboratories and deaerated via a nitrogen sparge prior to storage over activated 4 Å molecular sieves (EMD Millipore). Pentane (Fisher), diethyl ether (Millipore-Sigma), tetrahydrofuran (Fisher) were deaerated via a nitrogen sparge and further purified using a solvent purification system for usage inside the glovebox. Celite was purchased from Aqua Solutions and was dried under vacuum at 150 °C for 24 h for usage inside the glovebox. All glassware used in the glovebox was dried in an oven at 150 °C for at least 6 h and cooled under an inert atmosphere. All experiments and synthetic procedures were setup inside a nitrogen-filled glovebox unless otherwise mentioned.

EPR Spectra of Nickel Complexes

50 µL from a 10 mM (10 µmol in 1mL) stock solution of each Ni^{III} complex was diluted with 200 µL of toluene or PrCN. This 250 µL sample was placed in a septum capped EPR tube and cooled in liquid nitrogen until it glassed. EPR spectra were recorded for complexes at 100 K. EPR data are shown below.

Electrochemical Studies of Nickel Complexes

Cyclic voltammetry of Ni^{III} complexes were performed in a 3-electrode cell consisting of a 3 mm glassy carbon disc working electrode, a Pt wire counter electrode, and an $Ag/AgBF_4$ reference electrode with an Ag wire in a fritted chamber containing a solution of $AgBF_4$ (0.01 M) and

NBu4PF6 (0.1 M) in acetonitrile. A 2 mL solution of each complex (0.01 M) and NBu4PF6 (0.1 M) in acetonitrile was added to the electrochemical cell. Cyclic voltammograms were recorded at 50–250 mV/s.

### 5.6.2 Oxidative Reactivity of 2a-pic
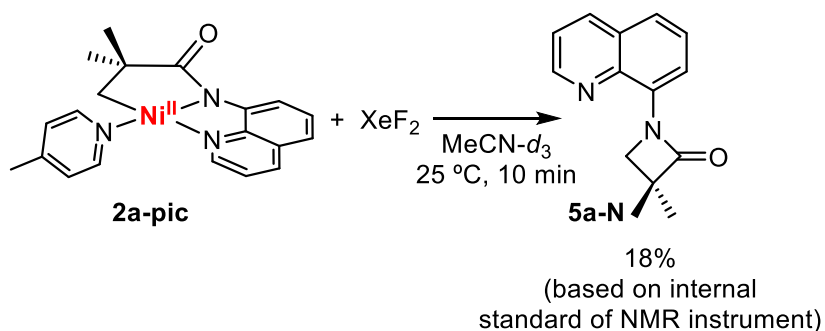
Complex **2a-pic** (3.8 mg, 10 µmol, 1 equiv) was dissolved in MeCN-d_3 (0.5 mL) and added to a 4 mL glass vial containing XeF2 (2.0 mg, 11 µmol, 1.1 equiv). There was an immediate color change from yellow to green and white fumes were observed. The sample was transferred an NMR tube that was sealed with a Teflon septum-lined screw cap. Then the NMR tube was removed from the glovebox and analyzed by ^{1}H NMR and ^{19}F NMR spectroscopy after 10 min. Formation of **5a-N** was noted in the ^{1}H NMR spectra (as indicated by the characteristic resonance at 4.29 ppm), and the crude ^{19}F NMR spectrum showed resonances in the aryl-fluoride region (-116.3 and -129.4 ppm), which are tentatively assigned as fluorination at the 5-position of the aminoquinoline. NMR data are shown below. No further change of the NMR spectra was observed even after 24 h.

Analogous to the above procedure, reactions were setup with other oxidants, including PhI(OAc)2, AgF2, Umemoto's reagent (CF3 oxidant), NFSI, NFTPT. In all of these cases, no diamagnetic signals indicative of a Ni^{IV} species were observed by ^{1}H NMR spectroscopy.
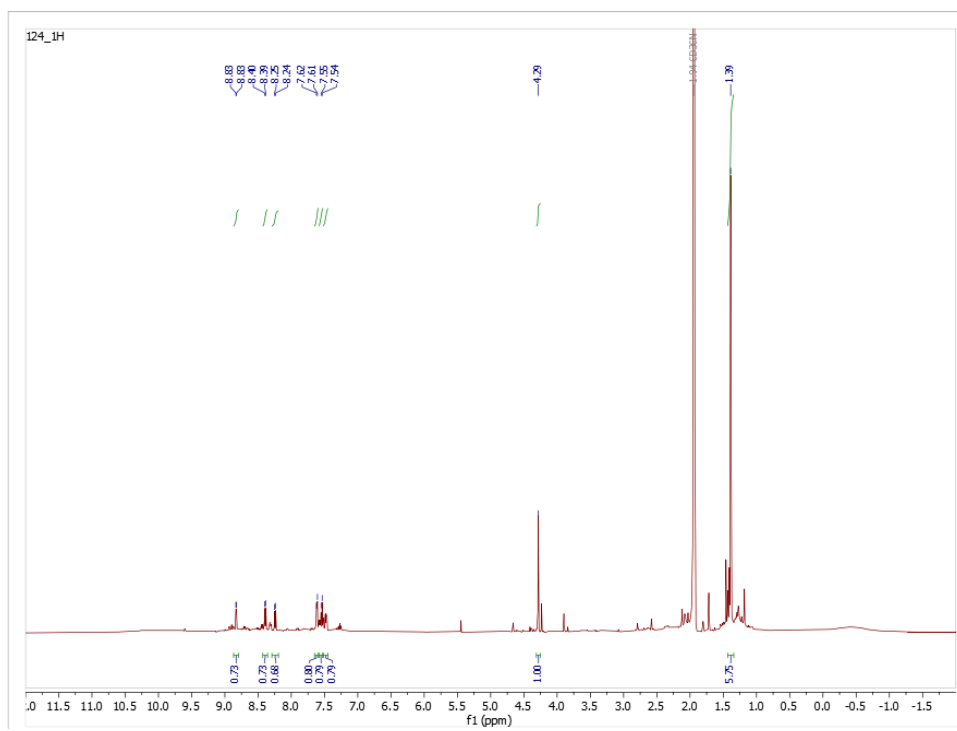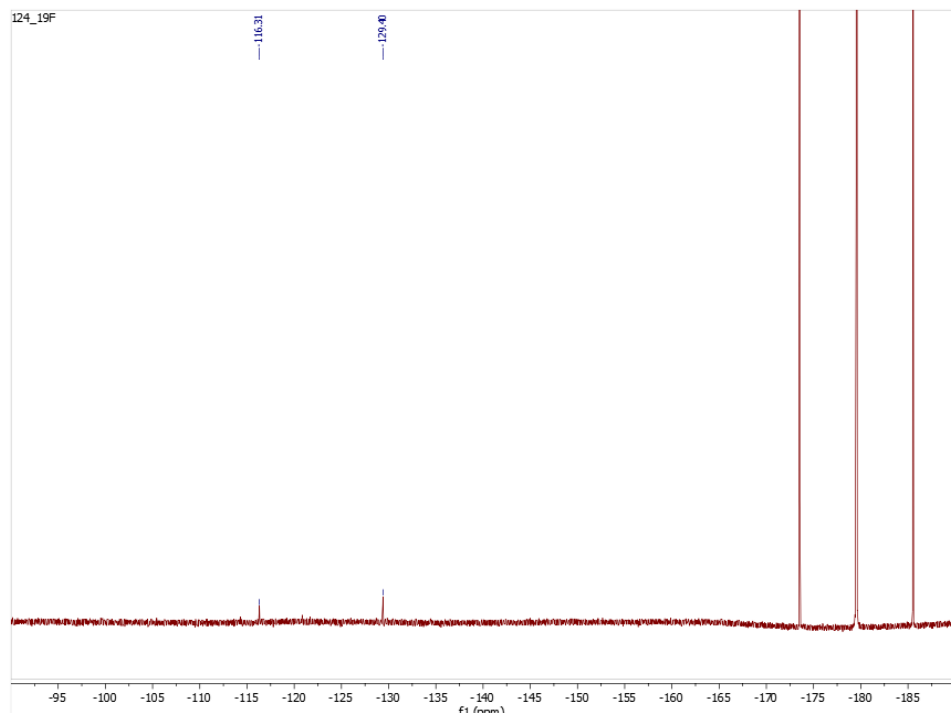
### 5.6.3 Synthesis and Characterization of Polydentate Ni^{III} Complexes
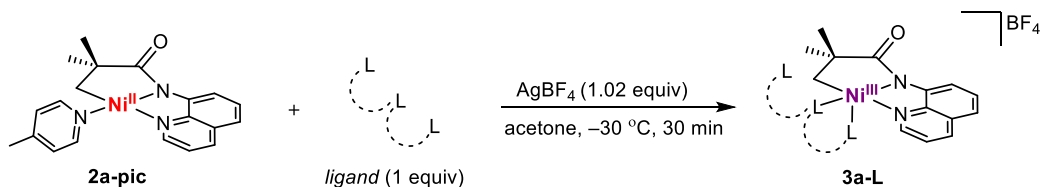
General Procedure: Complex **2a-pic** (189 mg, 0.5 mmol, 1 equiv) and ligand (0.5 mmol, 1 equiv) was weighed into a 20 mL vial and dissolved in anhydrous acetone (5 mL), and the resulting solution was cooled to –30 °C. This solution was added dropwise to a pre-cooled (–30 °C) solution of AgBF$_4$ (100 mg, 0.51 mmol, 1.02 equiv) in acetone (5 mL). The reaction was stirred for 30 min while it slowly warmed up to ambient temperature. A color change from orange to dark green or brown was observed, along with the formation of a gray precipitate. The solvent was removed under vacuum, and the resulting residue was re-dissolved in THF (5 mL). The reaction mixture was filtered through a Celite pad, and this pad was washed with THF (5 mL). The solvent was reduced under vacuum to ~2 mL and then a 1:1 mixture of pentane: diethyl ether (8 mL) was added to precipitate a brownish-green solid. This solid was recrystallized via slow diffusion of pentane into a THF solution and final yields were calculated (**3a-pic** = 78%, **3a-bipy** = 66%, and **3a-terpy** = 48%). The Ni^{III} complexes (**3a-pic** and **3a-bipy**) were characterized by EPR spectroscopy, and single crystal structures as described in section 5.6.5. All attempts to obtain a solid-state structure of **3a-terpy** were unsuccessful.
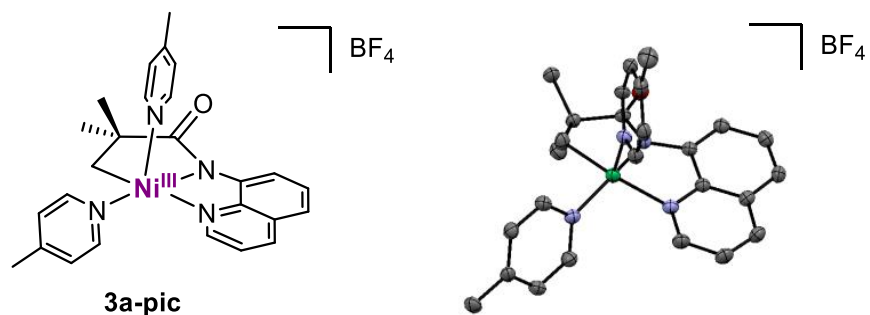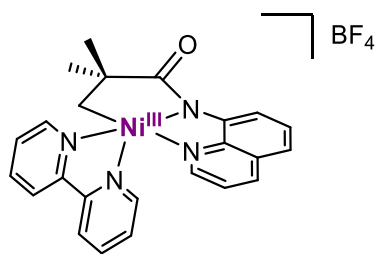
3a-pic

Elemental analysis: calculated for $C_{26}H_{28}N_4BF_4NiO$, C: 55.96, H: 5.06, N: 10.04; Found: C: 47.31, H: 4.28, N: 7.42
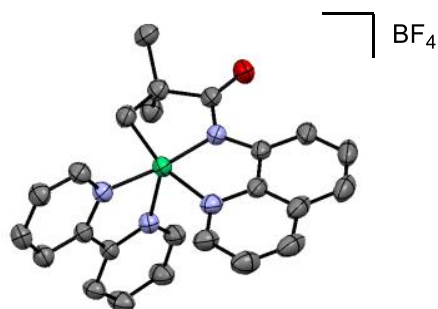
HRMS-electrospray (m/z): $[M^+-BF_4]$ calcd. for $C_{26}H_{28}N_4NiO$, 470.1616; found, 470.1618 [M-BF_4]

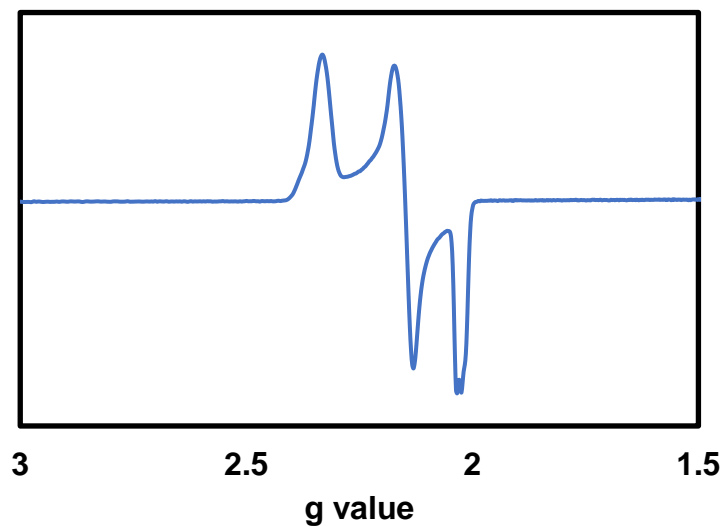EPR spectrum of **3a-pic** was recorded at 93 K in PrCN-glass.
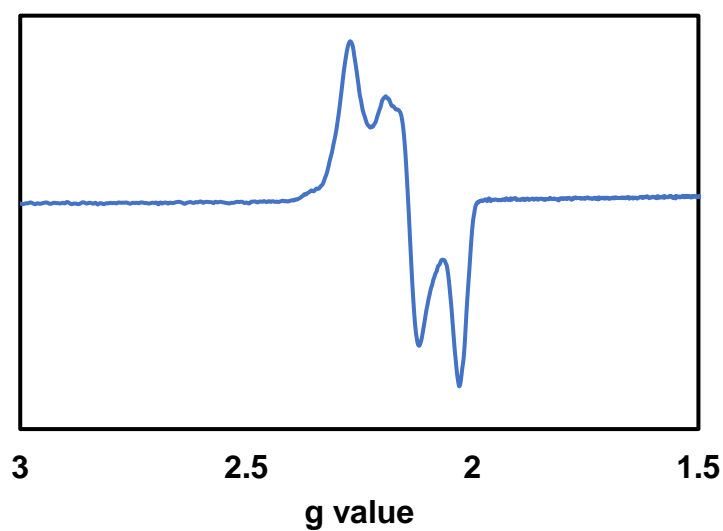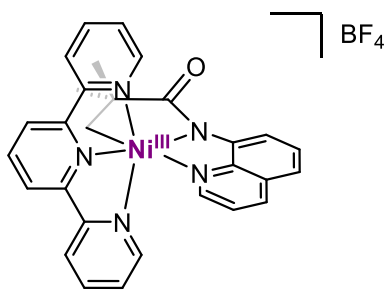
3a-bipy

Elemental analysis: calculated for $C_{24}H_{22}N_4BF_4NiO$, C: 54.60, H: 4.20, N: 10.61; Found: C: 57.16, H: 5.41, N: 9.41

HRMS-electrospray (m/z): $[M^+-BF_4]$ calcd. for $C_{24}H_{22}N_4NiO$, 440.1147; found, 440.1248 [M-BF_4]

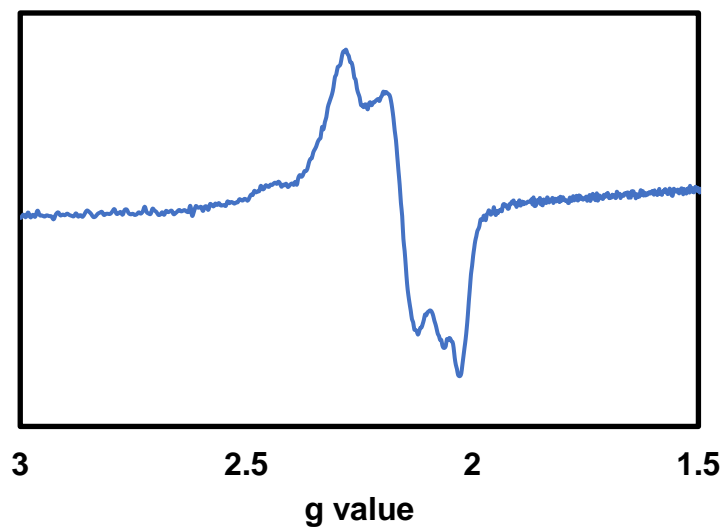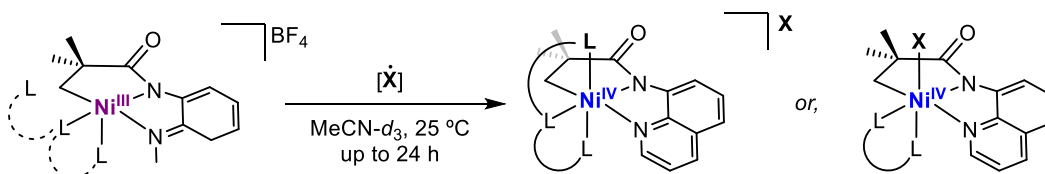EPR spectrum of **3a-bipy** was recorded at 93 K in PrCN-glass.

3a-terpy

HRMS-electrospray (m/z): [M$^+$-BF$_4$] calcd. for C$_{29}$H$_{25}$N$_5$NiO, 517.1413; found, 517.1527 [M-BF$_4$]

EPR spectrum of **3a-terpy** was recorded at 110 K in PrCN-glass.

## 5.6.4 Oxidative Reactivity of Polydentate Ni^{III} Complexes (3a-L)

Complex **3a-L** (10 µmol, 1 equiv) was dissolved in MeCN-d_3 (0.5 mL) and added to a 4 mL glass vial containing NOBF$_4$ (2.0 mg, 11 µmol, 1.1 equiv). There was an immediate color change from yellow to green. The sample was transferred an NMR tube that was sealed with a Teflon septum-lined screw cap. Then the NMR tube was removed from the glovebox and analyzed by ^{1}H NMR and ^{19}F NMR spectroscopy at 10 min. Upon monitoring up to 24 h, no diamagnetic signals consistent with a Ni^{IV} intermediate were observed.

Analogous to the above procedure, reactions were set up with other one-electron oxidants such as AgF$_2$ and ammonium cerium (IV) nitrate (CAN). These showed similar NMR spectra i.e., formation of a Ni^{IV} species was not observed by NMR spectroscopy.

X-Ray Crystallographic Data of 3a-pic
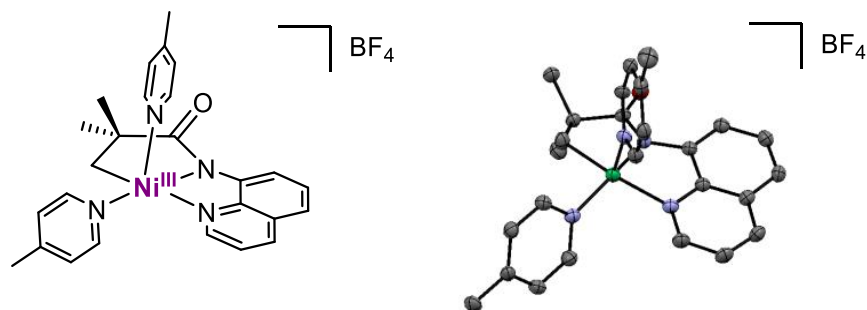
Orange blocks of **3a-pic** were grown from a acetone/tetrahydrofuran/pentane solution of the compound at -10 deg. C. A crystal of dimensions 0.06 x 0.04 x 0.04 mm was mounted on a Rigaku AFC10K Saturn 944+ CCD-based X-ray diffractometer equipped with a low temperature device and Micromax-007HF Cu-target micro-focus rotating anode (l = 1.54187 A) operated at 1.2 kW power (40 kV, 30 mA). The X-ray intensities were measured at 85(1) K with the detector placed at a distance 42.00 mm from the crystal. A total of 2028 images were collected with an oscillation width of 1.0° in w. The exposure times were 1 sec. for the low angle images, 5 sec. for high angle. Rigaku d*trek images were exported to CrysAlisPro for processing and corrected for absorption. The integration of the data yielded a total of 19576 reflections to a maximum 2q value of 138.64° of which 4593 were independent and 3833 were greater than 2s(I). The final cell constants (Table 1) were based on the xyz centroids of 5741 reflections above 10s(I). Analysis of the data showed negligible decay during data collection. The structure was solved and refined with the Bruker SHELXTL (version 2016/6) software package, using the space group P1bar with Z = 2 for the formula C26H28BN4F4ONi. All non-hydrogen atoms were refined anisotropically with the hydrogen atoms placed in idealized positions. The tetrafluoroborate anion is disordered over two positions. Full matrix least-squares refinement based on F2 converged at R1 = 0.0480 and wR2 =

0.1214 [based on I > 2sigma(I)], R1 = 0.0585 and wR2 = 0.1329 for all data. Additional details

are presented in Table 1 and are given as Supporting Information in a CIF file. Acknowledgement

is made for funding from NSF grant CHE-0840456 for X-ray instrumentation.

G.M. Sheldrick (2015) "Crystal structure refinement with SHELXL", Acta Cryst., C71, 3-8 (Open

Access).

CrystalClear Expert 2.0 r16, Rigaku Americas and Rigaku Corporation (2014), Rigaku Americas,

9009, TX, USA 77381-5209, Rigaku Tokyo, 196-8666, Japan.

CrysAlisPro 1.171.38.41 (Rigaku Oxford Diffraction, 2015).

Table 5.1 Crystal Data and Structure Refinement for **3a-pic**

Empirical formula	C26 H28 B F4 N4 Ni O
Formula weight	558.04
Temperature	85(2) K
Wavelength	1.54184 A
Crystal system, space group	Triclinic, P-1
Unit cell dimensions	a = 8.1631(4) A alpha = 75.846(3)° b = 9.5585(4) A beta = 81.795(3)° c = 17.5144(6) A gamma = 74.433(4)°
Volume	1272.15(10) A^3
Z, Calculated density	2, 1.457 Mg/m^3
Absorption coefficient	1.595 mm^-1
F(000)	578

Crystal size	0.060 x 0.040 x 0.040 mm
Theta range for data collection	2.611 to 69.321°
Limiting indices	-9<=h<=9, -11<=k<=10, -21<=l<=20
Reflections collected / unique	19576 / 4593 [R(int) = 0.0748]
Completeness to theta = 67.684	97.7%
Absorption correction	Semi-empirical from equivalents
Max. and min. transmission	1.00000 and 0.51245
Refinement method	Full-matrix least-squares on F^2
Data / restraints / parameters	4593 / 94 / 383
Goodness-of-fit on F^2	1.043
Final R indices [I>2sigma(I)]	R1 = 0.0480, wR2 = 0.1214
R indices (all data)	R1 = 0.0585, wR2 = 0.1329
Extinction coefficient	n/a
Largest diff. peak and hole	0.509 and -0.434 e.A^-3

X-Ray Crystallographic Data of 3a-bipy
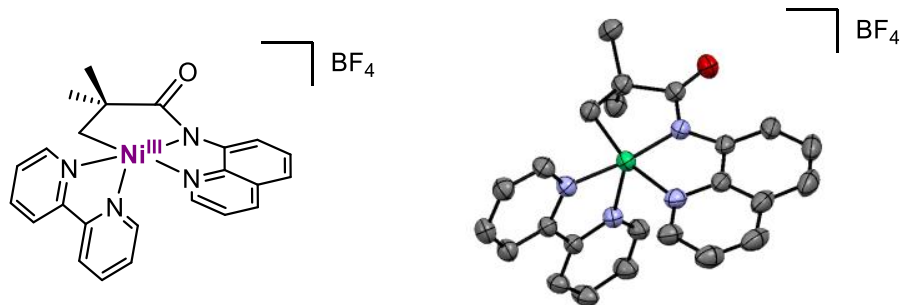
Colorless needles of **3a-bipy** were grown from a tetrahydrofuran/acetone solution of the compound at 22 deg. C. A crystal of dimensions 0.10 x 0.04 x 0.02 mm was mounted on a Rigaku AFC10K Saturn 944+ CCD-based X-ray diffractometer equipped with a low temperature device and Micromax-007HF Cu-target micro-focus rotating anode (l = 1.54187 A) operated at 1.2 kW power (40 kV, 30 mA). The X-ray intensities were measured at 85(1) K with the detector placed at a distance 42.00 mm from the crystal. A total of 2028 images were collected with an oscillation width of 1.0° in w. The exposure times were 5 sec. for the low angle images, 35 sec. for high angle. Rigaku d*trek images were exported to CrysAlisPro for processing and corrected for absorption. The integration of the data yielded a total of 81256 reflections to a maximum 2q value of 138.70° of which 10067 were independent and 8555 were greater than 2s(I). The final cell constants (Table 1) were based on the xyz centroids of 19741 reflections above 10s(I). Analysis of the data showed negligible decay during data collection. The structure was solved and refined with the Bruker SHELXTL (version 2018/3) software package, using the space group P2(1)/c with Z = 4 for the formula C54.4H58.2B2N8O4F8Ni2. All non-hydrogen atoms were refined anisotropically with the hydrogen atoms placed in idealized positions. Fractional atom counts are due to a solvent site with a mixture of acetone and water. Full matrix least-squares refinement based on F2 converged at R1 = 0.0736 and wR2 = 0.1910 [based on I > 2sigma(I)], R1 = 0.0835 and wR2 = 0.1992 for all data. Additional details are presented in Table 1 and are given as Supporting Information in a CIF

G.M. Sheldrick (2015) "Crystal structure refinement with SHELXL", Acta Cryst., C71, 3-8 (Open Access).

CrystalClear Expert 2.0 r16, Rigaku Americas and Rigaku Corporation (2014), Rigaku Americas, 9009, TX, USA 77381-5209, Rigaku Tokyo, 196-8666, Japan.

CrysAlisPro 1.171.38.41 (Rigaku Oxford Diffraction, 2015).

Table 5.2 Crystal Data and Structure Refinement for **3a-bipy**

Empirical formula	C54.40 H58.20 B2 F8 N8 Ni2 O4
Formula weight	1179.13
Temperature	85(2) K
Wavelength	1.54184 A
Crystal system, space group	Monoclinic, P2(1)/c
Unit cell dimensions	a = 27.3410(5) A alpha = 90° b = 10.2449(2) A beta = 96.382(2)° c = 19.4267(4) A gamma = 90°
Volume	5407.81(18) A^3
Z, Calculated density	4, 1.448 Mg/m^3
Absorption coefficient	1.562 mm^-1
F(000)	2442
Crystal size	0.100 x 0.040 x 0.020 mm

Theta range for data collection	3.253 to 69.345°
Limiting indices	-31<=h<=33, -12<=k<=12, -23<=l<=23
Reflections collected / unique	81256 / 10067 [R(int) = 0.0672]
Completeness to theta = 67.684	99.9%
Absorption correction	Semi-empirical from equivalents
Max. and min. transmission	1.00000 and 0.77153
Refinement method	Full-matrix least-squares on F^2
Data / restraints / parameters	10067 / 67 / 777
Goodness-of-fit on F^2	1.109
Final R indices [I>2sigma(I)]	R1 = 0.0736, wR2 = 0.1910
R indices (all data)	R1 = 0.0835, wR2 = 0.1992
Extinction coefficient	n/a
Largest diff. peak and hole	1.237 and -0.525 e.A^-3